

NANYANG TECHNOLOGICAL UNIVERSITY
SINGAPORE

Peroxytungstate Anions in Asymmetric Ion Pair Catalyzed Oxidations

YE XINYI

SCHOOL OF PHYSICAL AND MATHEMATICAL SCIENCES

2019

Peroxytungstate Anions in Asymmetric Ion Pair Catalyzed Oxidations

YE XINYI

SCHOOL OF PHYSICAL AND MATHEMATICAL SCIENCES

A thesis submitted to the Nanyang Technological University in partial fulfilment of the requirement for the degree of Doctor of Philosophy

2019

Statement of Originality

I hereby certify that the work embodied in this thesis is the result of original research done by me except where otherwise stated in this thesis. The thesis work has not been submitted for a degree or professional qualification to any other university or institution. I declare that this thesis is written by myself and is free of plagiarism and of sufficient grammatical clarity to be examined. I confirm that the investigations were conducted in accord with the ethics policies and integrity standards of Nanyang Technological University and that the research data are presented honestly and without prejudice.



7-Jan-2019

. . . . . .
Date

. . . . . .
YE XINYI

Supervisor Declaration Statement

I have reviewed the content and presentation style of this thesis and declare it of sufficient grammatical clarity to be examined. To the best of my knowledge, the thesis is free of plagiarism and the research and writing are those of the candidate's except as acknowledged in the Author Attribution Statement. I confirm that the investigations were conducted in accord with the ethics policies and integrity standards of Nanyang Technological University and that the research data are presented honestly and without prejudice.

7-Jan-2019



. . . . . .
Date

. . . . . .
Li Tianhu

Authorship Attribution Statement

This thesis contains material from 1 paper published in the following peer-reviewed journal(s) and 1 paper in manuscript where I was the first or corresponding author.

Chapter 3 is published as X. Ye, A.M.P. Moeljadi, K.F. Chin, H. Hirao, L. Zong, and C.-H.Tan. Enantioselective sulfoxidation catalyzed by a bisguanidinium diphosphatobisperoxotungstate ion pair. *Angew. Chem., Int. Ed. 55*, 7101-7105 (2016). DOI: 10.1002/ange.201601574.

The contributions of the co-authors are as follows:

- Prof Tan Choon-Hong provided the initial project direction and edited the manuscript drafts.
- I prepared the manuscript drafts. The manuscript was revised by Dr A.M.P. Moeljadi.
- I co-designed the computational study with A/Prof H. Hirao and performed all the laboratory work at the School of Physical and Mathematical Science. I also analyzed the data.
- All experiments, including sample preparation, was conducted by me in the Facility for Analysis, Characterization, Testing and Simulation.
- Dr K.F. Chin and Dr L. Zong assisted in the collecting optical rotation data and catalyst development.

Chapter 4 is in manuscript as K.F. Chin, X. Ye, Y. Li, L. Richmond, A.M. Kabylda, X. Zhang, E.C.X. Ang, and C.-H.Tan. Asymmetric Epoxidation of Allylic and Homoallylic Amines Catalyzed by Bisguanidinium Tetraperoxyditungstate. (Co-first author and corresponding author)

The contributions of the co-authors are as follows:

- Prof Tan Choon-Hong provided the initial project direction and edited the manuscript drafts.
- I prepared the manuscript drafts. The manuscript was revised by Dr K.F. Chin.
- I co-designed the IR and Raman study with Dr L. Richmond and A.M. Kabylda , and performed all the laboratory work at the School of Physical and Mathematical Science. I also analyzed the data.
- Most of experiments, including sample preparation, was conducted by Dr K.F. Chin and me in the Facility for Analysis, Characterization, Testing and Simulation.
- X. Zhang, E.C.X. Ang helped in part of substrates synthesis.
- Dr Yongxin Li assisted in the interpretation of the X-ray absorption spectroscopy data and carried out the spectral interpretation.

Note: If published materials are not inserted as thesis chapters, students must acknowledge co-worker contributions in the acknowledgement section of their thesis.

7-Jan-2019

. . . . . .
Date



. . . . . .
YE XINYI

Abstract

The aim of this study is to develop efficient asymmetric ion pair catalysis assisted by metal oxides to realize highly enantioselective oxidation reactions. In this thesis, two projects revealed the novel catalytic system as an excellent strategy in synthetic methodology. In each case, the essence of chemistry was studied mechanistically.

The first two chapters introduced the background from two aspects, which included the history of ion pair catalysis (Chapter 1) and application of tungstate salts in oxidation (Chapter 2). The following two chapters presented two projects utilizing the designed strategy.

Over the last few years, our group has developed a series of phase-transfer catalysts, which successfully solved problems in the enantioselective addition and substitution reaction under traditional base promoted conditions. Meanwhile, another precedent concept of ion pair catalysis was put forward as a branched subject in this field. Motivated by ion pair concept, the work discussed in this thesis proved the potential of the catalysts developed in our group under a novel working mode.

In Chapter 3, bisguanidinium diphosphatobisperoxotungstate $BG^{2+}[\{PO_2(OH)_2\}_2\{WO(O_2)_2\}]^{2-}$ successfully catalyzed asymmetric sulfoxidation, which was applied in synthesis of (*S*)-Lansoprazole ultimately. The active species was characterized by Raman spectroscopy and supported by computational data. In Chapter 4, according to the success of oxidizing electron poor allylic and homoallylic amines, a further development was established. The real catalyst was a stable compound and demonstrated as bisguanidinium tetraperoxyditungstate $BG^{2+}[W_2O_2(\mu\text{-}O)(O_2)_4]^{2-}$ by single crystal X-ray diffraction. Meanwhile, both experimental and computational data of Raman and IR were collected and compared for analysis and discussion. The perfectly matched spectra show the efficiency of information acquirability via Raman and IR, which has potential application in mechanism exploration in future work of this area.

Acknowledgements

First and foremost, I would like to express my most sincere gratitude to my supervisors, Associate Professor Li Tianhu (Main supervisor) and Professor Tan Choon-Hong (Co-supervisor) for their patience, guidance and providing me with valuable suggestions during my research. Not only that, they also greatly influenced me through their genius, serious working attitude and their enthusiasm in chemistry. They impart upon me with precious experience in academia. They also supported me financially when I was pursuing my doctorate degree.

Second, I am grateful to all the members of my dissertation committee for their valuable advice.

Third, I would like to thank my laboratory colleagues: Dr. Chin Kek Foo, Dr. Adhitya Mangala Putra Moeljadi, Dr. Chen Li, Dr. Chua Zhijie, Dr. Valerie Wong, Dr. Jackson Leow, Dr. Ren Jingyun, Mr. Song Zhijian, Mr. Zhang Xin, Mr. Chen Wenchao, Mr. Ye Ziyang Victor, Ms. Esther Ang Cai Xia and Mr. Adil M. Kabylda and other members, all of whom provided me with a lot of help and/or advice in my research work.

Fourth, I would like to thank all the support staff especially Ms. Lee Yeanchin, Ms. Janice Low, Ms. Zhu Wenwei, Ms Goh Eeling, Dr. Li Yongxin, Ms. Celine Hum Wei Mei, Ms. Cindy Goh, Ms. Tan Wei Ting for their help and support during my stay at NTU.

Fifth, I would like to give special thanks to my parents for their love, understanding and support allowing me to overcome all difficulties and hardships during this long journey.

Last but not the least, I would like to thank Nanyang Technological University, Division of Chemistry and Biological Chemistry for offering me this academic opportunity.

Table of Contents

Abstract 1

Acknowledgements 2

Table of Contents 3

Chapter 1 Ion Pair Catalysis **5**

1.1 Introduction 6

1.2 Chiral cation-directed catalysis 7

1.2.1 Ammonium cations 7

1.2.2 Phosphonium cations 13

1.3 Cation-binding catalysis 14

1.4 Chiral anion-directed catalysis 15

1.4.1 Borate anions 15

1.4.2 Phosphate anions 16

1.4.3 N-Triflylphoramidate cations 21

1.5 Anion-binding catalysis 23

1.6 Summary 28

References 28

Chapter 2 Tungstate Anion and Derivatives in Oxidation **33**

2.1 Introduction 34

2.2 Tungstate monomer in oxidation 35

2.3 Tungstate oligomer in oxidation 40

2.4 Tungstate polymer in oxidation 45

2.5 Summary 47

References.....47

Chapter 3 Bisguanidinium Diphosphatobisperoxotungstate Catalyzed Sulfoxidation 50

3.1 Introduction 51

3.2 Result and discussion 53

3.2.1 Reaction development 53

3.2.2 Mechanism study 62

3.3 Summary 68

3.4 Experimental 68

3.4.1 Experimental procedure 68

3.4.2 Characterization of asymmetric product 71

References.....83

Chapter 4 Bisguanidinium tetraperoxyditungstate Catalyzed Epoxidation ..85

4.1 Introduction 86

4.2 Results and discussions 88

4.2.1 Reaction development 88

4.2.2 Identification of catalyst 93

4.2.3 Characterization of catalyst 94

4.3 Summary 97

4.4 Experimental 98

4.4.1 Experimental procedure 98

4.4.2 Characterization of asymmetric products 99

4.4.3 Single crystal 107

References.....108

Appendix 110

Chapter 1

Ion Pair Catalysis

1.1 Introduction

Ion pair catalysis was presented for the first time in 1926 by Bjerrum.[1] Eighty years later, this concept was defined officially in textbook by Anslyn and Dougherty.[2] It said, a cation and an anion are close enough, and the required dissociation energy is higher than the thermal energy (at room temperature) available for separating them. From the other perspective, the lifetime of ion pair is longer than the time required for forming non-interacting ions caused by *Brownian motion*.

The progress of industrial asymmetric synthesis calls for the breakthrough in developing ion pair catalysis. Currently, the asymmetric catalysis systems could be concluded as organometallic catalysis, chiral Lewis acid catalysis, chiral organocatalysis, chiral ion pair catalysis, chiral enzymatic catalysis, and chiral photoredox catalysis. The most traditional field is referred to organometallic chemistry. Covalent bonds between a reaction intermediate and a metal catalyst are formed, and then the enantioselectivity is directed by a chiral ligand on the metal catalyst.[3] Chiral Lewis acid catalysis[4] utilizes a broad range of main group and transition metal Lewis acids coordinated by chiral ligands, which is distinguished from organometallic catalysis by dative bond directing mechanism. Chiral organocatalysis[5] has developed in recent few decades. It includes chiral enamine/iminium catalysis,[6] chiral NHC catalysis,[7] and chiral phosphine catalysis. Another field is ion pair catalysis, which could be subcategorized as chiral cationic and chiral anionic catalysis. The enantioselectivity can be induced through electrostatic or other noncovalent interactions between the charged intermediates and charged chiral ions.[8] Chiral enzymatic catalysis[9] also becomes a hot topic recently, which is human body benign and has large potential in application of drug modifications. The most novel field is different from the former in which free radicals are involved via chiral photoredox catalysts.[10] It burgeons recently with the discovery and application of metallic chiral ligand photoredox catalysts. However, radical relay progresses without any covalent interaction

between the intermediates and catalysts, which distinguishes itself from the first traditional catalytic mode. Among these strategies, ion pair catalysis is good for both homogenous and heterogenous reactions, and has the advantages of low catalyst loading and large scalability, which guarantees the prospective application in productive engineering.

According to the structural characteristics of ion pair catalysts, four categories of ion pair catalysis are concluded: chiral cation-directed catalysis, chiral anion-directed catalysis, cation-binding catalysis, and anion-binding catalysis (Figure 1.1).[8]

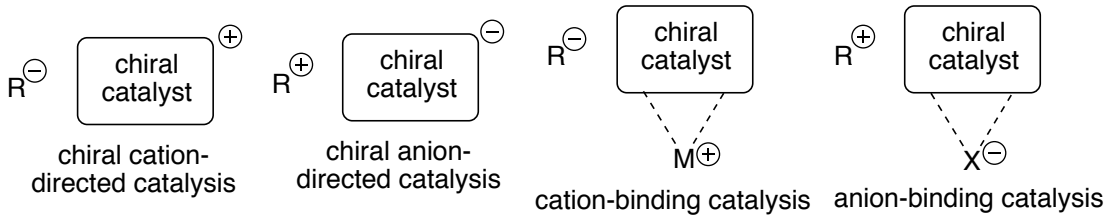
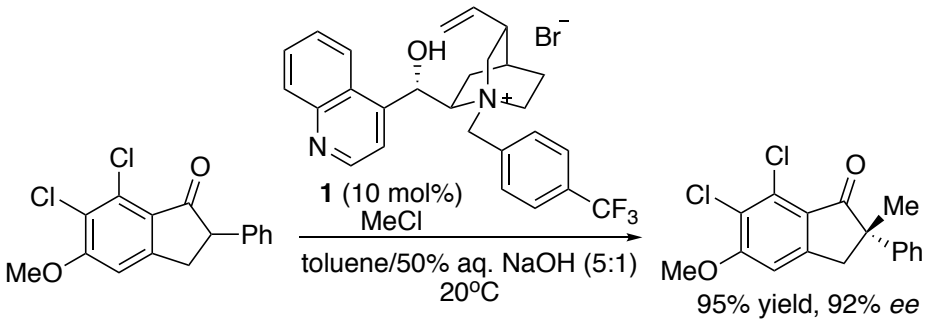


Figure 1.1 Four typical ion pair catalysis

1.2 Chiral cation-directed catalysis

1.2.1 Ammonium cations

The earliest report of using chiral ammonium salt can be traced back to the 1984, which was utilized in *C*-methylation of indanones (Scheme 1.1).[11] The skeleton of quaternary ammonium salt **1** is derived from natural product, cinchonidine. Since then, researchers found it worked efficiently in base promoted reaction, and this strategy was successfully applied in a wide range of reactions, such as aldol, Michael, Mannich and so on.



Scheme 1.1 First chiral quaternary ammonium catalyzed alkylation

However, the natural alkaloid is very costly, and sometimes it has to be further modified to improve results. Thus, researchers started to develop artificial ammonium catalyst with different skeletons. New generations of ammonium catalysts are classified into two groups: one possesses sp^3-nitrogen center, and another possesses sp^2-nitrogen center (Figure 1.2). Maruoka and co-workers developed C_2-symmetric bis-binaphthyl based sp^3-nitrogen centered spriocyclic catalyst **2**.[12] Shibasaki and co-workers developed two centered sp^3-nitrogen catalyst **3**.[13] Our group has contributed to two sp^2-nitrogen centered catalysts in recent decades. Pentanidinium (**PN**) **4** is the condensed product of one guanidine and one imidazole chloride.[14] Bisguanidinium (**BG**) **5** is a two charged cation catalyst, which is the condensed product of two molecular imidazole chloride salts and piperazine.[15,16]

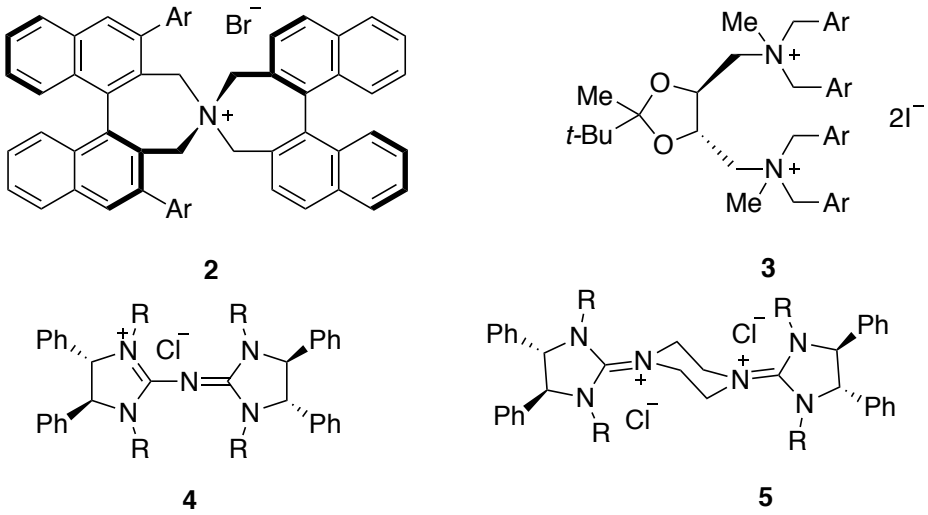
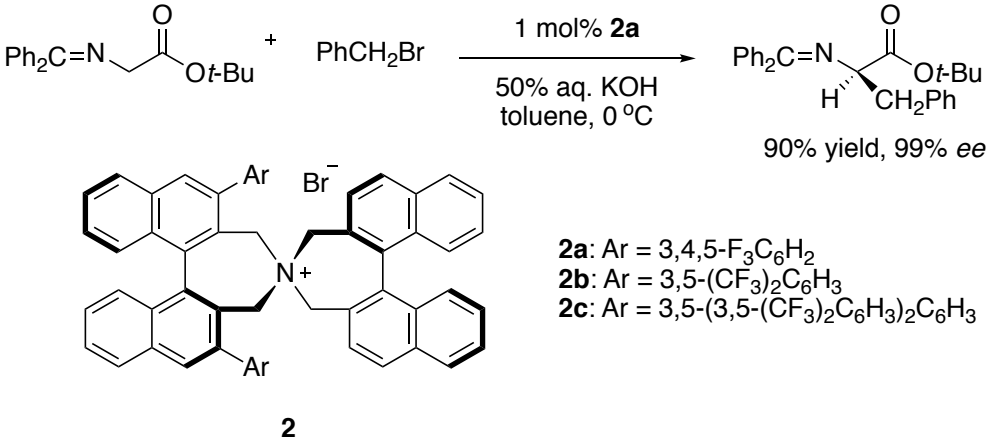


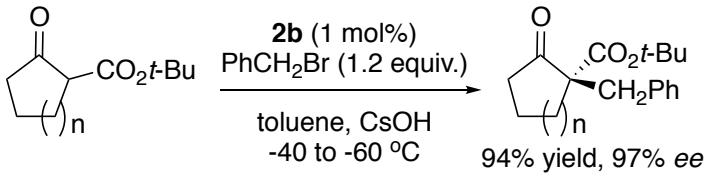
Figure 1.2 Representative examples about sp^3 and sp^2 centered ammonium salts

As one of the most popular quaternary ammonium cations, Maruoka's catalyst was widely used in methodology (Scheme 1.2). In the first report,[12] they described the skeleton of bis-binaphthyl based spiro-ammonium, and examined a series of modified derivatives in Schiff base alkylation. They found **2a** showed best performance with basic aqueous solution among these catalysts, producing 90% yield and 99% *ee* in a model reaction.



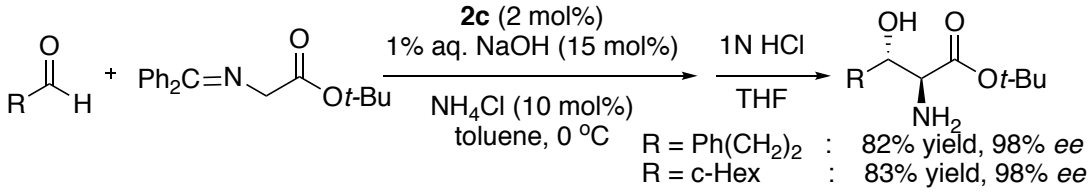
Scheme 1.2 First application of Maruoka catalyst

Later, the combination of phase transfer catalyst and base became an efficient method to build quaternary carbon centers. Additionally, with the development of catalysts, a broader substrate scope was explored (Scheme 1.3), where alkylation of tertiary carbanion formed by deprotonation of β-keto esters proved.[17]



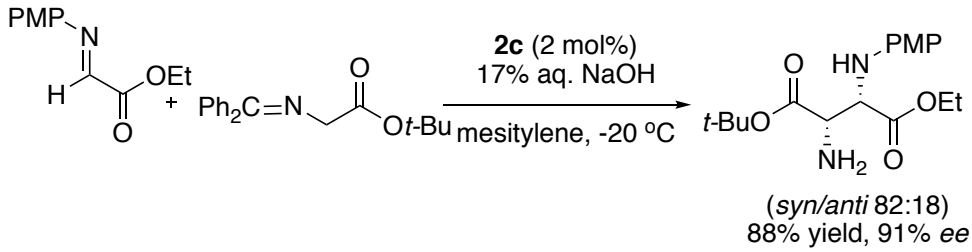
Scheme 1.3 C-H bond activation via Maruoka catalyst

Some other reactions involving similar deprotonation process were proved feasible with this catalytic system as well. The nucleophilic addition reactions were notable among them (Scheme 1.4). In the presence of **2c**, a direct aldol reaction[18,19] between Schiff base and aliphatic aldehydes were achieved in both high yield and *ee*%.



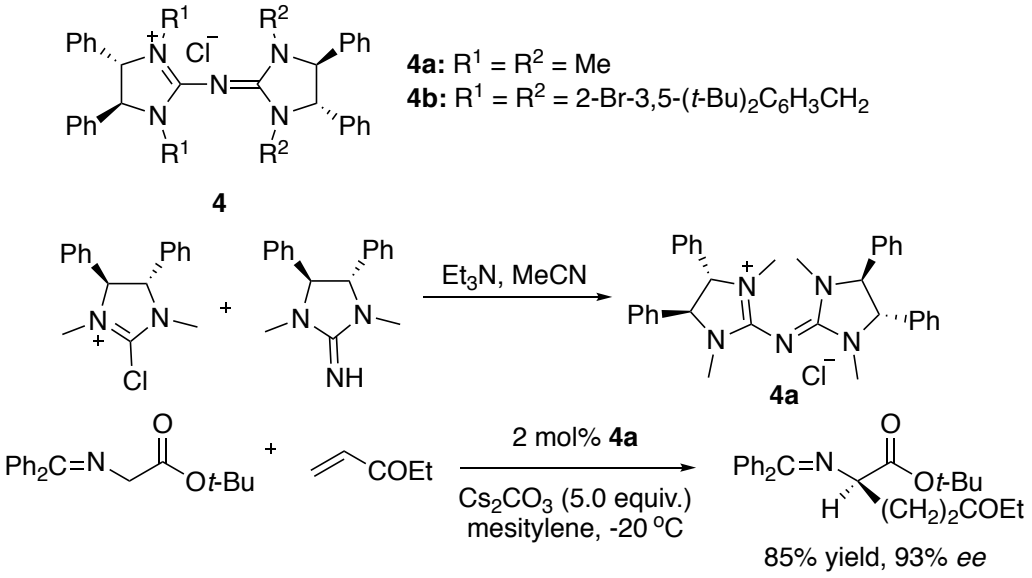
Scheme 1.4 aldol reaction via Maruoka catalyst

Similar to the aldol reaction, Mannich reaction[20] was easy to realize in this way. By replacing aldehydes with α-imino esters (Scheme 1.5), the analogues of chiral diamines were constructed in one step in both high regio and enantioselectivity.



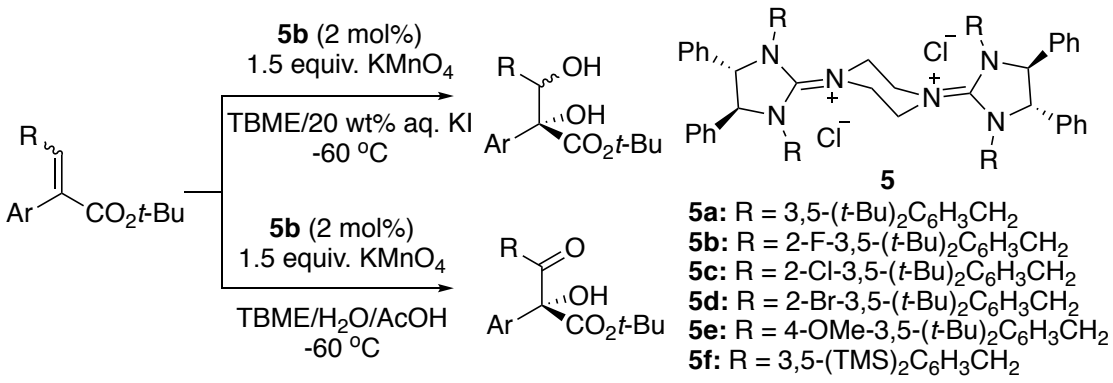
Scheme 1.5 Mannich reaction via Maruoka catalyst

When it comes to sp^2-nitrogen centered ammonium, the systematic work was done in our group in recent decade. In 2009, the concept of chiral guanidinium salt[21] was first put forward and used in phospha-Mannich reaction. Two years later, a landmark work of creating pentanidinium (**PN**) **4** was first demonstrated and applied to asymmetric Michael addition of Schiff base successfully.[14] The key step of preparation of **4** was the condensation between imidazole salt and guanidine. In this Michael addition reaction, **4a** was characterized by single crystal X-ray diffraction (Scheme 1.6).



Scheme 1.6 First application of pentanidinium catalyst

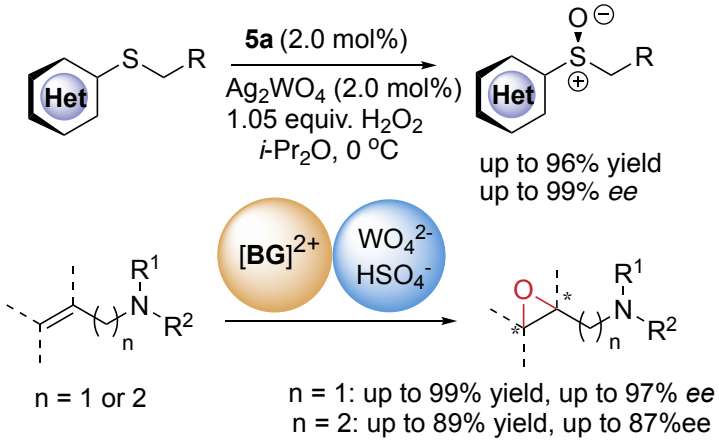
On the basis of preliminary models of catalysts, a new generation of guanidinium-based ion pair catalyst was established,[15] which was first reported and described as bisguanidinium (**BG**) **5** (Scheme 1.7). Motivated by the success of **PN** during 2011-2014, a strategy of changing the linker between the two guanidine units was attempted. In a series of catalyst derivatives, piperazine-linked **BG** was found to be the most potential catalyst for application in oxidation reaction. The main step to form **BG** was the condensation between two molecules of imidazole salts and one piperazine molecule in the presence of a base. In the first report of **BG**, trisubstituted enoates was chosen as the research object. The catalyst was modified with a specific side chain as **5b**. The terminal oxidant of dihydroxylation and oxohydroxylation was potassium permanganate. However, as potassium permanganate was so reactive, the reaction had to be conducted under extremely cold conditions. At the same time, potassium permanganate is not an ideal oxidant in industry. Thus, we work towards replacing the oxidant to hydrogen peroxide, which is widely used in practice.



Scheme 1.7 First application of bisguanidinium catalyst

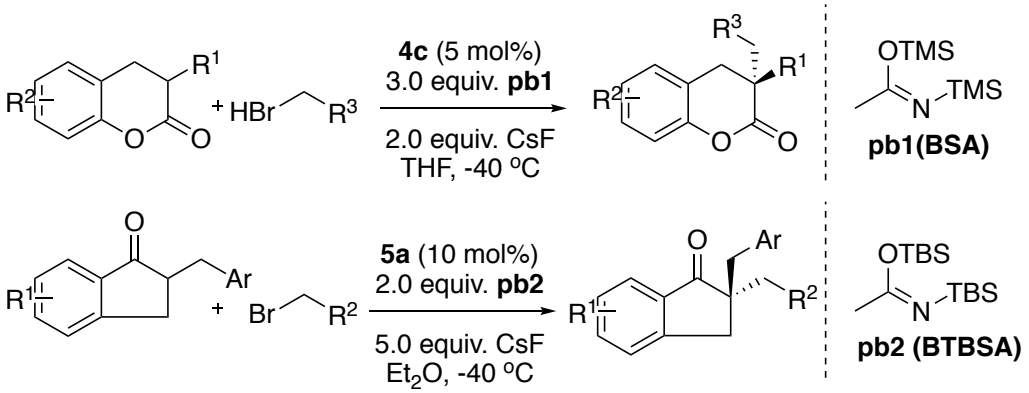
The industrial method of asymmetric oxidation is Kagan's sulfoxidation, which is famous for its application in synthesizing Esomeprazole by utilizing Ti-tartaric acid complex and cumene hydroperoxide. To challenge the existing method, we began to research on sulfoxidation (see more details in chapter 3).[22] Direct hydrogen peroxide transfer proved inefficient, but catalytic amount of metal oxide make the reaction work (Scheme 1.8). After

that, epoxidation was studied under the same catalytic system, and more information about ion pair catalysis was revealed during the mechanistic study (see more details in chapter 4).



Scheme 1.8 Bisguanidinium catalyzed oxidation reactions

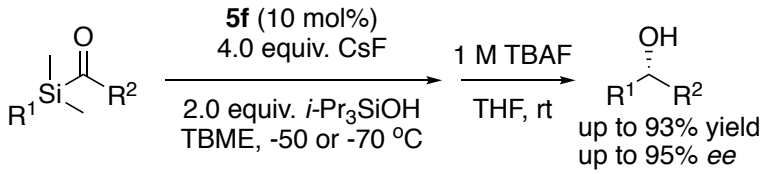
On the other hand, **BG** showed ability to capture the hypervalent silicate intermediate. In 2016, an asymmetric alkylation using silylamide as pro-base (**pb**) was accomplished when catalyzed by **PN** or **BG**.[23] In the substrate scope of dihydrocoumarins and benzochromenones, **PN** was applied. However, in the substrate scope of α-benzyl-1-indanones, **BG** was preferred over **PN**. The configuration of the pro-base was attributed to the difference in the choices of catalyst. It was obvious that **pb2** was bigger than **pb1** in terms of the TBS group (Scheme 1.9). As **BG** has a larger space in its ionic center, it was able to capture a bulkier silicate intermediate.



Scheme 1.9 Hypervalent silicate intermediates and pro-base strategy

The same strategy was applied to 1,2-anionotropic rearrangement of acylsilane to produce chiral secondary alcohol. The intramolecular 1,2-Brook rearrangement occurred in the

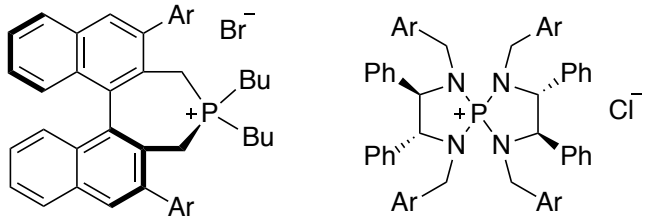
presence of CsF, and the extra additive of silanol in system was to provide a proton to the acyl group (Scheme 1.10).[24]



Scheme 1.10 1,2-Brook rearrangement activated by CsF

1.2.2 Phosphonium cations

Chiral quaternary phosphonium catalysts have been realized as another type of ion pair catalysts after the success of quaternary ammonium salts (Figure 1.3). In 2008, Maruoka and co-workers developed C_2-symmertric tetraalkyl phosphonium salt **6**,[25,26] with which they achieved enantioselective amination, Michael, and Mannich reactions. Ooi and co-workers developed *N*-benzylated D_2-symmetric *P*-spiro tetraaminophosphonium salt **7**.[27] The working principle of quaternary phosphonium cation is similar to that of the quaternary ammonium cation.



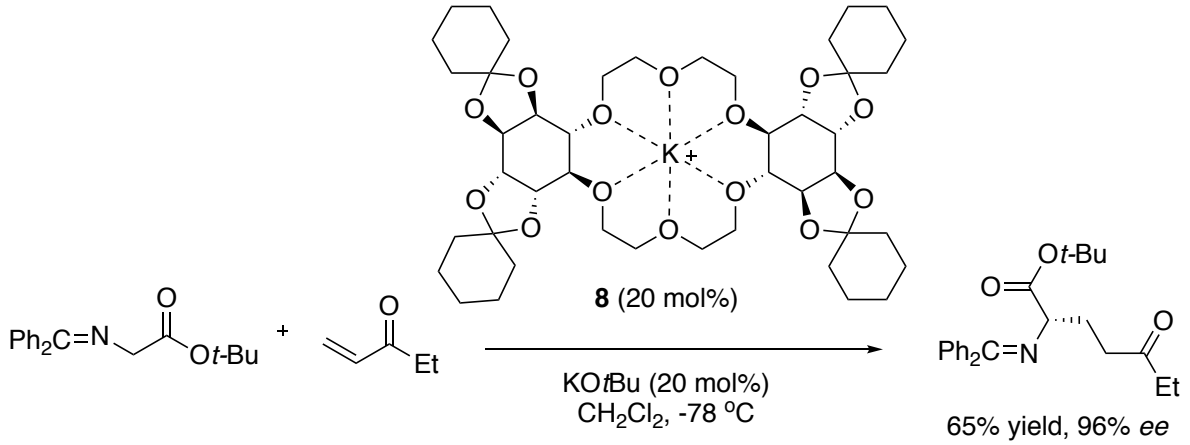
6 **7**

Figure 1.3 Quaternary phosphonium cations

1.3 Cation-binding catalysis

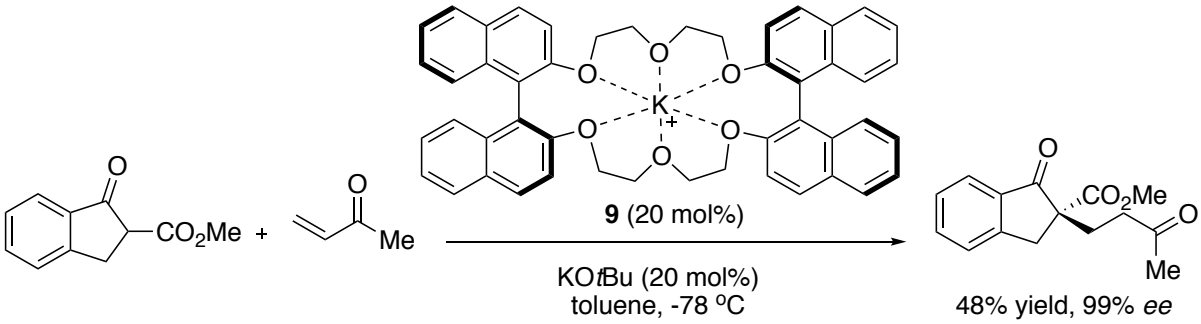
Compared to cation-directed catalysis, cation-binding catalysis works as well in form of ion state. This type of ion pair catalyst follows the structural character of crown-ether chelated metal cation catalyst, such as 18-crown-6/K^+ cation. Thus, a lot of modified crown polyethers were developed to improve their capability in terms of enantioselectivity.

The natural chiral-pool can be one of the most important motifs applied to polyethers. Akiyama and co-workers prepared chiral inositol derived crown ethers **8** to catalyze Michael addition reaction (Scheme 1.11).[28]



Scheme 1.11 Polyether-binding potassium catalyzed Michael addition reaction

Another chiral source is artificial chiral compound. Cram and Sogah created BINOL-based chiral crown ether **9** to accomplish Michael addition in 1981 (Scheme 1.12), which was the first example of highly enantioselective Michael addition catalyzed by phase transfer catalyst.[29]



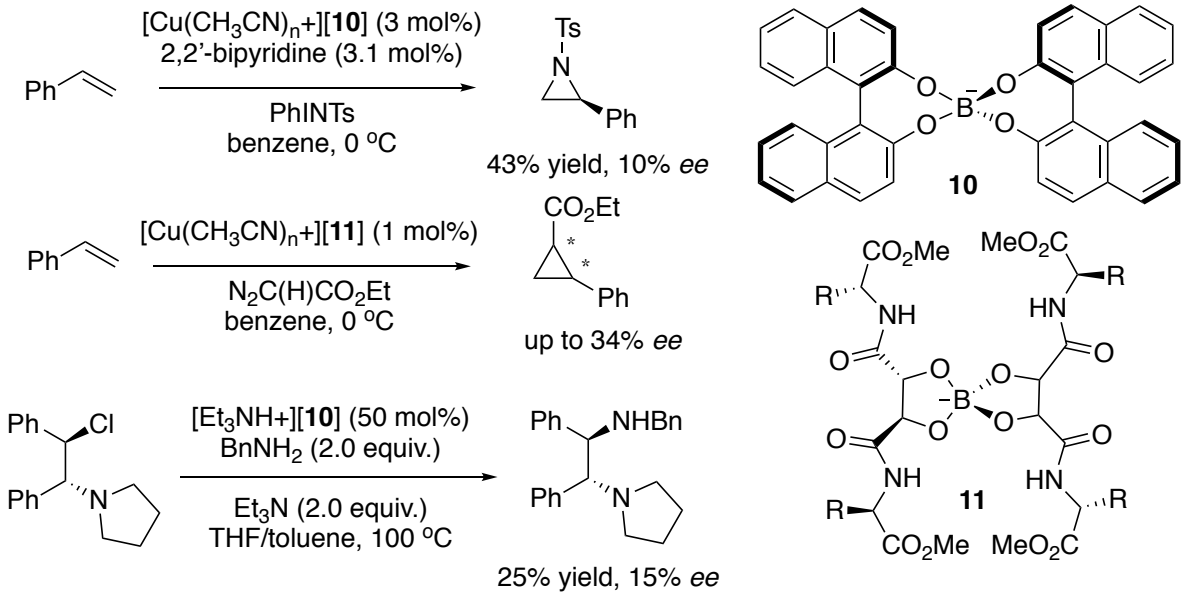
Scheme 1.12 BINOL-based chiral crown ether/K^+ catalyzed Michael addition reaction

1.4 Chiral anion-directed catalysis

1.4.1 Borate anions

Except for the Brønsted base deprotonated anion intermediates, the Brønsted acid activated cation intermediates also need to be controlled by chiral anion via ion-pairing. In 2000,

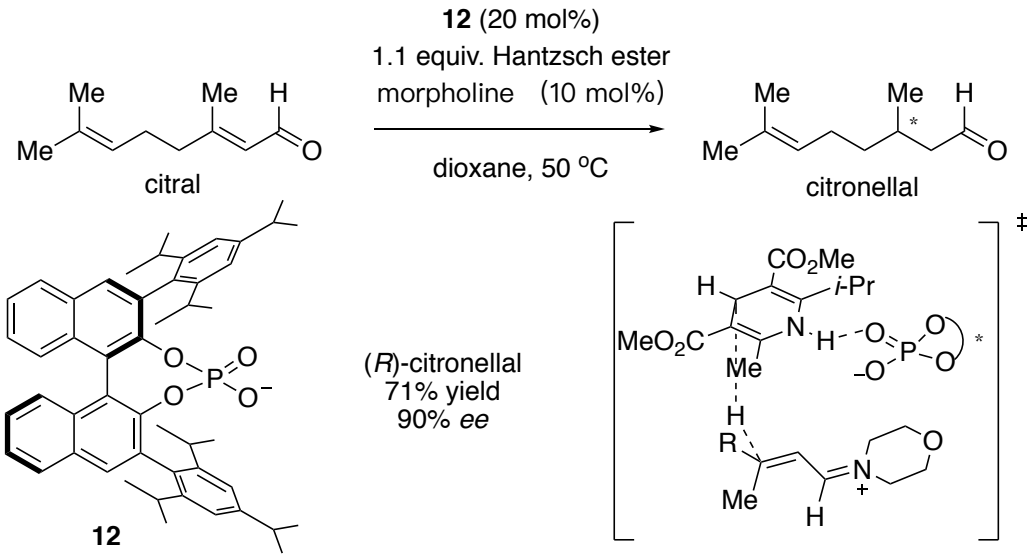
Arndtsen and co-workers reported the first application of chiral anion asymmetric catalysis (Scheme 1.13). A D_2-symmetric BINOL-based chiral borate **10**[30] was synthesized with an achiral copper complex as counterion, which was used in aziridination. However, poor enantioselectivity was achieved under chiral borate catalyst. Later, they used the condensation product of tartaric acid and α-amino acid to prepare a new borate anion **11**, which was applied in cyclopropanation on styrene. The capability of the modified catalyst was still weak, and the *ee*% was 34%, a less than moderate result. Nelson and co-workers thought the problem lay in the copper complex counterion.[31] It was assumed that the substrate formed a covalent bond with copper, thus weakening the directing effect of the borate. Thus, they used pure organocatalyst with achiral ammonium counterion. The substrate was dehalogenated[32] by the counterion, then an intramolecular reaction happened to form a cation intermediate. From the results, it seemed that the problem could not be solved in this stage and more explorations should be done.



Scheme 1.13 Applications of borate anion

1.4.2 Phosphate anions

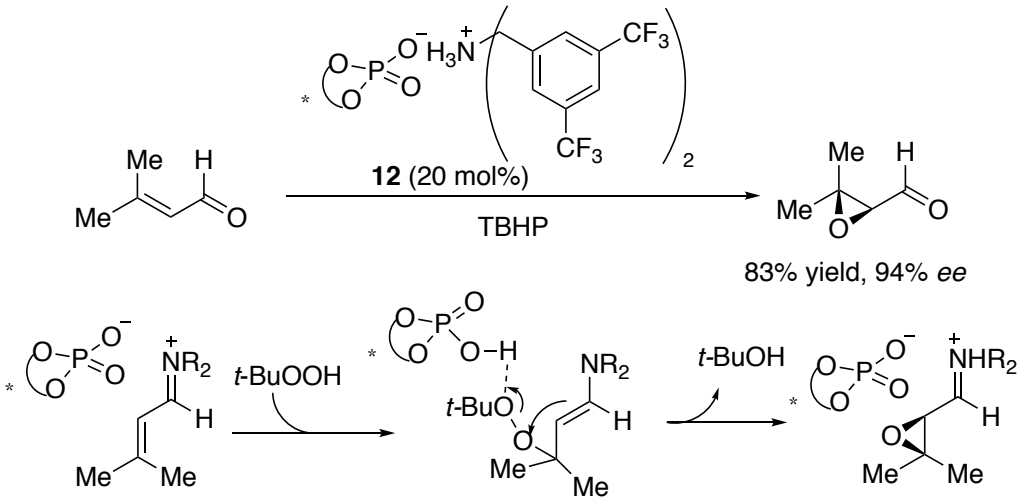
The BINOL-based phosphoric acid is an excellent hydrogen-bond directing asymmetric catalyst. Meanwhile, the conjugate base of acid proved to be an attractive candidate for ion pair catalyst as well. In 2006, List and co-workers reported chiral phosphate catalyzed reduction of citral to citronellal.[33] In previous work, both List[33] and MacMillan[34] gave their attention to chiral iminium ion strategy, and found the counterion affected the reactivity and enantioselectivity a lot. Then, List hypothesized the chiral inducing reagent could be a part of the counterion.[35] Thus, they used morpholine to activate aldehyde. At the same time, the Hantzsch ester was activated by phosphate ion **12** via hydrogen bonding. The whole species worked as a counterion pairing to the morpholine type iminium intermediate (Scheme 1.14). This strategy was a huge success, and this report became a landmark in phosphate catalyzed asymmetric catalysis.



Scheme 1.14 Iminium intermediate controlled by chiral phosphate

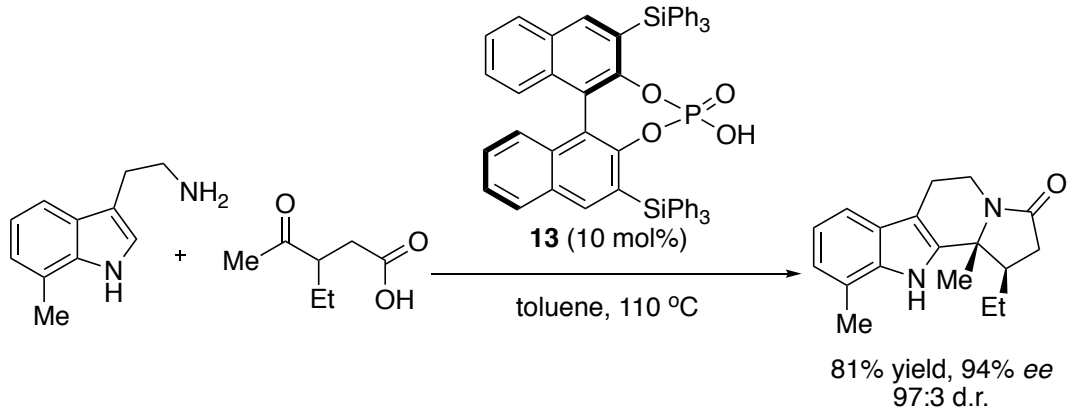
Subsequently, List's group applied this strategy to other types of reactions. For instance, they achieved epoxidation of α,β-unsaturated aldehydes (Scheme 1.15).[36] The oxidant, *tert*-butyl hydropeoxide (TBHP) was associated to phosphate anion via hydrogen bonding. The

ammonium counterion reacted with aldehyde to form the iminium cation intermediate, through which, the oxidation was realized with chiral-inducing process.



Scheme 1.15 Chiral phosphate catalyzed epoxidation

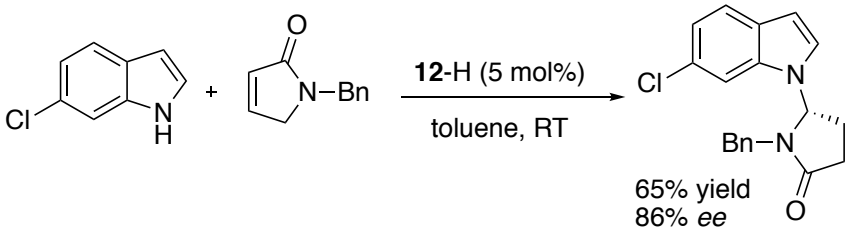
In 2010, Dixon and co-workers reported a condensation reaction between tryptamines and keto acid derivatives via 3-triphenyl silyl substituted BINOL-based phosphoric acid **13** (Scheme 1.16). The initial step of the reaction was formation of a pair of diastereomeric *N*-acyliminium phosphate salts. One of the diastereomers had a higher reactivity in cycloaddition, which led to the major product.[37,38]



Scheme 1.16 Chiral phosphate catalyzed cyclo-addition

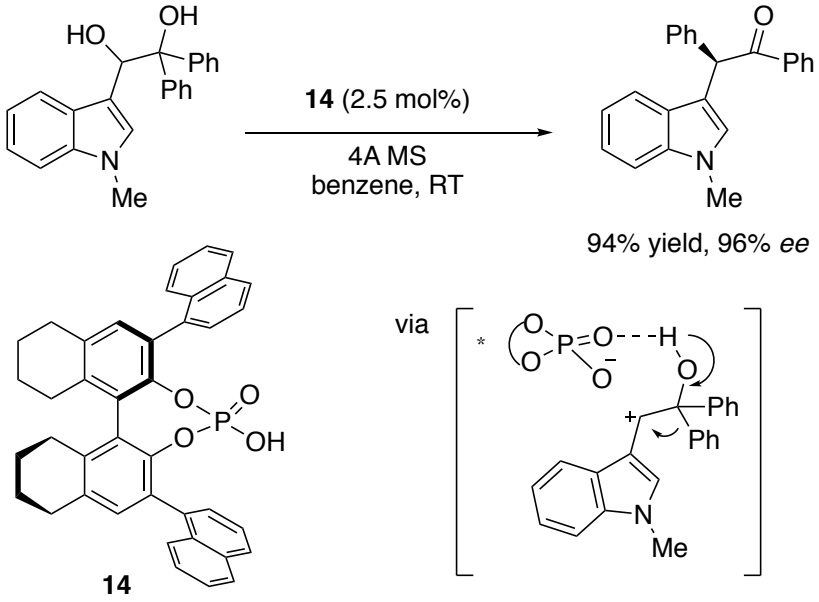
In 2011, Huang and co-workers reported *N*-alkylation between indole and α,β-unsaturated γ-lactams (Scheme 1.17).[39] Initially, α,β-unsaturated γ-lactam was protonated by

chiral phosphoric acid catalyst **12**-H. Once the *N*-acyliminium ions formed, it would pair with chiral anion. At last, a nucleophilic addition to benzopyrrole ring to give the alkylated product.



Scheme 1.17 Chiral phosphate catalyzed *N*-alkylation

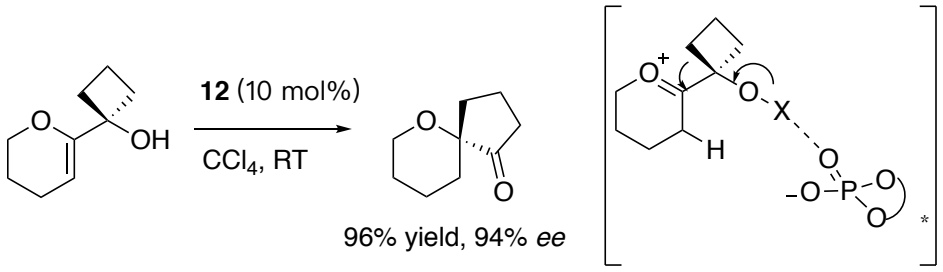
Above mentioned efficient strategy was continuously studied in more reaction mechanisms. For example, the carbocation intermediates are easy to be controlled by phosphate catalysts. Thus, Antilla and co-workers provided the first report of intramolecular pinacol rearrangement reaction (Scheme 1.18).[40] However, low enantioselectivity was observed in non-aryl group migration. They assumed that not only the hydrogen-bonding but also electrostatic interactions existed in catalytic process.



Scheme 1.18 Chiral phosphate catalyzed Pinacol rearrangement

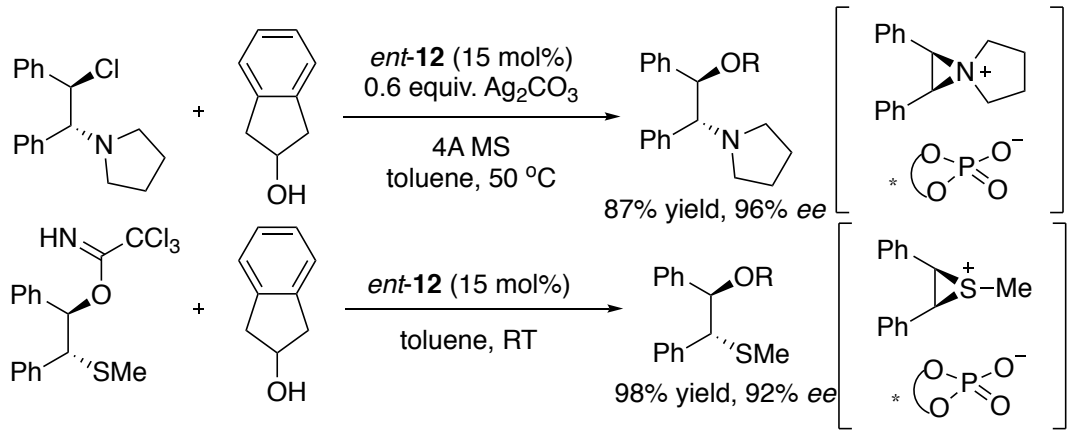
Motivated by the success with carbocations, oxocarbenium was considered as the next target to be controlled by phosphate anion. In 2009, Tu and co-workers accomplished a ring expansion semi-Pinacol rearrangement to produce spiroethers in high yield and *ee*% (Scheme

1.19).[41] The protonation on cyclohexylallylic ether led to form oxocarbenium intermediate. Then deprotonation on the alcohol pushed the rearrangement progress.



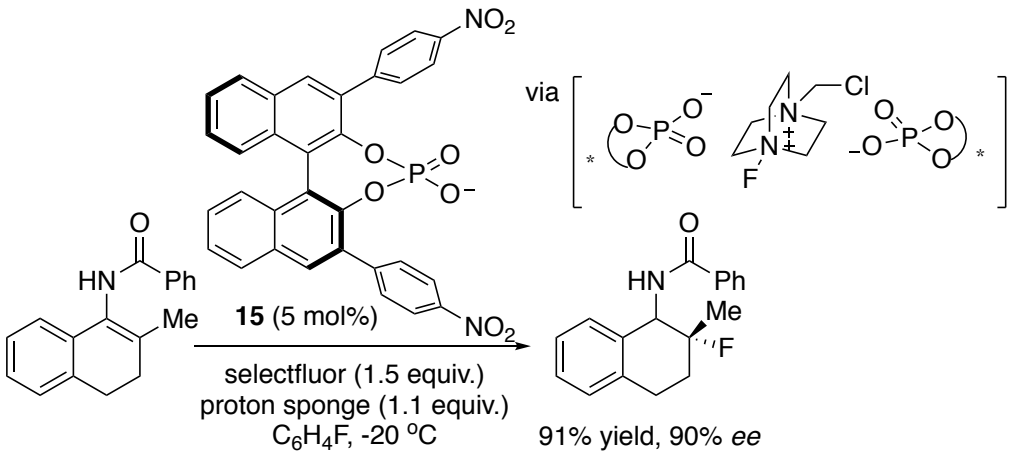
Scheme 1.19 Chiral phosphate catalyzed semi-Pinacol rearrangement

In the previous discussion, the application of a borate anion catalyst in S_N2 reaction was introduced, and the results were unsatisfying. Thus, by keeping the reaction under the same pathway, the ammonium intermediates were controlled by phosphate catalyst excellently. Later, Toste and co-workers applied the same strategy in the same type of reaction via episulfonium intermediates (Scheme 1.20).[42] In addition, the reaction condition was milder than the reaction with borate.



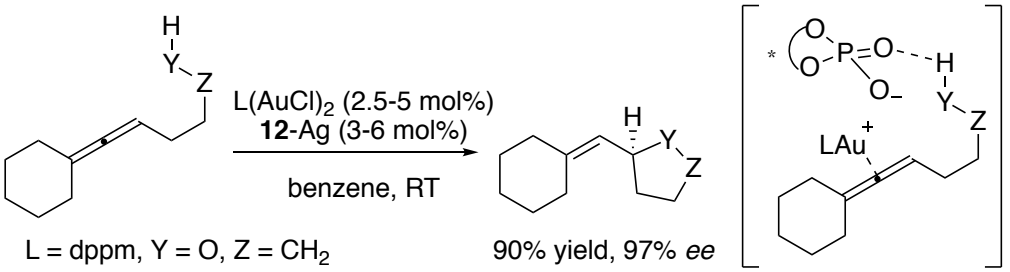
Scheme 1.20 Chiral phosphate catalyzed S_N2 reaction

Other than the cation intermediates, the cationic reagents could be controlled. For example, selectfluor[43-45] is a salt with two nitrogen centered cation of two charges (Scheme 1.21). The reagent itself can be captured by anion catalyst **15**, then passes the fluorine atom to the substrates.



Scheme 1.21 Chiral phosphate catalyzed fluorination

The last classical category is metallated intermediate. In this kind of catalytic cycle, the chiral anion catalyst **12**-Ag works as a dual catalyst with metal complex. In 2007, Toste and co-workers reported Au-catalyzed intramolecular cyclization reaction (Scheme 1.22).[46] Due to the linear geometry of allene, the ligand on gold catalyst was far from the reaction site, which made it difficult to induce enantioselectivity by chiral ligand on metal. Hence, they hypothesized that the counterion of Au-complex could approach the reaction site. Finally, they proved the design of the strategy, in which the hydrogen bonding effect helped in achieving excellent results.

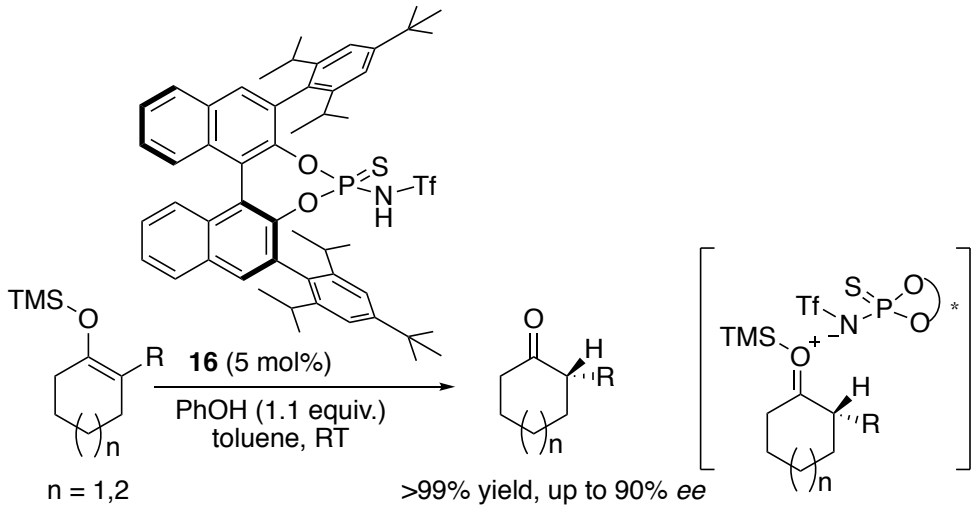


Scheme 1.22 Dual catalysis of chiral phosphate and gold catalyst

1.4.3 *N*-Triflylphosphoramidate anions

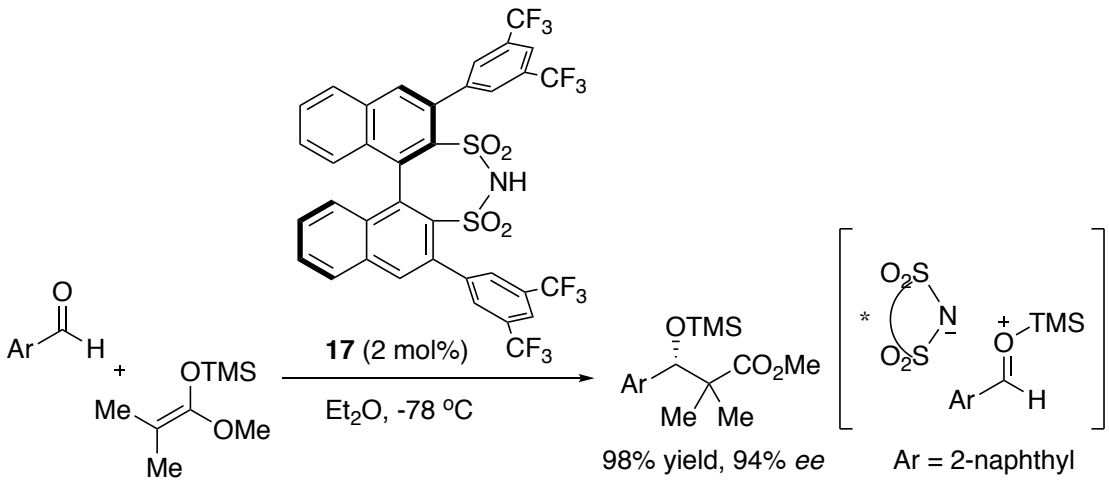
In 2008, Yamamoto and co-workers developed a *N*-Triflylphosphoramidate anion **16** by replacing one oxo-group on phosphate (Scheme 1.23), which was an excellent chiral Brønsted

acid catalyst in application of asymmetric protonation reaction. In presence of this novel Brønsted acid catalyst, the phenol substrate was protonated and paired with the chiral anion. A rapid proton transfer from achiral phenyl oxonium to silylether enolate substrate occurred, and it was followed by a desilylation with phenol to from the product. However, being the first generation of amide centered catalyst, the enantiomeric excess value was 90% at maximum in specific substrate.[47]



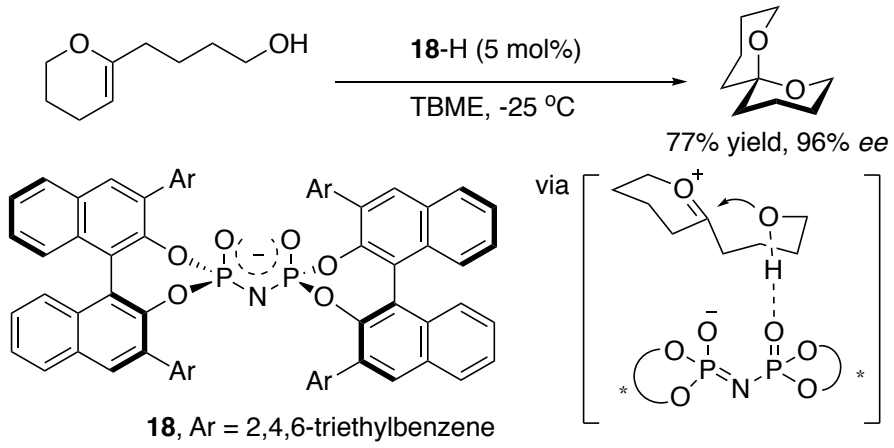
Scheme 1.23 *N*-Triflylphosphoramidate anion catalyst

List and co-workers continued to work on amide anion catalyst. They discovered binaphthyl disulfonimide catalyst **17** to activate aldehyde in Mukaiyama aldol reaction (Scheme 1.24).[48,49] The chiral amide salt paired with oxocarbenium, and both yield was up to 98%, and *ee*% was up to 94%.



Scheme 1.24 Binaphthyl disulfonimide catalyzed Mukaiyama aldol reaction

To broaden the scope of the reactions, they further developed a novel catalyst called imidodiphosphate anion **18** (Scheme 1.25). The structure of imidodiphosphate anion was constructed by two molecules of BINOL-based phosphate condensed with a mono amide group. They described it as a chiral pocket capturing the substrate and releasing the product after inducing the chiral center.[50] It successfully catalyzed the 5-, 6-, 7-membered cyclic enol ethers in spiroacetalization reaction.

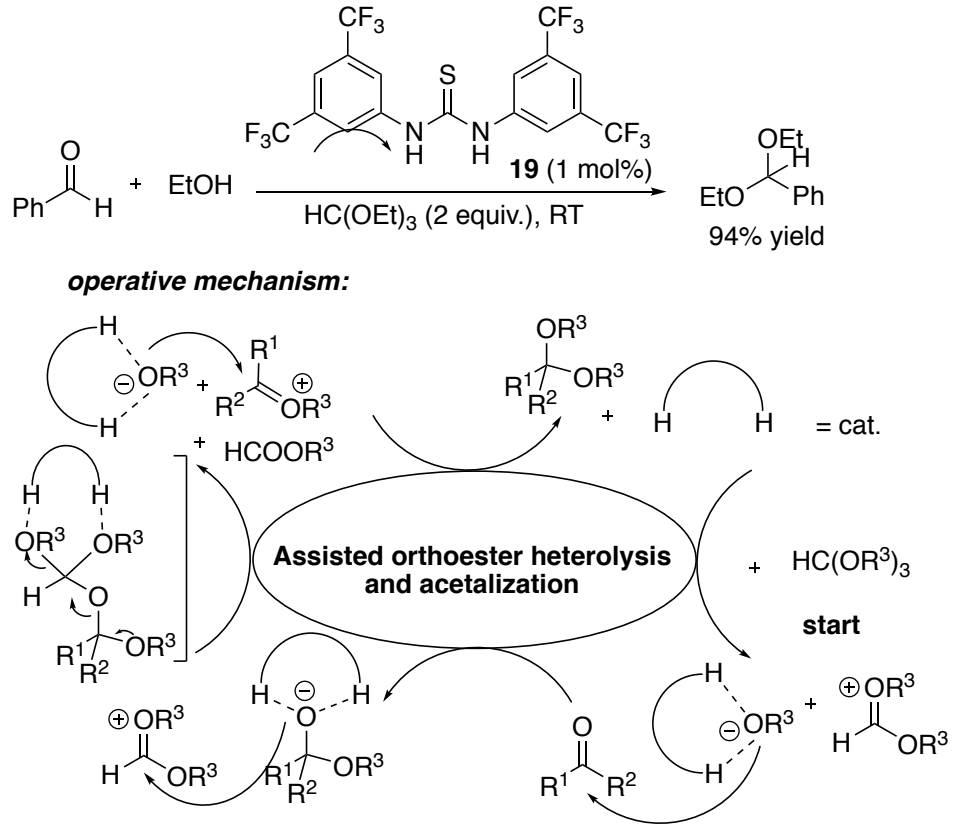


Scheme 1.25 Imidodiphosphate anion catalyzed spiroacetalization reaction

1.5 Anion-binding catalysis

Anion-binding catalysis was first recognized in achiral applications. It was discovered by Schreiner and co-workers in a thiourea catalyzed acetalization reaction (Scheme 1.26).[51] They

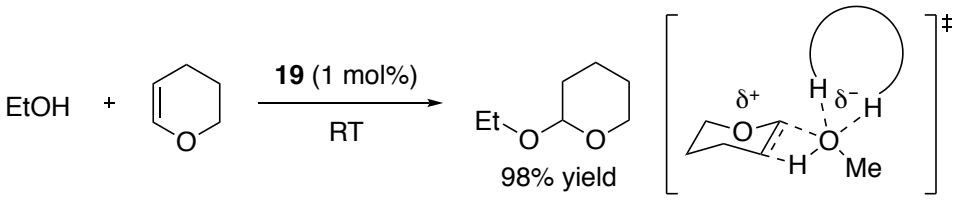
put forward two modes of catalytic behaviors. One mode was aldehyde carbonyl group binding to thiourea catalyst **19** via hydrogen bonding. The other mode involved orthoester in the mechanism where the incipient anion was generated by the reaction between thiourea catalyst and orthoester, which attacked rapidly on aldehyde. Until the hemiacetal oxocarbenium intermediate formed, it would be attacked by another molecule of the incipient anion in S_N2-like pathway. The evidence of this mechanism was provided when they applied thiols in the reaction. In principle, the thiol was a strong nucleophile and could achieve formal substitution on carbonyl and thiourea binding complex in priority. However, the product was only the normal ether from the orthoester.



Scheme 1.26 Thiourea catalyzed acetalization reaction via anion-binding mechanism

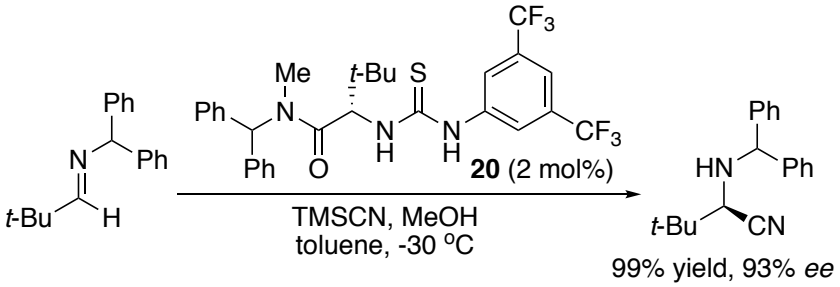
Subsequently, the same group used this catalytic mode in tetrahydropyranylation of alcohols (Scheme 1.27). The protonation of hydropyran olefin was followed by alkoxylation.[52]

The intermediate was a thiourea chelated alkoxide anion, which worked as nucleophile when attacking the protonated pyran ring.



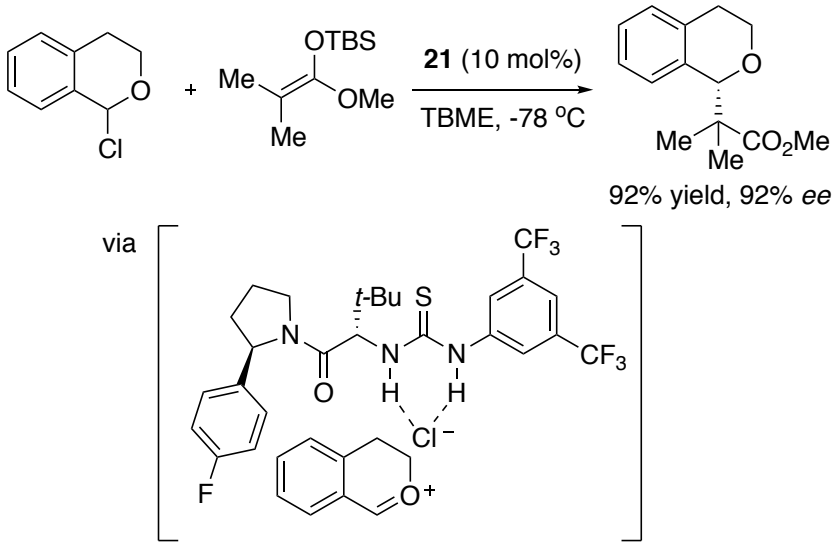
Scheme 1.27 Thiourea catalyzed tetrahydropyranylation reaction

The earliest application of a thiourea catalyst in asymmetric synthesis was reported by Jacobsen and co-workers (Scheme 1.28).[53] They found the cyanide anion was binding to the catalyst **20** and promoted an addition reaction to imine substrates. The yield was up to 99%, and the *ee*% was up to 93%.



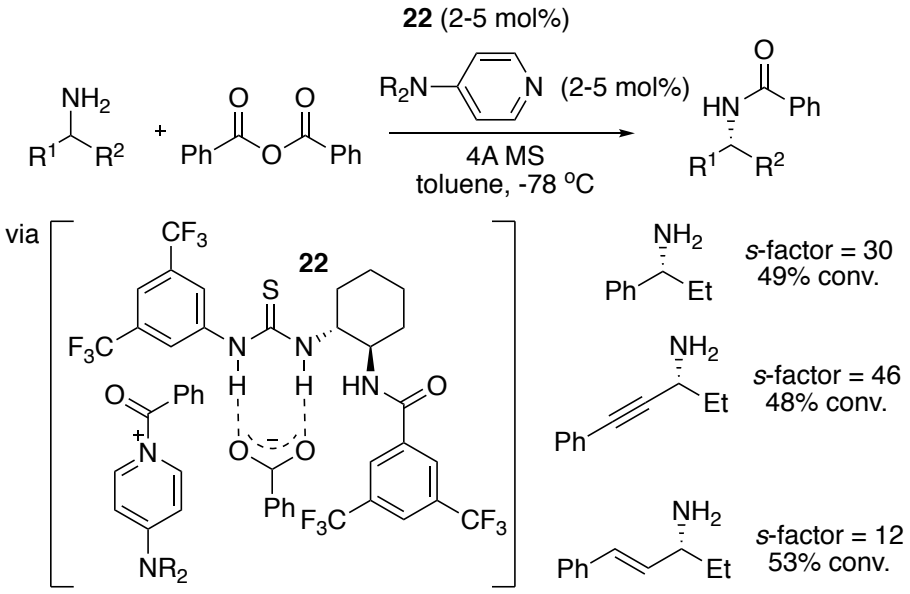
Scheme 1.28 Thiourea hydroxide-binding catalyzed cyanidation

Similarly, the halide anion could be a potential object to be discussed. In 2008, Jacobsen group continued in this area and used 1-chloroisochromans and silyl ketene acetals to furnish addition reaction (Scheme 1.29).[54] Initially, 1-chloroisochroman was dehalogenated by catalyst **21**, then a halide binding anion and an oxocarbenium cation were formed. Furthermore, the silyl ketene acetal was attacked by ion pair in specific direction to achieve high enantioselectivity.



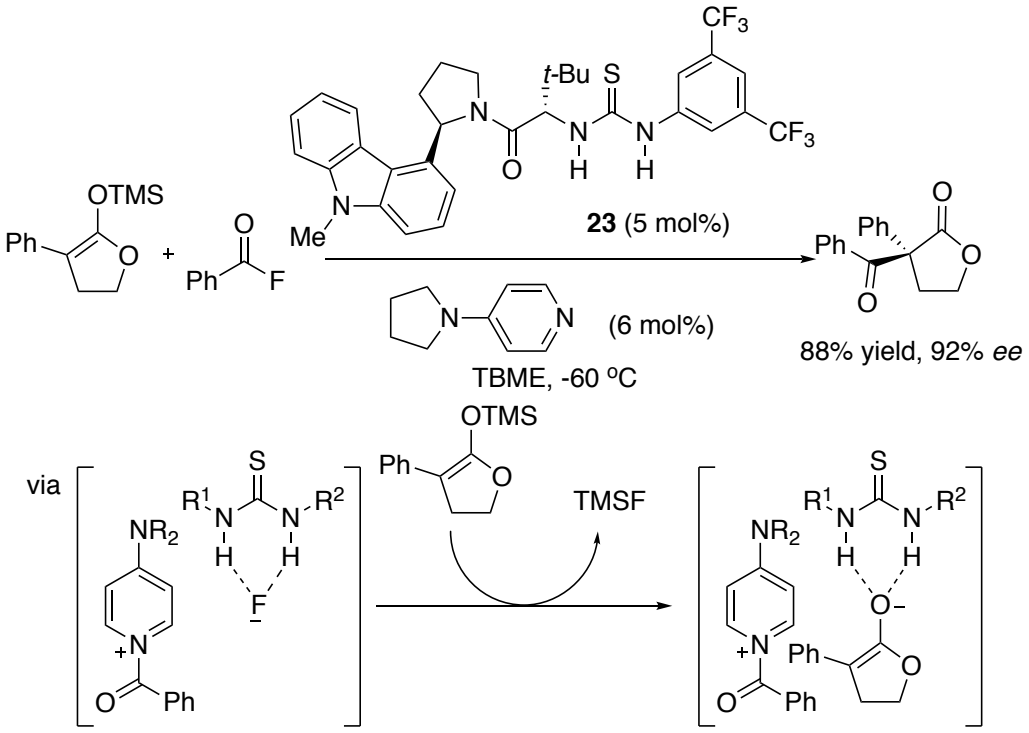
Scheme 1.29 Thiourea halide-binding catalyzed addition reaction

During 2009-2011, Seidel and co-workers accomplished a series of reactions utilizing carboxylate bound chiral thiourea anion (Scheme 1.30).[55-57] The 4-(dimethylamino)pyridine (DMAP) accepted one acyl group, then it paired with the chiral anion to attack the free amine.[58] The last step of this reaction was deprotonation to produce the chiral secondary amine. Since the starting material, free amine, was a racemic chiral reagent, the result was described by *s*-factor for the kinetic resolution progress. It was the first time that a dual catalyst system led ion pair complex worked as both donor and acceptor in the presence of thiourea **22** and DMAP at the same time.



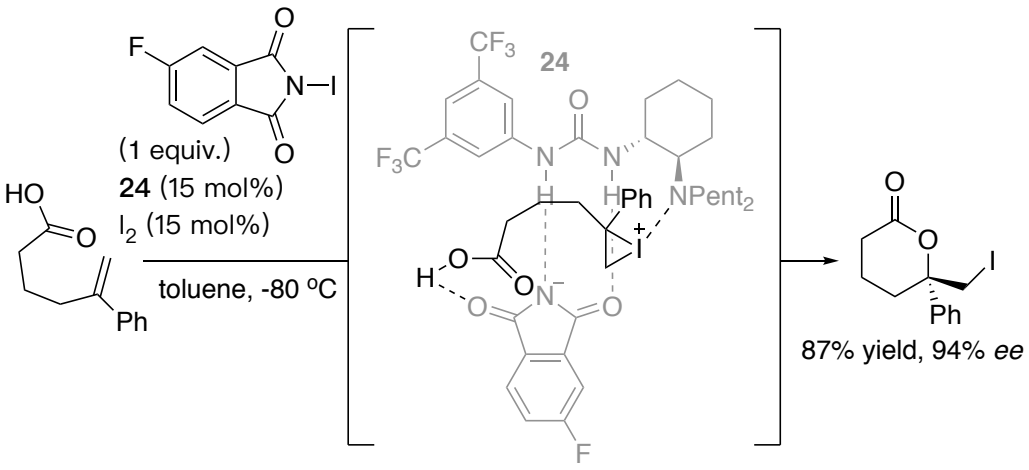
Scheme 1.30 Carboxylate bound chiral thiourea anion catalyzed *N*-alkylation

Inspired by the design of the dual catalytic mode, Jacobsen and co-workers applied it to enolate anion intermediates in 2011 (Scheme 1.31).[59] Initially, the benzoyl fluoride released fluoride, which bound to thiourea catalyst **23** to form the chiral anion. Immediately, the acyl group connected to DMAP to form the cation. The fluoride in ion pair cleaved the TMS-protected enol and was replaced by enolate anion. At last, the two components in ion pair reacted with each other, and the acylation product was obtained.



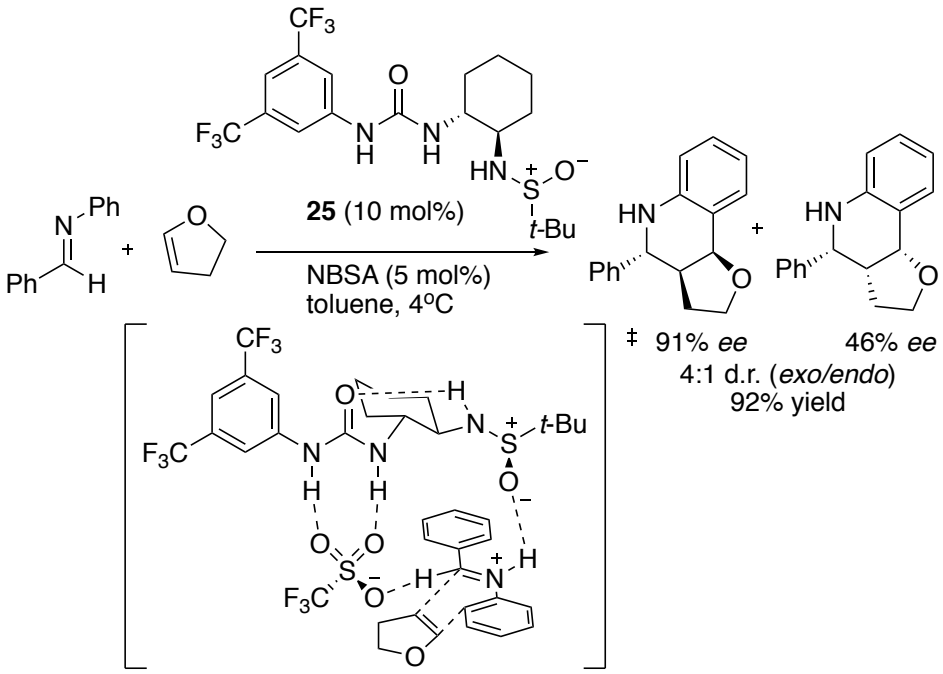
Scheme 1.31 Application of enolate bound chiral thiourea anion

In 2010, their group kept discovering new anion intermediate, and this time, they found *N*-iodophthalimide as a successful case (Scheme 1.32).[60] The iodonium source *N*-iodophthalimide was initiated by I_2. After forming the triiodide cation, it activated the carboxylic olefin to form iodonium cation. At the same time, the phthalimide anion bound to amino-urea catalyst **24**, and the I_2 regenerated to produce triiodide cation again.



Scheme 1.32 Application of iodide bound chiral thiourea anion

In the same year, they did some work of sulfonated anion. They chose *ortho*-nitrobenzensulfonic acid as proton source in Povarov reaction (Scheme 1.33).[61] The protonated imine underwent a [4+2] cycloaddition assisted by sulfonate-binding urea anion catalyst. They also modified the amino group on the catalyst **25**. The sulfinyl substituted chiral amine stabilized the protonated imine substrate via hydrogen bonding.



Scheme 1.33 Application of triflate bound chiral thiourea anion

1.6 Summary

In this chapter, the concept of ion pair catalysis was introduced from the beginning, and four types of ion pair catalysis were listed and illustrated using various examples. Since the new century, an explosion of related reports was contributed by researchers worldwide, which illustrated novelty of our research as well. In the section of chiral cation-directed catalysis, the recent development of our phase-transfer catalyst was reviewed, which includes the main content of this thesis.

References

(1) Bjerrum, N. Untersuchungen über ionenassoziation. *K. Dan. Videsk. Selesk. Math.-Fys. Medd.***1926**, *7*, 3.

(2) Anslyn, E. V.; Dougherty, D. A. Modern Physical Organic Chemistry, University Science Books, Sausalito, **2006**.

(3) Crabtree, R. H. The Organometallic Chemistry of the Transition Metals, 5th Edition, Wiley. **2009**.

(4) Narasaka, K. Chiral Lewis Acids in Catalytic Asymmetric Reactions. *Synthesis*, **1991**, *1*, 1.

(5) List, B. Introduction: Organocatalysis. *Chem. Rev.* **2007**, *107*, 5413.

(6) Erkkilä, A.; Majander, I.; Pihko, P. M. Iminium Catalysis. *Chem. Rev.* **2007**, *107*, 5416.

(7) César, V.; Bellemin-Laponnaz, S.; Gade, L. H. Chiral N-heterocyclic Carbenes as Stereodirecting Ligands in Asymmetric Catalysis. *Chem. Soc. Rev.* **2004**, *33*, 619.

(8) Brak, K.; Jacobsen, E. N. Asymmetric Ion-Pairing Catalysis. *Angew. Chem. Int. Ed.* **2013**, *52*, 534.

(9) Yoon, T. P.; Jacobsen, E. N. Privileged Chiral Catalysts. *Science*. **2003**, *299*, 1691.

(10) Huo, H.; Shen, X.; Wang, C.; Zhang, L.; Röse, P.; Chen, L. A.; Harms, K.; Marsch, M.; Hilt, G.; Meggers, E. Asymmetric Photoredox Transition-Metal Catalysis Activated by Visible Light. *Nature*. **2014**, *515*, 100.

(11) Dolling, U.-H.; Davis, P.; Grabowski, E. J. J. Efficient Catalytic Asymmetric Alkylations. 1. Enantioselective Synthesis of (+)-Indacrinone via Chiral Phase-Transfer Catalysis. *J. Am. Chem. Soc.* **1984**, *106,* 446.

(12) Ooi, T.; Kameda, M.; Maruoka, K. Molecular Design of a C_2-Symmetric Chiral Phase-Transfer Catalyst for Practical Asymmetric Synthesis of α-Amino Acids. *J. Am. Chem. Soc.* **1999**, *121*, 6519.

(13) Shibuguchi, T.; Fukuta, Y.; Akachi, Y.; Sekine, A.; Ohshima, T.; Shibasaki, M. Development of New Asymmetric Two-Center Catalysts in Phase-Transfer Reactions. *Tetrahedron Lett*. **2002**, *43*, 9539.

(14) Ma, T.; Fu, X.; Kee, C. W.; Zong, L.; Pan, Y.; Huang, K. W.; Tan, C. -H. Pentanidium-Catalyzed Enantioselective Phase-Transfer Conjugate Addition Reactions. *J. Am. Chem. Soc.* **2011**, *133*, 2828.

(15) Wang, C.; Zong, L.; Tan, C.-H. Enantioselective Oxidation of Alkenes with Potassium Permanganate Catalyzed by Chiral Dicationic Bisguanidinium. *J. Am. Chem. Soc.* **2015**, *137*, 10677.

(16) Zong, L.; Tan, C.-H. Phase-Transfer and Ion-Pairing Catalysis of Pentanidiums and Bisguanidiniums. *Acc. Chem. Res.* **2017**, *50*, 842.

(17) Ooi, T.; Miki, T.; Taniguchi, M.; Shiraishi, M.; Takeuchi, M.; Maruoka, K. Highly Enantioselective Construction of Quaternary Stereocenters on β-Keto Esters by Phase-Transfer Catalytic Asymmetric Alkylation and Michael Reaction. *Angew. Chem. Int. Ed.* **2003**, *42*, 3796.

(18) Ooi, T.; Taniguchi, M.; Kameda, M.; Maruoka, K. Direct Asymmetric Aldol Reactions of Glycine Schiff Base with Aldehydes Catalyzed by Chiral Quaternary Ammonium Salts. *Angew. Chem. Int. Ed.* **2002**, *41*, 4542.

(19) Ooi, T.; Kameda, M.; Taniguchi, M.; Maruoka, K. Development of Highly Diastereo- and Enantioselective Direct Asymmetric Aldol Reaction of a Glycinate Schiff Base with Aldehydes Catalyzed by Chiral Quaternary Ammonium Salts. *J. Am. Chem. Soc.* **2004**, *126*, 9685.

(20) Ooi, T.; Kameda, M.; Fujii, J. I.; Maruoka, K. Catalytic Asymmetric Synthesis of a Nitrogen Analogue of Dialkyl Tartrate by Direct Mannich Reaction under Phase-Transfer Conditions. *Org. Lett.* **2004**, *6*, 2397.

(21) Fu, X.; Loh, W. T.; Zhang, Y.; Chen, T.; Ma, T.; Liu, H.; Wang, J. M.; Tan, C.-H. Chiral Guanidinium Salt Catalyzed Enantioselective Phospha-Mannich Reactions. *Angew. Chem. Int. Ed.* **2009**, *48*, 7387.

(22) Ye, X.; Moeljadi, A. M. P.; Chin, K. F.; Hirao, H.; Zong, L.; Tan, C.-H. Enantioselective Sulfoxidation Catalyzed by a Bisguanidinium Diphosphatobisperoxotungstate Ion Pair. *Angew. Chem., Int. Ed.* **2016**, *55*, 7101.

(23) Teng, B.; Chen, W.; Dong, S.; Kee, C. W.; Gandamana, D. A.; Zong, L.; Tan, C.-H. Pentanidium- And Bisguanidinium-Catalyzed Enantioselective Alkylations Using Silylamide as Brønsted Probase. *J. Am. Chem. Soc.* **2016**, *138*, 9935.

(24) Cao, W.; Tan, D.; Lee, R.; Tan, C.-H. Enantioselective 1, 2-Anionotropic Rearrangement of Acylsilane through a Bisguanidinium Silicate Ion Pair. *J. Am. Chem. Soc.* **2018**, *140*, 1952.

(25) He, R.; Wang, X.; Hashimoto, T.; Maruoka, K. Binaphthyl-Modified Quaternary Phosphonium Salts as Chiral Phase-Transfer Catalysts: Asymmetric Amination of β-Keto Esters. *Angew. Chem., Int. Ed.* **2008**, *47*, 9466.

(26) He, R.; Ding, C.; Maruoka, K. Phosphonium Salts as Chiral Phase-Transfer Catalysts: Asymmetric Michael and Mannich Reactions of 3-Aryloxindoles. *Angew. Chem., Int. Ed.* **2009**, *48*, 4559.

(27) Uraguchi, D.; Asai, Y.; Ooi, T. Site-Directed Asymmetric Quaternization of a Peptide Backbone at a C-Terminal Azlactone. *Angew. Chem., Int. Ed.* **2009**, *48*, 733.

(28) Akiyama, T.; Hara, M.; Fuchibe, K.; Sakamoto, S.; Yamaguchi, K. Synthesis of a Novel Crown Ether Derived from Chiro-Inositol and Its Catalytic Activity on the Asymmetric Michael Addition. *Chem. Commun.* **2003**, 1734.

(29) Cram, D. J.; Sogah, G. D. Y. Chiral Crown Complexes Catalyse Michael Addition Reactions to Give Adducts in High Optical Yields. *J. Chem. Soc. Chem. Commun.* **1981**, 625.

(30) Llewellyn, D. B.; Adamson, D.; Arndtsen, B. A. A Novel Example of Chiral Counteranion Induced Enantioselective Metal Catalysis: the Importance of Ion-Pairing in Copper-Catalyzed Olefin Aziridination and Cyclopropanation. *Org. Lett.* **2000**, *2*, 4165.

(31) Llewellyn, D. B.; Arndtsen, B. A. Synthesis of a Library of Chiral α-Amino Acid-Based Borate Counteranions and Their Application to Copper Catalyzed Olefin Cyclopropanation. *Tetrahedron: Asymmetry* **2005**, *16*, 1789.

(32) Carter, C.; Fletcher, S.; Nelson, A. Towards Phase-Transfer Catalysts with a Chiral Anion: Inducing Asymmetry in the Reactions of Cations. *Tetrahedron: Asymmetry*, **2003**, *14*, 1995.

(33) Mayer, S.; List, B. Asymmetric Counteranion-Directed Catalysis. *Angew. Chem., Int. Ed.* **2006**, *45*, 4193.

(34) Yang, J. W.; Hechavarria Fonseca, M. T.; Vignola, N.; List, B. Metal-Free, Organocatalytic Asymmetric Transfer Hydrogenation of α, β-Unsaturated Aldehydes. *Angew. Chem., Int. Ed.* **2005**, *44*, 108.

(35) Ouellet, S. G.; Tuttle, J. B.; MacMillan, D. W. Enantioselective Organocatalytic Hydride Reduction. *J. Am. Chem. Soc.* **2005**, *127*, 32.

(36) Wang, X.; List, B. Asymmetric Counteranion-Directed Catalysis for the Epoxidation of Enals. *Angew. Chem., Int. Ed.* **2008**, *47*, 1119.

(37) Muratore, M. E.; Holloway, C. A.; Pilling, A. W.; Storer, R. I.; Trevitt, G.; Dixon, D. J. Enantioselective Brønsted Acid-Catalyzed N-Acyliminium Cyclization Cascades. *J. Am. Chem. Soc.* **2009**, *131*, 10796.

(38) Holloway, C. A.; Muratore, M. E.; Storer, R. L.; Dixon, D. J. Direct Enantioselective Brønsted Acid Catalyzed N-Acyliminium Cyclization Cascades of Tryptamines and Ketoacids. *Org. Lett.* **2010**, *12*, 4720.

(39) Xie, Y.; Zhao, Y.; Qian, B.; Yang, L.; Xia, C.; Huang, H. Enantioselective N–H Functionalization of Indoles with α, β-Unsaturated γ-Lactams Catalyzed by Chiral Brønsted Acids. *Angew. Chem., Int. Ed.* **2011**, 50, 5682.

(40) Liang, T.; Zhang, Z.; Antilla, J. C. Chiral Brønsted Acid Catalyzed Pinacol Rearrangement. *Angew. Chem., Int. Ed.* **2010**, *49*, 9734.

(41) Zhang, Q. W.; Fan, C. A.; Zhang, H. J.; Tu, Y. Q.; Zhao, Y. M.; Gu, P.; Chen, Z. M. Brønsted Acid Catalyzed Enantioselective Semipinacol Rearrangement for the Synthesis of Chiral Spiroethers. *Angew. Chem., Int. Ed.* **2009**, *48*, 8572.

(42) Hamilton, G. L.; Kanai, T.; Toste, F. D. Chiral Anion-Mediated Asymmetric Ring Opening of Meso-Aziridinium and Episulfonium Ions. *J. Am. Chem. Soc.* **2008**, *130*, 14984.

(43) Rauniyar, V.; Lackner, A. D.; Hamilton, G. L.; Toste, F. D. Asymmetric Electrophilic Fluorination Using an Anionic Chiral Phase-Transfer Catalyst. *Science*, **2011**, *334*, 1681.

(44) Phipps, R. J.; Hiramatsu, K.; Toste, F. D. Asymmetric Fluorination of Enamides: Access to a Fluoroimines Using an Anionic Chiral Phase-Transfer Catalyst. *J. Am. Chem. Soc.* **2012**, *134*, 8376.

(45) Alix, A.; Lalli, C.; Retailleau, P.; Masson, G. Highly Enantioselective Electrophilic a Bromination of Enecarbamates: Chiral Phosphoric Acid and Calcium Phosphate Salt Catalysts. *J. Am. Chem. Soc.* **2012**, *134*, 10389.

(46) Hamilton, G. L.; Kang, E. J.; Mba, M.; Toste, F. D. A Powerful Chiral Counterion Strategy for Asymmetric Transition Metal Catalysis. *Science*, **2007**, *317*, 496.

(47) Cheon, C. H.; Yamamoto, H. A Brønsted Acid Catalyst for the Enantioselective Protonation Reaction. *J. Am. Chem. Soc.* **2008**, *130*, 9246.

(48) García-García, P.; Lay, F.; García-García, P.; Rabalakos, C.; List, B. A Powerful Chiral Counteranion Motif for Asymmetric Catalysis. *Angew. Chem., Int. Ed.* **2009**, *48*, 4363.

(49) Ratjen, L.; García-García, P.; Lay, F.; Beck, M. E.; List, B. Disulfonimide-Catalyzed Asymmetric Vinylogous and Bisvinylogous Mukaiyama Aldol Reactions. *Angew. Chem., Int. Ed.* **2011**, *50*, 754.

(50) Čorić, I.; List, B. Asymmetric Spiroacetalization Catalysed by Confined Brønsted Acids. *Nature*, **2012**, *483*, 315.

(51) Kotke, M.; Schreiner, P. R. Acid-Free, Organocatalytic Acetalization. *Tetrahedron* **2006**, *62*, 434.

(52) Kotke, M.; Schreiner, P. R. Generally Applicable Organocatalytic Tetrahydropyranylation of Hydroxy Functionalities with Very Low Catalyst Loading. *Synthesis* **2007**, *2007*, 779.

(53) Zuend, S. J.; Jacobsen, E. N. Mechanism of Amido-Thiourea Catalyzed Enantioselective Imine Hydrocyanation: Transition State Stabilization via Multiple Non-Covalent Interactions. *J. Am. Chem. Soc.* **2009**, *131*, 15358.

(54) Reisman, S. E.; Doyle, A. G.; Jacobsen, E. N. Enantioselective Thiourea-Catalyzed Additions to Oxocarbenium Ions. *J. Am. Chem. Soc.* **2008**, *130*, 7198.

(55) De, C. K.; Klauber, E. G.; Seidel, D. Merging Nucleophilic and Hydrogen Bonding Catalysis: an Anion Binding Approach to The Kinetic Resolution of Amines. *J. Am. Chem. Soc.* **2009**, *131*, 17060.

(56) Klauber, E. G.; De, C. K.; Shah, T. K.; Seidel, D. Merging Nucleophilic and Hydrogen Bonding Catalysis: an Anion Binding Approach to The Kinetic Resolution of Propargylic Amines. *J. Am. Chem. Soc.* **2010**, *132*, 13624.

(57) Mittal, N.; Sun, D. X.; Seidel, D. Kinetic Resolution of Amines via Dual Catalysis: Remarkable Dependence of Selectivity on the Achiral Cocatalyst. *Org. Lett.* **2012**, *14*, 3084.

(58) Fu, G. C. Asymmetric Catalysis with "Planar-Chiral" Derivatives of 4-(Dimethylamino) Pyridine. *Acc. Chem. Res.* **2004**, *37*, 542.

(59) Birrell, J. A.; Desrosiers, J. N.; Jacobsen, E. N. Enantioselective Acylation of Silyl Ketene Acetals through Fluoride Anion-Binding Catalysis. *J. Am. Chem. Soc.* **2011**, *133*, 13872.

(60) Veitch, G. E.; Jacobsen, E. N. Tertiary Aminourea-Catalyzed Enantioselective Iodolactonization. *Angew. Chem., Int. Ed.* **2010**, *49,* 7332.

(61) Xu, H.; Zuend, S. J.; Woll, M. G.; Tao, Y.; Jacobsen, E. N. Asymmetric Cooperative Catalysis of Strong Brønsted Acid–Promoted Reactions Using Chiral Ureas. *Science*, **2010**, *327*, 986.

Chapter 2

Tungstate Anion and Derivatives in Oxidation

2.1 Introduction

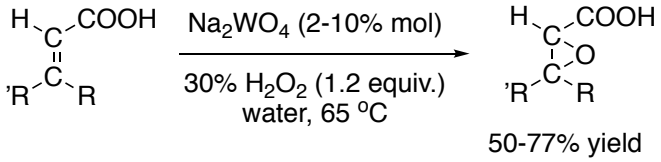
Tungsten is a transition metal with elemental symbol W.[1] Its atomic number is 74, which is in period 6, group 6. The electron configuration is $[Xe]4f^{14}5d^{4}6s^{2}$, so it can exhibit oxidation states from -2 to 6. Molybdenum and tungsten are in the same group, which show the similar reactivity in many applications. Therefore, these two metals are usually compared, studied and discussed at the same time, and in most cases, they show the same principles. The most common oxidized product of tungsten is WO_3, which can further dissolve in alkaline water to form WO_4^{2-}. Molybdenum oxide is often used as an oxidant in organic synthesis. The tungsten catalysts with coordination of various ligands have also been studied a lot in oxidation reactions.[2,3] Due to the structural feature of chiral cation catalyst developed in our group, we focused on anionic form of tungstate to start our research. We aim to utilize the oxidative property of tungstate, and have accomplished some asymmetric oxidation reaction via ion pair catalysis.

Tungstates and congeners are known to polymerize in aqueous solutions in different forms according to the miscellaneous additives, pH and concentrations. The most famous example is Keggin's structure, which represented a series of anions with a general formula of $[XM_{12}O_{40}]^{n-}$. The first α-Keggin structure was $(NH_3)_3[PMo_{12}O_{40}]$, reported by Berzelius in 1826.[4]

In this chapter, in-depth introductions to tungstate are constructed according to the active species, and there will be three categories: tungstate monomer, tungstate oligomer, and tungstate polymer. All selected applications are organic oxidation reactions, including epoxidation, cleavage of double-bond (to carboxylic acids, aldehydes or ketones), oxidation of alcohols, oxidation of amines, sulfoxidation, and oxidation of imines.

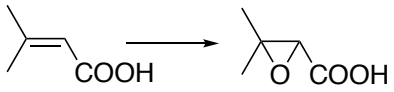
2.2 Tungstate monomer in oxidation

The pioneering work of using tungstate as a catalyst in oxidation was demonstrated by Payne in 1959.[5] They used 2-10 mole % of tungstate catalyst and 1.2 equivalent of hydrogen peroxide solution (30%, w/w) to oxidize α,β-unsaturated acids to epoxy acids in heated water (Scheme 2.1). Before their study, other groups tried to use tungstic acid to catalyze the epoxidation, but they obtained a lot of hydroxylated side product. They assumed the epoxide was easily hydrolyzed under extremely acidic conditions. Thus, Payne hypothesized to restrict the pH of the system, by which they could prevent the side reaction happening. Owing to the mild condition established by replacing the tungstic acid to sodium tungstate salts, they avoided hydroxylation of the substrates successfully.



Scheme 2.1 First example of catalytic tungstate in oxidation

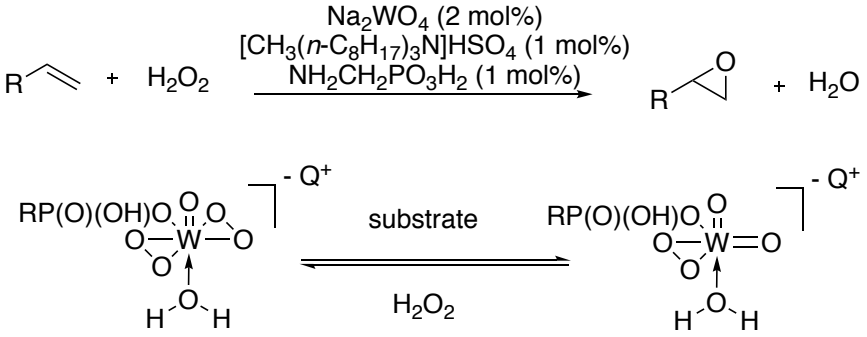
In 1985, Sharpless and co-workers improved the procedure and substrate scope based on the work done by Payne (Scheme 2.2).[6] First of all, they expanded the scope of substrates and concluded the differences of reactivities of olefins with different substitutions. They found tri-substitution substrates performed better under Payne's condition, even when it was conducted at room temperature. Later, they compared Payne's strategy with their Ti-complex oxidation system, and thought the tungstate anion might be chelated to some acid, by which the capability of catalyst was increased significantly. They tried to prove it by tuning additive and checking the relative reaction rate of a model substrate. The experimental data supported their assumptions.



entry	additive	ratio additive/catalyst	relative rate
1	picolinic acid	1.19	3.0
2	no additive		5.1
3	ethylene glycol	1.19	14.9
4	D-(-)-butanediol	1.21	23.2
5	*dl*-lactic acid	1.20	25.0
6	L-(+)-tartaric acid	1.19	28.9

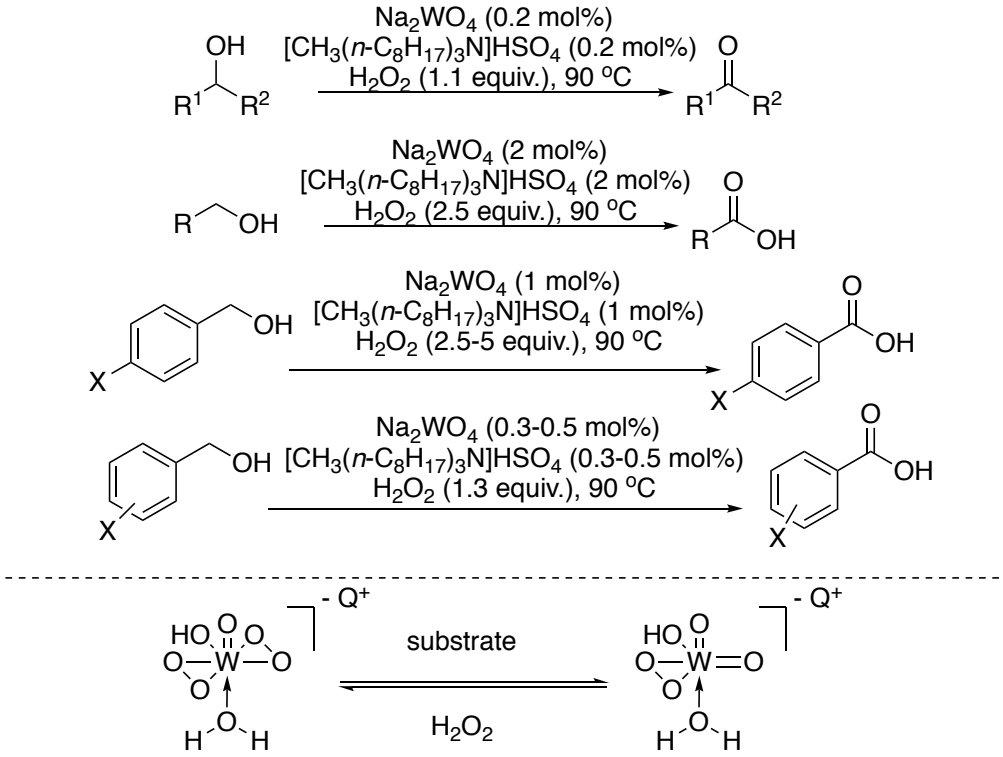
Scheme 2.2 More explorations contributed by Sharpless

In 1996, Noyori and co-workers used phase transfer catalyst with sodium tungstate in epoxidation of terminal olefins (Scheme 2.3).[7] They overcame the problem of substrate scope limitation and promoted the efficiency of the reaction, achieving excellent yields. However, they pointed out that styrene could not be converted to epoxide in high yield, which was due to the hydrolytic decomposition at the interface. About the additive (aminomethyl)phosphonic acid, they gave an explaination as follows: the conjugated base of phosphonic acid became a ligand coordinating to tungstate anion, which improved the activity of the catalyst.



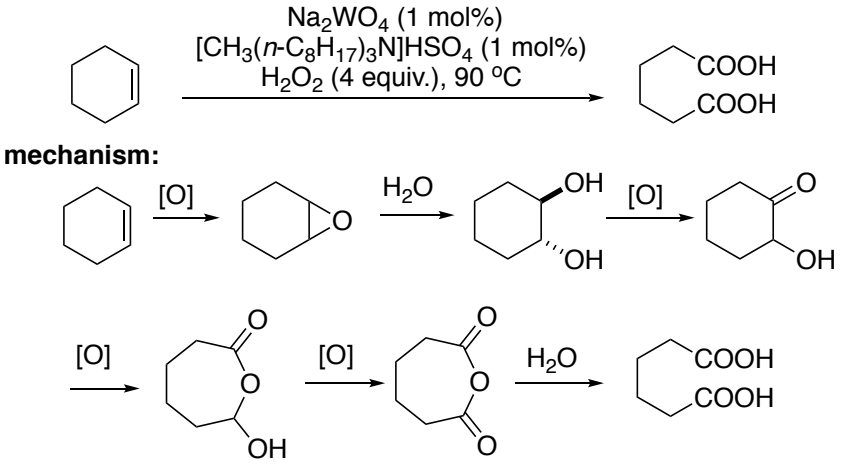
Scheme 2.3 Tungstate catalyst assisted by phase transfer catalyst

In 1997, Noyori group applied this phase transfer catalyzed strategy to the oxidation of alcohols, secondary alcohols to ketones and primary alcohols to aldehydes or to acids when over-oxidized (Scheme 2.4).[8,9] As alcohols were more easily oxidized than olefins, they found the tungstate anion along with the phase transfer catalyst was active enough. Hence, they proposed the active species was a tungstate with a hydroxyl group. By controlling the loading of the oxidant and adjusting the concentration of the reaction, over-oxidation could be promoted or inhibited.



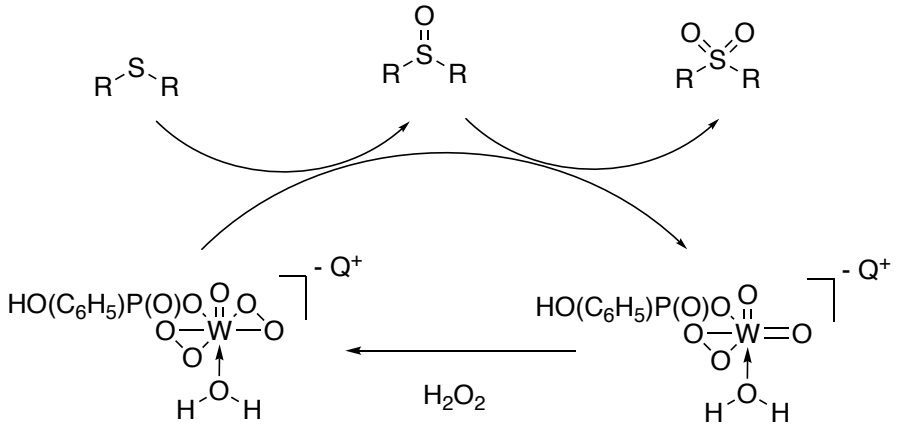
Scheme 2.4 More types of oxidation under Noyori's system

A huge success of phase transfer tungstate catalyst was achieved in producing the adipic acid from cyclohexene in 1999 by Noyori group (Scheme 2.5).[10] In their previous work, they had already proposed the catalyst structure. This time, they described the mechanism of the over-oxidation reaction. Cyclohexene was oxidized to an epoxide first, then the epoxide was hydrolyzed to a diol. The diol was further oxidized to give α-hydroxy ketone product, which continuously underwent the Baeyer-Villiger oxidation to form seven-membered ring. After one step of oxidation followed by a hydrolysis, adipic acid was obtained ultimately.



Scheme 2.5 Mechanism study of over-oxidized reaction catalyzed by phase transfer catalyst with tungstate

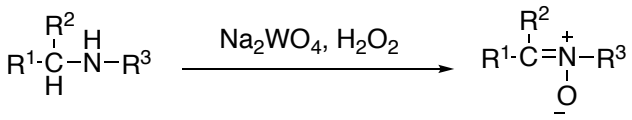
In 2001, the Noyori group complemented the tungstate catalytic system by investigating the sulfide oxidation.[11] A tungstate anion coordinated with a phenylphosphoric acid in 1 to 1 ratio, pairing with a phase transfer cation (Scheme 2.6). The starting material could be oxidized to sulfoxide, or over-oxidized to sulfone. Even though the dominant product was determined by the amount of the oxidant, the sulfone could not be excluded when producing the sulfoxide. Hence, the chemoselectivity was one main problem in this reaction.



Scheme 2.6 Tungstate monomer with phosphate ligand

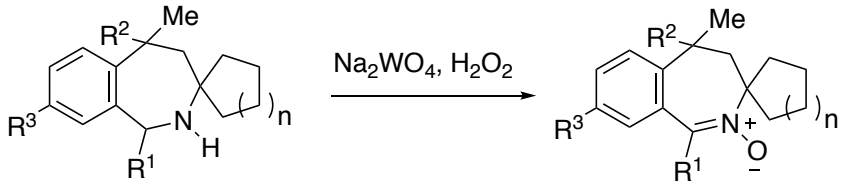
Besides, the oxidation of nitrogen atom was researched using tungstate catalyst. In 1990, Murahashi and co-workers established simple reaction conditions for the oxidation of secondary amines (Scheme 2.7).[12] Only a catalytic amount of tungstate and stoichiometric

hydrogen peroxide were applied to the substrate in water or methanol. As a result, acyclic and cyclic nitrones were obtained in good to excellent yield.



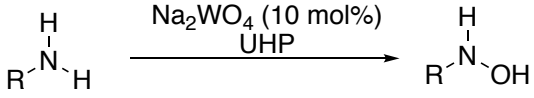
Scheme 2.7 Oxidation of nitrogen atom via tungstate

In 2001, Varlamov and co-workers complemented the cyclic nitrones synthesis with the same strategy (Scheme 2.8).[13] 2-Benzazepine derivatives was an important building block of drug moieties for Alzheimer's disease.



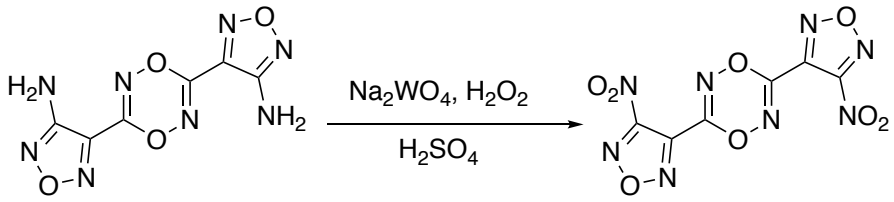
Scheme 2.8 Cyclic nitrone synthesis via tungstate

In 2005, Aslanzadeh reported an oxidation of primary amines by using sodium tungstate as a catalyst and hydrogen peroxide in urea (UHP) as an oxidant (Scheme 2.9).[14] This method was applied to a large scope of substrates including benzylic amines and α-amino esters, in which the yields ranged from 65% to 80%.



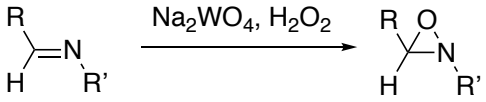
Scheme 2.9 Oxidation of primary amines via tungstate

In 2011, Leonard and co-workers discovered a new method to oxidize diamines to directly produce unstable nitro-compounds (Scheme 2.10).[15] The reaction conditions were harsh and dangerous, as the hydrogen peroxide was used with concentrated sulfuric acid. The procedure demanded researchers with rich experiences.



Scheme 2.10 Tungstate oxidized amines to nitro-compounds

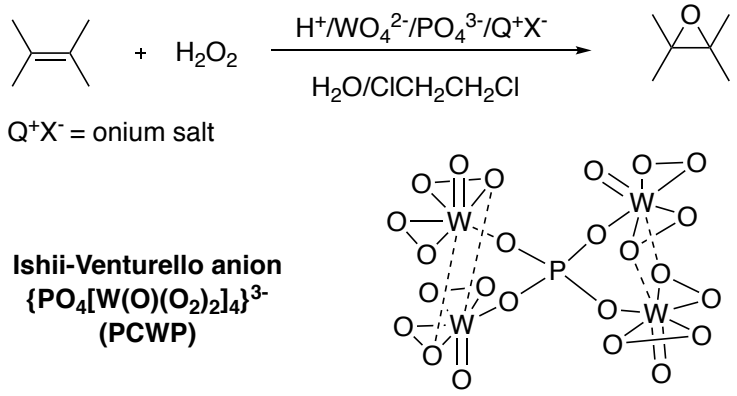
The oxidation N-alkyl imine was also studied under the catalysis of tungstate salts (Scheme 2.11). The imine was oxidized to oxaziridine in the presence of 10 mol% tungstate, and the yield of reaction was up to 96%.[16]



Scheme 2.11 Tungstate oxidized imines to oxaziridines

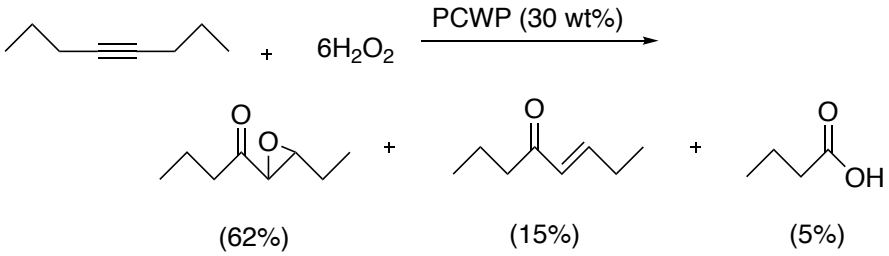
2.3 Tungstate oligomer in oxidation

In 1983, Venturello and co-workers reported an epoxidation reaction catalyzed by tungstate and phosphoric acid under phase transfer conditions.[17] Initially, they found the effectiveness of the reaction depended highly on the pH of the reaction solution, where the rate of the reaction increased drastically as the pH decreased. Later, they recognized that the buffer solution of H_3PO_4/NaH_2PO_4 was effective in producing the acid-sensitive epoxides. Thus, they considered that the reactivity was not merely influenced by pH. Two years later, they successfully prepared and isolated the catalyst using the previously reported conditions.[18] They had strong evidence through single crystal X-ray crystallography and examined the activity in the reported reaction (Scheme 2.12). The fundamental structure was phosphorus centered salt with four coordinated tungstates $[PW_4O_{24}]^{3-}$, and the overall charge of the anion was -3. Almost at the same time, Ishii group was studying the oxidation application of Keggin's structure. They realized a novel catalyst was generated in the presence of a phase transfer catalyst in hydrogen peroxide solutions, which was called PCWP. In 1990, they compared the IR data with Venturello's crystal and confirmed the structure.[19]



Scheme 2.12 Ishii-Venturello anion application

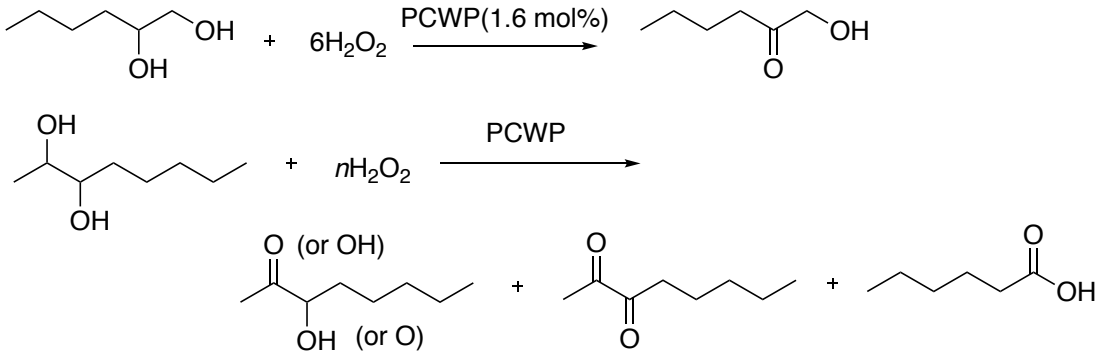
In Ishii's report, they described the catalyst was with three tetrahexylammonium cations, and they tried to oxidize various alkynes by PCWP (Scheme 2.13). During their research, they found several products. Except for the main product α,β-epoxy ketones, there were other side products, such as α,β-epoxy ketones and acids.



Scheme 2.13 Alkyne oxidation catalyzed by PCWP

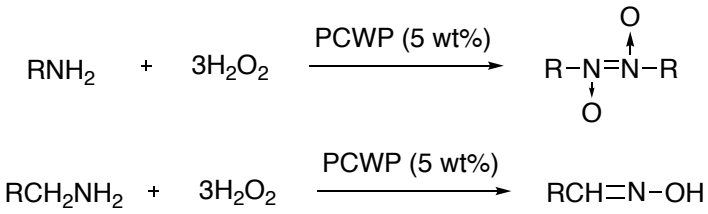
Inspired by the interesting discovery and motivated by more challenging reactions, Ishii's group reported a diol oxidation in 1991.[20] Only 1.6 mol% of PCWP catalyst and 6 equivalents of hydrogen peroxide were used for acyclic aliphatic diols, benzylic diols, and cyclic diols. They found that a secondary alcohol is specifically oxidized in the presence of a primary alcohol. Additionally, the cyclic diols could be hydrolyzed to acids. In 1995, Ishii group supplemented this work by studying the chemoselectivity among the α-hydroxy ketone, diketone and acid products.[21] They found using stoichiometric amount of PCWP resulted in highly specific oxidation to diketones. Meanwhile, in the presence of a catalytic amount of PCWP, adding the hydrogen peroxide dropwise could lead to efficient oxidation to diketones

as well. With the same catalytic amount of PCWP, the adding of hydrogen peroxide in one portion afforded the α-hydroxy ketone as a main product. This study clearly revealed the oxidative efficiency of PCWP was much higher than the common oxidant (Scheme 2.14).



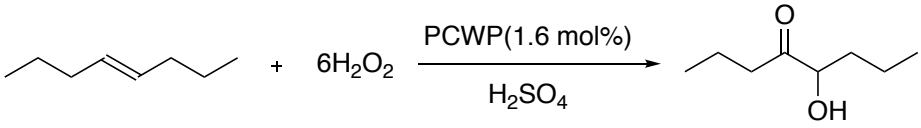
Scheme 2.14 Diol oxidation catalyzed by PCWP

Meanwhile, Ishii group also applied the system to the oxidation of primary amines (Scheme 2.15).[22] Non-aromatic amines were oxidized to oximes, and some of the products could be dried over and dehydrolyzed to N-oxides. Aromatic amines were oxidized to the corresponding nitroso compounds.



Scheme 2.15 N-oxidation catalyzed by PCWP

Likewise, the direct oxidation of olefins to α-hydroxy ketones was realized by this strategy. Ishii's group continued their study on the application of PCWP, and reported this result in 1992 (Scheme 2.16).[23] As shown below, sulfuric acid was a crucial component in this reaction. Without sulfuric acid, the olefins would be oxidized to epoxides (see Scheme 2.12). However, in the presence of the sulfuric acid, the reaction led to the formation of the α-hydroxy ketone as the dominant product.



Scheme 2.16 Alkene oxidation catalyzed by PCWP

In 1964, inorganic chemists Einstein and Penfold identified the potassium dihydrated tetraperoxyditungstate $[\{W(=O)(O_2)_2(H_2O)\}_2(\mu\text{-}O)]^{2-}K_2^+$ by X-ray analysis (Figure 2.1).[24] The typical dinuclear tungstate was isolated from a cold aqueous solution, which crystalized colorlessly in shape of blade. The article focused on discussing the fundamental parameters of this inorganic compound, and no application of this novel species was explored.

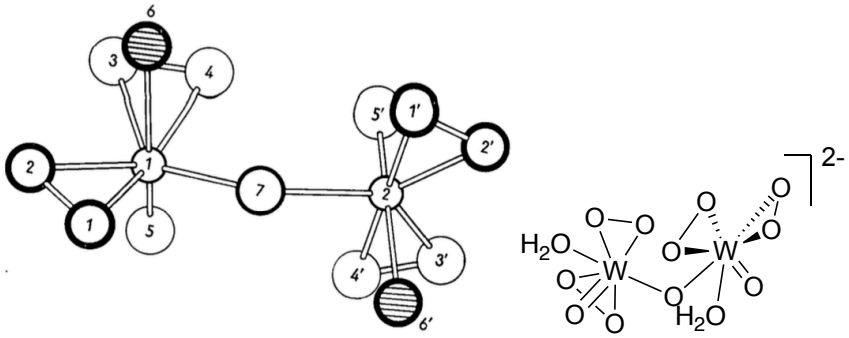
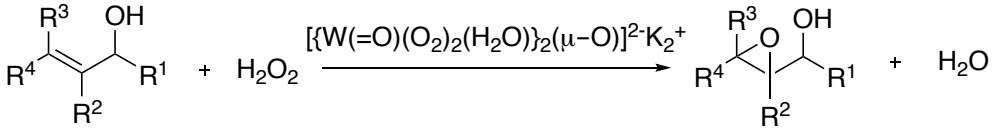


Figure 2.1 X-ray of $[\{W(=O)(O_2)_2(H_2O)\}_2(\mu\text{-}O)]^{2-}K_2^+$

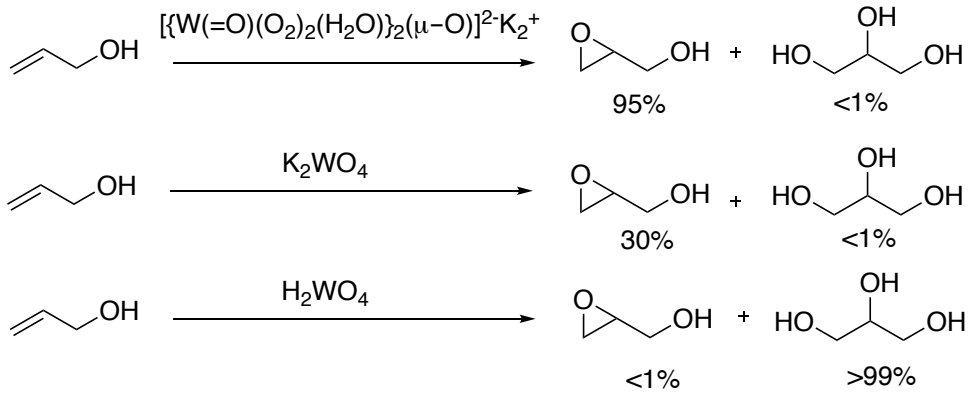
In 2003, Mizuno and co-workers occasionally found the potassium dinuclear dihydrated tetraperoxyditungstate was effective in epoxidation of α,β-unsaturated alcohols (Scheme 2.17).[25] By utilizing this catalyst, the utilization rate of hydrogen peroxide reached 97%, and the yield of epoxides were from 83-98%.



Scheme 2.17 Epoxidation of α,β-unsaturated alcohols via $[\{W(=O)(O_2)_2(H_2O)\}_2(\mu\text{-}O)]^{2-}K_2^+$

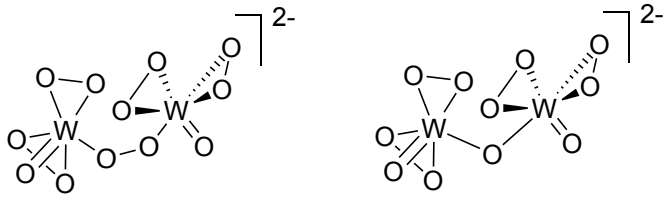
In 2004, they continued this work and concluded that the neutral solution of the catalyst promoted highly selective epoxidation of allylic alcohols. The reactivity of the whole reaction decreased by replacing the catalyst with K_2WO_4. (Scheme 2.18).[26] As a result, the conversion

of the reaction was terminated at 30%. On the other hand, if the catalyst directly replaced with H_2WO_4, they observed triols as products in high selectivity and yield. It was obvious that the triols was formed from the epoxy alcohol via hydrolysis in acid solution. Nonetheless, it could not be claimed that H_2WO_4 could transform to dinuclear dihydrated tetraperoxyditungstate automatically in acid solution, because hydrolysis step could break the equilibrium of epoxide progress in the first step.



Scheme 2.18 Comparison of catalytic differences among $[\{W(=O)(O_2)_2(H_2O)\}_2(\mu\text{-}O)]^{2-}K_2^+$, K_2WO_4, and H_2WO_4

In 2007, Mizuno's group successfully synthesized μ-η^1:η^1-peoxo-bridging dinuclear tetraperoxyditungstate and dehydrate tetraperoxyditungstate (Figure 2.2).[27] They took both to oxidize alkyl olefins, benzylic alcohols, allylic alcohols, and phosphines. Interestingly, these two catalysts showed the same performance in these reactions. As early as 1989, Griffith and co-workers predicted the structure of dehydrate tetraperoxyditungstate accurately by analyzing the IR and Raman data of those ionic compounds with different counterions.[28]



$[\{W(=O)(O_2)_2\}_2(\mu\text{-}O_2)]^{2-}$ **$[\{W(=O)(O_2)_2\}_2(\mu\text{-}O)]_{2-}$**

Figure 2.2 X-ray of μ-η^1:η^1-peoxo-bridging dinuclear tetraperoxyditungstate and dehydrate tetraperoxyditungstate

2.4 Tungstate polymer in oxidation

The most famous tungstate polymeric structure is Keggin's structure, which was first reported by Berzelius in 1826.[4] They proposed the configuration as chain or ring. Until 1934, James Fargher Keggin determined the α-Keggin's anion by X-ray diffraction (Figure 2.3), since then the Keggin's structure has been deeply researched, and 5 types of isomers have been identified (α-, β-, γ-, δ-, ε-).[29]

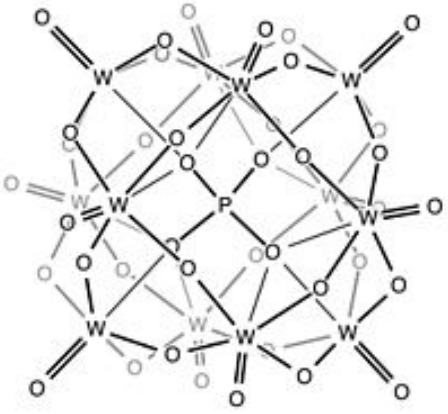
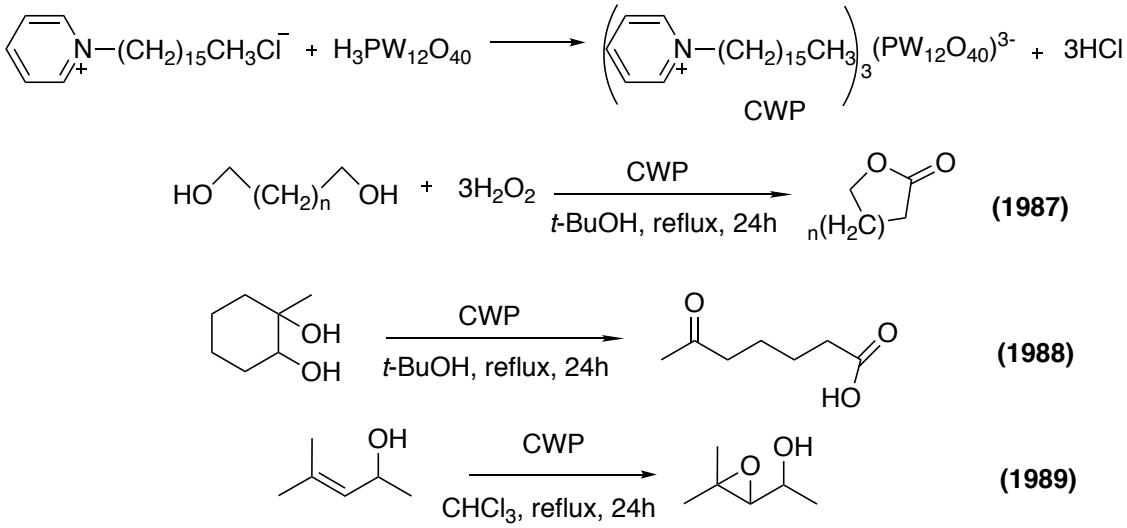


Figure 2.3 Keggin's structure

Ishii and co-workers synthesized tris(cetylpyridinium)12-tungustophosphate (CWP), which was an ion exchanged product between cetylpyridinium chloride and α-Keggin acid. They reported some reactions using CWP as a catalyst. In 1987, they achieved a facile lactonization of α,ω-diols in the presence of CWP.[30] One year later, a carboxylation reaction of pinacols was realized with the use of CWP.[31] In 1989, CWP was applied to epoxidation of allylic alcohols.[32] They discussed the influence of the solvent, the phase transfer catalyst, the pH, and the difference between tungstate and molybdenum on reactions (Scheme 2.19).



Scheme 2.19 CWP applications developed by Ishii's group

Another famous tungstate polymeric catalyst is tetra-*n*-butylammonium decatungstate ($[(C_4H_9)_4N]_4`W_{10}O_{32}$, TBADT, Figure 2.4). Moreover, TBADT is a photoredox catalyst, and it can promote single electron transfer process in oxidation.

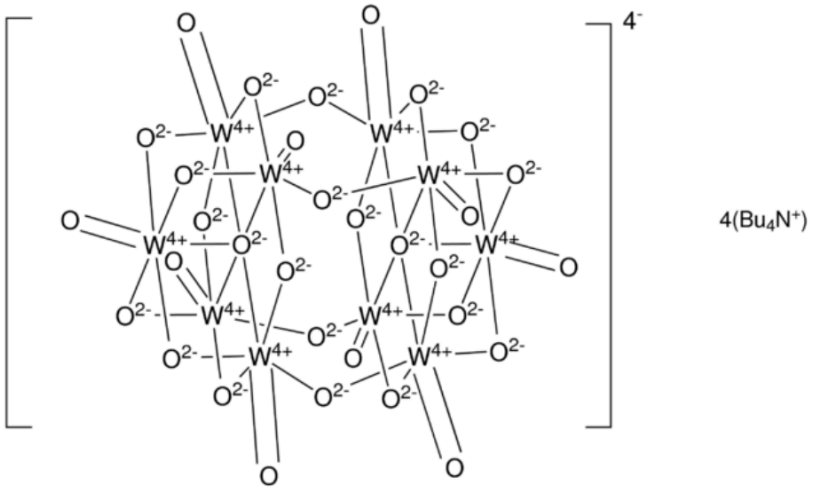
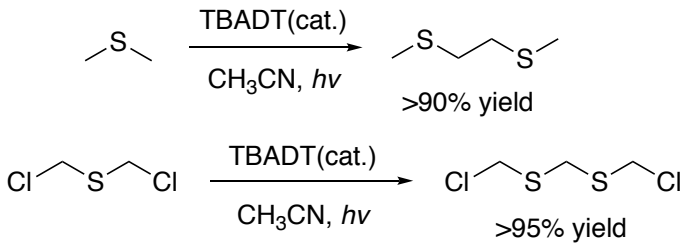


Figure 2.4 Structure of TBADT

For example, Craig and co-workers described the preparation, application, and kinetic study of TBADT in 1990 (Scheme 2.20).[33] The catalyst was activated by UV-light to form a radical anion. Then the radical anion worked as an oxidant in dehydrogenation homocoupling reaction, which obtained one electron from thioethers. Consequently, the thioether radical cation dissociated to one proton and one free neutral radical for the homocoupling step.



Scheme 2.20 Photocatalytic capability of TBADT

2.5 Summary

Tungstate salts have worked as oxidants in organic reactions for more than 70 years. Initially, it worked merely as an oxidant in stoichiometric amount. Later, it was developed into a catalyst by bringing the oxygen atom from a terminal oxidant, such as hydrogen peroxide, to the target molecules. The structures of catalytically active tungstate salts can be classified into monomer, oligomer, and polymer. Thus, pairing tungstate with a chiral cation catalyst is a plausible strategy for asymmetric oxidation. Exploration of this concept would not only lead to novel asymmetric oxidation reactions but also provide new insight into the structure and reactivity of tungstate.

References

(1) Lassner, E.; Schubert, W. D. Tungsten in Hardmetals. *Springer, Boston, MA.* **1999**, 321.

(2) Jørgensen, K. A. Transition-Metal-Catalyzed Epoxidations. *Chem. Rev.* **1989**, *89*, 431.

(3) Wang, C.; Yamamoto, H. Tungsten-Catalyzed Asymmetric Epoxidation of Allylic and Homoallylic Alcohols with Hydrogen Peroxide. *J. Am. Chem. Soc.* **2014**, *136*, 1222.

(4) Berzelius, J. The Preparation of the Phosphomolybdate Ion $[PMo_{12}O_{40}]^{3-}$. *Pogg Ann*, **1826**, *6*, 369.

(5) Payne, G. B.; Williams, P. H. Reactions of Hydrogen Peroxide. IV. Sodium Tungstate Catalyzed Epoxidation of α,β-Unsaturated Acids. *J. Org. Chem.* **1959**, *24*, 54.

(6) Kirshenbaum, K. S.; Sharpless, K. B. Improved Procedure for the Tungstate-Catalyzed Epoxidation of Alpha, Beta-Unsaturated Acids. *J. Org. Chem.* **1985**, *50*, 1979.

(7) Sato, K.; Aoki, M.; Ogawa, M.; Hashimoto, T.; Noyori, R. A Practical Method for Epoxidation of Terminal Olefins with 30% Hydrogen Peroxide under Halide-Free Conditions. *J. Org. Chem.* **1996**, *61*, 8310.

(8) Sato, K.; Aoki, M.; Takagi, J.; Noyori, R. Organic Solvent- and Halide-Free Oxidation of Alcohols with Aqueous Hydrogen Peroxide. *J. Am. Chem. Soc.* **1997**, *119*, 12386.

(9) Sato, K.; Takagi, J.; Aoki, M.; Noyori, R. Hydrogen Peroxide Oxidation of Benzylic Alcohols to Benzaldehydes and Benzoic Acids under Halide-Free Conditions. *Tetrahedron Lett* **1998**, *39*, 7549.

(10) Sato, K.; Aoki, M.; Noyori, R. A" Green" Route to Adipic Acid: Direct Oxidation of Cyclohexenes with 30 Percent Hydrogen Peroxide. *Science* **1998**, *281*, 1646.

(11) Sato, K.; Hyodo, M.; Aoki, M.; Zheng, X. Q.; Noyori, R. Oxidation of Sulfides to Sulfoxides and Sulfones with 30% Hydrogen Peroxide under Organic Solvent- and Halogen-Free Conditions. *Tetrahedron* **2001**, *57*, 2469.

(12) Murahashi, S.; Mitsui, H.; Shiota, T.; Tsuda, T.; Watanabe, S. Tungstate-Catalyzed Oxidation of Secondary Amines to Nitrones. Alpha-Substitution of Secondary Amines via Nitrones. *J. Org. Chem.* **1990**, *55*, 1736.

(13) Varlamov, A.; Kouznetsov, V.; Zubkov, F.; Chernyshev, A.; Alexandrov, G.; Palma, A.; Salas, S. Efficient Synthesis and Spectroscopic Analysis of 8-Nitro Spiro C3-Annulated 2-Benzazepines and Their N-Oxides. *Synthesis* **2001**, 0849.

(14) Heydari, A.; Aslanzadeh, S. Oxidation of Primary Amines to N-Monoalkylhydroxylamines Using Sodium Tungstate and Hydrogen Peroxide-Urea Complex. *Adv. Syn. Catal.* **2005**, *347*, 1223.

(15) Leonard, P. W.; Pollard, C. J.; Chavez, D. E.; Rice, B. M.; Parrish, D. A. 3, 6-Bis (4-nitro-1, 2, 5-oxadiazol-3-yl)-1, 4, 2, 5-dioxadiazene (BNDD): A Powerful Sensitive Explosive. *Synlett* **2011**, *22*, 2097.

(16) Shailaja, M.; Manjula, A.; Rao, B. V. An Inexpensive and Selective Oxygenation of N-Alkyl Imines to Oxaziridines. *Synlett* **2005**, 1176.

(17) Venturello, C.; Alneri, E.; Ricci, M. A New, Effective Catalytic System for Epoxidation of Olefins by Hydrogen Peroxide under Phase-Transfer Conditions. *J. Org. Chem.* **1983**, *48*, 3831.

(18) Venturello, C.; D'Aloisio, R.; Bart, J. C. J.; Ricci, M. A New Peroxotungsten Heteropolyanion with Special Oxidizing Properties: Synthesis and Structure of Tetrahexylammonium Tetra(diperoxotungsto)phosphate (3-). *J. Mol. Catal.* **1985**, *32*, 107.

(19) Ishii, Y.; Sakata, Y. A Novel Oxidation of Internal Alkynes with Hydrogen Peroxide Catalyzed by Peroxotungsten Compounds. *J. Org. Chem.* **1990**, *55*, 5545.

(20) Sakata, Y.; Ishii, Y. A Versatile Transformation of Vic-diols into Alpha-Hydroxy Ketones with Hydrogen Peroxide Catalyzed by Peroxotungstophosphates. *J. Org. Chem.* **1991**, *56*, 6233.

(21) Iwahama, T.; Sakaguchi, S.; Nishiyama, Y.; Ishii, Y. A Direct Conversion of Vic-Diols into 1, 2-Diketones with Aqueous Hydrogen Peroxide Catalyzed by Peroxotungstophosphate (PCWP). *Tetrahedron Lett.* **1995**, *36*, 1523

(22) Sakaue, S.; Sakata, Y.; Nishiyama, Y.; Ishii, Y. Oxidation of Aliphatic and Aromatic Amines with Hydrogen Peroxide Catalyzed by Peroxoheteropoly Oxometalates. *Chem. Lett.* **1992**, *21*, 289.

(23) Sakata, Y.; Katayama, Y.; Ishii, Y. Direct Catalytic Transformation of Olefins into α-Hydroxy Ketones with Hydrogen Peroxide Catalyzed by Peroxotungstophosphate. *Chem. Lett.* **1992**, *21*, 671.

(24) Einstein, F. W. B.; Penfold, B. R. The Crystal Structure of Hydrated Potassium Tetraperoxyditungstate(VI), $K_2W_2O_{11}.4H_2O$. *Acta. Crystallogr.* **1964**, *17*, 1127.

(25) Kamata, K.; Yamaguchi, K.; Hikichi, S.; Mizuno, N. $[\{W(=O)(O_2)_2(H_2O)\}_2(\mu\text{-}O)]^{2-}$-Catalyzed Epoxidation of Allylic Alcohols in Water with High Selectivity and Utilization of Hydrogen Peroxide. *Adv. Syn. Catal*. **2003**, *345*, 1193.

(26) Kamata, K.; Yamaguchi, K.; Mizuno, N. Highly Selective, Recyclable Epoxidation of Allylic Alcohols with Hydrogen Peroxide in Water Catalyzed by Dinuclear Peroxotungstate. *Chem. Eur. J*. **2004**, *10*, 4728.

(27) Kamata, K.; Kuzuya, S.; Uehara, K.; Yamaguchi, S.; Mizuno, N. μ-η1: η1-Peroxo-Bridged Dinuclear Peroxotungstate Catalytically Active for Epoxidation of Olefins. *Inorg. Chem.* **2007**, *46*, 3768.

(28) Campbell, N. J.; Dengel, A. C.; Edwards, C. J.; Griffith, W. P. Studies on Transition Metal Peroxo Complexes. Part 8. The Nature of Peroxomolybdates and Peroxotungstates in Aqueous Solution. *J. Chem. Soc., Dalton Trans.* **1989**, *6*, 1203.

(29) Keggin, J. F. The Structure and Formula of 12-Phosphotungstic Acid. *Proc. R. Soc. Lond. A*. **1934**, *144*, 75.

(30) Ishii, Y.; Yamawaki, K.; Yoshida, T.; Ura, T.; Ogawa, M. Oxidation of Olefins and Alcohols by Peroxo-Molybdenum Complex Derived from Tris(cetylpyridinium) 12-molybdophosphate and Hydrogen Peroxide. *J. Org. Chem.* **1987**, *52*, 1868.

(31) Ishii, Y.; Yamawaki, K.; Ura, T.; Yamada, H.; Yoshida, T.; Ogawa, M. Hydrogen Peroxide Oxidation Catalyzed by Heteropoly Acids Combined with Cetylpyridinium Chloride. Epoxidation of Olefins and Allylic Alcohols, Ketonization of Alcohols and Diols, and Oxidative Cleavage of 1,2-diols and Olefins. *J. Org. Chem.* **1988**, *53*, 3587.

(32) Oguchi, T.; Sakata, Y.; Takeuchi, N.; Kaneda, K.; Ishii, Y.; Ogawa, M. Epoxidation of α,β-Unsaturated Carboxylic Acids with Hydrogen Peroxide by Heteropoly Acids. *Chem. Lett.* **1989**, *18*, 2053.

(33) Duncan, D. C.; Chambers, R. C.; Hecht, E.; Hill, C. L. Mechanism and Dynamics in the $H_3[PW_{12}O_{40}]$-Catalyzed Selective Epoxidation of Terminal Olefins by H_2O_2. Formation, Reactivity, and Stability of $\{PO_4[WO(O_2)_2]_4\}^{3-}$. *J. Am. Chem. Soc.* **1995**, *117*, 681.

Chapter 3

Bisguanidinium Diphosphatobisperoxotungstate Catalyzed Sulfoxidation

3.1 Introduction

Chiral sulfoxides are a vital moiety of enantioenriched drugs, such as Esomeprazole, Lansoprazole, and Armodafinil. Therefore, we are interested in the practical preparation of enantiopure chiral sulfoxides.[1-4] Kagan oxidation has been widely adopted for asymmetric sulfoxidation in industry for a long time (Figure 3.1, Eqn. 1),[5] which utilizing Ti(O-*i*Pr)$_4$ and chiral diethyl tartrate in extra mole equivalent of water to produce a homogeneous reagent to get clean chiral sulfoxide. There are emerging methods[6-9] to prepare chiral sulfoxides including some recent breakthroughs utilizing imidodiphosphoric acid (Figure 3.1, Eqn. 2),[10] or binuclear titanium chiral complex (Figure 3.1, Eqn. 3).[11]

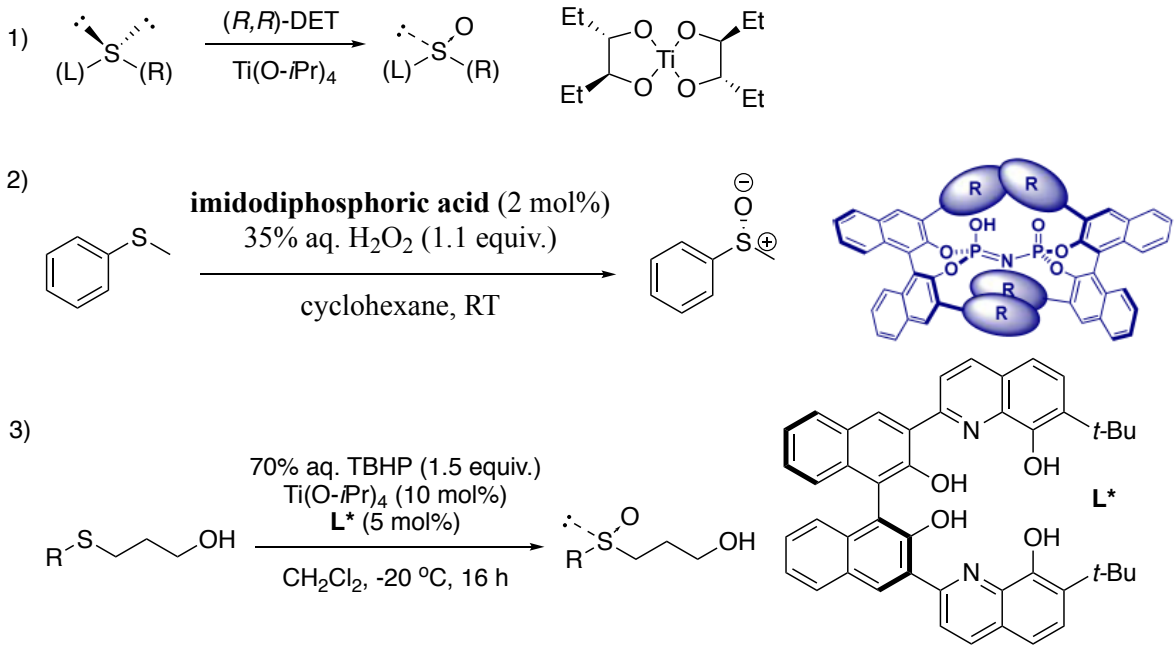


Figure 3.1 Some representative work of asymmetric sulfoxidation

Chiral cationic ion-pairing catalysis using inorganic salts is well known. The oxidizing anionic salts can be stoichiometric as in the epoxidation of chalcone with sodium hypochlorite using Maruoka catalyst (Figure 3.2, Eqn. 1).[12-14] Alternatively, the actual oxidant, (hypo)iodite, can be generated *in situ* through the use of iodide and stoichiometric oxidant such as cumene

hydroperoxide (CHP) (Figure 3.2, Eqn. 2). Ishihara demonstrated that enantioselective oxidative cycloetherification can be accomplished with this approach.[15-16] We recently demonstrated that by using potassium permanganate salt in the presence of a chiral dicationic bisguanidinium, highly enantioselective dihydroxylation and oxohydroxylation of *α,β*-unsaturated esters can be achieved (Figure 3.2, Eqn. 3).[17] This strategy is highly complementary to the chiral anion ion-pairing catalysis that was demonstrated to be compatible with a variety of cationic metal species.[18-20] Herein, we wish to report the enantioselective sulfoxidation using a catalytic amount of silver tungstate in the presence of chiral dicationic bisguanidinium (Figure 3.2, Eqn. 4).

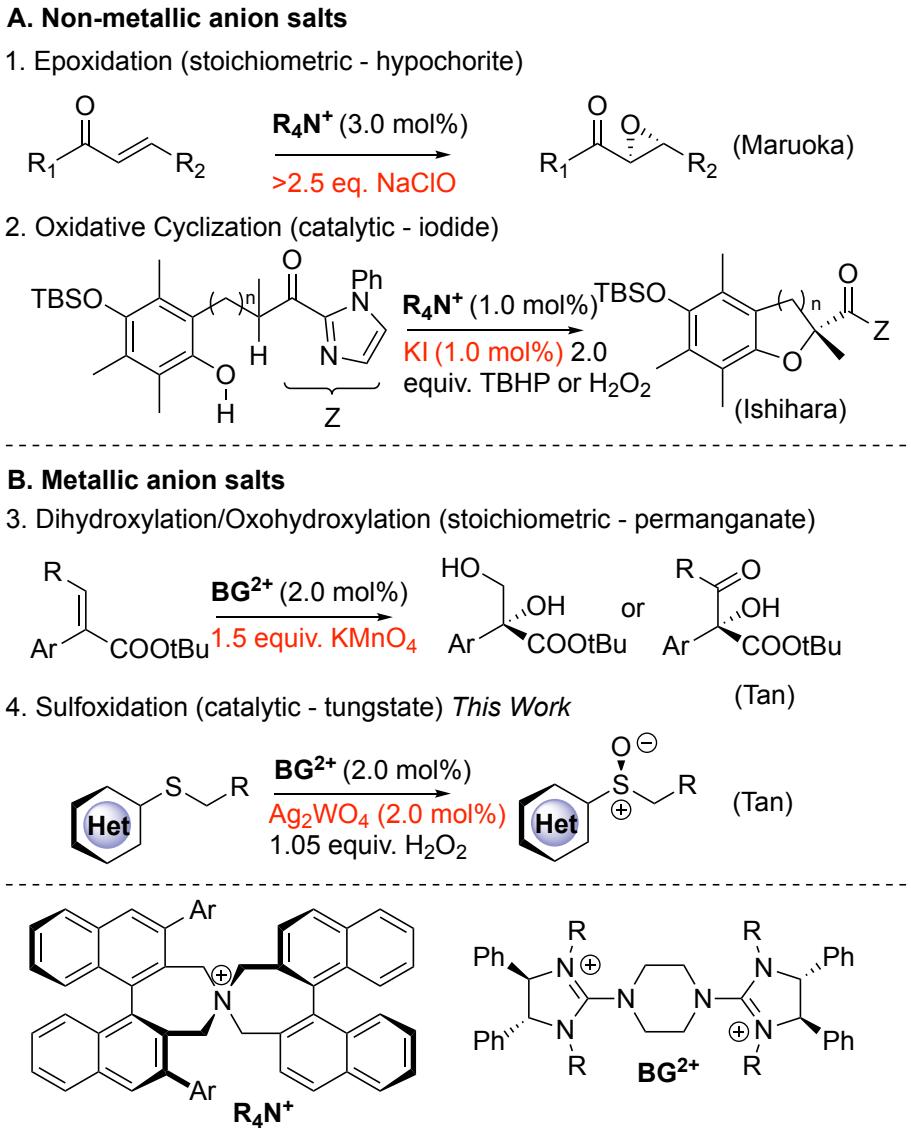


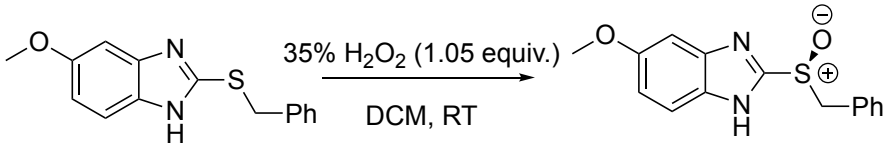
Figure 3.2 Enantioselective chiral cation ion-pairing oxidations.

3.2 Results and discussion

3.2.1 Reaction development

Initially, we mimicked the structures of target medicines, which was with heterocyclic substituted sulfoxides. Therefore, we prepared some heterocyclic substituted sulfides as model precursors. The first set of experiments we did were used to exclude the possibility of background reaction in presence of tungstate. As it showed in Table 3.1, either without tungstate or without **5a**, reaction did not work at all.

Table 3.1 Oxidative activity test of tungstate [a]

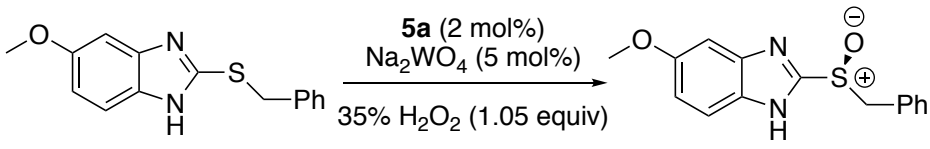


Entry	**5a** (mol%)	Na_2WO_4 (mol%)	Result [b,c]
1	2	-	N.R
2	-	5	N.R
3	2	5	isolated yield % = 79 ee % = 0

[a]Reaction conditions: substrate (0.05 mmol), H_2O_2 (0.0525 mmol, 1.05 equiv, 35%w/w), 0.5 mL DCM at room temperature. [b]Yield of isolated product. [c]Determined by HPLC analysis on a chiral stationary phase.

Because solvent is one of the most important factors to produce enantioselectivity, we changed the solvent and observed ee% for the first time (see in Table 3.2). It seemed the reaction working in toluene (entry 2) could give best reaction in these conditions.

Table 3.2 Screening of solvent [a]

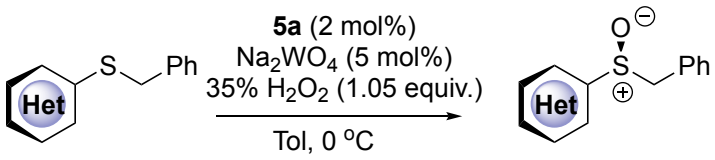


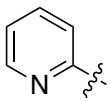
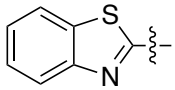
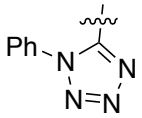
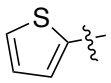
Entry	Temp (°C)	Solvent	yield (%)[b]	ee (%)[c]
1	0	Et_2O	42	17
2	0	Tol	41	32
3	0	CPME	35	19
4	-20	CPME	-	30

[a]Reaction conditions: substrate (0.05 mmol), H_2O_2 (0.0525 mmol, 1.05 equiv, 35%w/w), **5a** (0.001 mmol, 2.0 mol%), Na_2WO_4 (0.0025 mmol, 5.0 mol%), 0.5 mL solvent. [b]Yield of isolated product. [c]Determined by HPLC analysis on a chiral stationary phase.

With current condition in hand, we tried to apply it in different substrates. Among these structures, we found sulphide with aromatic tetrazole ring could be oxidized to corresponding sulfoxide in 27% yield, 30% ee (Table 3.3, entry 3).

Table 3.3 Exploration of heterocyclic compounds scope [a]



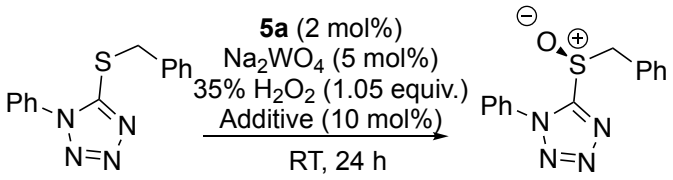
Entry	**Het**	yield (%)[b]	ee (%)[c]
1		Trace	8
2		17	8
3		27	30
4		Trace	6

[a]Reaction conditions: substrate (0.05 mmol), H_2O_2 (0.0525 mmol, 1.05 equiv, 35%w/w), **5a** (0.001 mmol, 2.0 mol%), Na_2WO_4 (0.0025 mmol, 5.0 mol%), 0.5 mL toluene at 0°C. [b]Yield of isolated product. [c]Determined by HPLC analysis on a chiral stationary phase.

Thus, we used the tetrazole compound as model reactant and put extra additive to improve reaction. Some Brønsted acid and Lewis acid were examined. Obviously, the

enantioselectivities under the reaction conditions with weak Brønsted acid were improved a lot (Table 3.4, entry 1-4). Under the basic and neutral conditions, the reactions were inhibited (entry 5-8).

Table 3.4 Screening of additive [a]

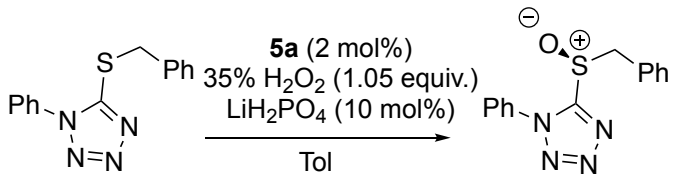


Entry	Additive (10 mol%)	Solvent	yield (%)[b]	ee (%)[c]
1	NaH_2PO_4	Tol	60	42
2	KH_2PO_4	Tol	60	41
3	LiH_2PO_4	Tol	66	42
4	LiH_2PO_4	*p*-CF_3Tol	74	38
5	K_2HPO_4	Tol	Trace	-
6	LiOAc	Tol	N.R	-
7	LiCl	Tol	N.R	-
8	LiBr	Tol	N.R	-

[a]Reaction conditions: substrate (0.05 mmol), H_2O_2 (0.0525 mmol, 1.05 equiv, 35%w/w), **5a** (0.001 mmol, 2.0 mol%), Na_2WO_4 (0.0025 mmol, 5.0 mol%), additive (0.005 mmol, 10.0 mol%), 0.5 mL solvent at room temperature. [b]Yield of isolated product. [c]Determined by HPLC analysis on a chiral stationary phase.

Because the condition was changed a lot after deciding to use additive, the tungstate should be rescreened on the same reaction model (Table 3.5). The results showed $(NH_4)_2WO_4$ might be the best choice (entry 2). Yield of product reached to 85%, and ee% reached to 56% at 0 °C. Furthermore, we lowered the temperature to -20 °C (entry 4) and -40 °C (entry 5). Yield of reaction reached as high as 98%, and ee% was more than moderate.

Table 3.5 Further screening of tungstate in presence of additive [a]

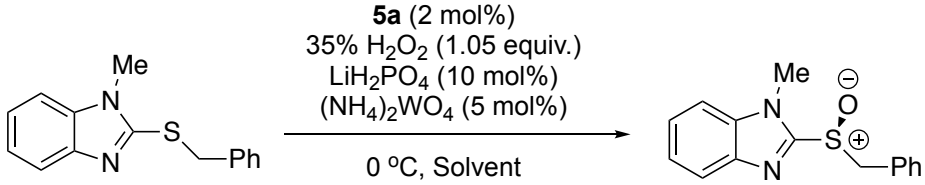


Entry	Temp (°C)	$M_x(WO_4)_y$ (5 mol%)	Time (h)	yield (%)[b]	ee (%)[c]
1	0	Na_2WO_4	24	28	40
2	0	$(NH_4)_2WO_4$	48	85	56
3	0	$Bi_2(WO_4)_3$	48	70	17
4	-20	$(NH_4)_2WO_4$	72	83	62
5	-40	$(NH_4)_2WO_4$	90	98	70

[a]Reaction conditions: substrate (0.05 mmol), H_2O_2 (0.0525 mmol, 1.05 equiv, 35%w/w), **5a** (0.001 mmol, 2.0 mol%), $M_x(WO_4)_y$ (0.0025 mmol, 5.0 mol%), LiH_2PO_4 (0.005 mmol, 10.0 mol%), 0.5 mL toluene at room temperature. [b]Yield of isolated product. [c]Determined by HPLC analysis on a chiral stationary phase.

Based on the current condition, sulphide with *N*-methylbenzoimidazole ring was oxidized. It was very disappointing that only trace amount of product was obtained (Table 3.6, entry 1). Hence, the solvent was switched to ether. Fortunately, unexpected results were obtained in diisopropyl ether (entry 2) and diethyl ether (entry 3).

Table 3.6 Condition test on drug analogues [a]

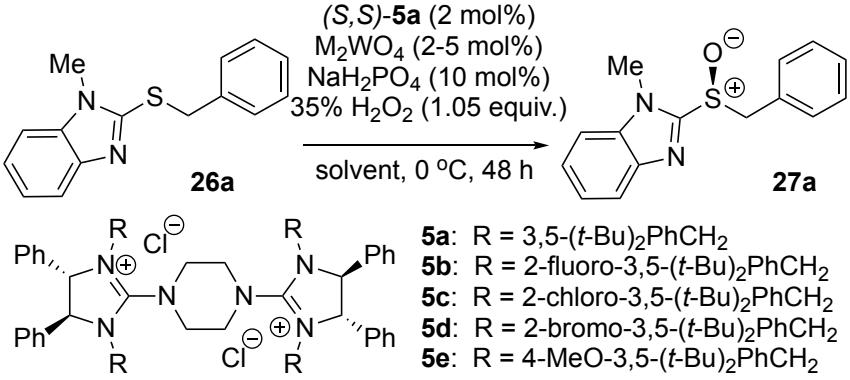


Entry	Solvent	yield (%)[b]	ee (%)[c]
1	Tol	trace	18
2	*i*-Pr_2O	60	88
3	Et_2O	75	90

[a]Reaction conditions: substrate (0.05 mmol), H_2O_2 (0.0525 mmol, 1.05 equiv, 35%w/w), **5a** (0.001 mmol, 2.0 mol%), $(NH_4)_2WO_4$ (0.0025 mmol, 5.0 mol%), LiH_2PO_4 (0.005 mmol, 10.0 mol%), 0.5 mL solvent at 0°C. [b]Yield of isolated product. [c]Determined by HPLC analysis on a chiral stationary phase.

After a period of condition tuning, we concluded all factors and applied them in one substrate **26a** to determine the final condition. The systematic and general information was as shown in Table 3.7 below.

Table 3.7 Final optimization of the reaction conditions



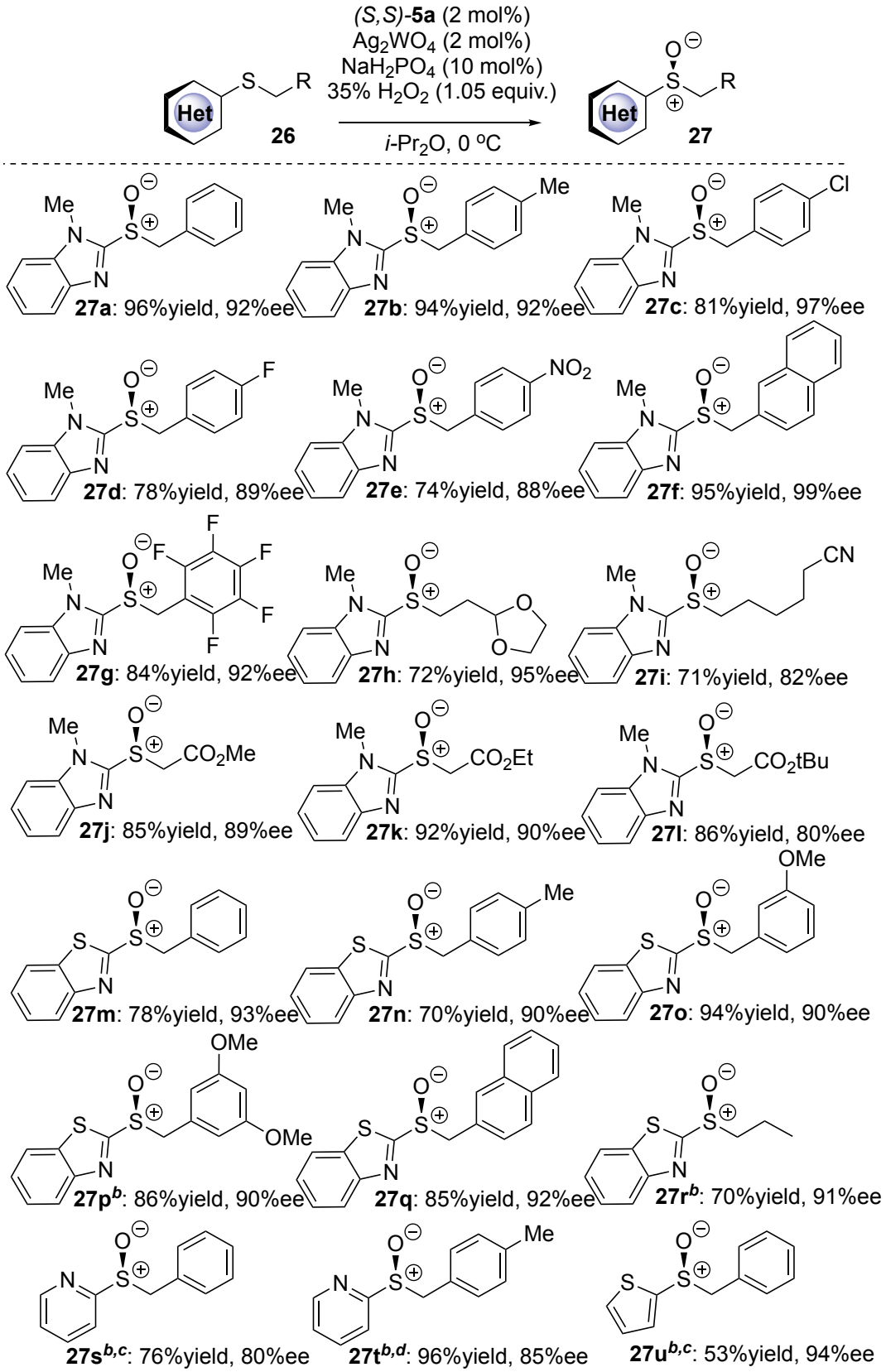
Entry	**BG**	$M_x(WO_4)_y$	Additive	Solvent	yield (%)[b]	ee (%)[c]
1[d]	*(S,S)*-**5a**	--	--	Et_2O	N.R.	N.A.
2	*(S,S)*-**5a**	Na_2WO_4	--	Et_2O	20	−5
3	*(S,S)*-**5a**	Na_2WO_4	NaH_2PO_4	Et_2O	36	20
4	*(S,S)*-**5a**	K_2WO_4	NaH_2PO_4	Et_2O	18	−2
5	*(S,S)*-**5a**	$(NH_4)_2WO_4$	NaH_2PO_4	Et_2O	48	42
6	*(S,S)*-**5a**	**Ag_2WO_4**	**NaH_2PO_4**	**Et_2O**	**83**	**88**
7	*(R,R)*-**5a**	**Ag_2WO_4**	**NaH_2PO_4**	**Et_2O**	**90**	**-89**
8	*(S,S)*-**5a**	Ag_2WO_4	LiH_2PO_4	Et_2O	70	90
9	*(S,S)*-**5a**	Ag_2WO_4	KH_2PO_4	Et_2O	83	84
10	*(S,S)*-**5a**	Ag_2WO_4	$NH_4H_2PO_4$	Et_2O	82	82
11	*(S,S)*-**5a**	Ag_2WO_4	$NaHSO_4$	Et_2O	52	80
12	*(S,S)*-**5a**	Ag_2WO_4	NaH_2PO_4	Tol	60	74
13	*(S,S)*-**5a**	Ag_2WO_4	NaH_2PO_4	DCM	68	20
14	*(S,S)*-**5a**	Ag_2WO_4[e]	NaH_2PO_4	Et_2O	55	50
15	*(S,S)*-**5a**	**Ag_2WO_4[e]**	**NaH_2PO_4**	***i*-Pr_2O**	**96**	**92**
16	*(S,S)*-**5b**	Ag_2WO_4[e]	NaH_2PO_4	*i*-Pr_2O	63	50
17	*(S,S)*-**5c**	Ag_2WO_4[e]	NaH_2PO_4	*i*-Pr_2O	52	32
18	*(S,S)*-**5d**	Ag_2WO_4[e]	NaH_2PO_4	*i*-Pr_2O	84	8
19	*(S,S)*-**5e**	Ag_2WO_4[e]	NaH_2PO_4	*i*-Pr_2O	65	63
20	*(S,S)*-**5a**	--	NaH_2PO_4	*i*-Pr_2O	19	N.A.

[a]Reaction conditions: **26a** (0.05 mmol), H_2O_2 (0.0525 mmol, 1.05 equiv, 35%w/w), **5** (0.001 mmol, 2.0 mol%), $M_x(WO_4)_y$ (0.0025 mmol, 5.0 mol%), 1.0 mL Et_2O at 0 °C. [b]Yield of isolated product. [c]Determined by HPLC analysis on a chiral stationary phase. [d]No reaction was also observed at room temperature. [e]2.0 mol% of Ag_2WO_4 was used.

At the outset, benzimidazole-derived benzyl sulfide **26a** was chosen as the model substrate to investigate the reaction conditions (Table 3.7). In the presence of 2.0 mol% of bisguanidinium *(S,S)*-**5a** with Et_2O as solvent, no reaction was found when only H_2O_2 was used (Table 3.7, entry 1); indicating that *(S,S)*-**5a** alone cannot catalyze the reaction. When 5.0 mol% of Na_2WO_4 was added, the reaction gave sulfoxide **27a** in poor yield and low enantioselectivity (entry 2). When 10 mol% NaH_2PO_4 was added, the yield of sulfoxide **27a** improved significantly to 36% and its *ee* value improved to 20% (entry 3). When Na_2HPO_4 and Na_3PO_4 were used instead, the reactions were inhibited. Next, a range of commercially available tungstate salts, such as K_2WO_4, $(NH_4)_2WO_4$ and Ag_2WO_4 were evaluated (entries 4-6). Sulfoxide **27a** was obtained in 83% yield with 88% *ee* value when Ag_2WO_4 was used (entry 6). We assumed that Ag^+ forced the Cl^- to be exchanged from **BG**, forming precipitate of AgCl, which decreased the competition between the counter ions of **BG**. Moreover, *ent*-**5a** afforded the antipode with similar efficiency and enantioselectivity (entry 7). Various additives were tested, and both yield and *ee*% were compared to Na_2HPO_4 (entry 8-11). Above all, solvent was examined (entry 6,12,13). When the catalyst loading of Ag_2WO_4 was decreased to 2.0 mol%, it is necessary to change the solvent to diisopropyl ether to provide the best results (entry 15). the best solvent was Et_2O in previous conclusions, hence, the Et_2O was re-examined under the same condition (entry 14). Other bisguanidiniums *(S,S)*-**5b-5e** featuring different benzyl groups was unable to improve the results obtained with *(S,S)*-**5a** (entries 16-19). We also confirm that NaH_2PO_4 in the absence of Ag_2WO_4 did not promote the sulfoxidation reaction (entry 20).

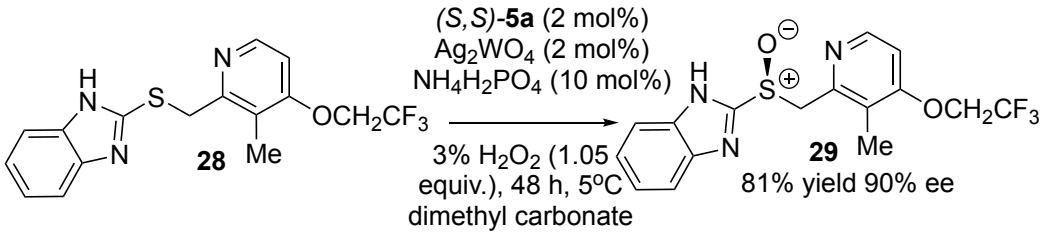
With the optimized reaction conditions in hand, the substrate scope of benzimidazole-derived sulfides was examined (Scheme 3.1, **27a**-**27i**). The benzimidazole group does not seem

to act as a ligand and inhibit the reaction. Both electron donating and electron withdrawing substitutions on the benzyl group worked well, affording the corresponding sulfoxidation products in good to excellent yields with good levels of enantioselectivities. The oxidation ability of the catalyst is able to override even highly electron withdrawing group such as pentafluorobenzyl (**27g**). Besides benzyl groups, simple alkyl groups or esters are also tolerated in this reaction (**27h**-**1**). Other heterocyclic systems such as benzothiazole (**27m**-**r**), pyridine (**27s**-**t**) and thiophene (**27u**) also worked well providing products with excellent *ee* values. However, thiophene heterocyclic sulfides gave lower yields with significant amount of sulfone detected. We were also able to scale the reaction to gram scale (3.5 mmol) to give **27q** in 91% yield and 92% *ee*. The established strategy was also successfully applied to the preparation of *(S)*-Lansoprazole **29**, a commercial proton-pump inhibitor (Scheme 3.2).



Reactions were carried out on 0.2 mmol scale in 4.0 mL solvent for 36 hours unless otherwise noted; yield values refer to isolated yields after purification and *ee* was determined by chiral HPLC. [a] 5.0 mol% of Ag_2WO_4 was used. [b] Et_2O as the solvent. [c] 8.0 mL iPr_2O was used.

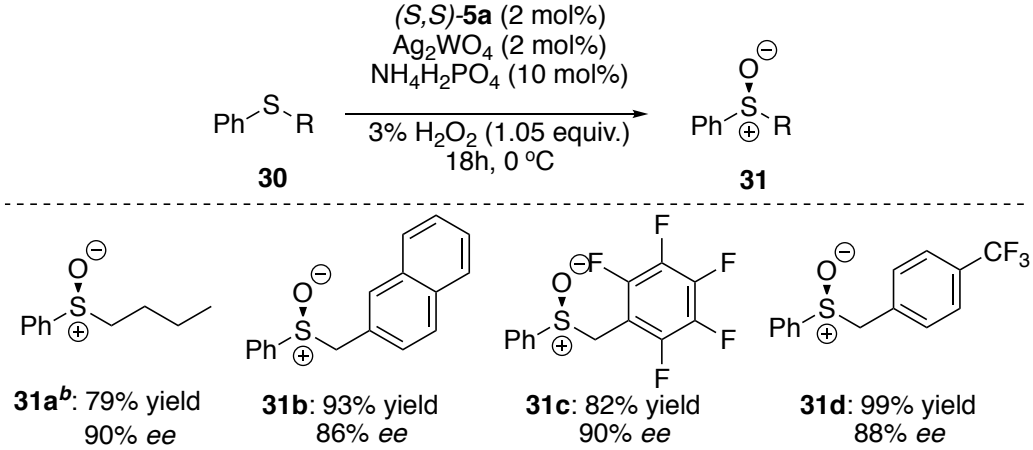
Scheme 3.1 Enantioselective sulfoxidation of heterocyclic sulfides.



Scheme 3.2 Enantioselective synthesis of *(S)*-Lansoprazole.

Simple phenyl substituent sulfoxides were also created (Table 3.8, **6a-6d**). Due to the activity differences existing among the substrates, the concentration and solvent can influence the results. When using iPr$_2$O as the sole solvent, the conventional sulphide was over-oxidized to sulfone. In Et$_2$O, the conversion was limited. In DMC (dimethyl carbonate), it terminated in 4 hours under 5 °C, while only moderate yield and ee were obtained. Surprisingly, when the mixed solvent system was examined, both chemoselectivity and enantioselectivity increased.

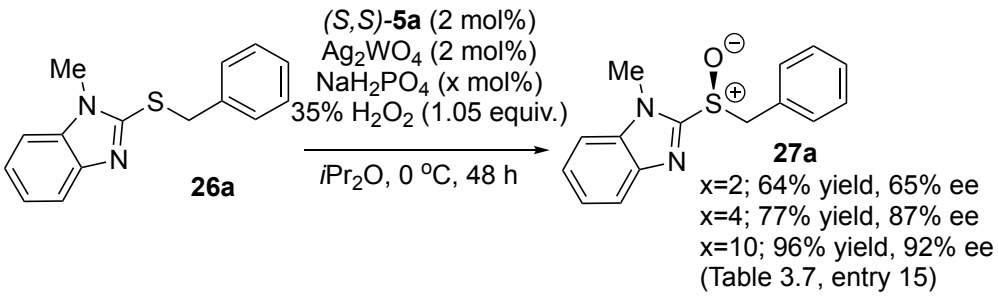
Table 3.8 Other conventional substrates of sulphides[a]



[a] Reactions were carried out on 0.2 mmol scale in a solvent mixture of DMC (4.0 mL)/Et$_2$O (4.0 mL). (DMC=dimethyl carbonate) [b] Reactions were carried out in a solvent mixture of DMC (4.0 mL)/iPr$_2$O (4.0 mL).

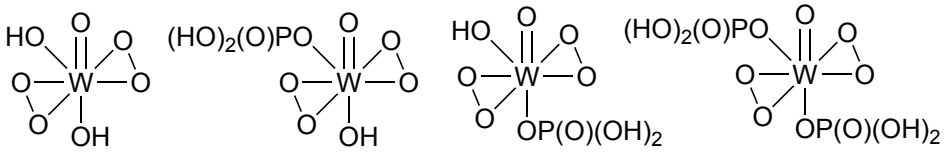
3.2.2 Mechanism study

During optimization of the reaction conditions, we realized that the ratio of Ag_2WO_4 to NaH_2PO_4 is crucial in obtaining good yields and enantioselectivities (Scheme 3.3). The most significant improvement was achieved when the ratio of phosphate to tungstate reached 1:2. As the amount of phosphate in this current methodology is in excess over tungstate, we speculated that the Ishii-Venturello catalyst, $[PO_4\{WO(O_2)_2\}_4]^{3-}$, is not the active catalyst in this methodology. When we replaced the Ag_2WO_4/NaH_2PO_4 with $H_3PW_{12}O_{40}$ (Keggin's reagent) as in Ishii's protocol, the reaction provided sulfoxides in 40% yield and 30% *ee*.



Scheme 3.3 Influence of phosphate loading.

Ligand coordination or substitution has been previously shown to be an important factor that can influence the catalytic activities of peroxotungstates. Under the current experimental condition, monomeric and oligomeric dihydroxide species **i** (Figure 3.3) should exist and in the presence of phosphate additive, form substituted phosphate species **ii-iv**.[21-23] These complexes assume distorted pentagonal bipyramid geometry and obey the 18-electron rule. As a result, coordination of three or more phosphates to the tungstate center can be considered to be unlikely. It is also important to note that due to the short O-O bond distances (1.45 to 1.47 Å)[24] in the peroxo group, the oxygen atoms will most likely lie in the equatorial plane, instead of occupying both axial and equatorial positions in the complex. Based on these premises, the four possible configurations of substituted peroxotungstate species are presented (Figure 3.3).



i **ii** **iii** **iv**

Figure 3.3 Four possible peroxotungstate species.

Raman spectra was computed for candidate structure **i-iv** by performing vibrational frequency analysis on stationary points optimized at the B3LYP/B1 theory level in gas phase. The result is shown in Figure 3.4. The peak at 1014 cm^{-1} in experimental Raman spectra was found to be the peak with the highest intensity, which corresponds to the W=O bond stretching vibrations. Computed Raman spectra showed this peak at 920-1000 cm^{-1} region. Additionally, characteristic bands from $W(O_2)$ group appear in 500-600 cm^{-1} region, while bands above 1000 cm^{-1} generally correspond to vibrational modes from phosphate group.

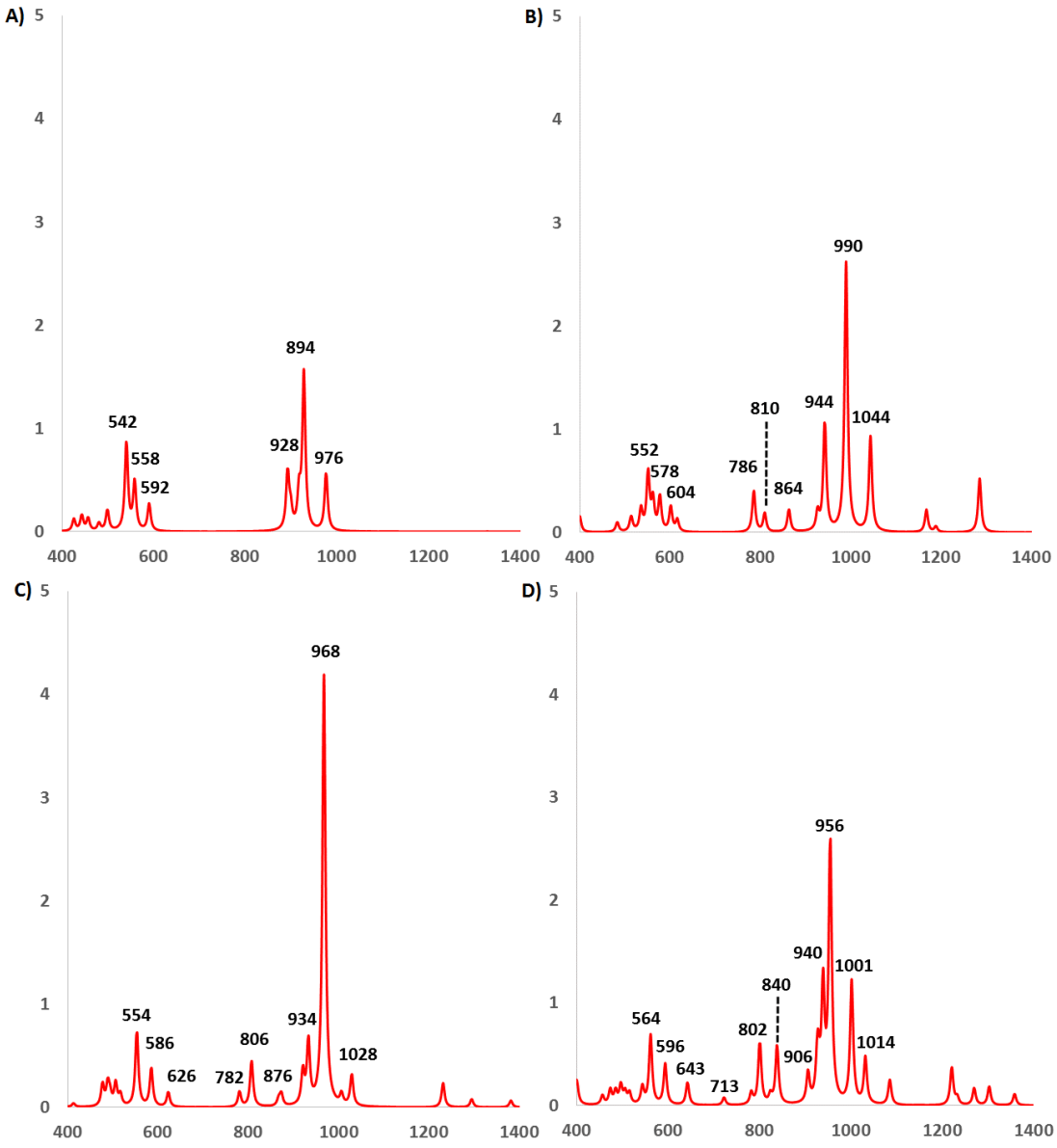
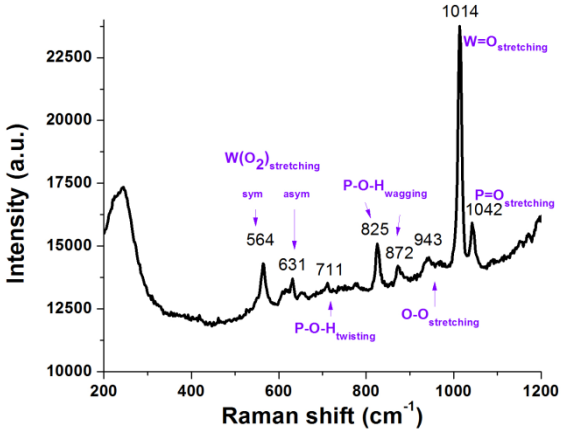


Figure 3.4 Predicted Raman spectra of active species candidates, computed at B3LYP/B1 theory level for (A) dihydroxide **i**, (B) equatorial monophosphate **ii**, (C) axial monophosphate **iii**, (D) diphosphate **iv**.



	P=O	W=O	O-O	P-O-H	P-O-H	$W(O_2)$
Calc.	1014	1001	940	840, 802	713	643_{asym}, 564_{sym}
Expt.[a,b]	1042	1014	943	872, 825	711	631_{asym}, 564_{sym}

[a] Preparation: In a 4mL sample vial, BG-1 (0.01 mmol, 1.0 equiv), tungstate oxide (0.01 mmol, 1.0 equiv), phosphate monobasic (0.05 mmol, 5.0 equiv), hydrogen peroxide (0.1 mmol, 10.0 equiv, 35%, w/w) and diethyl ether in a proper amount were added at room temperature. Keep stirring for 6 hours, and filtrate the precipitate. Blow drying the mixture, then remove water on vacuo. [b] Raman setting: 2mW, 532 laser power, 30 seconds.

Figure 3.5 Experimental Raman spectrum and vibration diagram of [**P2W**]$^{2-}$, $[\{PO_2(OH)_2\}_2\{WO(O_2)_2\}]^{2-}$

Raman spectra of the active species were obtained and compared with predicted Raman spectra of the four possible intermediates. Computed Raman spectra were obtained by performing vibrational frequency analysis on stationary points optimized at the B3LYP/B1 level of theory in gas phase, where B1 is a combination of LANL2DZ effective core potential basis set for W and the 6-31g* basis set for remaining atoms. A peak was observed experimentally at 711 cm^{-1}, which corresponds to the twisting of P-O-H group in the phosphate ligand (Figure 3.5). This same peak was found only in the computed spectra of [**P2W**]$^{2-}$ (713 cm^{-1}).

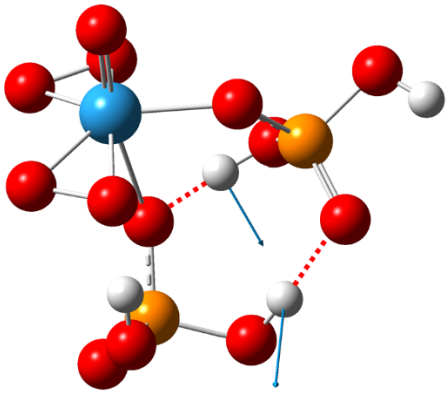


Figure 3.6 Vector representations of the vibrational mode corresponding to the band at 713 cm^{-1} in the computed Raman spectra of diphosphate **4**. Dotted lines represent hydrogen bond interactions.

A more thorough analysis of the $[\mathbf{P2W}]^{2-}$ structures revealed that intramolecular hydrogen bond interaction between the two phosphate ligands is important for this peak (Figure 3.6); absence of such interaction will shift the vibrational frequency towards 800 cm^{-1}. We thus propose that the active anion of this enantioselective sulfoxidation is diphosphatobisperoxotungstate, $[\{PO_2(OH)_2\}_2\{WO(O_2)_2\}]^{2-}$.

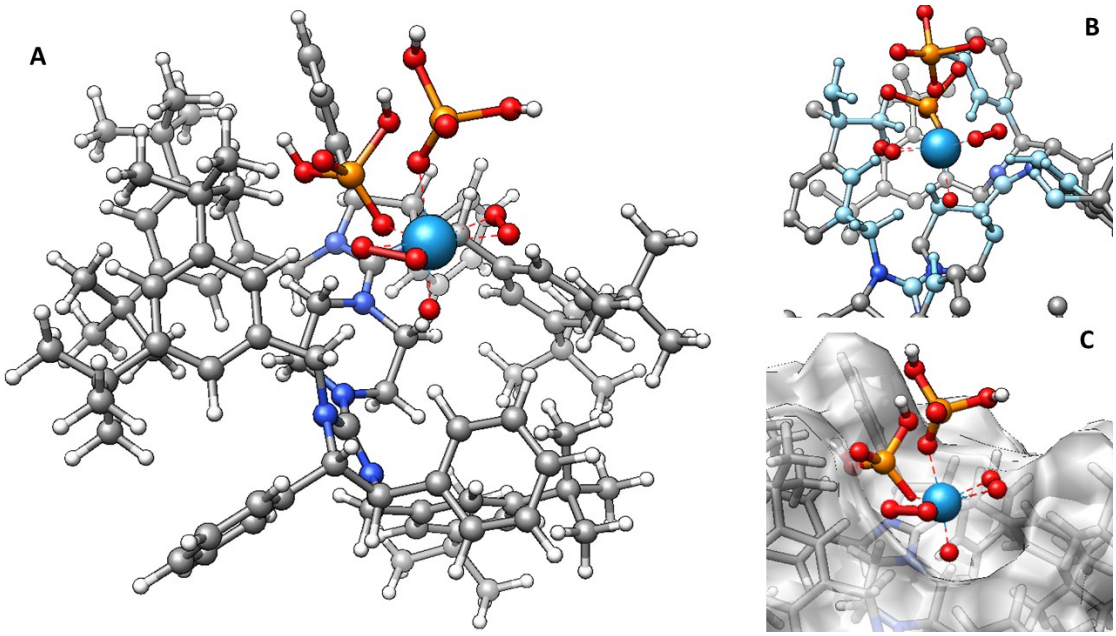


Figure 3.7 Representation of $[\mathbf{BG}]^{2+}[\mathbf{P2W}]^{2-}$ ion pair.

(a) ONIOM optimization result, color coded as grey: C, blue: N, white: H, orange: P, red: O. (b) Atoms in close distance to $[\mathbf{P2W}]^{2-}$ core is highlighted. (c) Surface of $[\mathbf{BG}]^{2+}$ structure is displayed.

Preliminary computational studies of the complete $[\mathbf{BG}]^{2+}[\mathbf{P2W}]^{2-}$ structure using two-layer ONIOM $(QM:QM')^2$ method revealed a stable ion-pair interaction, where $[\mathbf{P2W}]^{2-}$ is buried in the chiral cavity of $[\mathbf{BG}]^{2+}$ (Figure 3.7).

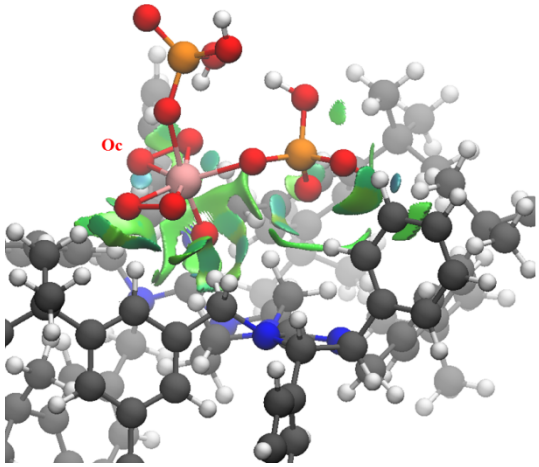


Figure 3.8 Representation of $[\mathbf{BG}]^{2+}[\mathbf{P2W}]^{2-}$ ion-pair from ONIOM optimization result, color-coded as grey: C, blue: N, white: H, orange: P, red: O, pink: W. NCI surface of BG1 structure is displayed: green indicates attractive non-covalent interactions.

This configuration results in only one of the peroxo-oxygen (marked as **Oc** in Figure 3.8) being exposed, leaving it as the only possible reaction site. This will restrict the direction of approach of the sulfide, thereby providing fertile condition for an enantioselective reaction. We thus propose a simple working model, which includes the initial formation of $[\mathbf{P2W}]^{2-}$ in the aqueous phase through the interactions of silver tungstate, phosphate and hydrogen peroxide (Figure 3.9). The formation of the ion-pair $[\mathbf{BG}]^{2+}[\mathbf{P2W}]^{2-}$ in the organic phase is facilitated by $[\mathbf{BG}]^{2+}$. After oxidation, $[\mathbf{P2W}]^{2-}$ is regenerated in the aqueous phase by H_2O_2.

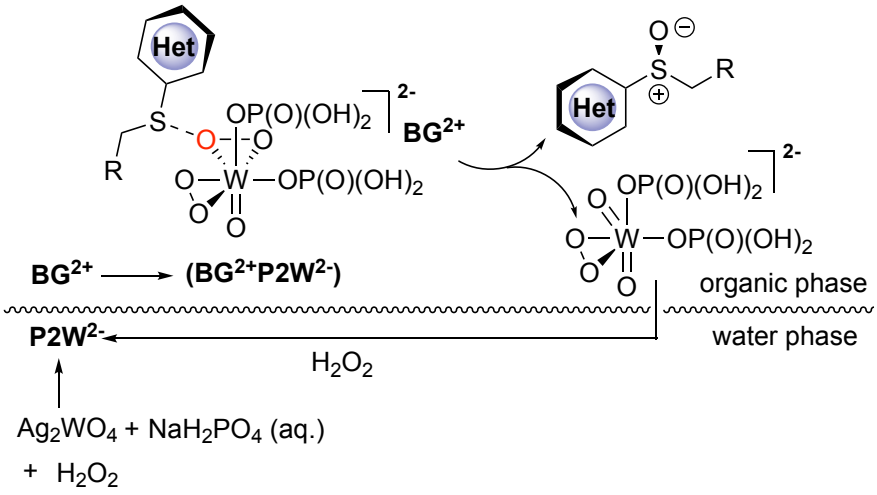


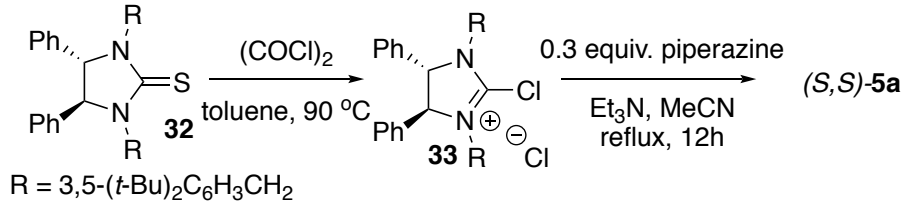
Figure 3.9 Working Model.

3.3 Summary

In summary, we report the first enantioselective tungstate-catalyzed oxidation reaction. Especially, with the aid of a chiral bisguanidinium diphosphatobisperoxotungstate ion pairing catalyst, high enantioselectivities were achieved for a variety of drug-like heterocyclic sulfides under mild condition with H_2O_2, a cheap and environmentally friendly oxidant. Except for Kagan-Sharpless Ti-complex catalysis, heterocyclic sulfides were less investigated in the research history of enantioselective sulfoxidations. In addition, the ion-pair catalysis was also applied to conventional sulfides successfully. With the advantage of low-catalyst loading and large-scale producing, synthetic utility was demonstrated through the preparation of *(S)*-Lansoprazole, a commercial proton-pump inhibitor. The active ion-pair catalyst was identified to be bisguanidinium diphosphatobisperoxotungstate using Raman spectroscopy and computational studies.

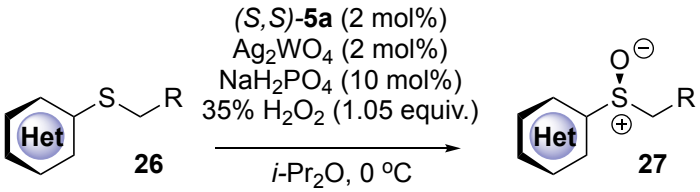
3.4 Experimental

3.4.1 Experimental procedure



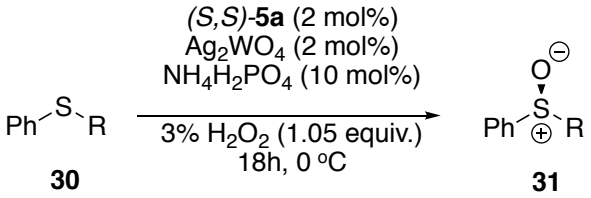
Scheme 3.4 Preparation and characterization of bisguanidinium catalysts (**5a** as the representative example)

1,4-Bis((4*S*,5*S*)-1,3-bis(3,5-di-*tert*-butylbenzyl)-4,5-diphenylimidazolidin-2-ylidene)piperazine-1,4-diium chloride (5a): Thiourea **32** was prepared according to literature procedure[1]. A 25 mL RBF was charged with a solution of thiourea (1.59 g, 2.41 mmol, 1.0 equiv) in toluene (8 mL) with a condenser under N_2 atmosphere. $(COCl)_2$ (1.66 mL, 19.3 mmol, 8.0 equiv) was added via syringe in one portion. The mixture was heated to 90 °C for about 12 h, and then refluxed for 1 h. Toluene was removed under reduced pressure and solid imidazoline salt **33** was obtained directly for the next step without any purification. The imidazoline salt was dissolved in dry MeCN (2 mL) under nitrogen atmosphere, and then piperazine (62 mg, 0.72 mmol, 0.3 equiv) was added, followed by the addition of Et_3N (1 mL, 7.23 mmol, 3.0 equiv). Then the whole solution was heated to reflux for 12 h and cooled to rt. Add 1M HCl (20 mL) to the reaction solution and the mixture was extracted by CH_2Cl_2 (20 mL × 3). Solvent was removed under reduced pressure and bis-guanidinium salt **5a** was obtained by flash chromatography (silica gel, DCM-Methanol 100:1-30:1), as a beige powder, 695 mg, 68% yield. **5a**[2]**:** ^{1}H NMR (400 MHz, CDCl3) δ 7.30 (dd, J = 5.0, 1.5 Hz, 12H), 7.20 (s, 4H), 7.05 (dd, J = 6.5, 2.8 Hz, 8H), 6.96 (d, J = 1.5 Hz, 8H), 5.19 (d, J = 14.7 Hz, 4H), 4.82 (d, J = 14.7 Hz, 4H), 4.73 (d, J = 9.5 Hz, 4H), 4.48 (d, J = 9.5 Hz, 4H), 4.32 (s, 1H), 1.14 (s, 72H); ^{13}C NMR (100 MHz, CDCl3) δ 162.68, 151.30, 137.67, 131.89, 129.58, 129.16, 126.51, 123.37, 122.26, 70.39, 54.52, 48.99, 34.69, 31.37, 31.28; HRMS (ESI) calc. for C94H124Cl2N6 m/z $[M\text{-}2Cl^-]^{2+}$: 668.4944; found: 668.4941.



Scheme 3.5 Preparation of **5a** catalyzed sulfoxidation of heterocyclic sulfides

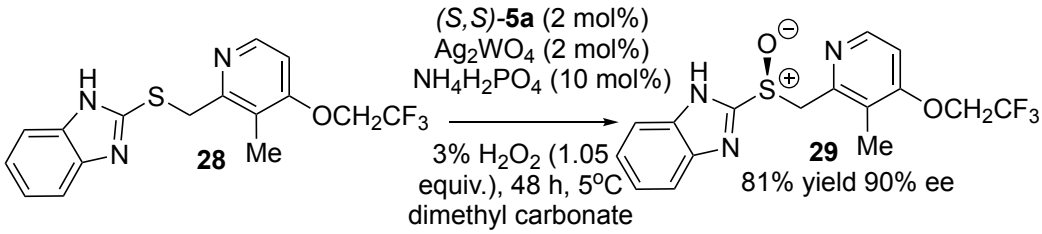
In a 4 mL sample vial, sulfides **26** (0.2 mmol, 1.0 equiv), bisguanidium chloride (0.004 mmol, 0.02 equiv), silver tungstate oxide (0.004 mmol, 0.02 equiv), sodium phosphate monobasic (0.02 mmol, 0.1 equiv) and solvent were added. Then lower the solution to the presupposed temperature. After stabilizing, H_2O_2 (1.05 equiv, 35% w/w) was injected in one portion into the system. The mixture was stirred for 24 hours to 48 hours, and the termination of reaction was monitored by TLC. The resulting suspension was quenched by saturated $Na_2S_2O_3$ (sat.). EtOAc (0.5 mL×3) was used for extraction, and the organic layers was combined and dried over anhydrous Na_2SO_4. The organic solvent was removed in rotary evaporator (the water-bathing temperature is under 38 °C), and the residues was purified by chromatography on silica gel to afford the desired products **27**.



Scheme 3.6 Preparation of **5a** catalyzed sulfoxidation of phenyl sulfides

In a 10 mL sample vial, sulfides **30** (0.2 mmol, 1.0 equiv), bisguanidium chloride (0.004 mmol, 0.02 equiv), silver tungstate oxide (0.004 mmol, 0.02 equiv), ammonium phosphate monobasic (0.02 mmol, 0.1 equiv) and 8mL mixed solvent were added. The solvent mixture was consisted of 4 mL dimethyl carbonate and 4 mL diethyl ether (diisopropyl ether in **5a**). Then lower the solution to the presupposed temperature. After stabilizing, H_2O_2 (1.05 equiv, 3% w/w) was injected in one portion into the system. The mixture was stirred for 18hours, and the termination of reaction was monitored by TLC. The resulting suspension was quenched by saturated

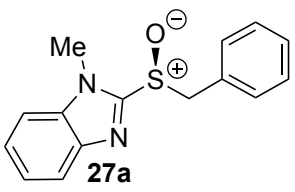
$Na_2S_2O_{3\,(sat.)}$. EtOAc (0.5 mL×3) was used for extraction, and the organic layers was combined and dried over anhydrous Na_2SO_4. The organic solvent was removed in rotary evaporator (the water-bathing temperature is under 38 °C), and the residues was purified by chromatography on silica gel to afford the desired products **31**.



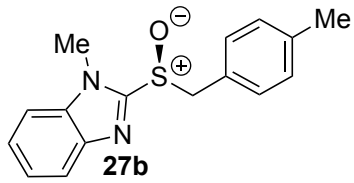
Scheme 3.7 Application of Lansoprazole

In a 25 mL RBF, sulfides **28** (0.2 mmol, 1.0 equiv), bisguanidium chloride **5a** (0.004 mmol, 0.02 equiv), silver tungstate oxide (0.004 mmol, 0.02 equiv), ammonium phosphate monobasic (0.02 mmol, 0.1 equiv) and 8 mL solvent were added. Then lower the solution to the presupposed temperature in a constant incubator. After stabilizing, H_2O_2 (1.05 equiv, 3% w/w) was injected in one portion into the system. The mixture was stirred for 48hours, and the termination of reaction was monitored by TLC. The resulting suspension was quenched by saturated $Na_2S_2O_{3\,(sat.)}$. Use $NaHCO_3$ to wash, and then EtOAc (0.5 mL×3) was used for extraction, and the organic layers was combined and dried over anhydrous Na_2SO_4. The organic solvent was removed in rotary evaporator (the water-bathing temperature is under 38 °C), and the residues was purified by chromatography on silica gel to afford the desired products **29**.

3.4.2 Characterization of asymmetric products

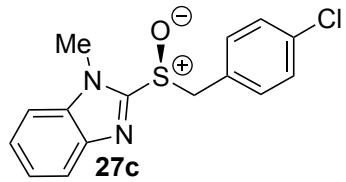


(*S*)-2-(Benzylsulfinyl)-1-methyl-1*H*-benzo[*d*]imidazole (27a): 96% yield; white solid; ^{1}H NMR (400 MHz, $CDCl_3$) δ 7.87–7.82 (m, 1H), 7.38–7.35 (m, 2H), 7.32–7.26 (m, 2H), 7.21 (td, *J* = 10.4, 4.7 Hz, 2H), 7.03 (dd, 2H), 4.64 (d, *J* = 12.9 Hz, 1H), 4.50 (d, *J* = 12.9 Hz, 1H), 3.45 (s, 3H); ^{13}C NMR (101 MHz, $CDCl_3$) δ 150.01, 141.54, 136.47, 130.61, 128.89, 128.77, 124.68, 123.77, 120.59, 109.83, 60.96, 29.97; HRMS (ESI) calcd for $C_{15}H_{14}N_2OS$ *m/z* $[M+H]^+$: 271.0905; found: 271.0904; $[\alpha]_D^{22}$= -29.16 (*c* 3.8, CH_2Cl_2); HPLC analysis: Chiralcel OJ-H (Hex/IPA = 70/30, 1.0 mL/min, 254 nm, 22°C), 17.1, 29.0 (major) min, 92% ee.



27b

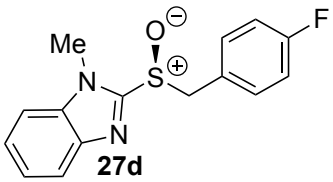
(*S*)-1-Methyl-2-((4-methylbenzyl)sulfinyl)-1*H*-benzo[*d*]imidazole (27b): 94% yield; white solid; ^{1}H NMR (400 MHz, $CDCl_3$) δ 7.89–7.78 (m, 1H), 7.38–7.33 (m, 2H), 7.32–7.27 (m, 1H), 7.03 (d, *J* = 7.9 Hz, 2H), 6.93 (d, *J* = 8.0 Hz, 2H), 4.62 (d, *J* = 12.9 Hz, 1H), 4.45 (d, *J* = 12.9 Hz, 1H), 3.49 (s, 3H), 2.30 (s, 3H); ^{13}C NMR (101 MHz, $CDCl_3$) δ 150.38, 142.01, 138.80, 136.58, 130.50, 129.45, 125.73, 124.51, 123.53, 120.78, 109.78, 60.62, 30.03, 21.27; HRMS (ESI) calcd for $C_{16}H_{16}N_2OS$ *m/z* $[M+H]^+$: 285.1062; found: 285.1056; $[\alpha]_D^{22}$= -29.41 (*c* 2.2, CH_2Cl_2); HPLC analysis: Daicel Corporation IB3 (Hex/IPA = 70/30, 1.0 mL/min, 254 nm, 22°C), 8.4, 15.4 (major) min, 94% ee.



27c

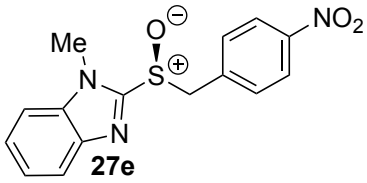
(*S*)-2-((4-Chlorobenzyl)sulfinyl)-1-methyl-1*H*-benzo[*d*]imidazole (27c): 81% yield; white solid; ^{1}H NMR (400 MHz, $CDCl_3$) δ 7.82 (dd, *J* = 8.0, 6.6 Hz, 1H), 7.36 (qd, *J* = 12.8, 8.0 Hz, 3H), 7.22 (d, *J* = 8.3 Hz, 2H), 7.01 (d, *J* = 8.3 Hz, 2H), 4.63 (d, *J* = 13.0 Hz, 1H), 4.47 (d, *J* = 13.0 Hz, 1H), 3.59 (s, 3H); ^{13}C NMR (101 MHz, $CDCl_3$) δ 149.73, 141.95, 136.67, 135.11,

131.96, 128.97, 127.55, 124.75, 123.74, 120.80, 109.88, 59.90, 30.23; HRMS (ESI) calcd for $C_{15}H_{13}ClN_2OS$ *m/z* $[M+H]^+$: 305.0515; found: 305.0518; $[\alpha]_D^{22}$= -41.21 (*c* 3.2, CH_2Cl_2); HPLC analysis: Daicel Corporation IB3 (Hex/IPA = 70/30, 1.0 mL/min, 254 nm, 22°C), 9.3, 30.4 (major) min, 97% ee.



27d

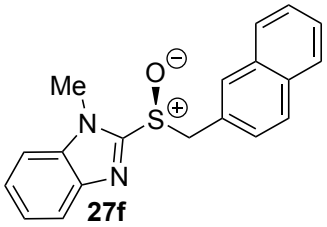
(*S*)-2-((4-Fluorobenzyl)sulfinyl)-1-methyl-1*H*-benzo[*d*]imidazole (27d): 78% yield; white solid; ^{1}H NMR (400 MHz, $CDCl_3$) δ 7.87–7.78 (m, 1H), 7.43–7.29 (m, 3H), 7.04 (dd, *J* = 8.4, 5.5 Hz, 2H), 6.91 (t, *J* = 8.6 Hz, 2H), 4.60 (dd, *J* = 30.8, 13.2 Hz, 2H), 3.56 (s, 3H); ^{13}C NMR (101 MHz, $CDCl_3$) δ 164.47, 162.00, 149.54, 140.37, 136.17, 132.38, 132.30, 125.06, 124.75, 124.71, 124.30, 120.10, 115.91, 115.70, 110.00, 59.95, 30.23; HRMS (ESI) calcd for $C_{15}H_{13}FN_2OS$ *m/z* $[M+H]^+$: 289.0811; found: 289.0808; $[\alpha]_D^{22}$= -33.38 (*c* 4.3, CH_2Cl_2); HPLC analysis: Daicel Corporation IB3 (Hex/IPA = 70/30, 1.0 mL/min, 254 nm, 22°C), 8.9, 29.7 (major) min, 88% ee.



27e

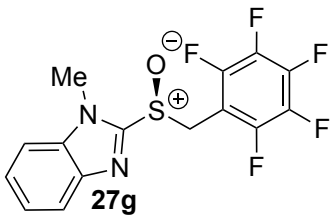
(*S*)-1-Methyl-2-((4-nitrobenzyl)sulfinyl)-1*H*-benzo[*d*]imidazole (27e): 74% yield; yellow solid; ^{1}H NMR (400 MHz, $CDCl_3$) δ 8.10 (d, *J* = 8.3 Hz, 1H), 7.82 (d, *J* = 7.4 Hz, 1H), 7.60–7.27 (m, 2H), 4.72 (dd, *J* = 42.3, 12.9 Hz, 1H), 3.69 (s, 1H); ^{13}C NMR (101 MHz, $CDCl_3$) δ 149.17, 148.18, 141.87, 136.73, 136.60, 131.66, 124.99, 123.91, 123.72, 120.84, 109.96, 59.48, 30.46; HRMS (ESI) calcd for $C_{15}H_{13}N_3O_3S$ *m/z* $[M+H]^+$: 316.0756; found: 316.0761; $[\alpha]_D^{22}$= -

213.88 (*c* 2.3, CH_2Cl_2); HPLC analysis: Daicel Corporation IA3 (Hex/IPA = 70/30, 1.0 mL/min, 254 nm, 22°C), 14.3, 25.0 (major) min, 88% ee.



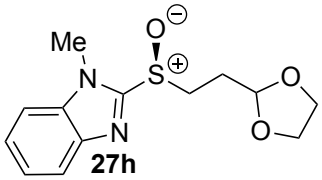
27f

(*S*)-1-Methyl-2-((naphthalen-2-ylmethyl)sulfinyl)-1*H*-benzo[*d*]imidazole (27f): 95% yield; white solid; ^{1}H NMR (400 MHz, $CDCl_3$) δ 7.92–7.85 (m, 1H), 7.77 (d, *J* = 7.8 Hz, 1H), 7.66 (d, *J* = 8.4 Hz, 1H), 7.62 (dd, 1H), 7.58 (s, 1H), 7.50–7.34 (m, 4H), 7.23–7.17 (m, 1H), 7.06 (dd, *J* = 8.4, 1.7 Hz, 1H), 4.82 (d, *J* = 12.9 Hz, 1H), 4.69 (d, *J* = 12.9 Hz, 1H), 3.35 (s, 3H); ^{13}C NMR (101 MHz, $CDCl_3$) δ 149.98, 141.18, 136.34, 133.09, 133.08, 130.23, 128.35, 127.90, 127.65, 127.51, 126.67, 126.54, 126.18, 124.70, 123.83, 120.40, 109.79, 61.21, 30.00; HRMS (ESI) calcd for $C_{19}H_{16}N_2OS$ *m/z* $[M+H]^+$: 321.1062; found: 321.1062; $[\alpha]_D^{22}$= -222.58 (*c* 2.2, CH_2Cl_2); HPLC analysis: Daicel Corporation IB3 (Hex/IPA = 70/30, 1.0 mL/min, 254 nm, 22°C), 10.7, 38.0 (major) min, 99% ee.

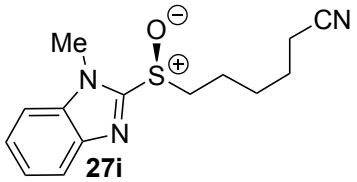


27g

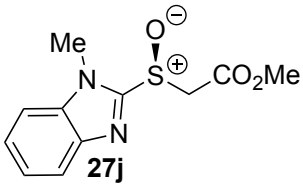
(*S*)-1-Methyl-2-(((perfluorophenyl)methyl)sulfinyl)-1*H*-benzo[*d*]imidazole (27g): 84% yield; white solid; ^{1}H NMR (400 MHz, $CDCl_3$) δ 7.80 (d, *J* = 8.1 Hz, 1H), 7.48–7.33 (m, 3H), 4.88 (d, *J* = 13.2 Hz, 1H), 4.71 (d, *J* = 13.1 Hz, 1H), 4.09 (s, 3H); ^{13}C NMR (101 MHz, $CDCl_3$) δ 149.60, 141.96, 137.04, 125.30, 123.95, 121.11, 109.99, 47.47, 30.92; HRMS (ESI) calcd for $C_{15}H_9F_5N_2OS$ *m/z* $[M+H]^+$: 361.0434; found: 361.0435; $[\alpha]_D^{22}$= -141.82 (*c* 2.2, CH_2Cl_2); HPLC analysis: Daicel Corporation IB3 (Hex/IPA = 70/30, 1.0 mL/min, 254 nm, 22°C), 10.2, 15.6 (major) min, 92% ee.



(*S*)-2-((2-(1,3-Dioxolan-2-yl)ethyl)sulfinyl)-1-methyl-1*H*-benzo[*d*]imidazole (27h): 72% yield; colorless oil; ^{1}H NMR (400 MHz, $CDCl_3$) δ 7.81 (d, *J* = 7.9 Hz, 1H), 7.45–7.36 (m, 2H), 7.34 (ddd, *J* = 8.3, 6.6, 1.8 Hz, 1H), 5.04 (t, *J* = 3.9 Hz, 1H), 4.11 (s, 3H), 4.01–3.92 (m, 2H), 3.89–3.80 (m, 2H), 3.59 (ddd, *J* = 8.3, 6.8, 1.8 Hz, 2H), 2.28 (dddd, *J* = 14.8, 8.0, 6.9, 4.0 Hz, 1H), 2.14 (dddd, *J* = 9.9, 7.5, 6.6, 3.5 Hz, 1H); ^{13}C NMR (101 MHz, $CDCl_3$) δ 151.13, 141.62, 136.73, 124.84, 123.71, 120.85, 109.98, 102.46, 65.26, 47.86, 31.01, 26.58; HRMS (ESI) calcd for $C_{13}H_{16}N_2O_3S$ *m/z* $[M+H]^+$: 281.0960; found: 281.0959; $[\alpha]_D^{22}$= +8.45 (*c* 0.9, $CHCl_3$); HPLC analysis: Daicel Corporation IB3 (Hex/IPA = 70/30, 1.0 mL/min, 254 nm, 22°C), 15.1, 19.3 (major) min, 95% ee.

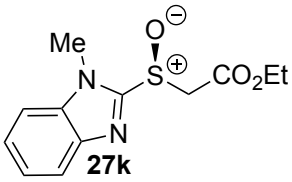


(*S*)-6-((1-Methyl-1*H*-benzo[*d*]imidazol-2-yl)sulfinyl)hexanenitrile (27i): 71% yield; colorless oil; ^{1}H NMR (400 MHz, $CDCl_3$) δ 7.84–7.78 (m, 1H), 7.47–7.39 (m, 2H), 7.37 (ddd, 1H), 4.14 (s, 3H), 3.57 (ddd, *J* = 13.2, 9.4, 5.6 Hz, 1H), 3.45 (ddd, *J* = 13.2, 9.5, 6.3 Hz, 1H), 2.36 (t, *J* = 6.8 Hz, 2H), 2.05–1.81 (m, 2H), 1.79–1.63 (m, 4H); ^{13}C NMR (101 MHz, $CDCl_3$) δ 150.80, 141.27, 136.74, 125.02, 123.96, 120.68, 119.40, 110.09, 52.84, 31.13, 27.71, 25.06, 21.66, 17.05; HRMS (ESI) calcd for $C_{14}H_{17}N_3OS$ *m/z* $[M+Na]^+$: 298.0990; found: 298.0996; $[\alpha]_D^{22}$= +7.71 (*c* 0.7, $CHCl_3$); HPLC analysis: Daicel Corporation IB3 (Hex/IPA = 70/30, 1.0 mL/min, 254 nm, 22°C), 24.6, 41.0 (major) min, 82% ee.



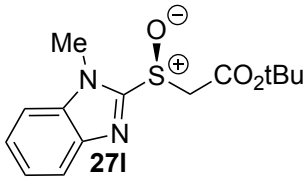
27j

(*S*)-Methyl-2-((1-methyl-1*H*-benzo[*d*]imidazol-2-yl)sulfinyl)acetate (27j): 85% yield; white solid; ^{1}H NMR (400 MHz, $CDCl_3$) δ 7.84–7.77 (m, 1H), 7.46–7.39 (m, 2H), 7.36 (ddd, *J* = 8.3, 6.4, 2.0 Hz, 1H), 4.69 (d, *J* = 15.1 Hz, 1H), 4.44 (d, *J* = 15.1 Hz, 1H), 4.11 (s, 3H), 3.74 (s, 3H); ^{13}C NMR (101 MHz, $CDCl_3$) δ 165.45, 165.43, 150.83, 141.38, 136.67, 125.25, 125.18, 123.97, 121.01, 120.92, 110.20, 57.21, 53.12, 31.04; HRMS (ESI) calcd for $C_{11}H_{12}N_2O_3S$ *m/z* $[M+H]^+$: 253.0647; found: 253.0645; $[\alpha]_D^{22}$= +5.25 (*c* 1.2, CH_2Cl_2); HPLC analysis: Daicel Corporation IB3 (Hex/IPA = 70/30, 1.0 mL/min, 254 nm, 22°C), 15.6, 22.0 (major) min, 89% ee.



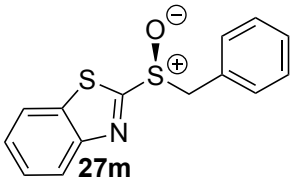
27k

(*S*)-Ethyl-2-((1-methyl-1*H*-benzo[*d*]imidazol-2-yl)sulfinyl)acetate (27k): 92% yield; white solid; ^{1}H NMR (400 MHz, $CDCl_3$) δ 7.80 (d, *J* = 8.0 Hz, 1H), 7.46–7.38 (m, 2H), 7.35 (ddd, *J* = 8.2, 6.5, 1.9 Hz, 1H), 4.65 (t, *J* = 14.3 Hz, 1H), 4.41 (d, *J* = 15.0 Hz, 1H), 4.18 (q, *J* = 7.1 Hz, 2H), 4.10 (s, 3H), 1.21 (t, *J* = 7.1 Hz, 3H); ^{13}C NMR (101 MHz, $CDCl_3$) δ 164.92, 150.95, 141.46, 136.66, 125.11, 123.89, 120.93, 110.16, 62.39, 57.45, 31.01, 14.05; HRMS (ESI) calcd for $C_{12}H_{14}N_2O_3S$ *m/z* $[M+H]^+$: 267.0803; found: 267.0807; $[\alpha]_D^{22}$= +4.62 (*c* 1.2, CH_2Cl_2); HPLC analysis: Daicel Corporation IB3 (Hex/IPA = 70/30, 1.0 mL/min, 254 nm, 22°C), 11.4, 16.6 (major) min, 90% ee.



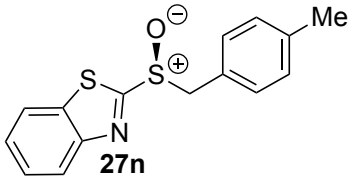
27l

(*S*)-*tert*-Butyl-2-((1-methyl-1*H*-benzo[*d*]imidazol-2-yl)sulfinyl)acetate (27l): 86% yield; white solid; ^{1}H NMR (400 MHz, $CDCl_3$) δ 7.83–7.75 (m, 1H), 7.46–7.38 (m, 2H), 7.35 (ddd, *J* = 8.3, 6.5, 1.9 Hz, 1H), 4.57 (d, *J* = 14.8 Hz, 1H), 4.34 (d, *J* = 14.8 Hz, 1H), 4.11 (s, 3H), 1.39 (s, 9H); ^{13}C NMR (101 MHz, $CDCl_3$) δ 163.93, 151.09, 141.45, 136.64, 125.06, 123.86, 120.89, 110.13, 83.86, 58.46, 31.01, 27.97; HRMS (ESI) calcd for $C_{14}H_{18}N_2O_3S$ *m/z* $[M+Na]^+$: 317.0936; found: 317.0937; $[\alpha]_D^{22}$= +13.78 (*c* 1.1, $CHCl_3$); HPLC analysis: Daicel Corporation IB3 (Hex/IPA = 70/30, 1.0 mL/min, 254 nm, 22°C), 7.3, 8.6 (major) min, 80% ee.



27m

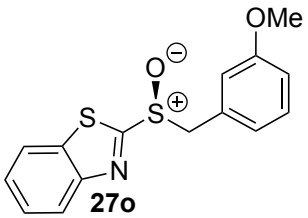
(*S*)-2-(Benzylsulfinyl)benzo[*d*]thiazole (27m): 78% yield; white solid; ^{1}H NMR (400 MHz, $CDCl_3$) δ 8.09 (d, *J* = 8.2 Hz, 1H), 7.93 (d, *J* = 8.1 Hz, 1H), 7.57 (t, *J* = 7.3 Hz, 1H), 7.47 (t, *J* = 7.6 Hz, 1H), 7.34–7.23 (m, 3H), 7.17 (d, *J* = 6.8 Hz, 2H), 4.51 (d, *J* = 13.1 Hz, 1H), 4.33 (d, *J* = 13.1 Hz, 1H); ^{13}C NMR (101 MHz, $CDCl_3$) δ 176.99, 153.74, 136.04, 130.47, 128.75, 128.71, 128.39, 126.93, 126.16, 123.93, 122.26, 118.61, 62.85; HRMS (ESI) calcd for $C_{14}H_{11}NOS_2$ *m/z* $[M+H]^+$: 274.0360; found: 274.0356; $[\alpha]_D^{22}$= -47.99 (*c* 3.3, CH_2Cl_2); HPLC analysis: Chiralcel OD-H (Hex/IPA = 90/10, 1.0 mL/min, 254 nm, 22°C), 13.4 (major), 16.4 min, 93% ee.



27n

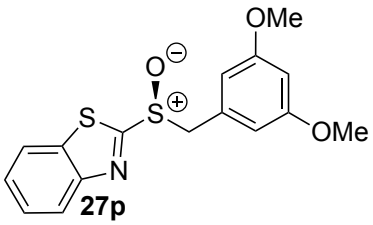
(*S*)-2-((4-Methylbenzyl)sulfinyl)benzo[*d*]thiazole (27n): 70% yield; white solid; ^{1}H NMR (400 MHz, $CDCl_3$) δ 8.10 (d, *J* = 8.2 Hz, 1H), 7.95 (d, *J* = 8.0 Hz, 1H), 7.57 (ddd, *J* = 8.3, 7.3, 1.2 Hz, 1H), 7.48 (ddd, 1H), 7.15–7.01 (m, 4H), 4.48 (d, *J* = 13.1 Hz, 1H), 4.31 (d, *J* = 13.1 Hz, 1H), 2.31 (s, 3H); ^{13}C NMR (101 MHz, $CDCl_3$) δ 177.27, 153.84, 138.80, 136.13, 130.46,

129.56, 127.00, 126.22, 125.37, 124.00, 122.37, 62.82, 21.32; HRMS (ESI) calcd for $C_{15}H_{13}NOS_2$ *m/z* $[M+Na]^+$: 310.0336; found: 310.0333; $[\alpha]_D^{22}$= -74.52 (*c* 1.6, CH_2Cl_2); HPLC analysis: Chiralcel OD-H (Hex/IPA = 90/10, 1.0 mL/min, 254 nm, 22°C), 12.4 (major), 15.9 min, 90% ee.



27o

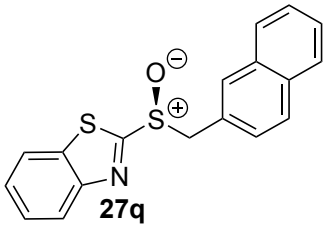
(*S*)-2-((3-Methoxybenzyl)sulfinyl)benzo[*d*]thiazole (27o): 94% yield; white solid; ^{1}H NMR (400 MHz, $CDCl_3$) δ 8.10 (d, *J* = 8.2 Hz, 1H), 7.95 (d, *J* = 8.1 Hz, 1H), 7.57 (ddd, 1H), 7.48 (ddd, 1H), 7.18 (t, *J* = 7.9 Hz, 1H), 6.84 (dd, *J* = 8.2, 2.3 Hz, 1H), 6.79 (d, *J* = 7.5 Hz, 1H), 6.66 (d, *J* = 1.8 Hz, 1H), 4.48 (d, *J* = 13.1 Hz, 1H), 4.30 (d, *J* = 13.1 Hz, 1H), 3.60 (s, 3H); ^{13}C NMR (101 MHz, $CDCl_3$) δ 177.19, 159.82, 153.84, 136.17, 129.86, 129.82, 127.05, 126.29, 124.00, 122.95, 122.39, 115.26, 115.21, 63.17, 55.18, 25.48; HRMS (ESI) calcd for $C_{15}H_{13}NO_2S_2$ *m/z* $[M+H]^+$: 304.0466; found: 304.0467; $[\alpha]_D^{22}$= -59.08 (*c* 3.1, CH_2Cl_2); HPLC analysis: Daicel Corporation IB3 (Hex/IPA = 70/30, 1.0 mL/min, 254 nm, 22°C), 7.3 (major), 7.6 min, 91% ee.



27p

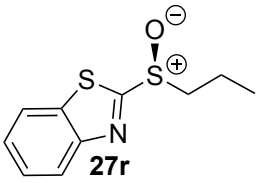
(*S*)-2-((3,5-Dimethoxybenzyl)sulfinyl)benzo[*d*]thiazole (27p): 86% yield; white solid; ^{1}H NMR (400 MHz, $CDCl_3$) δ 8.09 (d, *J* = 8.2 Hz, 1H), 7.96 (d, *J* = 8.1 Hz, 1H), 7.56 (ddd, 1H), 7.48 (ddd, *J* = 11.2, 4.1 Hz, 1H), 6.41–6.35 (m, 1H), 6.31 (d, *J* = 2.2 Hz, 2H), 4.43 (d, *J* = 13.0 Hz, 1H), 4.26 (d, *J* = 13.0 Hz, 1H), 3.60 (s, 6H); ^{13}C NMR (101 MHz, $CDCl_3$) δ 177.30, 160.97, 153.85, 136.20, 130.55, 127.07, 126.32, 124.00, 122.41, 108.22, 101.57, 63.57, 55.35; HRMS

(ESI) calcd for $C_{16}H_{15}NO_3S_2$ *m/z* $[M+H]^+$: 334.0572; found: 334.0574; $[\alpha]_D^{22}$= -166.21 (*c* 3.1, $CHCl_3$); HPLC analysis: Chiralcel OD-H (Hex/IPA = 90/10, 0.5 mL/min, 254 nm, 22°C), 37.8 (major), 42.4 min, 92% ee.



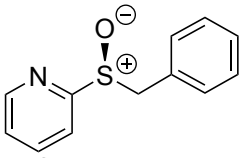
27q

(*S*)-2-((Naphthalen-2-ylmethyl)sulfinyl)benzo[*d*]thiazole (27q): 85% yield; white solid; ^{1}H NMR (400 MHz, $CDCl_3$) δ 8.12 (d, *J* = 8.2 Hz, 1H), 7.90 (d, *J* = 8.1 Hz, 1H), 7.83–7.76 (m, 1H), 7.72 (dd, *J* = 8.7, 4.9 Hz, 3H), 7.58 (ddd, 1H), 7.51–7.41 (m, 3H), 7.25 (dd, *J* = 8.5, 1.7 Hz, 1H), 4.68 (d, *J* = 13.1 Hz, 1H), 4.50 (d, *J* = 13.1 Hz, 1H); ^{13}C NMR (101 MHz, $CDCl_3$) δ 177.12, 153.87, 136.14, 133.27, 133.26, 130.36, 128.59, 128.10, 127.79, 127.58, 127.05, 126.66, 126.51, 126.26, 124.02, 122.38, 63.41.; HRMS (ESI) calcd for $C_{18}H_{13}NOS_2$ *m/z* $[M+H]^+$: 324.0517; found: 324.0523; $[\alpha]_D^{22}$= -78.47 (*c* 2.2, CH_2Cl_2); HPLC analysis: Chiralcel AS-H (Hex/IPA = 90/10, 1.0 mL/min, 254 nm, 22°C), 36.1, 43.4 (major) min, 91% ee.



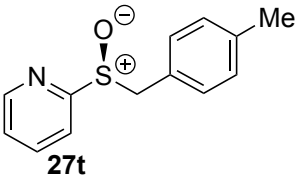
27r

(*S*)-2-(Propylsulfinyl)benzo[*d*]thiazole (27r): 70% yield; colorless oil; ^{1}H NMR (400 MHz, $CDCl_3$) δ 8.04 (d, *J* = 8.2 Hz, 1H), 7.98 (d, *J* = 8.0 Hz, 1H), 7.54 (t, *J* = 7.7 Hz, 1H), 7.47 (t, *J* = 7.6 Hz, 1H), 3.26–3.11 (m, 2H), 1.99 (tq, *J* = 14.8, 7.4 Hz, 1H), 1.76 (tq, 1H), 1.08 (t, *J* = 7.4 Hz, 3H); ^{13}C NMR (101 MHz, $CDCl_3$) δ 177.86, 153.99, 136.02, 126.99, 126.21, 123.97, 122.36, 116.21, 58.61, 15.53, 13.24; HRMS (ESI) calcd for $C_{10}H_{11}NOS_2$ *m/z* $[M+Na]^+$: 248.0180; found: 248.0176; $[\alpha]_D^{22}$= -1.15 (*c* 2.0, CH_2Cl_2); HPLC analysis: Chiralcel OB-H (Hex/IPA = 90/10, 1.0 mL/min, 254 nm, 22°C), 12.3 (major), 14.5 min, 91% ee.



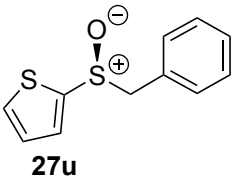
27s

(*S*)-2-(Benzylsulfinyl)pyridine (27s): 76% yield; white solid; ^{1}H NMR (400 MHz, $CDCl_3$) δ 8.69 (d, *J* = 4.3 Hz, 1H), 7.80 (td, *J* = 7.7, 1.7 Hz, 1H), 7.63 (d, *J* = 7.9 Hz, 1H), 7.37 (ddd, *J* = 7.6, 4.7, 1.1 Hz, 1H), 7.31 – 7.21 (m, 3H), 7.04 (dd, *J* = 7.7, 1.6 Hz, 2H), 4.40 (d, *J* = 13.1 Hz, 1H), 4.10 (d, *J* = 13.1 Hz, 1H); ^{13}C NMR (101 MHz, $CDCl_3$) δ 163.64, 149.11, 137.86, 130.27, 129.31, 128.31, 128.17, 124.67, 120.73, 59.97; HRMS (ESI) calcd for $C_{12}H_{11}NOS$ *m/z* $[M+H]^+$: 218.0640; found: 218.0639; $[\alpha]_D^{22}$= -205.63 (*c* 2.6, $CHCl_3$); HPLC analysis: Chiralcel OD-H (Hex/IPA = 90/10, 1.0 mL/min, 254 nm, 22°C), 17.7 (major), 21.9 min, 80% ee.



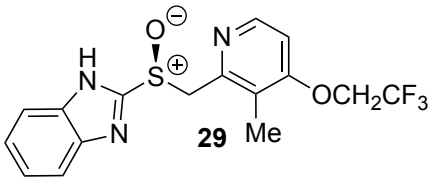
27t

(*S*)-2-((4-Methylbenzyl)sulfinyl)pyridine (27t): 96% yield; white solid; ^{1}H NMR (400 MHz, $CDCl_3$) δ 8.71–8.51 (m, 1H), 7.78 (td, *J* = 7.7, 1.7 Hz, 1H), 7.62 (dt, *J* = 7.9, 0.9 Hz, 1H), 7.33 (ddd, *J* = 7.6, 4.7, 1.2 Hz, 1H), 7.02 (d, *J* = 7.8 Hz, 2H), 6.89 (d, *J* = 8.0 Hz, 2H), 4.33 (d, *J* = 13.1 Hz, 1H), 4.03 (d, *J* = 13.1 Hz, 1H), 2.28 (s, 3H); ^{13}C NMR (101 MHz, $CDCl_3$) δ 163.90, 149.26, 138.08, 137.84, 130.25, 129.14, 126.26, 124.67, 120.77, 59.87, 21.24; HRMS (ESI) calcd for $C_{13}H_{13}NOS$ *m/z* $[M+Na]^+$: 254.0616; found: 254.0620; $[\alpha]_D^{22}$= -253.06 (*c* 3.4, $CHCl_3$); HPLC analysis: Chiralcel OB-H (Hex/IPA = 90/10, 0.5 mL/min, 254 nm, 22°C), 21.7 (major), 25.5 min, 85% ee.



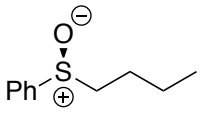
27u

(*S*)-2-(Benzylsulfinyl)thiophene (27u): 53% yield; white solid; ^{1}H NMR (400 MHz, $CDCl_3$) δ 7.62 (d, *J* = 4.9 Hz, 1H), 7.32–7.24 (m, 3H), 7.13 (t, *J* = 4.1 Hz, 1H), 7.08 (dd, *J* = 7.2, 1.9 Hz, 2H), 7.05–6.98 (m, 1H), 4.36 (d, *J* = 12.4 Hz, 1H), 4.15 (d, *J* = 12.4 Hz, 1H); ^{13}C NMR (101 MHz, $CDCl_3$) δ 144.93, 131.19, 130.33, 129.89, 129.34, 128.80, 128.58, 127.28, 65.14; HRMS (ESI) calcd for $C_{11}H_{10}OS_2$ *m/z* $[M+H]^+$: 245.0071; found: 245.0071; $[\alpha]_D^{22}$= +73.96 (*c* 1.0, $CHCl_3$); HPLC analysis: Chiralcel OD-H (Hex/IPA = 90/10, 1.0 mL/min, 254 nm, 22°C), 18.5, 25.0 (major) min, 95% ee.



29

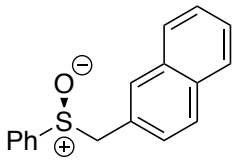
(*S*)-2-(((3-Methyl-4-(2,2,2-trifluoroethoxy)pyridin-2-yl)methyl)sulfinyl)-1*H*-benzo[*d*]imidazole or (*S*)-Lansoprazole (29): 81% yield; white solid; ^{1}H NMR (400 MHz, Acetone) δ 8.38 (d, *J* = 5.6 Hz, 1H), 7.75 (d, *J* = 3.1 Hz, 2H), 7.40 (dd, *J* = 6.1, 3.2 Hz, 2H), 7.13 (d, *J* = 5.7 Hz, 1H), 4.93–4.90 (AB-system, *J* = 13.5 Hz, 2H), 4.89–4.84 (q, *J* = 7.8 Hz, 2H), 2.33 (s, 3H); ^{13}C NMR (101 MHz, Acetone) δ 162.69, 155.37, 152.14, 149.15, 126.02, 124.16, 123.71, 123.27, 107.52, 66.50, 66.15, 65.80, 65.44, 61.80, 61.75, 11.07; HRMS (ESI) calcd for $C_{16}H_{14}F_3N_3O_2S$ *m/z* $[M+H]^+$: 370.0837; found: 370.0838; $[\alpha]_D^{22}$= -253.8 (*c* 0.5, Acetone); HPLC analysis: Chiralcel OD-H (Hex/IPA = 80/20, 0.7 mL/min, 254 nm, 22°C), 22.9 (major), 33.3min, 90% ee.



31a

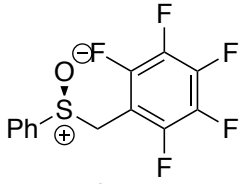
(*S*)-(Butylsulfinyl)benzene (31a): 79% yield; colorless oil; ^{1}H NMR (400 MHz, $CDCl_3$) δ 7.63–7.58 (m, 2H), 7.52–7.45 (m, 3H), 2.77 (dt, 2H), 1.79–1.65 (m, 1H), 1.64–1.51 (m, 1H), 1.50–1.34 (m, 2H), 0.89 (t, *J* = 7.3 Hz, 3H); ^{13}C NMR (101 MHz, $CDCl_3$) δ 143.97, 130.91,

129.18, 124.04, 57.01, 24.13, 21.87, 13.62; HRMS (ESI) calcd for $C_{10}H_{14}OS$ *m/z* $[M+H]^+$: 183.0844; found: 183.0849; $[\alpha]_D^{22}$= -165.82 (*c* 0.73, CH_2Cl_2); HPLC analysis: Chiralcel OB-H (Hex/IPA = 50/50, 0.5 mL/min, 254 nm, 22°C), 9.5 (major), 12.2 min, 90% ee.



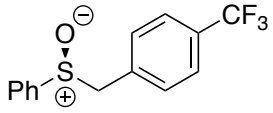
31b

(*S*)-2-((Phenylsulfinyl)methyl)naphthalene (31b): 93% yield; white solid; ^{1}H NMR (400 MHz, $CDCl_3$) δ 7.83–7.76 (m, 2H), 7.71 (dd, *J* = 8.6, 5.9 Hz, 2H), 7.50–7.42 (m, 4H), 7.39 (d, *J* = 4.3 Hz, 4H), 7.08 (dd, *J* = 8.4, 1.7 Hz, 1H), 4.25 (d, *J* = 12.6 Hz, 1H), 4.16 (d, *J* = 12.6 Hz, 1H); ^{13}C NMR (101 MHz, $CDCl_3$) δ 142.88, 133.18, 133.02, 131.30, 129.93, 128.98, 128.23, 127.95, 127.81, 127.75, 126.71, 126.44, 126.41, 124.56, 64.00; HRMS (ESI) calcd for $C_{17}H_{14}OS$ *m/z* $[M+H]^+$: 267.0844; found: 267.0850; $[\alpha]_D^{22}$= -41.85 (*c* 1.3, CH_2Cl_2); HPLC analysis: Chiralcel OD-H (Hex/IPA = 90/10, 1.0 mL/min, 254 nm, 22°C), 18.7, 22.2 (major) min, 86% ee.



31c

(*S*)-1,2,3,4,5-Pentafluoro-6-((phenylsulfinyl)methyl)benzene (31c): 82% yield; white solid; ^{1}H NMR (400 MHz, $CDCl_3$) δ 7.63–7.38 (m, 5H), 4.19 (d, *J* = 13.0 Hz, 1H), 4.09 (d, *J* = 13.0 Hz, 1H); ^{13}C NMR (101 MHz, $CDCl_3$) δ 142.57, 132.14, 129.45, 124.05, 50.40; HRMS (ESI) calcd for $C_{13}H_7F_5OS$ *m/z* $[M+H]^+$: 307.0216; found: 307.0221; $[\alpha]_D^{22}$= -102.15 (*c* 1.5, CH_2Cl_2); HPLC analysis: Chiralcel OD-H (Hex/IPA = 90/10, 1.0 mL/min, 254 nm, 22°C), 10.7, 12.1 (major) min, 90% ee.



31d

(*S*)-1-((Phenylsulfinyl)methyl)-4-(trifluoromethyl)benzene (31d): 99% yield; white solid; ^{1}H NMR (400 MHz, $CDCl_3$) δ 7.56–7.30 (m, 7H), 7.07 (d, *J* = 8.0 Hz, 2H), 4.10 (d, *J* = 12.7 Hz, 1H), 4.01 (d, *J* = 12.7 Hz, 1H); ^{13}C NMR (101 MHz, $CDCl_3$) δ 142.36, 133.18, 131.55, 130.81, 129.15, 125.37, 125.33, 124.39, 62.60; HRMS (ESI) calcd for $C_{14}H_{11}F_3OS$ *m/z* $[M+H]^+$: 285.0561; found: 285.0555; $[\alpha]_D^{22}$= -88.63 (*c* 1.5, CH_2Cl_2); HPLC analysis: Chiralcel OD-H (Hex/IPA = 90/10, 1.0 mL/min, 254 nm, 22°C), 12.7, 14.0 (major) min, 88% ee.

References

(1) Fernandez, I.; Khiar, N. Recent Developments in the Synthesis and Utilization of Chiral Sulfoxides. *Chem. Rev.* **2003**, *103*, 3651.

(2) Kagan, H. B.; Luukas, T. O. Transition Metals for Organic Synthesis: Building Blocks and Fine Chemicals, *Second Revised and Enlarged Edition.* **2004**: 479.

(3) Kagan, H. B. *Wiley-VCH: Weinheim, Germany,* **2008**.

(4) O'Mahony, G. E.; Ford, A.; Maguire, A. R. Asymmetric Oxidation of Sulfides. *J. Sulfur Chem.* **2013**, *34*, 301.

(5) Kagan, H. B.; Rebiere, F. Some Routes to Chiral Sulfoxides with Very High Enantiomeric Excesses. *Synlett* **1990**, *11*, 643.

(6) Davis, F. A.; Reddy, R. T.; Han, W.; Carroll, P. J. Chemistry of Oxaziridines. 17. N-(Phenylsulfonyl)(3, 3-dichlorocamphoryl) Oxaziridine: a Highly Efficient Reagent for the Asymmetric Oxidation of Sulfides to Sulfoxides. *J. Am. Chem. Soc.* **1992**, *114*, 1428.

(7) Legros, J.; Bolm, C. Highly Enantioselective Iron-Catalyzed Sulfide Oxidation with Aqueous Hydrogen Peroxide under Simple Reaction Conditions. *Angew. Chem. Int. Ed.* **2004**, *43*, 4225.

(8) Drago, C.; Caggiano, L.; Jackson, R. F. Vanadium-Catalyzed Sulfur Oxidation/Kinetic Resolution in the Synthesis of Enantiomerically Pure Alkyl Aryl Sulfoxides. *Angew. Chem. Int. Ed.* **2005**, *44*, 7221.

(9) Fujisaki, J.; Matsumoto, K.; Matsumoto, K.; Katsuki, T. Catalytic Asymmetric Oxidation of Cyclic Dithioacetals: Highly Diastereo-and Enantioselective Synthesis of the S-Oxides by a Chiral Aluminum (Salalen) Complex. *J. Am. Chem. Soc.* **2011**, *133*, 56.

(10) Liao, S.; Čorić, I.; Wang, Q.; List, B. Activation of H2O2 by Chiral Confined Brønsted Acids: a Highly Enantioselective Catalytic Sulfoxidation. *J. Am. Chem. Soc.* **2012**, *134*, 10765.

(11) Bhadra, S.; Akakura, M.; Yamamoto, H. Design of a New Bimetallic Catalyst for Asymmetric Epoxidation and Sulfoxidation. *J. Am. Chem. Soc.* **2015**, *137*, 15612.

(12) Ooi, T.; Ohara, D.; Tamura, M.; Maruoka, K. Design of New Chiral Phase-Transfer Catalysts with Dual Functions for Highly Enantioselective Epoxidation af α,β-Unsaturated Ketones. *J. Am. Chem. Soc.* **2004**, *126*, 6844.

(13) Shirakawa, S.; Wu, X.; Maruoka, K. Kinetic Resolution of Axially Chiral 2-Amino-1, 1′-Biaryls by Phase-Transfer-Catalyzed N-Allylation. *Angew. Chem. Int. Ed.* **2013**, *52*, 4312.

(14) Ooi, T.; Maruoka, K. Recent Advances in Asymmetric Phase-Transfer Catalysis. *Angew. Chem. Int. Ed.* **2007**, *46*, 4222.

(15) Uyanik, M.; Okamoto, H.; Yasui, T.; Ishihara, K. Quaternary Ammonium (hypo) Iodite Catalysis for Enantioselective Oxidative Cycloetherification. *Science*. **2010**, *328*, 1376.

(16) Uyanik, M.; Hayashi, H.; Ishihara, K. High-Turnover Hypoiodite Catalysis for Asymmetric Synthesis of Tocopherols. *Science*. **2014**, *345*, 291.

(17) Wang, C.; Zong, L.; Tan, C. H. Enantioselective Oxidation of Alkenes with Potassium Permanganate Catalyzed by Chiral Dicationic Bisguanidinium. *J. Am. Chem. Soc.* **2015**, *137*, 10677.

(18) Brak, K.; Jacobsen, E. N. Asymmetric Ion-Pairing Catalysis. *Angew. Chem. Int. Ed.* **2013**, *52*, 534.

(19) Mahlau, M.; List, B. Asymmetric Counteranion-Directed Catalysis: Concept, Definition, and Applications. *Angew. Chem. Int. Ed.* **2013**, *52*, 518.

(20) Phipps, R. J.; Hamilton, G. L.; Toste, F. D. The Progression of Chiral Anions from Concepts to Applications in Asymmetric Catalysis. *Nat. Chem.* **2012**, *4*, 603.

(21) Campestrini, S. A. N. D. R. O.; Conte, V.; Di Furia, F.; Modena, G.; Bortolini, O. Metal Catalysis in Oxidation by Peroxides. 30. Electrophilic Oxygen Transfer from Anionic, Coordinatively Saturated Molybdenum Peroxo Complexes. *J. Org. Chem.* **1988**, *53*, 5721.

(22) Yang, C. H.; Dzugan, S. J.; Goedken, V. L. Structure and Reactivity of an Unusual Tungsten (Vi) Porphyrin Complex Having Cis Oxo And Peroxo Groups. *J. Chem. Soc., Chem. Commun.* **1985**, *20*, 1425.

(23) Amato, G.; Arcoria, A.; Ballistreri, F. P.; Tomaselli, G. A.; Bortolini, O.; Conte, V.; Valle, G. Oxidations with Peroxotungsten Complexes: Rates and Mechanism of Stoichiometric Olefin Epoxidations. *J. Mol. Catal.* **1986**, *37*, 165.

(24) Jacobson, S. E.; Tang, R.; Mares, F. Group 6 Transition Metal Peroxo Complexes Stabilized by Polydentate Pyridinecarboxylate Ligands. *Inorg. Chem.* **1978**, *17*, 3055.

Chapter 4

Bisguanidinium Tetraperoxyditungstate Catalyzed Epoxidation

4.1 Introduction

Asymmetric epoxidation of allylic amines is one of the most versatile reactions, as the chiral amino-epoxides obtained can be further derivatized to amino alcohols, which are present in the scaffold of many drugs and natural products.[1-2] Due to the competitive *N*-oxidation of amines,[3] there are only few reports on peracid-mediated epoxidations of allylic amines.[4-8] Chemo- and diastereoselective epoxidation of allylic amines have been developed either through *N*-oxide[9-12] or protonated ammonium cation.[13] For similar reasons, there are also few reports on chiral ligand mediated metal-catalyzed asymmetric epoxidation of allylic amines.[14-15] The few examples included Yamamoto's report on the use of Hf(IV)-bishydroxamic acid complex-catalyzed asymmetric epoxidation that was successful for a wide range of substrates including allylic sulfonamides, homoallylic sulfonamides, aldimine and ketimine (Figure 4.1).[14] Separately, he utilized chiral Schiff base/titanium(IV) catalyst for asymmetric epoxidation of the *N*-alkenyl sulfonamides and homoallylic sulfonamides.[15]

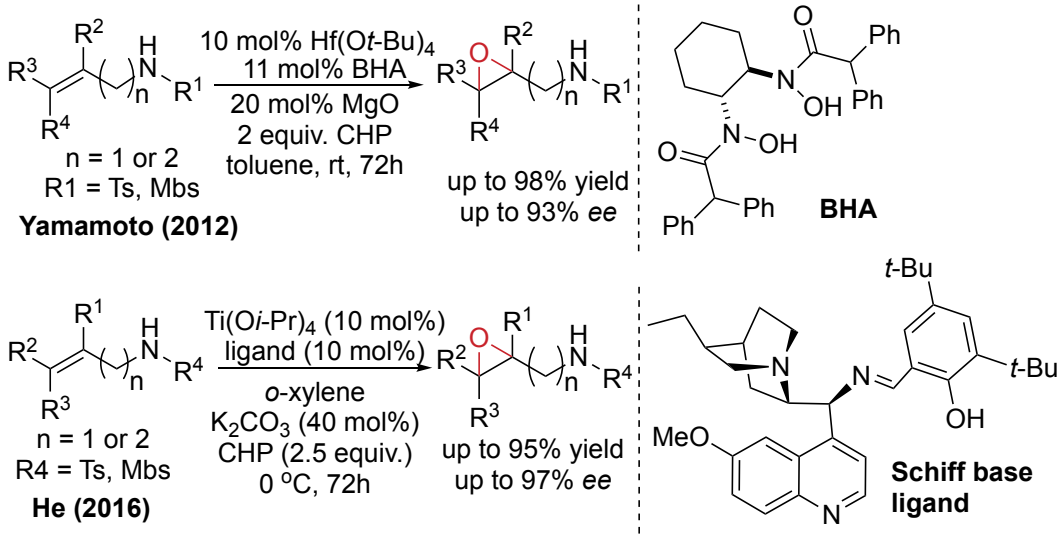


Figure 4.1 Highly enantioselective epoxidation of allylic and homoallylic amines using chiral ligand-mediated metal-catalyzed reactions.

We recently demonstrated that ion pair catalyst consisting of a chiral cationic and an inorganic anionic salt can catalyze several reactions with high stereoselectivity.[16-20] We demonstrated that bisguanidinium permanganate can mediate enantioselective dihydroxylation and oxohydroxylation[17] of α,β-unsaturated esters. We have also developed highly efficient and highly enantioselective bisguanidinum-catalyzed sulfoxidation[18,21] of heterocyclic sulfides and alkyl aryl sulfides using aqueous hydrogen peroxide as oxidant. Diphosphatobisperoxotungstate[21] and dinuclear oxodiperoxomolybdosulfate[18] were identified to be the active anionic species respectively (Figure 4.2).

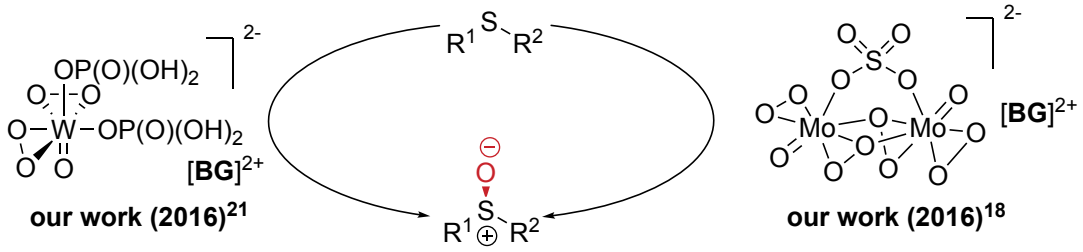


Figure 4.2 Our previous studies of highly enantioselective sulfoxidations using ion pair catalysts.

Thus, we like to expand the scope of ion pair catalysis of anionic metal oxides to include asymmetric epoxidation of challenging olefin substrates (Figure 4.3).

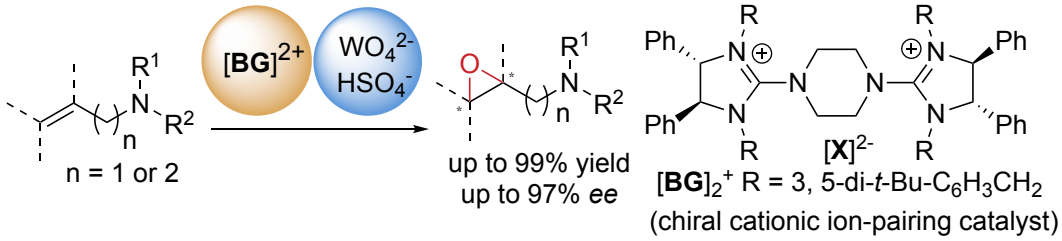


Figure 4.3 This work using chiral cationic ion pair strategy for asymmetric epoxidation of allylic and homoallylic amines.

In this report, we disclose a highly enantioselective epoxidation of allylic amines using a new ion pair catalyst that consists of a chiral cationic bisguanidinium [**BG**]$^{2+}$and achiral tetraperoxyditungstate anion $[W_2O_2(\mu\text{-}O)(O_2)_4]^{2-}$ (Figure 4.4).

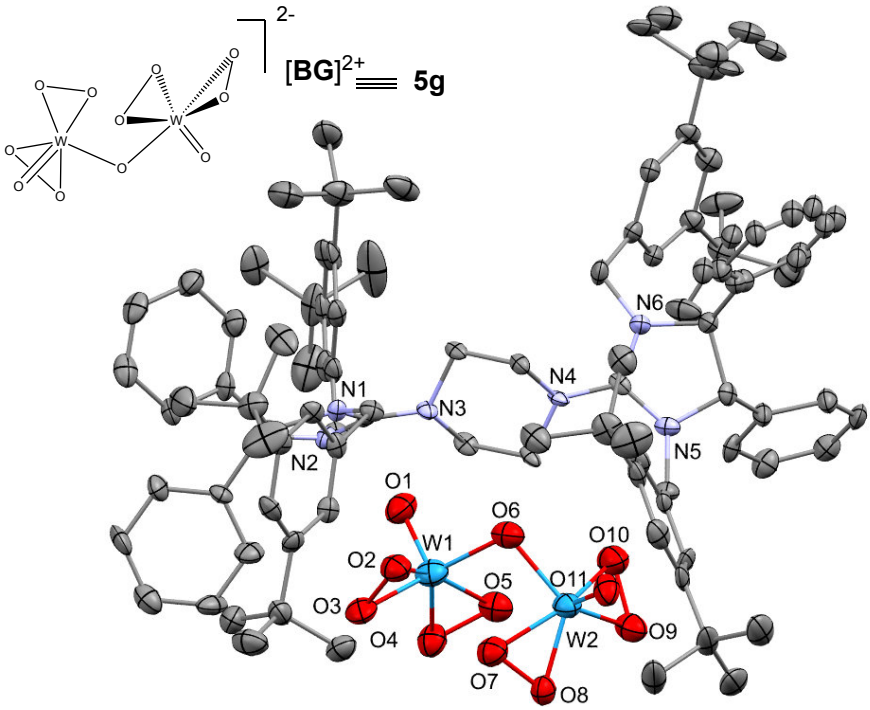


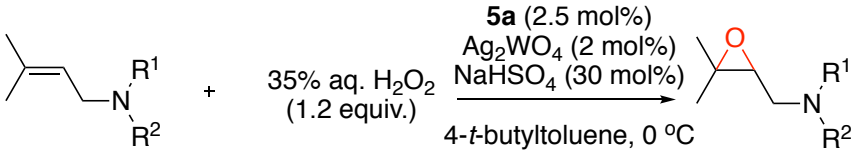
Figure 4.4 *X*-Ray crystallographic structure of $[\mathbf{BG}]^{2+}[W_2O_2(\mu\text{-}O)(O_2)_4]^{2-}$ **5g** (ellipsoids at 50% probability).

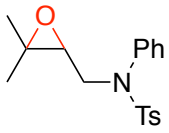
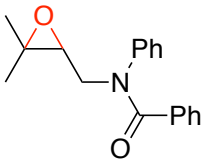
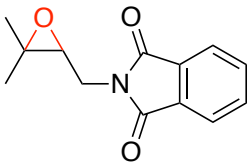
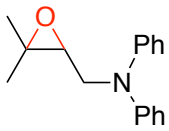
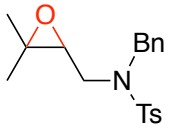
4.2 Results and discussion

4.2.1 Reaction development

As amines are more prone to be oxidized than olefin, protecting groups were added to the amines to circumvent this chemoselectivity issue. Initially, we chose a series of 1,1'-allylic amides as reactant. It was obvious that the substrates with tosyl group led to better results than others (Table 4.1, entry 1,5). Thus, in the following work, we applied tosyl group in most substrates to established the epoxidation reaction.

Table 4.1 Exploration of substrate scope [a]



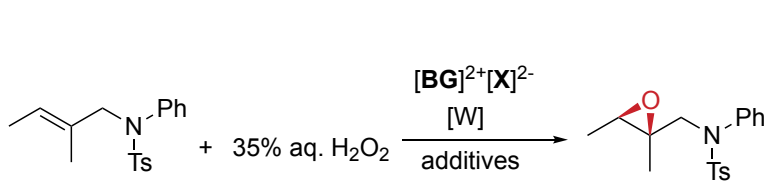
Entry	**Substrate**	yield (%)[b]	ee (%)[c]
1		77	63
2		22	40
3		10	11
4		45	11
5		83	54

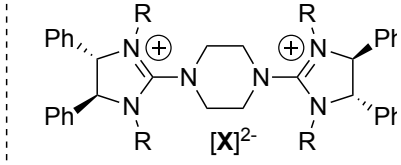
[a]Reaction conditions: **substrate** (0.05 mmol), H_2O_2 (0.06 mmol, 1.20 equiv., 35%w/w), **5a** (0.0025 mmol, 2.5 mol%), Ag_2WO_4 (0.002 mmol, 2.0 mol%), $NaHSO_4$ (0.015mmol, 30.0 mol%), 500 µL solvent at 0 °C. [b]Yield of isolated product. [c]Determined with HPLC analysis using a chiral stationary phase.

We have previously shown that a highly efficient and highly enantioselective bisguanidinum-catalyzed sulfoxidation was achieved using bisguanidinium diphosphatobisperoxotungstate as the catalyst.[21] Using this catalyst, we tested tosyl and phenyl di-protected allylic amine **34a** and found that low yield (5%) of allylic expoxide **35a** was isolated (Table 4.2, entry 3). We then tested conditions without any additive (entry 1), with acetic acid (entry 2) and with sodium hydrogen sulfate, $NaHSO_4$ (entry 4). We found that moderate yield (52%) and good *ee* value (60%) were obtained for allylic expoxide **35a**, when $NaHSO_4$ was used as the additive in a sub-stoichiometric amount (0.3 equiv.) (entry 4). No side products from the oxidation of nitrogen was observed. When the reaction temperature was carried out at 0 °C, *ee* value of allylic expoxide **35a** improved to 67%; however, the yield

decreased to 16% (entry 5). The counterion effect of the tungstate was also examined (entries 5-8) and Ag_2WO_4 was found to give the best results. We propose that the efficient formation of AgCl from Ag_2WO_4 and bisguanidinium chloride allows the complete formation of the ion pair catalyst and this was important to improve the reactivity and selectivity of the reaction (entry 8). Solvent also play a vital role in determining the reactivity and stereoselectivity of this reaction (entry 8-11). After screening a large number of solvents, it was revealed that 4-*tert*-butyltoluene proved to give the best yield (89%) and best enantioselectivity (94% *ee*) (entry 11). We also examined the additives, and $NaHSO_4$ promoted the reaction best (entry 11-14). Later, we found a premade catalyst **5g** could work in the system alone and give high *ee* value. If $NaHSO_4$ is used as an additive (entry 16), both the yield and *ee* value reached to the same level as the *in situ* condition (entry 11).

Table 4.2 Optimization of Asymmetric Epoxidation of Protected 1,2-Allylic Amine[a]





[**BG**]$^{2+}$: R = 3, 5-di-*t*-Bu-C_6H_3CH
5a = [**BG**]$^{2+}$.2[**Cl**]$^-$
5g = [**BG**]$^{2+}$[$\mathbf{W_2O_2(\mu\text{-}O)(O_2)_4}$]$^{2-}$

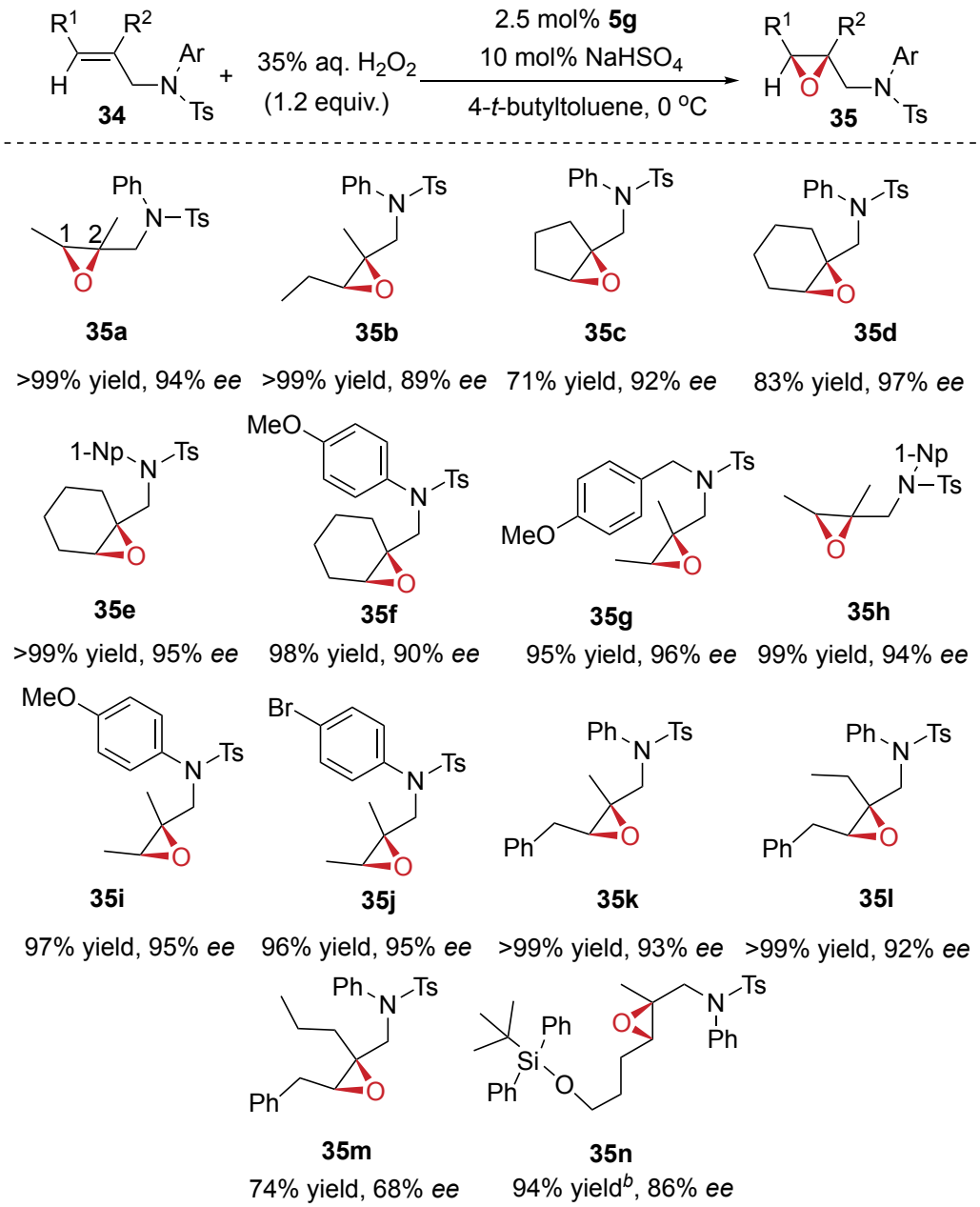
Entr	[**BG**]$^{2+}$[**X**]$^{2-}$	[W]	Additive	Solvent	T (°C)	yield (%)[b]	*ee* (%)[c]
1	**5a**	Na_2WO_4	-	toluene	r.t.	N.R.	N.A.
2	**5a**	Na_2WO_4	CH_3CO_2H	toluene	r.t.	<5	10
3	**5a**	Na_2WO_4	$NaH_2PO_4.H_2O$	toluene	r.t.	5	-13
4	**5a**	Na_2WO_4	$NaHSO_4$	toluene	r.t.	52[d]	60
5	**5a**	Na_2WO_4	$NaHSO_4$	toluene	0	16	67
6	**5a**	Cs_2WO_4	$NaHSO_4$	toluene	0	50	70
7	**5a**	$CaWO_4$	$NaHSO_4$	toluene	0	15	60
8	**5a**	Ag_2WO_4	$NaHSO_4$	toluene	0	38	75
9	**5a**	Ag_2WO_4	$NaHSO_4$	CH_2Cl_2	0	13	20
10	**5a**	Ag_2WO_4	$NaHSO_4$	*i*-Pr_2O	0	47	86
11	**5a**	Ag_2WO_4	$NaHSO_4$	4-*t*-butyltoluene	0	89	94
12	**5a**	Ag_2WO_4	$KHSO_4$	4-*t*-butyltoluene	0	89	90
13	**5a**	Ag_2WO_4	$TBAHSO_4$	4-*t*-butyltoluene	0	10	90
14	**5a**	Ag_2WO_4	$NaH_2PO_4.H_2O$	4-*t*-butyltoluene	0	17	-28

15[e]	**5g**	-	-	4-*t*-butyltoluene	0	57	92
16[f]	**5g**	-	$NaHSO_4$	4-*t*-butyltoluene	0	>99	94

[a]Reaction conditions: **34a** (0.05 mmol), H_2O_2 (0.06 mmol, 1.20 equiv., 35%w/w), $[\mathbf{BG}]^{2+}[\mathbf{X}]^{2-}$ (0.0025 mmol, 2.5 mol%), $M_x(WO_4)_y$ (0.002 mmol, 2.0 mol%), additive (0.015mmol, 30.0 mol%), 500 μL solvent at 0 °C. [b]Yield of isolated product. [c]Determined with HPLC analysis using a chiral stationary phase. [d]39% of **34a** was recovered. [e]The ion pair catalyst **5g** (0.0025 mmol, 2.5 mol%) was premade and used directly with substrate (0.05 mmol) and H_2O_2 (0.06 mmol, 1.20 equiv., 35%w/w) in 500 μL solvent. [f]Based on the condition with premade catalyst **5g** (0.0025 mmol, 2.5 mol%), add extra $NaHSO_4$ (0.005 mol, 10.0 mol%) at the beginning of the experiment.

With the optimized conditions in hand, we are keen to know how the protecting groups on the amine and substitution pattern of the olefin affect the reactivity and enantioselectivity of the epoxidation. We used **5g** along with $NaHSO_4$ as the additive (condition of Table 4.2, entry 16) to explore the substrates scope of 1,2-allylic amines, and the results showed moderate to excellent yields (71 to 99% yield) and good to excellent enantioselectivities (68 to 97% *ee*). Compared to **35a**, increasing the alkyl chain length at 1-position to two carbons saw a drop in enantioselectivity of the epoxide **35b** (89% *ee*). However, when the 1- and 2-position were linked to form cyclic allylic amines, the *ee* values increased to 92% and 97% respectively for epoxides **35c** and **35d**. Next, the effect of the aromatic protecting groups on nitrogen was investigated. 1-Napthyl (abbreviated as 1-Np in Scheme 4.1) protected cyclic epoxide **35e** and *para*-methoxyphenyl protected cyclic epoxide **35f** were obtained in excellent enantioselectivities (90-95% *ee*). The effect of other protecting groups was also evaluated; *para*-methoxylbenzyl, 1-napthyl, *para*-methoxyphenyl, and *para*-bromophenyl protected acyclic epoxide **35g-j** were obtained in 94-96% *ee*. From these results, it was observed that aryl-protecting group on nitrogen does not affect the enantioselectivity of the epoxides significantly. When a phenyl group was added to the terminal position of alkene on 1-position, both yields and *ee* values remained unaffected; but when the length of alkyl chain on 2-position was increased to 3-carbons, the yields are slightly decreased (**35k-m**). When we lengthen the alkyl chain on position-1 with silyl-protected alcohol group, acyclic epoxide **35n** was obtained

in good yield but slightly lower *ee* value. A single crystal of amino-epoxide **35e**, suitable for X-ray structural analysis, was obtained and the absolute stereochemistry was determined to be (*R*,*R*).

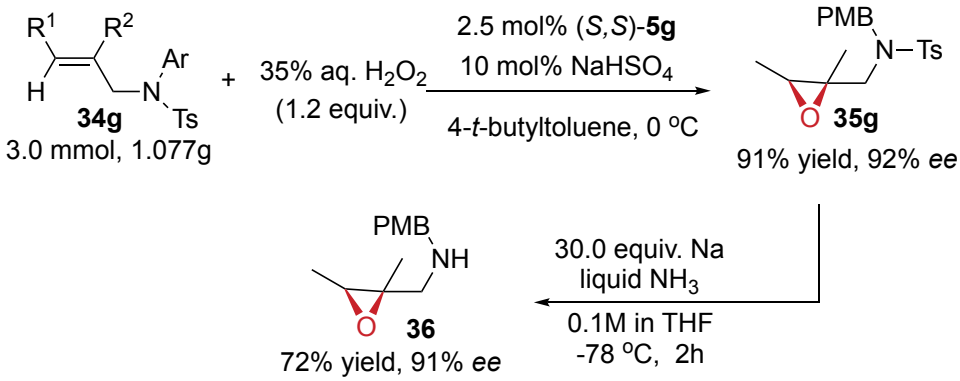


[a]Reaction conditions: **34** (0.1 mmol), H_2O_2 (0.12 mmol, 1.20 equiv, 35%w/w), **5g** (0.0025 mmol, 2.5 mol%), $NaHSO_4$ (0.01 mmol, 10.0 mol%), 1.0 mL solvent at 0 °C. Yields were obtained by chromatographic purification. Enantiomeric excess was determined using chiral HPLC. [b]Reaction was conducted at R.T. 1-Np is 1-napthyl.

Scheme 4.1 Asymmetric epoxidation of protected 1,2-allylic amine 34[a]

The ability of this methodology to be carried out on a larger scale was demonstrated with the formation of epoxide **35g** on a 3.0 mmol-scale with an *ee* value of 92% and yield of 91% (Scheme 4.2). Deprotection of the tosyl-group was achieved using sodium in liquid ammonia, with epoxide **8** obtained without losing much *ee* value. It is interesting to note that the epoxide was retained intact under the basic reaction conditions.

Scheme 4.2 Scale-up experiment and deprotection



4.2.2 Identification of catalyst

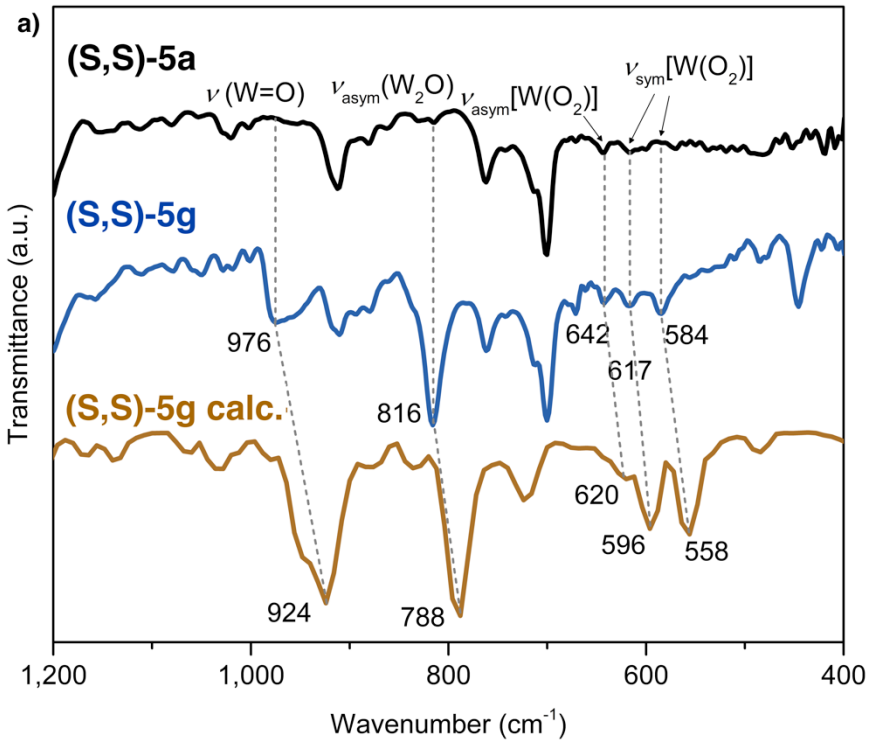
We were able to prepare the ion pair catalyst **5g** as a white powder and $NaHSO_4$ has a crucial role in the formation of the catalyst (Figure 4.4). When $NaHSO_4$ was not added or replaced with NaH_2PO_4, the preparation of the ion pair catalyst was not successful. We initially speculated that the structure of the ion pair to be an analogue of dinuclear oxodiperoxomolybdosulfate ion pair, containing a bridging sulfate between two tungsten atoms (Figure 4.3)[18]. After several attempts, we were able to obtain a single crystal suitable for X-ray diffraction, grown from DMF at room temperature. While we did indeed obtain a bimetallic anion, there was no sulfate bridge. The achiral tetraperoxyditungstate anion[22] species $[W_2O_2(\mu\text{-}O)(O_2)_4]^{2-}$ is found to fit nicely into the central cavity of the chiral dication. Each tungsten is coordinated to two peroxo-groups and a terminal oxo ligand, and both tungsten atoms in the anion are linked by a non-linear oxygen bridge [W_1-O_6-W_2: 103.4(4)°]. Thus, the coordination number is 6 on tungsten and in a distorted octahedral arrangement of oxygen atoms. It is

interesting to note that the bond length of O_6-W_2 (1.962(10) Å) is slightly longer than O_6-W_1 (1.942(11) Å). Both O_1-W_1 (1.761(10) Å) and O_{11}-W_2 (1.690(10) Å) bonds fall in the typical range for the W=O bond. Influenced by the adjacent metal, the bond lengths of O_5-W_1 (2.003(10) Å) and O_7-W_2 (1.942(10) Å) are longer than the other bone lengths between peroxo-group and tungsten (Fig. 1d). The crystal was added in catalytic amount (2.5 mol%) into a solution containing di-protected allylic amine **34a**, and epoxide **35a** was obtained in 92% *ee* and moderate yield (Table 4.2, entry 15), demonstrating that the crystal is the active catalyst of the epoxidation. If we repeat the same experiment in the presence of $NaHSO_4$, the yield improved significantly (entry 16). While $NaHSO_4$ is not part of the active catalyst, we speculate that it is important for maintaining the structure of the active catalyst and allowing the catalyst to be re-oxidized by hydrogen peroxide.

4.2.3 Characterization of catalyst

Einstein and Penfold identified the hydrated tetraperoxyditungstate $[W_2O_{11}(H_2O)_2]^{2-}K_2^+$ using X-ray crystallography and showed that each tungstate has a pentagonal bipyramidal arrangement. Each tungstate is 7-coordinated with 2 peroxy groups, a bridging oxo between the two tungstate and the apical positions are occupied by an oxo group and water[23]. The structure of dehydrated tetraperoxyditungstate $[\{W(=O)(O_2)_2\}_2(\mu\text{-}O)]^{2-}$ or $[W_2O_2(\mu\text{-}O)(O_2)_4]^{2-}$ (anion of our ion pair catalyst) was first proposed by Griffith in 1995.[24] Without an X-ray crystal structure, the catalyst was characterized through IR and Raman analysis. By changing the counterion for $[\{W(=O)(O_2)_2\}_2(\mu\text{-}O)]^{2-}$, several useful sets of data were obtained, and characteristic IR and Raman spectroscopic peaks were identified.[25] In this regard, we conducted spectroscopic studies with FT-IR and FT-Raman for our ion pair catalyst, **5g** $[\mathbf{BG}]^{2+}[W_2O_2(\mu\text{-}O)(O_2)_4]^{2-}$. This is followed by density functional theory (DFT) calculation to provide qualitative simulated frequencies in a bid to understand the experimental spectra. Based on the

spectra overlay for **5a** $[\mathbf{BG}]^{2+}.2[Cl]^-$ and the ion pair catalyst **5g** $[\mathbf{BG}]^{2+}[W_2O_2(\mu\text{-}O)(O_2)_4]^{2-}$ (Figure 4.5), the appearance of new peaks could be attributed to the tetraperoxyditungstate, $[W_2O_2(\mu\text{-}O)(O_2)_4]^{2-}$. Frequency analysis of the optimized electronic structure of **5g** shows that there are two $\nu_{sym}[W(O_2)]$, one $\nu_{asym}[W(O_2)]$, one $\nu(W{=}O)$ and one $\nu_{asym}(W_2O)$ stretching. These vibrations were assigned to the new peaks attributed to the tungstate anion for Raman and IR. The $\nu_{asym}(W_2O)$ stretching has a strong absorbance peak in IR but is very weak in Raman. In general, the experimental and theoretical spectra are overall a good fit, with difference in wavenumber of up to 40 cm^{-1} for IR. The calculated scaled values for Raman spectra are in excellent agreement with the experimentally observed data and are consisted with previously reported tungstate vibrational wavelengths[49]. As a result, we have demonstrated the reliability of the B3LYP method in predicting Raman spectra of the ion pair catalyst and suggest that it can be more accurate to estimate experimental data. Meanwhile, the IR can supplement information, which may be lost in Raman.



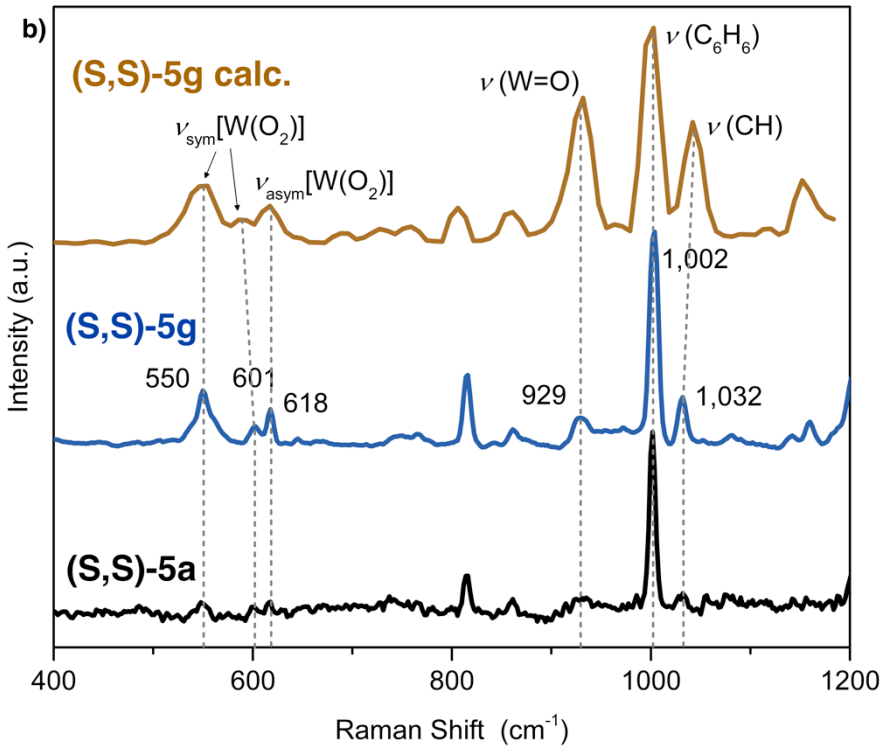


Figure 4.5 Experimental (in blue) and computational (in khaki) characters of 5g, and 5a was set as blank control (in black). **a**, Infrared spectra of **5a**, **5g** and **5g** (calc.). **b**, Raman spectra of **5g** (calc.), **5g** and **5a**.

With the elucidation of the active catalytic species, we propose a plausible mechanism (Figure 4.6). Firstly, the tungstate anion was oxidized and dimerized in the presence of $NaHSO_4$ and oxidant. The solubility of Na_2WO_4 and $NaHSO_4$ were initially poor in water but after the addition of hydrogen peroxide, a clear homogeneous solution was formed. This indicated that the tetraperoxyditungstate $[W_2O_2(\mu\text{-}O)(O_2)_4]^{2-}$ anion is highly soluble and it is then carried into the organic phase by the bisguanidinium $[\mathbf{BG}]^{2+}$, forming the ion pair catalyst **5g**. After the epoxidation reaction, the reduced form of tetraperoxyditungstate is regenerated by hydrogen peroxide at the interphase region between the organic solvent and water.

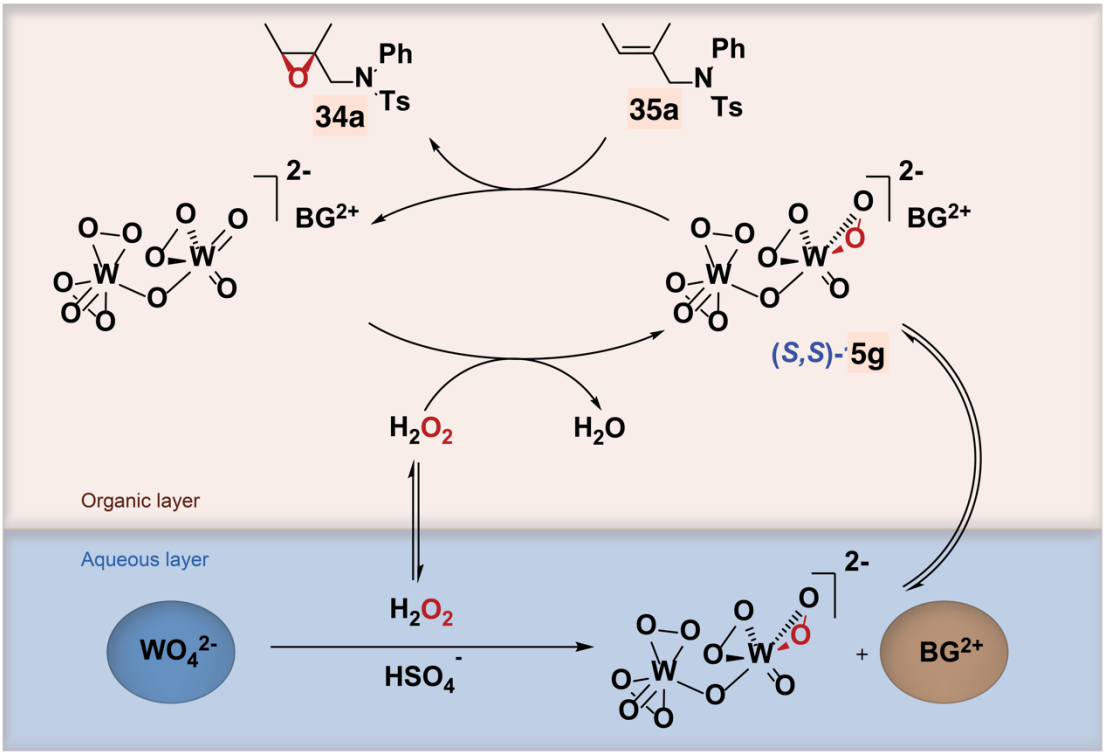


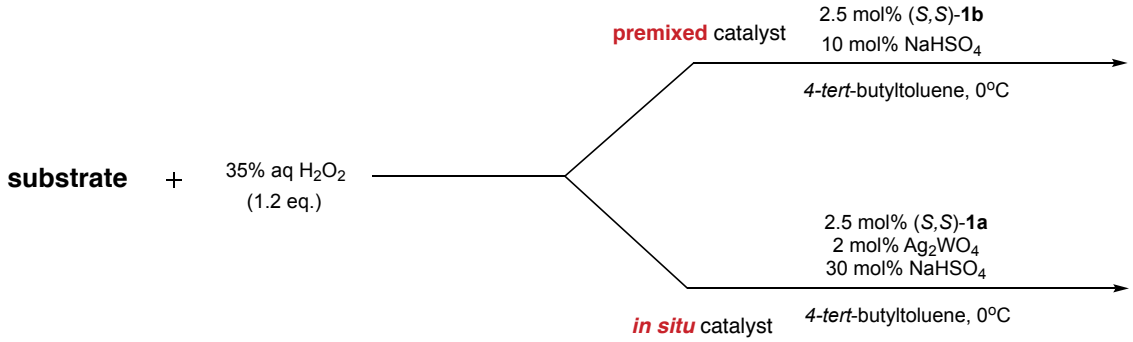
Figure 4.6 Proposed reaction pathway of ion pair phase transfer catalysis.

4.3 Summary

In summary, we have developed an ion pair strategy for epoxidation of allylic amines in high enantioselectivity using bisguanidinium tetraperoxyditungstate as a catalyst. Environmentally benign aqueous hydrogen peroxide is used as the terminal oxidant in stoichiometric amount. The catalytic oxidation process provided excellent yields and enantioselectivities for 1,1'-allylic protected amines. Low catalyst loading, ease of operation (under air), scalability, and tolerance to functional groups demonstrate the versatility of this method. The structure of the ion pair catalyst $[\mathbf{BG}]^{2+}[W_2O_2(\mu\text{-}O)(O_2)_4]^{2-}$ was elucidated by using X-ray crystallography and further characterized with IR and Raman spectroscopies. Analysis of the IR and Raman spectra allow to identify specific structures on the anion, which will be useful for the identification of related anions in the absence of X-ray crystallography.

4.4 Experimental

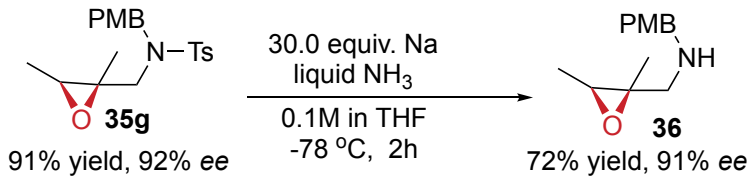
4.4.1 Experimental procedure



Premixed catalyst: To a 4 mL glass vial, **substrate** (1.0 mmol, 1.0 equiv.), **5g** (0.025 mmol, 0.025 equiv.), sodium hydrogen sulfate (0.1 mmol, 0.1 equiv.) were added, followed by addition of *t*-butyltoluene (1 mL). The mixture was then cooled in a 0 °C incubator with stirring for 15 minutes. 35% aq. H_2O_2 (1.2 mmol, 1.2 equiv.) was then added in one portion into reaction at 0°C. The mixture was left to stir at 0°C for 48 h.

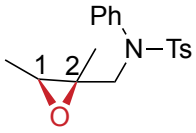
In situ catalyst: To a 4 mL glass vial, **substrate** (1.0 mmol, 1.0 equiv.), Ag_2WO_4 (0.02 mmol, 0.02 equiv.), **5a** (0.025 mmol, 0.025 equiv.), sodium hydrogen sulfate (0.3 mmol, 0.3 equiv.) were added, followed by addition of *t*-butyltoluene (1 mL). The mixture was then cooled in a 0 °C incubator with stirring for 15 minutes. 35% aq. H_2O_2 (1.2 mmol, 1.2 equiv.) was then added in one portion into reaction at 0 °C .The mixture was continue to stir at 0 °C for 48 h.

Work-up: After the reaction was complete (monitored by TLC), sat. $Na_2S_2O_3$ (aq.) was added into reaction to quench any unreacted oxidant. The aq. layer was extracted with Ethyl Acetate 3 times. The combined organic extracts was dried over anhydrous Na_2SO_4, concentrated under reduced pressure to get crude. Purification by flash column chromatography on silica gel (Eluent: Hexane-Ethyl Acetate 20:1 to 4:1) to obtain desired product.



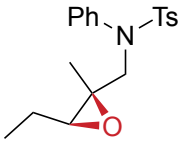
To a 50 mL Schlenk flask, sodium(washed by distilled hexane for twice) and magnetic stir-bar was added, followed equipped with a cold-finger condenser. The cold-finger condenser was connected to ammonia gas cylinder. After the gas condensed to liquid, the mixture in flask turned to dark blue. Then the cold-finger condenser was removed and replaced by rubber stopper with balloon. A solution of **3g** (2 mmol) in THF (5.0 mL) was injected into flask. The reaction was quenched by solid ammonium chloride after 2 h. The work-up step was terminated until the blue disappeared. A filtration separation followed and the filter residue was washed by DCM. Combine the THF solution and DCM solution, and remove the organic solvent under reduced pressure to get crude. Purification by flash column chromatography on silica gel (Eluent: DCM-Ethyl Acetate 1:1) to obtain desired product.

4.4.2 Characterization of asymmetric products



35a

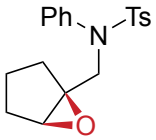
***N*-((2,3-dimethyloxiran-2-yl)methyl)-4-methyl-*N*-phenylbenzenesulfonamide (35a):** >99% yield, white solid, ^{1}H NMR (500 MHz, $CDCl_3$) δ 7.48 (d, J = 8.0 Hz, 2H), 7.33 (d, J = 4.4 Hz, 3H), 7.27 (t, J = 7.3 Hz, 2H), 7.09 – 7.00 (m, 2H), 3.92 (d, J = 13.6 Hz, 1H), 3.31 (d, J = 13.6 Hz, 1H), 2.57 (q, J = 5.3 Hz, 1H), 2.44 (s, 3H), 1.40 (s, 3H), 1.08 (d, J = 5.4 Hz, 3H). ^{13}C NMR (126 MHz, $CDCl_3$) δ 143.74, 139.92, 135.37, 129.60, 129.19, 128.95, 128.31, 127.82, 59.02, 58.41, 58.39, 21.68, 14.79, 13.75. HRMS: (ESI) $[M+Na]^+$ calcd. for $C_{18}H_{21}NNaO_3S$, 354.1140, found 354.1130. HPLC analysis: Chiralcel OD-H (Hex/IPA = 95/05, 1.0 mL/min, 254 nm, 23°C), 9.4min (major), 11.6 min, 94% ee. $[\alpha]^{22.4}_D$ +3.4° (c 0.58, $CHCl_3$).



35b

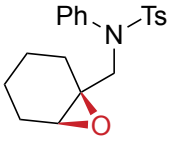
***N*-((3-ethyl-2-methyloxiran-2-yl)methyl)-4-methyl-*N*-phenylbenzenesulfonamide**

(35b): >99% yield, white solid, ^{1}H NMR (500 MHz, $CDCl_3$) δ 7.45 (d, *J* = 8.0 Hz, 2H), 7.30 (d, *J* = 5.0 Hz, 3H), 7.25 (t, *J* = 7.8 Hz, 2H), 7.10 – 6.94 (m, 2H), 3.97 (d, *J* = 13.4 Hz, 1H), 3.20 (d, *J* = 13.4 Hz, 1H), 2.42 (s, 3H), 2.35 (t, *J* = 6.4 Hz, 1H), 1.46 (dt, *J* = 14.0, 7.1 Hz, 1H), 1.38 (s, 3H), 1.22 (td, *J* = 14.5, 7.3 Hz, 1H), 0.66 (t, *J* = 7.5 Hz, 3H). ^{13}C NMR (126 MHz, $CDCl_3$) δ 143.74, 139.62, 135.20, 129.59, 129.18, 128.95, 128.30, 127.84, 64.23, 58.99, 58.25, 21.67, 21.65, 14.77, 9.84. HRMS: (ESI) $[M+Na]^+$ calcd. for $C_{19}H_{23}NNaO_3S$, 368.1296, found 368.1301. HPLC analysis: Chiralcel OD-H (Hex/IPA = 95/05, 1.0 mL/min, 254 nm, 23°C), 9.8.min (major), 13.6 min, 89% ee. $[\alpha]^{22.6}_D$ +4.8° (*c* 0.75, $CHCl_3$).



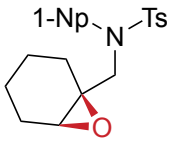
35c

***N*-(6-oxabicyclo[3.1.0]hexan-1-ylmethyl)-4-methyl-*N*-phenylbenzenesulfonamide (35c):** 71% yield, white solid, ^{1}H NMR (400 MHz, $CDCl_3$) δ 7.43 (d, *J* = 8.3 Hz, 2H), 7.32 – 7.24 (m, 3H), 7.24 – 7.16 (m, 2H), 7.08 – 6.91 (m, 2H), 4.01 (d, *J* = 14.1 Hz, 1H), 3.70 (d, *J* = 14.1 Hz, 1H), 2.97 (s, 1H), 2.39 (s, 3H), 1.92 – 1.73 (m, 3H), 1.56 – 1.31 (m, 3H). ^{13}C NMR (101 MHz, $CDCl_3$) δ 143.73, 139.96, 135.34, 129.60, 129.15, 128.89, 128.25, 127.84, 65.96, 62.09, 52.92, 27.79, 27.38, 21.69, 19.40. HRMS: (ESI) $[M+Na]^+$ calcd. for $C_{19}H_{21}NNaO_3S$, 366.1140, found 366.1145. HPLC analysis: Chiralcel OD-H (Hex/IPA = 95/05, 1.0 mL/min, 254 nm, 23°C), 10.2min (major), 12.1 min, 92% ee. $[\alpha]^{22.4}_D$ +2.3° (*c* 0.49, $CHCl_3$).



35d

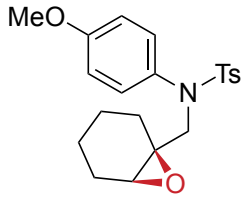
***N*-(7-oxabicyclo[4.1.0]heptan-1-ylmethyl)-4-methyl-*N*-phenylbenzenesulfonamide (35d):** 83% yield, white solid, ^{1}H NMR (400 MHz, $CDCl_3$) δ 7.42 (d, *J* = 8.3 Hz, 2H), 7.31 – 7.24 (m, 3H), 7.24 – 7.16 (m, 2H), 6.98 (dd, *J* = 6.7, 3.0 Hz, 2H), 3.88 (d, *J* = 13.5 Hz, 1H), 3.23 (d, *J* = 13.5 Hz, 1H), 2.57 (d, *J* = 2.9 Hz, 1H), 2.38 (s, 3H), 2.29 – 2.02 (m, 1H), 1.74 (ddd, *J* = 21.3, 14.6, 6.9 Hz, 2H), 1.46 – 0.97 (m, 5H). ^{13}C NMR (101 MHz, $CDCl_3$) δ 143.72, 139.86, 135.38, 129.60, 129.14, 129.09, 128.33, 127.84, 58.11, 58.04, 57.55, 25.49, 24.60, 21.68, 20.16, 19.14. HRMS: (ESI) $[M+Na]^+$ calcd. for $C_{20}H_{23}NNaO_3S$, 380.1296, found 380.1300. HPLC analysis: Chiralcel AD-H (Hex/IPA = 95/05, 1.0 mL/min, 254 nm, 23°C), 15.8min (major), 19.2 min, 97% ee. $[\alpha]^{22.4}_D$ +3.4° (*c* 0.52, $CHCl_3$).



35e

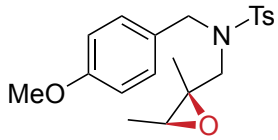
***N*-((7-oxabicyclo[4.1.0]heptan-1-yl)methyl)-4-methyl-*N*-(naphthalen-1-yl)benzenesulfonamide (35e):** >99% yield, white solid ^{1}H NMR (400 MHz, $CDCl_3$) δ 8.13 (dd, *J* = 191.9, 8.4 Hz, 1H), 7.86 – 7.21 (m, 8H), 6.88 (dd, *J* = 138.7, 7.1 Hz, 1H), 4.43 (d, *J* = 13.0 Hz, 1H), 3.76 (dd, *J* = 78.6, 13.9 Hz, 1H), 2.91 (d, *J* = 13.0 Hz, 1H), 2.45 (t, *J* = 10.1 Hz, 2H), 2.03 – 1.62 (m, 1H), 1.53 – 0.51 (m, 5H). ^{13}C NMR (101 MHz, $CDCl_3$) δ143.97, 143.80, 137.39, 136.50, 135.74, 134.94, 134.85, 134.69, 133.35, 132.09, 129.70, 129.64, 129.32, 129.28, 128.45, 128.30, 128.08, 127.72, 127.00, 126.81, 126.69, 126.46, 125.37, 125.08, 124.94, 124.63, 124.11, 60.30, 58.98, 58.42, 58.30, 57.71, 57.37, 25.97, 25.46, 24.52, 24.39, 21.72, 21.68, 20.15, 20.09, 19.00, 18.37. HRMS: (ESI) $[M+Na]^+$ calcd. for $C_{24}H_{25}NO_3S$,

407.1555, found 407.1558. HPLC analysis: Chiralcel AD-H (Hex/IPA = 95/5, 1.0 mL/min, 254 nm, 23°C), 22.7 min, 26.5 min (major), 95% ee. $[\alpha]^{22.4}_{D}$ +51.6° (*c* 1.72, CH_2Cl_2).



35f

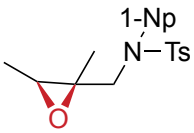
***N*-(7-oxabicyclo[4.1.0]heptan-1-ylmethyl)-*N*-(4-methoxyphenyl)-4-methylbenzenesulfonamide (35f):** 98% yield, white solid ^{1}H NMR (500 MHz, CDCl3) δ 7.46 (d, *J* = 8.3 Hz, 2H), 7.30 – 7.19 (m, 2H), 6.96 – 6.88 (m, 2H), 6.86 – 6.72 (m, 2H), 3.86 (d, *J* = 13.4 Hz, 1H), 3.79 (s, 3H), 3.22 (d, *J* = 13.4 Hz, 1H), 2.60 (d, *J* = 2.6 Hz, 1H), 2.42 (s, 3H), 2.19 (dt, *J* = 14.9, 6.0 Hz, 1H), 1.96 – 1.69 (m, 2H), 1.54 – 1.36 (m, 2H), 1.28 (ddd, *J* = 15.0, 8.7, 5.1 Hz, 1H), 1.22 – 1.07 (m, 2H). ^{13}C NMR (126 MHz, CDCl3) δ 159.30, 143.63, 135.42, 132.29, 130.20, 129.58, 127.85, 114.31, 58.12, 57.91, 57.79, 55.52, 25.48, 24.64, 21.68, 20.20, 19.16. HRMS: (ESI) $[M+Na]^+$ calcd. for $C_{21}H_{25}NNaO_4S$, 410.1402, found 410.1413. HPLC analysis: Chiralcel IB-3 (Hex/IPA = 97/03, 0.8 mL/min, 254 nm, 23°C), 16.0min (major), 17.7 min, 90% ee. $[\alpha]^{21.4}_{D}$ -0.46° (*c* 0.71, $CHCl_3$).



35g

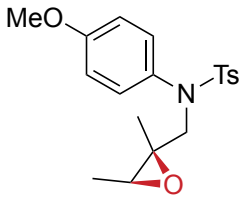
***N*-(((2*S*,3*S*)-2,3-dimethyloxiran-2-yl)methyl)-*N*-(4-methoxybenzyl)-4-methylbenzenesulfonamide (35g):** 95% yield, white solid ^{1}H NMR (400 MHz, $CDCl_3$) δ 7.68 (d, *J* = 8.3 Hz, 2H), 7.30 (d, *J* = 8.0 Hz, 2H), 7.15 (d, *J* = 8.7 Hz, 2H), 6.80 (d, *J* = 8.7 Hz, 2H), 4.46 (d, *J* = 14.9 Hz, 1H), 4.11 (d, *J* = 14.9 Hz, 1H), 3.78 (s, 3H), 3.38 (d, *J* = 14.6 Hz, 1H), 2.91 (d, *J* = 14.6 Hz, 1H), 2.61 (q, *J* = 5.4 Hz, 1H), 2.42 (s, 3H), 1.13 (s, 3H), 1.02 (d, *J* = 5.5 Hz, 3H). ^{13}C NMR (101 MHz, $CDCl_3$) δ 159.37, 143.52, 136.94, 130.14, 129.84, 128.08,

127.31, 113.92, 59.49, 58.34, 55.39, 55.37, 54.89, 52.70, 21.62, 14.61, 13.65. HRMS: (ESI) $[M+H]^+$ calcd. for $C_{20}H_{26}NO_4S$, 376.1583, found 376.1581. HPLC analysis: Chiralcel AD-H (Hex/IPA = 95/05, 1.0 mL/min, 254 nm, 23°C), 32.0min (major), 42.9 min, 96% ee. $[\alpha]^{22.4}_D$ +10.48° (*c* 0.84, CH_2Cl_2).



35h

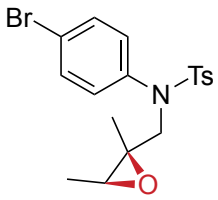
***N*-((2,3-dimethyloxiran-2-yl)methyl)-4-methyl-*N*-(naphthalen-1-yl)benzenesulfonamide (35h):** 99% yield, white solid ^{1}H NMR (300 MHz, $CDCl_3$) δ 8.30 – 7.88 (m, 1H), 7.84 (dd, *J* = 8.5, 4.8 Hz, 2H), 7.62 – 7.17 (m, 7H), 6.90 (dd, *J* = 74.1, 7.4 Hz, 1H), 4.39 (d, *J* = 13.2 Hz, 1H), 3.90 (d, *J* = 13.9 Hz, 1H), 3.62 (d, *J* = 13.9 Hz, 1H), 3.00 (d, *J* = 13.2 Hz, 1H), 2.51 (q, *J* = 5.5 Hz, 1H), 2.43 (d, *J* = 6.9 Hz, 3H), 2.05 (q, *J* = 5.4 Hz, 1H), 1.38 (d, *J* = 65.1 Hz, 3H), 0.85 (dd, *J* = 129.3, 5.5 Hz, 3H). ^{13}C NMR (75 MHz, $CDCl_3$) δ 129.70, 129.64, 129.31, 128.24, 128.10, 126.92, 126.49, 125.02, 124.29, 123.99, 61.19, 58.57, 58.31, 58.24, 21.72, 15.29, 13.72, 13.52, 6.71. HRMS: (ESI) $[M+Na]^+$ calcd. for $C_{22}H_{23}NaNO_3S$, 381.1399, found 381.1400. HPLC analysis: Chiralcel OJ-H (Hex/IPA = 95/5, 1.5 mL/min, 254 nm, 23°C), 19.2 min, 28.3 min (major), 94% ee. $[\alpha]^{22.4}_D$ +35.6° (*c* 1.28, CH_2Cl_2).



35i

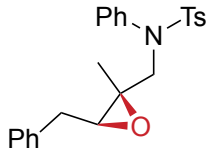
***N*-((2,3-dimethyloxiran-2-yl)methyl)-*N*-(4-methoxyphenyl)-4-methylbenzenesulfonamide (35i):** 97% yield, colorless oil, ^{1}H NMR (500 MHz, $CDCl_3$) δ 7.48 (d, *J* = 8.0 Hz, 2H), 7.27 (t, *J* = 6.8 Hz, 2H), 6.94 (d, *J* = 8.7 Hz, 2H), 6.83 (d, *J* = 8.7 Hz, 2H), 3.86 (d, *J* = 13.5 Hz, 1H), 3.82 (s, 3H), 3.28 (d, *J* = 13.5 Hz, 1H), 2.57 (q, *J* = 5.4 Hz, 1H),

2.44 (s, 3H), 1.41 (s, 3H), 1.11 (d, J = 5.4 Hz, 3H). ^{13}C NMR (126 MHz, $CDCl_3$) δ 159.17, 143.51, 135.32, 132.24, 129.96, 129.45, 127.72, 114.24, 58.90, 58.52, 58.11, 55.39, 21.55, 14.64, 13.67. HRMS: (ESI) $[M+Na]^+$ calcd. for $C_{21}H_{23}NNaO_4S$, 384.1245, found 384.1237; HPLC analysis: Chiralcel AS-H (Hex/IPA = 95/05, 1.0 mL/min, 254 nm, 23°C), 26.7min, 33.6 min(major), 95% ee. $[\alpha]^{21.4}_D$ +2.7° (*c* 0.51, $CHCl_3$)



35j

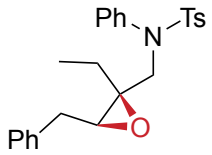
***N*-(4-bromophenyl)-*N*-((2,3-dimethyloxiran-2-yl)methyl)-4-methylbenzenesulfonamide (35j):** 96% yield, white solid, ^{1}H NMR (500 MHz, $CDCl_3$) δ 7.45 (dt, J = 9.6, 2.5 Hz, 4H), 7.27 (s, 2H), 7.00 – 6.84 (m, 2H), 3.75 (d, J = 13.8 Hz, 1H), 3.42 (d, J = 13.8 Hz, 1H), 2.64 (q, J = 5.5 Hz, 1H), 2.44 (s, 3H), 1.58 (s, 3H), 1.37 (s, 3H), 1.13 (d, J = 5.5 Hz, 3H). ^{13}C NMR (126 MHz, $CDCl_3$) δ 144.06, 144.04, 135.01, 135.00, 132.43, 132.41, 130.50, 130.49, 129.76, 129.75, 127.80, 127.78, 122.25, 77.41, 77.16, 76.91, 59.12, 58.06, 57.90, 21.72, 21.70, 14.79, 14.78, 13.78, 13.76. HRMS: (ESI) $[M+Na]^+$ calcd. for $C_{18}H_{20}BrNNaO_3S$, 432.0245, found 432.0247. HPLC analysis: Chiralcel OD-H (Hex/IPA = 90/10, 1.0 mL/min, 254 nm, 23°C), 9.1 min (major), 10.8 min, 95% ee. $[\alpha]^{22.4}_D$ +36.0° (*c* 0.53, CH_2Cl_2).



35k

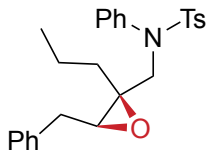
***N*-((3-benzyl-2-methyloxiran-2-yl)methyl)-4-methyl-*N*-phenylbenzenesulfonamide (35k):** >99% yield, white solid, ^{1}H NMR (500 MHz, $CDCl_3$) δ 7.42 (d, J = 8.3 Hz, 2H), 7.29 – 7.17 (m, 9H), 7.03 – 6.98 (m, 2H), 6.98 – 6.92 (m, 2H), 3.91 (d, J = 13.7 Hz, 1H), 3.31 (d, J = 13.7 Hz, 1H), 2.75 (dd, J = 14.4, 6.0 Hz, 1H), 2.67 (t, J = 6.0 Hz, 1H), 2.59 (dd, J = 14.4, 5.9

Hz, 1H), 2.41 (s, 3H), 1.53 (s, 3H). ^{13}C NMR (126 MHz, $CDCl_3$) δ 143.76, 139.55, 137.36, 135.18, 129.59, 129.18, 128.78, 128.74, 128.72, 128.28, 127.82, 126.59, 62.93, 59.49, 58.23, 35.00, 21.67, 15.28. HRMS: (ESI) $[M+Na]^+$ calcd. for $C_{24}H_{25}NO_3SNa$, 430.1453, found 430.1462; HPLC analysis: Chiralcel OD-H (Hex/IPA = 95/05, 1.0 mL/min, 254 nm, 23°C), 19.2 min (major), 24.1 min, 93% ee. $[\alpha]^{21.2}_D$ + 5.5° (*c* 0.76, $CHCl_3$)



35l

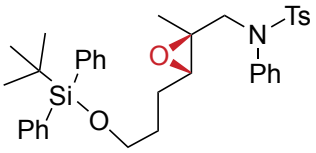
***N*-((3-benzyl-2-ethyloxiran-2-yl)methyl)-4-methyl-*N*-phenylbenzenesulfonamide (35l):** >99% yield, white solid, ^{1}H NMR (400 MHz, $CDCl_3$) δ 7.41 (d, *J* = 8.1 Hz, 2H), 7.28 – 7.15 (m, 9H), 7.02 – 6.90 (m, 4H), 4.06 (d, *J* = 13.7 Hz, 1H), 3.20 (d, *J* = 13.7 Hz, 1H), 2.69 (dd, *J* = 14.1, 10.1 Hz, 2H), 2.59 (dd, *J* = 12.6, 3.4 Hz, 1H), 2.41 (s, 3H), 1.92 (dd, *J* = 14.3, 7.4 Hz, 1H), 1.69 (dd, *J* = 14.4, 7.3 Hz, 1H), 1.16 (t, *J* = 7.5 Hz, 3H). ^{13}C NMR (101 MHz, $CDCl_3$) δ 143.78, 139.49, 137.58, 134.83, 129.56, 129.09, 128.75, 128.73, 128.66, 128.27, 127.88, 126.52, 77.48, 77.16, 76.84, 63.86, 62.66, 54.72, 34.65, 21.67, 21.12, 8.93. HRMS: (ESI) $[M+Na]^+$ calcd. for $C_{25}H_{27}NNaO_3S$, 444.1609, found 444.1620; HPLC analysis: Chiralcel AD-H (Hex/IPA = 95/05, 1.0 mL/min, 254 nm, 23°C), 13.4 min (major), 14.9 min, 92% ee. $[\alpha]^{21.2}_D$ +4.3° (*c* 0.72, $CHCl_3$)



35m

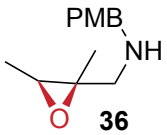
***N*-((3-benzyl-2-propyloxiran-2-yl)methyl)-4-methyl-*N*-phenylbenzenesulfonamide (35m):** 74% yield, white solid, ^{1}H NMR (400 MHz, $CDCl_3$) δ 7.41 (d, *J* = 8.0 Hz, 2H), 7.21 (dd, *J* = 15.1, 7.9 Hz, 8H), 6.96 (dd, *J* = 10.5, 7.6 Hz, 4H), 4.08 (d, *J* = 13.7 Hz, 1H), 3.16 (d, *J* = 13.7 Hz, 1H), 2.74 – 2.54 (m, 3H), 2.41 (s, 3H), 1.94 – 1.81 (m, 1H), 1.66 – 1.49 (m, 4H), 1.01 (t, *J*

= 7.1 Hz, 3H). ^{13}C NMR (101 MHz, $CDCl_3$) δ 143.78, 139.52, 137.62, 134.84, 129.56, 129.09, 128.75, 128.66, 128.28, 127.90, 126.51, 63.57, 61.89, 55.29, 34.71, 30.25, 21.68, 18.03, 14.67. HRMS: (ESI) $[M+Na]^+$ calcd. for $C_{26}H_{29}NNaO_3S$, 458.1766, found 458.1763. HPLC analysis: Chiralcel OD-H (Hex/IPA = 95/05, 1.0 mL/min, 254 nm, 23°C), 10.6 min, 13.0 min (major), 68% ee. $[\alpha]^{22.7}_D$ +3.5° (*c* 0.57, $CHCl_3$).



35n

***N*-((3-(3-((*tert*-butyldiphenylsilyl)oxy)propyl)-2-methyloxiran-2-yl)methyl)-4-methyl-*N*-phenylbenzenesulfonamide (35n):** 94% yield, colourless oil, ^{1}H NMR (500 MHz, CD_3CN) δ 7.57 (dt, *J* = 8.1, 1.6 Hz, 4H), 7.45 – 7.32 (m, 9H), 7.28 (d, *J* = 8.1 Hz, 2H), 7.26 – 7.18 (m, 3H), 7.02 – 6.89 (m, 2H), 3.82 (d, *J* = 13.6 Hz, 1H), 3.46 (ddd, *J* = 10.3, 8.3, 4.2 Hz, 2H), 3.21 (d, *J* = 13.6 Hz, 1H), 2.37 (s, 3H), 2.31 (t, *J* = 6.2 Hz, 1H), 1.23 (s, 7H), 0.95 (s, 9H). ^{13}C NMR (126 MHz, $CDCl_3$) δ 143.74, 139.57, 135.66, 135.17, 133.98, 129.74, 129.59, 129.18, 128.90, 128.30, 127.84, 127.75, 63.28, 62.83, 58.95, 58.19, 28.74, 26.97, 24.90, 21.68, 19.31, 14.81. HRMS: (ESI) $[M+Na]^+$ calcd. for $C_{36}H_{43}NNaO_4SSi$, 636.2580, found 636.2584. HPLC analysis: Chiralcel OD-H (Hex/IPA = 95/5, 0.5 mL/min, 254 nm, 23°C), 16.7min (major), 20.8 min, 86% ee. $[\alpha]^{22.4}_D$ +35.3° (*c* 2.31, CH_2Cl_2).



36

1-((2*S*,3*S*)-2,3-dimethyloxiran-2-yl)-*N*-(4-methoxybenzyl)methanamine (36): 72% yield, colorless oil, ^{1}H NMR (400 MHz, $CDCl_3$) δ 7.22 (d, *J* = 8.6 Hz, 2H), 6.85 (d, *J* = 8.6 Hz, 2H), 3.79 (s, 3H), 3.71 (s, 2H), 3.05 (q, *J* = 5.5 Hz, 1H), 2.80 – 2.59 (q, 2H), 1.30 (s, 3H), 1.28 (d, *J* = 5.5 Hz, 3H). ^{13}C NMR (101 MHz, $CDCl_3$) δ 158.72, 132.55, 129.29, 113.86, 60.50, 57.22, 55.36, 55.20, 53.34, 15.63, 13.91. HRMS: (ESI) $[M+H]^+$ calcd. for $C_{13}H_{20}NO_2$, 222.1494,

found 222.1502. HPLC analysis: Chiralcel AS-H (Hex/IPA = 80/20, 1.0 mL/min, 254 nm, 23°C), 7.2 min, 10.7 min (major), 92% ee. $[\alpha]^{23}_{D}$ -5.2° (*c* 2.16, CH_2Cl_2).

4.3.3 Single crystal

35% H_2O_2 (3.45 mL , 40.0 mmol) was added dropwise to a mixture of $Na_2WO_4 \cdot 2H_2O$ (330 mg, 1.13 mmol) and $NaHSO_4$ (1.8 g, 15.0 mmol) in 10 mL deionized water. Before adding the H_2O_2, the $Na_2WO_4 \cdot 2H_2O$ and $NaHSO_4$ were partially dissolved. After finishing the dropping, all components were dissolved, giving a colorless solution at room temperature. Then the above solution was added dropwise to a turbid solution of (*S,S*)-**5a**[4] (564 mg, 0.4 mmol) in Et_2O (20 mL). After vigorously stirring for 15 min, the Et_2O layer turned to a yellow solution. After further stirring for 2 h and removal of Et_2O by evaporation, (*S,S*)-**5g** precipitated from organic phase. 4.0 mL deionized water was added and the resulting heterogeneous mixture was submitted to ultra sonicator for 1 min. Then the pale white solid was filtered off and washed with deionized water (20 mL). After drying under vacuum at room temperature, (*S,S*)-**5g** was obtained as a pale white powder (731.5 mg, 97% yield) and its structure was characterized and determined by X-ray single-crystal diffraction. ^{1}H NMR (400 MHz, $CDCl_3$) δ 7.46 – 6.65 (m, 32H), 5.28 – 4.63 (dd, 8H), 4.58 – 4.03 (d, 8H), 3.32 (s, 4H), 1.15 (s, 72H).

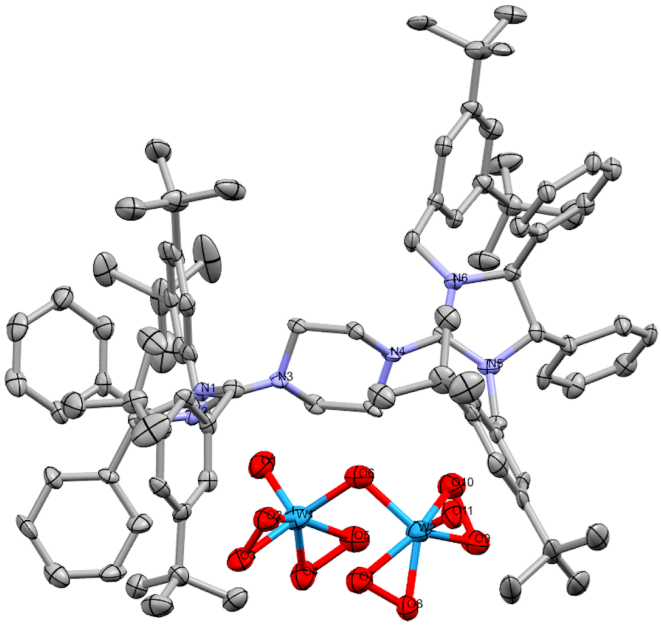


Fig. 2 X-ray structure of (*S,S*)-**5g**.(CCDC: 1868566)

References

(1) Sova, M.; Kovac, A.; Turk, S.; Hrast, M.; Blanot, D.; Gobec, S. Phosphorylated Hydroxyethylamines as Novel Inhibitors of the Bacterial Cell Wall Biosynthesis Enzymes MurC to MurF. *Bioorg. Chem.* **2009**, *37*, 217.

(2) Getman, D. P.; DeCrescenzo, G. A.; Heintz, R. M.; Reed, K. L.; Talley, J. J.; Bryant, M.L.; Clare, M.; Houseman, K. A.; Marr, J. J.; Mueller, R. A.; Vazquez, M. L.; Shieh, H.-S.; Stallings, W. C.; Stegeman, R. A. Discovery of a Novel Class of Potent HIV-1 Protease Inhibitors Containing the (*R*)-(Hydroxyethyl)Urea Isostere. *J. Med. Chem.* **1993**, *36*, 288.

(3) Miyano, S.; Lu, L. D.-L.; Viti, S. M.; Sharpless, K. B. Kinetic Resolution of Racemic Beta-Hydroxy Amines by Enantioselective N-Oxide Formation. *J. Org. Chem.* **1985**, *50*, 4350.

(4) Quick, J.; Khandelwal, Y.; Meltzer, P. C.; Weinberg, J. S. Synthetic Studies on the Lythraceae Alkaloids. 11. Model Studies for the Synthesis of Lythracine V. *J. Org. Chem.* **1983**, *48*, 5199.

(5) Quick, J.; Mondello, C.; Humora, M.; Brennan, T. Synthesis of 2,6-Diacetonylpiperidine. X-Ray Diffraction Analysis of Its N-Benzoyl Derivative. *J. Org. Chem.* **1978**, *43*, 2705.

(6) Emmons, W. D.; Pagano, A. S.; Freeman, J. P. Peroxytrifluoroacetic Acid. III. The Hydroxylation of Olefins. *J. Am. Chem. Soc.* **1954**, *76*, 3472.

(7) Gil, L.; Compère, D.; Guilloteau-Bertin, B.; Chiaroni, A.; Marazano, C. An Enantioselective Entry to Substituted 6-Membered Nitrogen Heterocycles from Chiral Pyridinium Salts via Selective Epoxidation of Tetrahydropyridine Intermediates. *Synthesis* **2000**, *14*, 2117.

(8) Grishina, G. V.; Borisenko, A. A.; Veselov, I. S.; Petrenko, A. M. Russ. Synthesis and Stereochemistry of 3-Hydroxy-1,2,3,6-Tetrahydropyridines. *J. Org. Chem.* **2005**, *41*, 272.

(9) Davies, S. G.; Fletcher A. M.; Thomson, J. E. Hydrogen Bond Directed Epoxidation: Diastereoselective Olefinic Oxidation of Allylic Alcohols and Amines. *Org. Biomol. Chem.* **2014**, *12*, 4544.

(10) Aciro, C.; Claridge, T. D. W.; Davies, S. G.; Roberts, P. M.; Russell, A. J.; Thomson, J. E. Ammonium-Directed Dihydroxylation of 3-Aminocyclohex-1-Enes: Development of a Metal-Free Dihydroxylation Protocol. *Org. Biomol. Chem.* **2008**, *6*, 3751.

(11) Aciro, C.; Davies, S. G.; Roberts, P. M.; Russell, A. J.; Smith, A. D.; Thomson, J. E. Ammonium-Directed Dihydroxylation: Metal-Free Synthesis of the Diastereoisomers of 3-Aminocyclohexane-1,2-Diol. *Org. Biomol. Chem.* **2008**, *6*, 3762.

(12) Davies, S. G.; Fletcher, A. M.; Kurosawa, W.; Lee, J. A.; Poce, G.; Roberts, P. M.; Thomson, J. E.; Williamson, D. M. One-Pot Conversions of Olefins to Cyclic Carbonates and Secondary Allylic and Homoallylic Amines to Cyclic Carbamates. *J. Org. Chem.* **2010**, *75*, 7745.

(13) Aggarwal, V. K.; Fang, G. Y. Highly Regioselective and Diastereoselective Epoxidation of Allylic Amines with Oxone. *Chem. Commun.* **2005**, 3448.

(14) Olivares-Romero, J. L.; Li, Z.; Yamamoto, H. Hf(IV)-Catalyzed Enantioselective Epoxidation of *N*-Alkenyl Sulfonamides and *N*-Tosyl Imines. *J. Am. Chem. Soc.* **2012**, *134*, 5440.

(15) Ji, N.; Yuan, J.; Liu, M.; Lan, T.; He, W. Novel Chiral Schiff Base/Ti(IV) Catalysts for the Catalytic Asymmetric Epoxidation of *N*-Alkenyl Sulfonamides. *Chem. Commun.* **2016**, *52*, 7731.

(16) Zong, L.; Ban, X.; Kee, C. W.; Tan, C.-H. Catalytic Enantioselective Alkylation of Sulfenate Anions to Chiral Heterocyclic Sulfoxides Using Halogenated Pentanidium Salts. *Angew. Chem., Int. Ed.* **2014**, *53*, 11849.

(17) Wang, C.; Zong, L.; Tan, C.-H. Enantioselective Oxidation of Alkenes with Potassium Permanganate Catalyzed by Chiral Dicationic Bisguanidinium. *J. Am. Chem. Soc.* **2015**, *137*, 10677.

(18) Zong, L.; Wang, C.; Moeljadi, A. M. P.; Ye, X.; Hirao, H.; Tan, C.-H. Bisguanidinium Dinuclear Oxodiperoxomolybdosulfate Ion Pair-Catalyzed Enantioselective Sulfoxidation. *Nat. Commun.* **2016**, *7*, 13455.

(19) Teng, B.; Chen, W.; Dong, S.; Kee, C. W.; Gandamana, D. A.; Zong, L.; Tan, C.-H. Pentanidium- And Bisguanidinium-Catalyzed Enantioselective Alkylations Using Silylamide as Brønsted Probase. *J. Am. Chem. Soc.* **2016**, *138*, 9935.

(20) Zong, L.; Tan, C.-H. Phase-Transfer and Ion-Pairing Catalysis of Pentanidiums and Bisguanidiniums. *Acc. Chem. Res.* **2017**, *50*, 842.

(21) Ye, X.; Moeljadi, A. M. P.; Chin, K. F.; Hirao, H.; Zong, L.; Tan, C.-H. Enantioselective Sulfoxidation Catalyzed by a Bisguanidinium Diphosphatobisperoxotungstate Ion Pair. *Angew. Chem., Int. Ed.* **2016**, *55*, 7101.

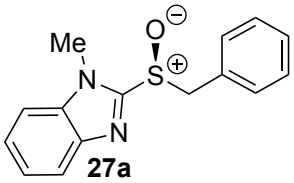
(22) Kamata, K.; Kuzuya, S.; Uehara, K.; Yamaguchi, S.; Mizuno, N. μ-η^1:η^1-Peroxo-Bridged Dinuclear Peroxotungstate Catalytically Active for Epoxidation of Olefins. *Inorg. Chem.* **2007**, *46*, 3768.

(23) Einstein, F. W. B.; Penfold, B. R. The Crystal Structure of Hydrated Potassium Tetraperoxyditungstate(VI), $K_2W_2O_{11}.4H_2O$. *Acta. Crystallogr.* **1964**, *17*, 1127.

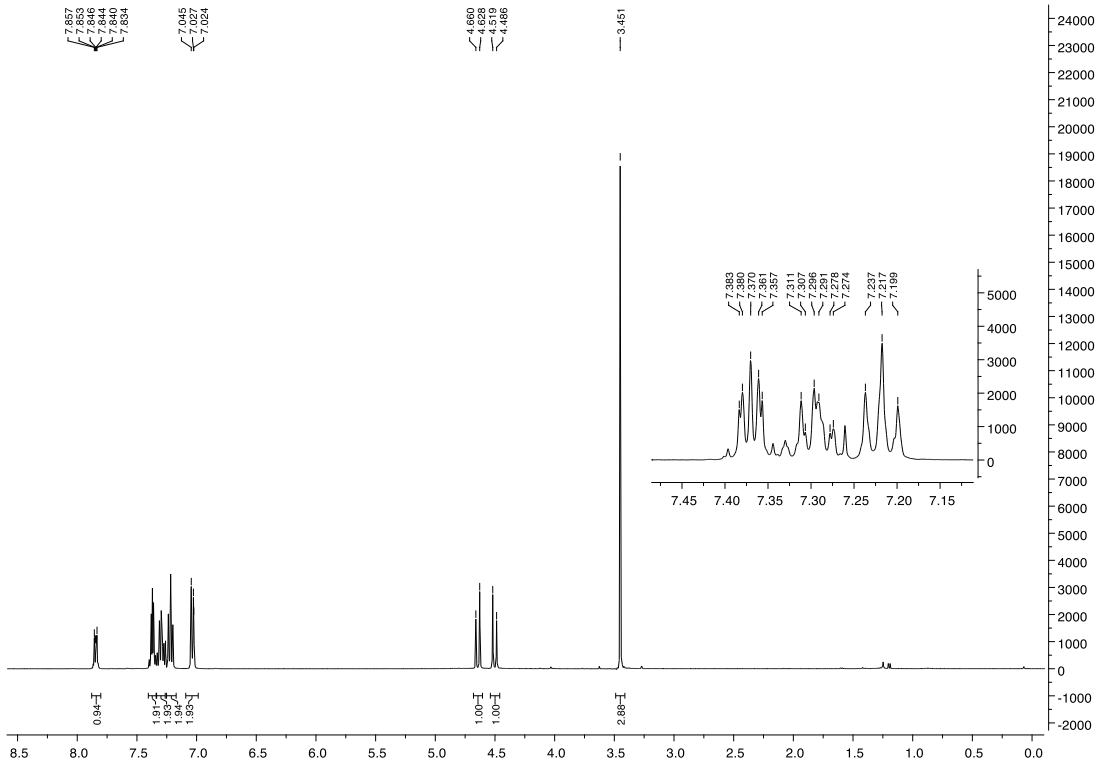
(24) Campbell, N. J.; Dengel, A. C.; Edwards, C. J.; Griffith, W. P. Studies on Transition Metal Peroxo Complexes. Part 8. The Nature of Peroxomolybdates and Peroxotungstates in Aqueous Solution. *J. Chem. Soc., Dalton Trans.* **1989**, *6*, 1203.

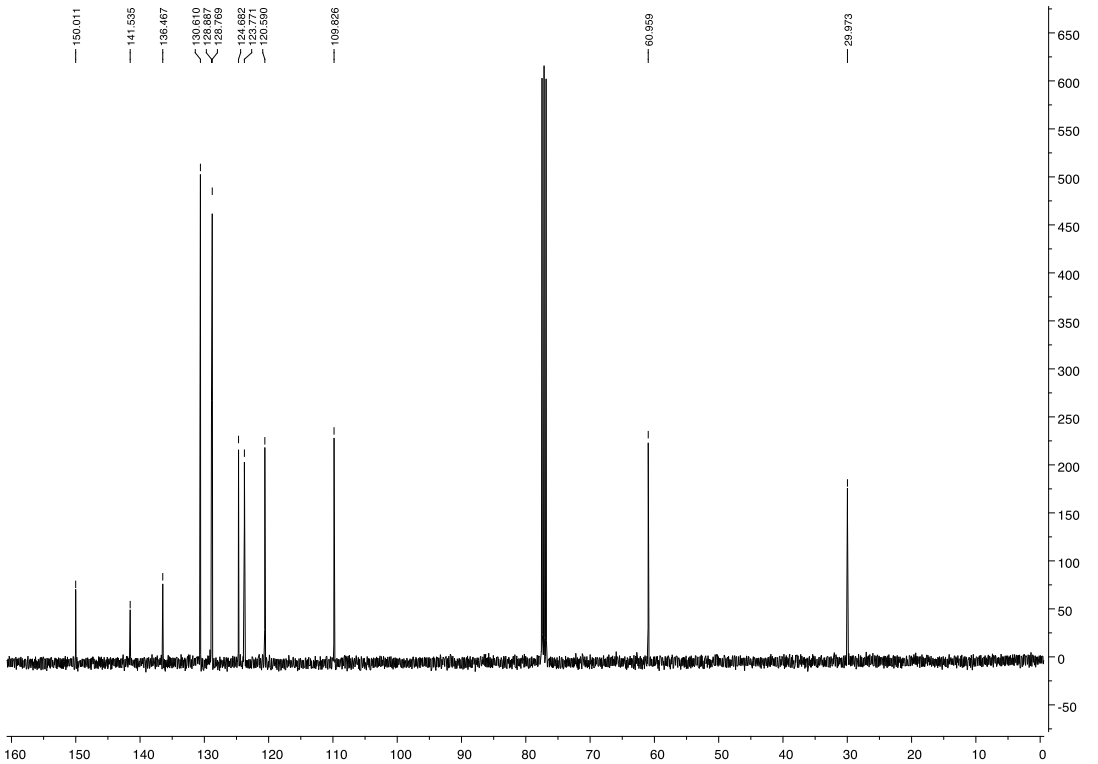
(25) Yang, H.-M.; Wu, H.-S. Interfacial Mechanism and Kinetics of Phase-Transfer Catalysis. *Catal. Rev.* **2003**, *45*, 463.

Appendix

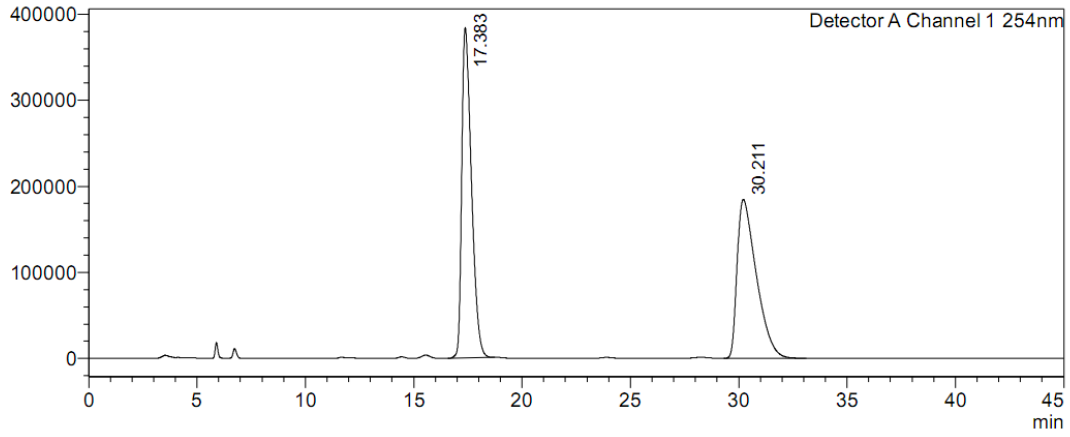


27a





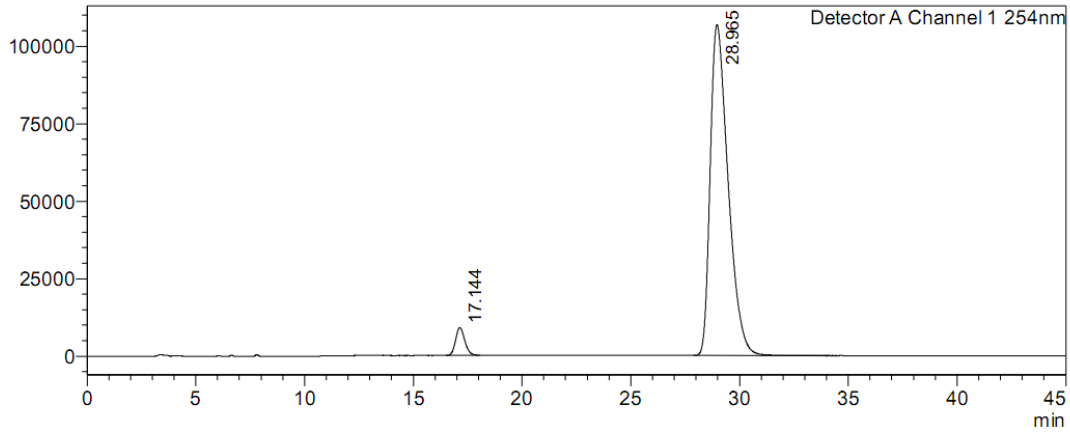
YXY3174B-OJH3010254230-50 YXY3174B-OJH3010254230-50.lcd



Detector A Channel 1 254nm

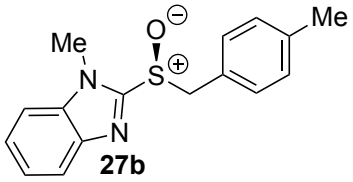
Peak#	Ret. Time	Area	Height	Height%	Area%
1	17.383	11828226	384055	67.514	51.004
2	30.211	11362426	184801	32.486	48.996
Total		23190652	568856	100.000	100.000

YXY3164A-OJH3010254230-50 YXY3164A-OJH3010254230-50.lcd

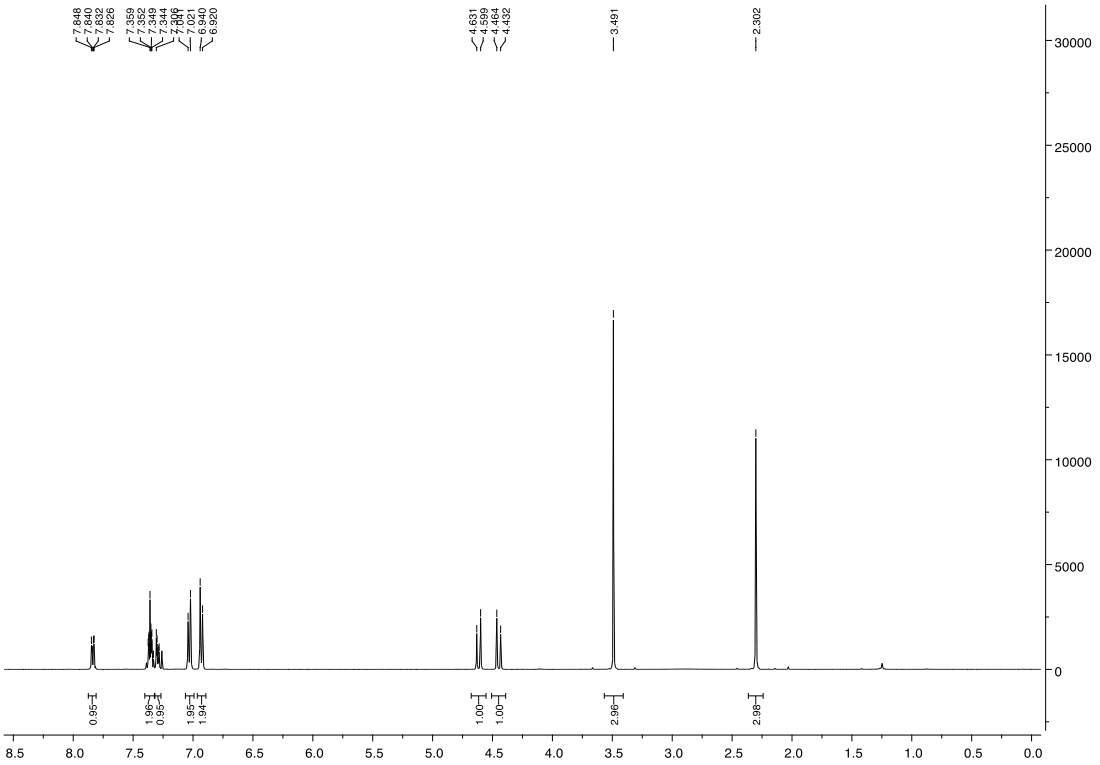


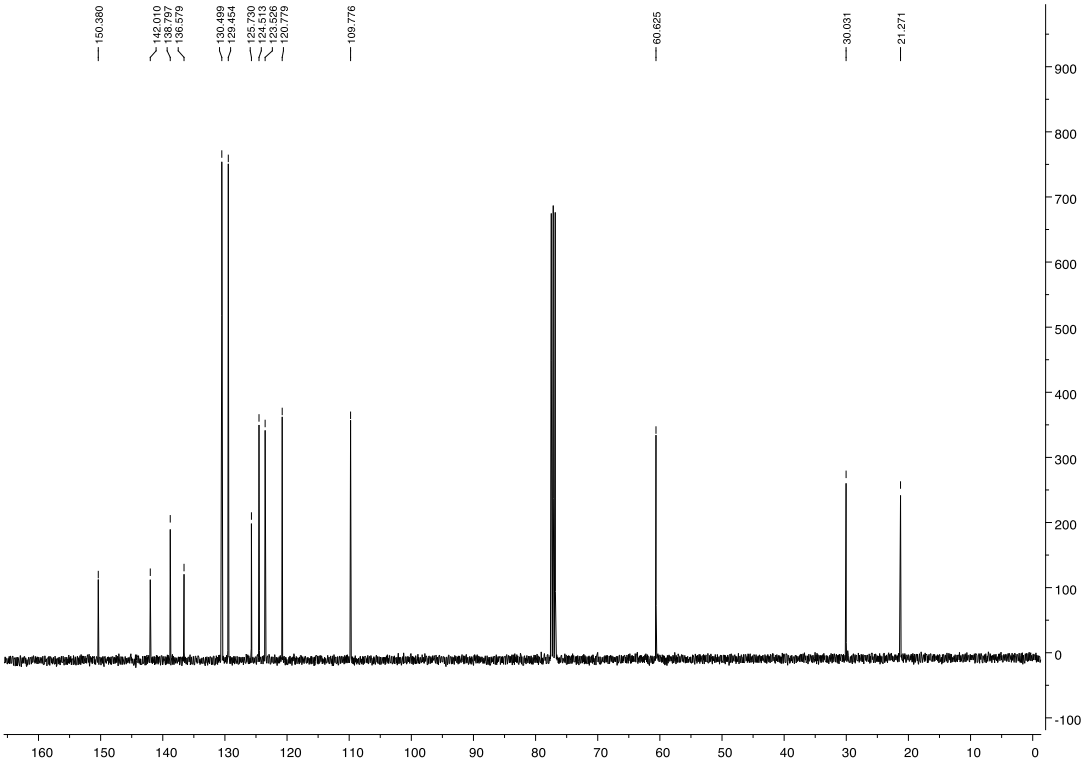
Detector A Channel 1 254nm

Peak#	Ret. Time	Area	Height	Height%	Area%
1	17.144	258746	8918	7.707	4.049
2	28.965	6131967	106799	92.293	95.951
Total		6390713	115718	100.000	100.000

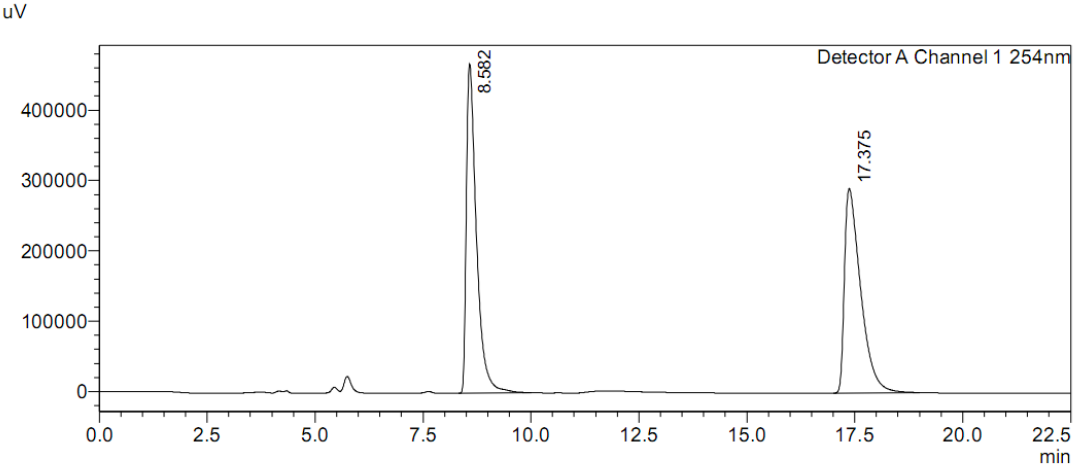

Me
O
S
Me
N
N

27b


7.848
7.840
7.832
7.826
7.359
7.352
7.349
7.344
7.021
6.940
6.920
4.631
4.599
4.464
4.432
3.491
2.302
0.95
1.96
0.95
1.95
1.94
1.00
1.00
2.96
2.98


150.380
142.010
138.797
136.579
130.499
129.454
125.790
124.513
123.526
120.779
109.776
60.625
30.031
21.271

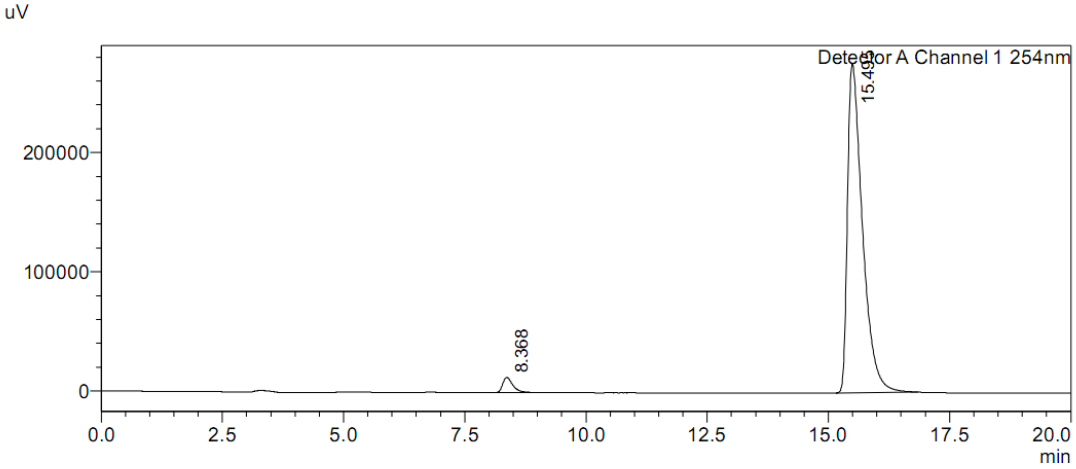
YZY1083A-IB3-3010254230-100-R YZY1083A-IB3-3010254230-100-R.lcd



Detector A Channel 1 254nm

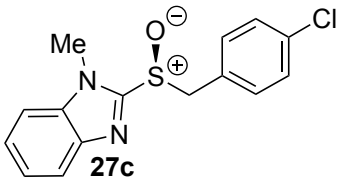
Peak#	Ret. Time	Area	Height	Height%	Area%
1	8.582	7605917	468032	61.694	50.142
2	17.375	7562819	290606	38.306	49.858
Total		15168736	758638	100.000	100.000

YXY3098A-IB3-3010254230-25 YXY3098A-IB3-3010254230-25.lcd

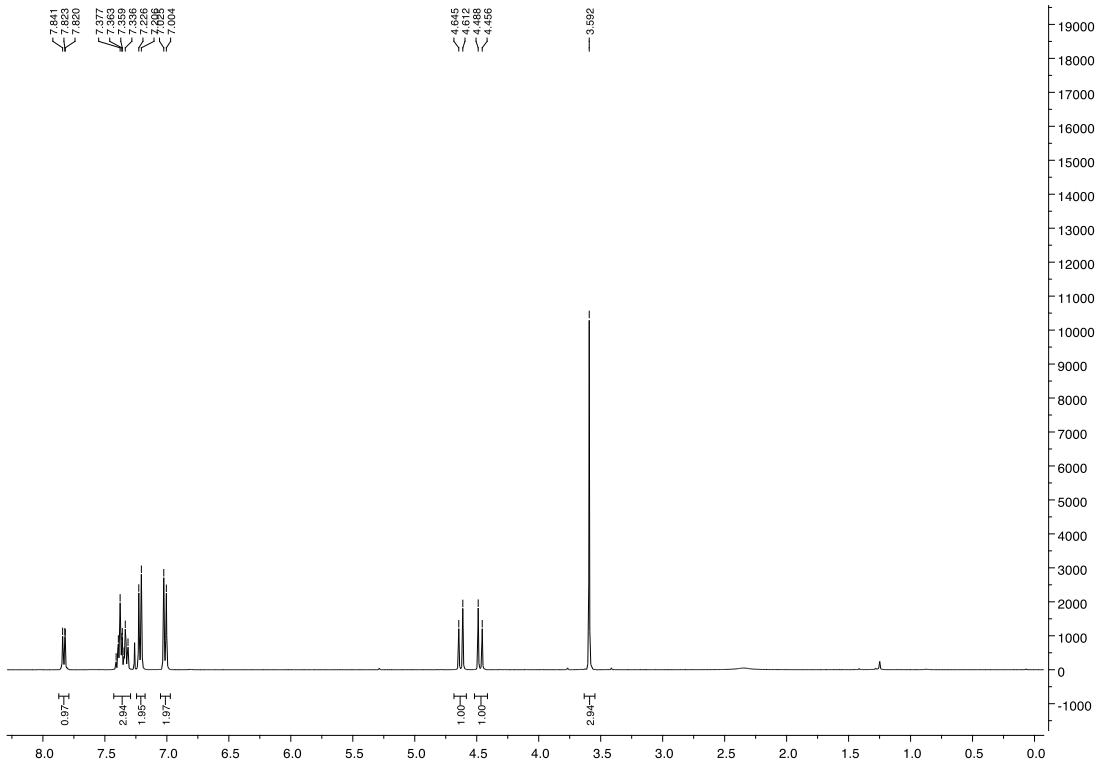


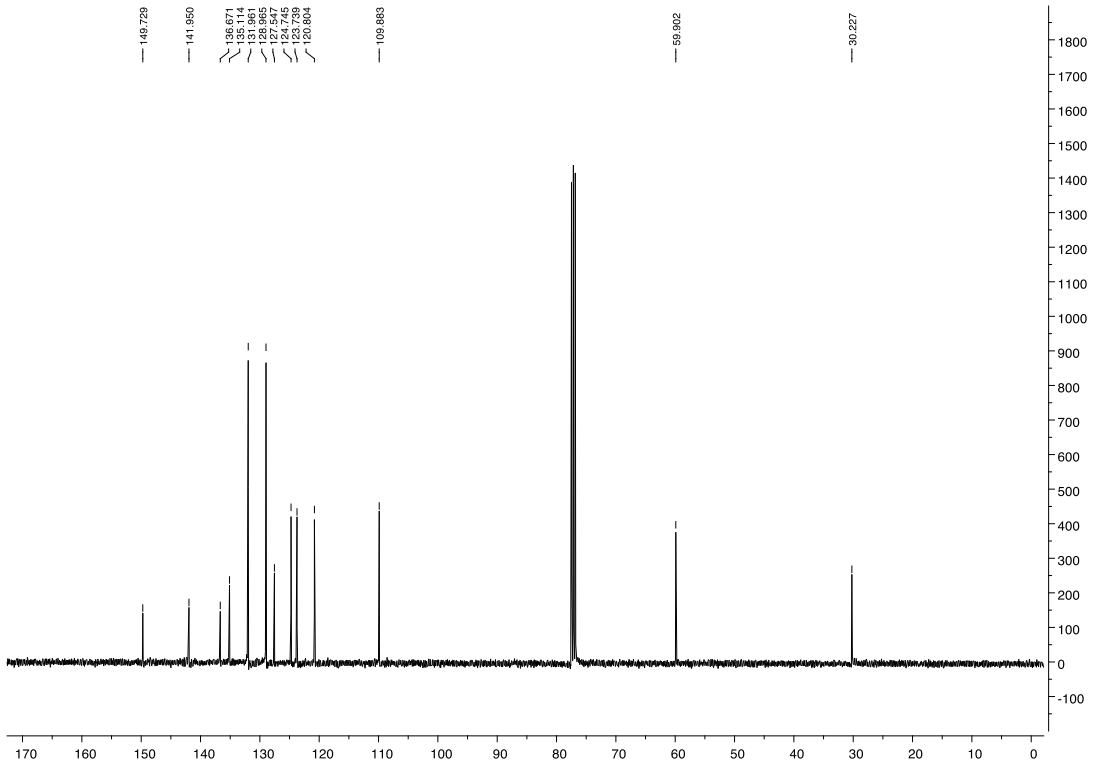
Detector A Channel 1 254nm

Peak#	Ret. Time	Area	Height	Height%	Area%
1	8.368	181149	12725	4.412	2.960
2	15.495	5939401	275660	95.588	97.040
Total		6120550	288385	100.000	100.000

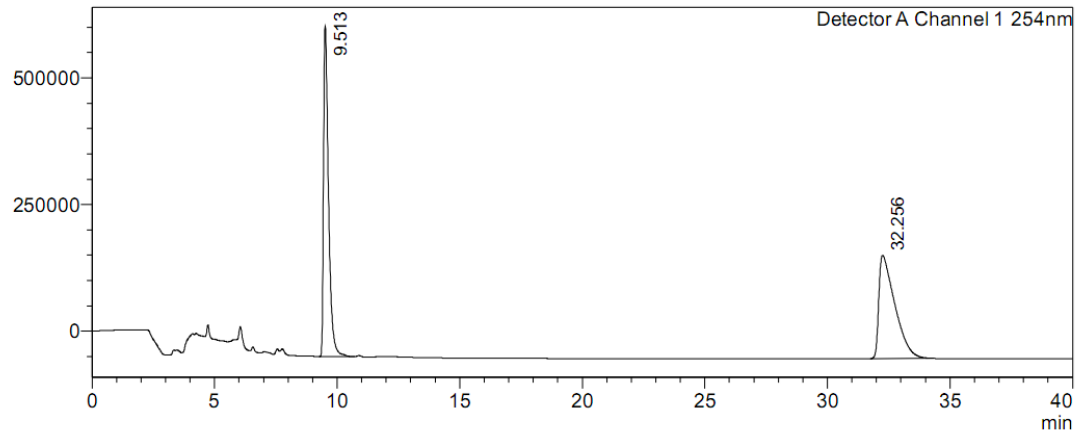

Me
N
O
S
N
Cl

27c


7.841
7.823
7.820
7.377
7.363
7.359
7.336
7.226
7.098
7.095
7.004
4.645
4.612
4.498
4.466
3.592
0.97
2.94
1.95
1.97
1.00
1.00
2.94


149.729
141.950
136.671
135.114
131.961
128.965
127.547
124.745
120.709
120.694
109.883
59.902
30.227

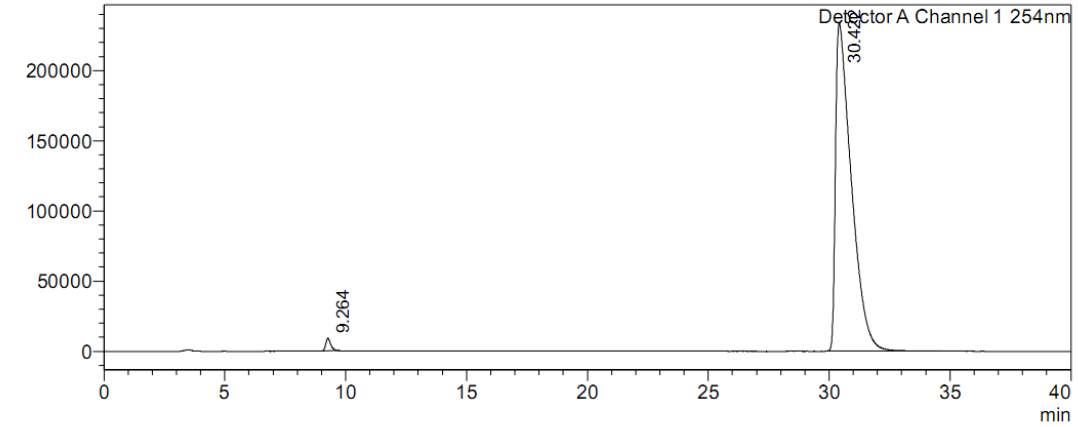
YZY1083C-IB3-3010254230-100-R YZY1083C-IB3-3010254230-100-R.lcd
uV



Detector A Channel 1 254nm

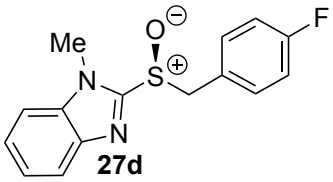
Peak#	Ret. Time	Area	Height	Height%	Area%
1	9.513	9270799	652125	76.174	50.018
2	32.256	9264079	203976	23.826	49.982
Total		18534878	856101	100.000	100.000

YXY3132A-IB3-3010254230-40 YXY3132A-IB3-3010254230-40.lcd
uV

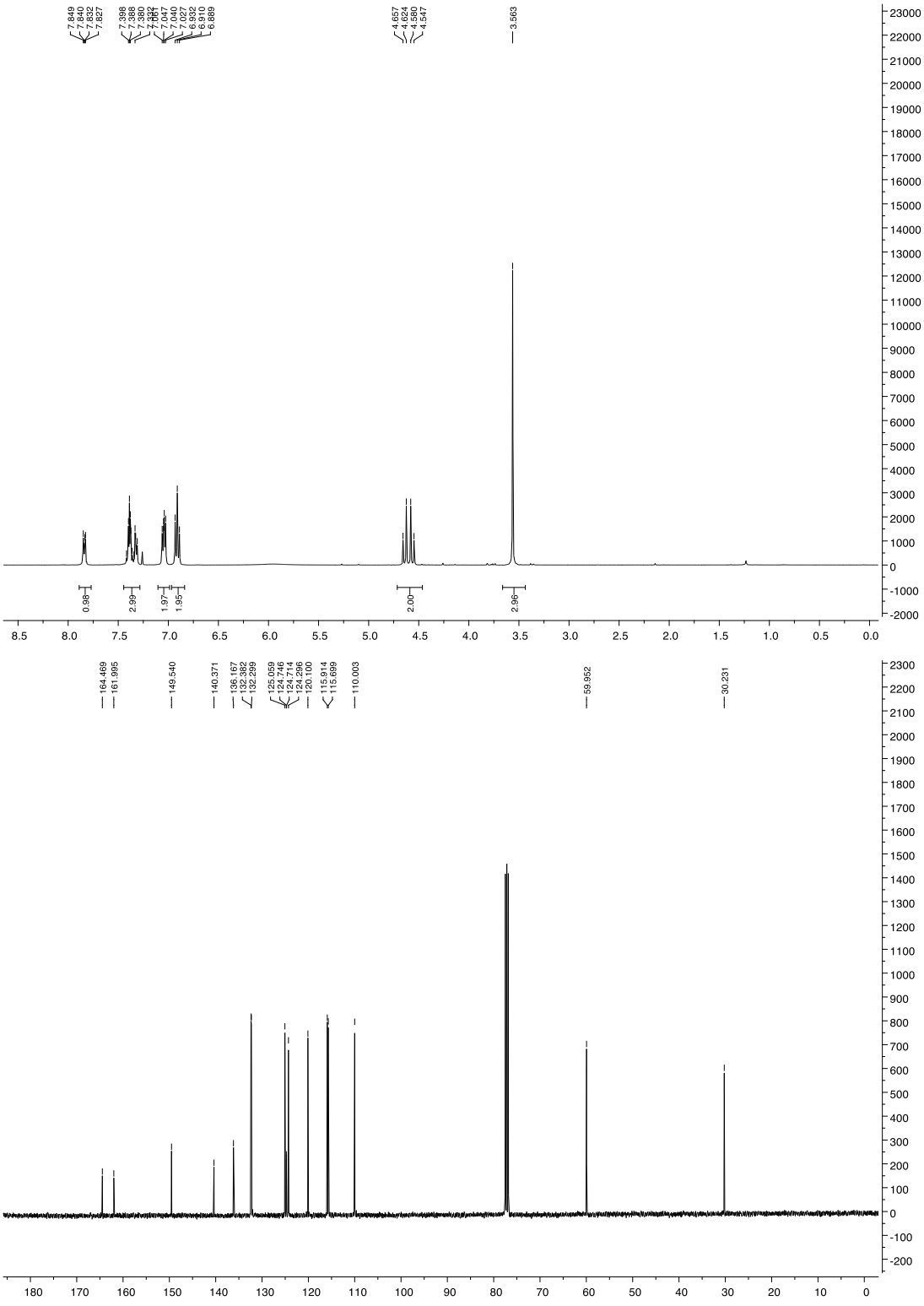


Detector A Channel 1 254nm

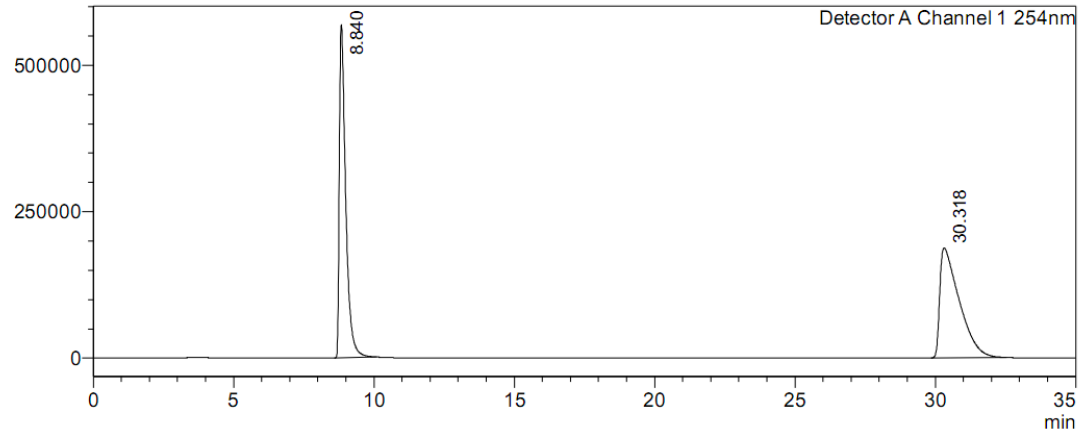
Peak#	Ret. Time	Area	Height	Height%	Area%
1	9.264	130431	8985	3.706	1.207
2	30.422	10673637	233449	96.294	98.793
Total		10804068	242434	100.000	100.000


Me
N
O
S
F
N

27d


7.849
7.840
7.832
7.827
7.398
7.388
7.380
7.372
7.061
7.047
7.040
7.027
6.932
6.910
6.889
4.657
4.624
4.580
4.547
3.563
0.98
2.99
1.97
1.95
2.00
2.96
164.469
161.995
149.540
140.371
136.167
132.382
132.299
125.059
124.946
124.714
124.296
120.100
115.914
115.699
110.003
59.952
30.231

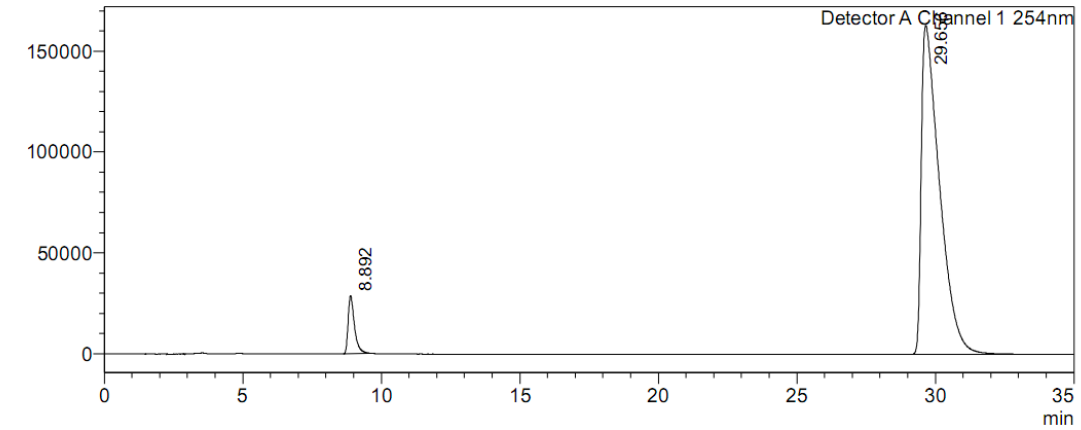
YXY3154A-IB3-3010254230-100-R YXY3154A-IB3-3010254230-100-R.lcd
uV



Detector A Channel 1 254nm

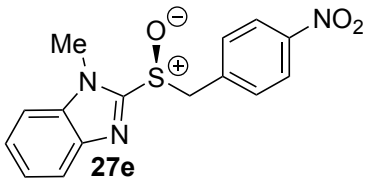
Peak#	Ret. Time	Area	Height	Height%	Area%
1	8.840	9031234	568421	75.153	49.912
2	30.318	9062975	187934	24.847	50.088
Total		18094209	756355	100.000	100.000

YXY3154B-IB3-3010254230-40 YXY3154B-IB3-3010254230-40.lcd
uV

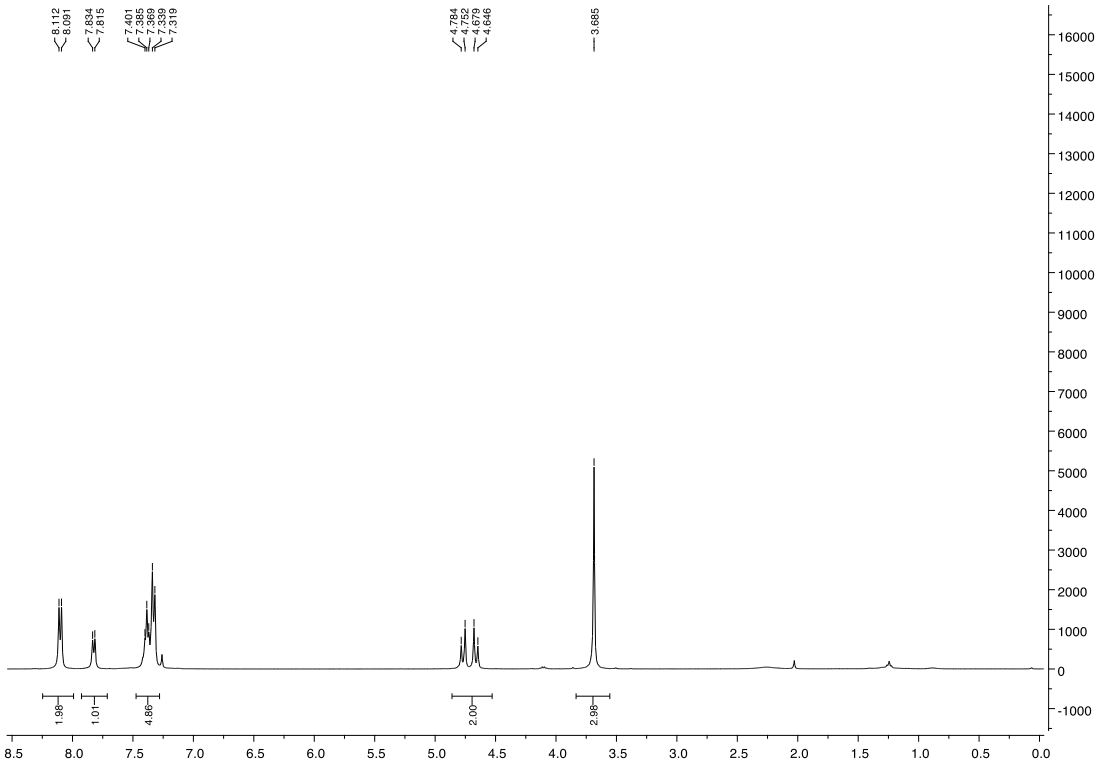


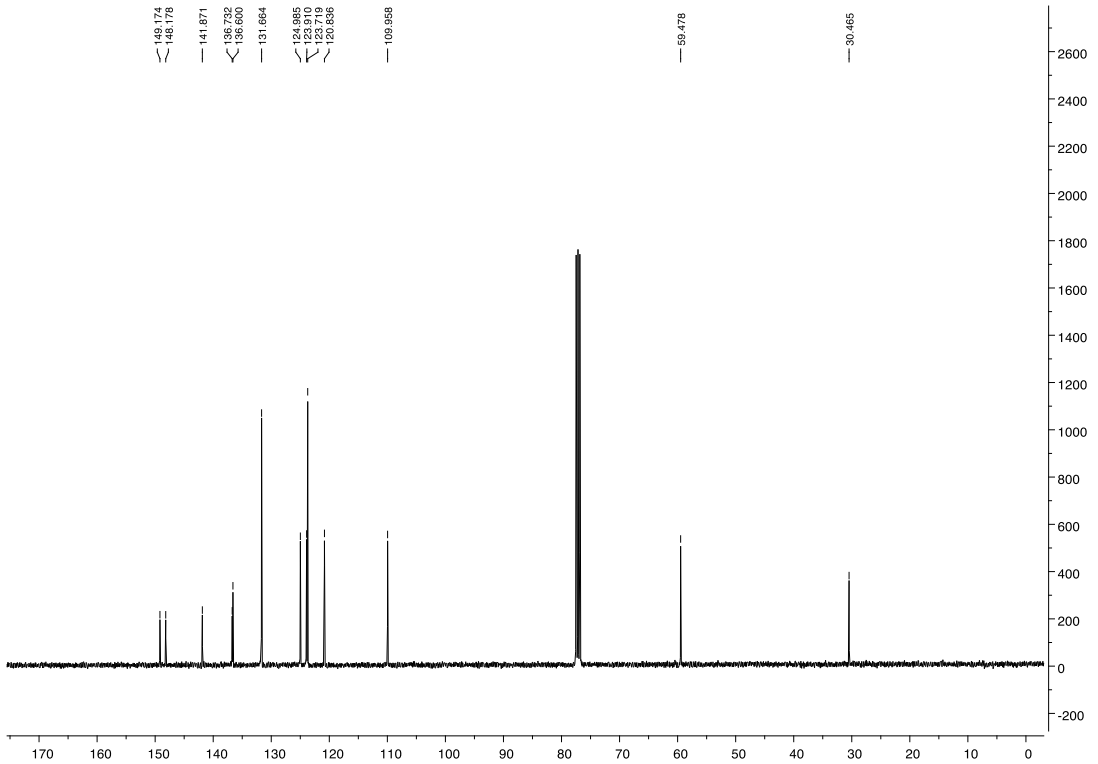
Detector A Channel 1 254nm

Peak#	Ret. Time	Area	Height	Height%	Area%
1	8.892	456992	28775	14.998	5.777
2	29.656	7453577	163083	85.002	94.223
Total		7910569	191859	100.000	100.000

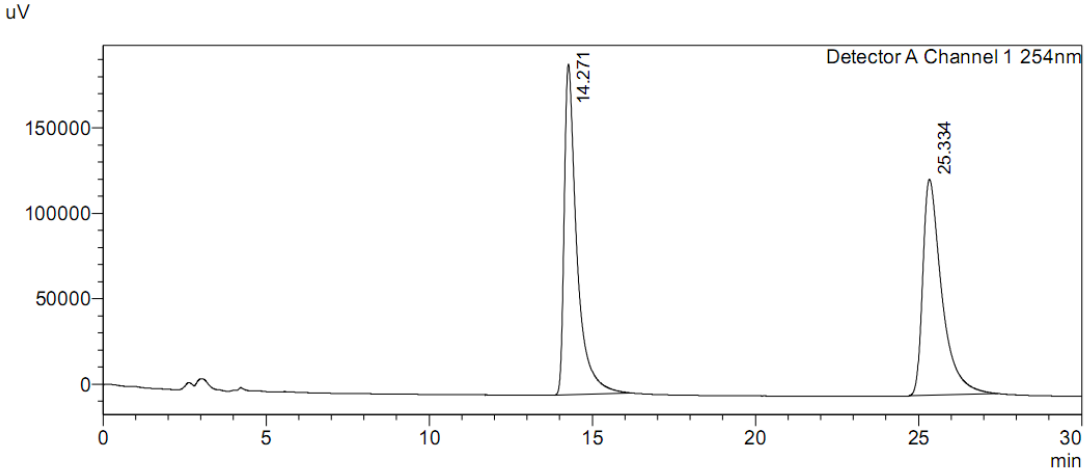

Me
N
O
S
N
NO2

27e


8.112
8.091
7.834
7.815
7.401
7.385
7.369
7.339
7.319
4.784
4.752
4.679
4.646
3.685
1.98
1.01
4.86
2.00
2.98


149.174
148.178
141.871
136.732
136.600
131.664
124.985
123.910
123.719
120.836
109.958
59.478
30.465

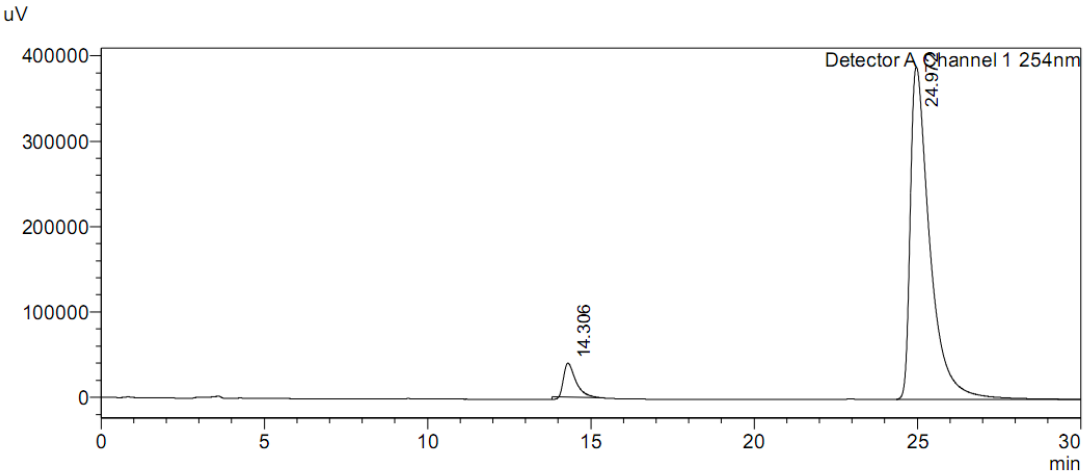
YXY3172A-IA3-3010254230-100-R YXY3172A-IA3-3010254230-100-R.lcd



Detector A Channel 1 254nm

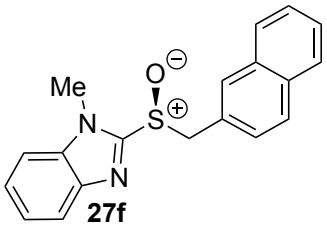
Peak#	Ret. Time	Area	Height	Height%	Area%
1	14.271	5209509	193648	60.479	50.325
2	25.334	5142280	126542	39.521	49.675
Total		10351789	320190	100.000	100.000

YXY3184-IA3-3010254230-40 YXY3184-IA3-3010254230-40.lcd

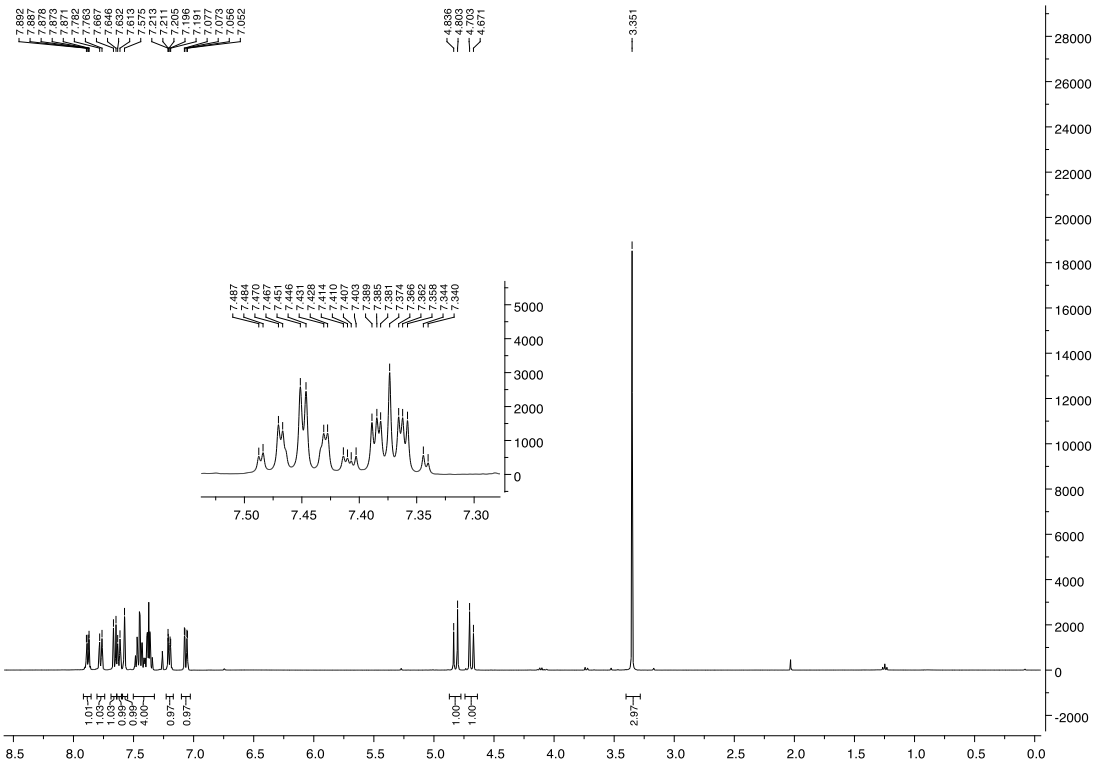


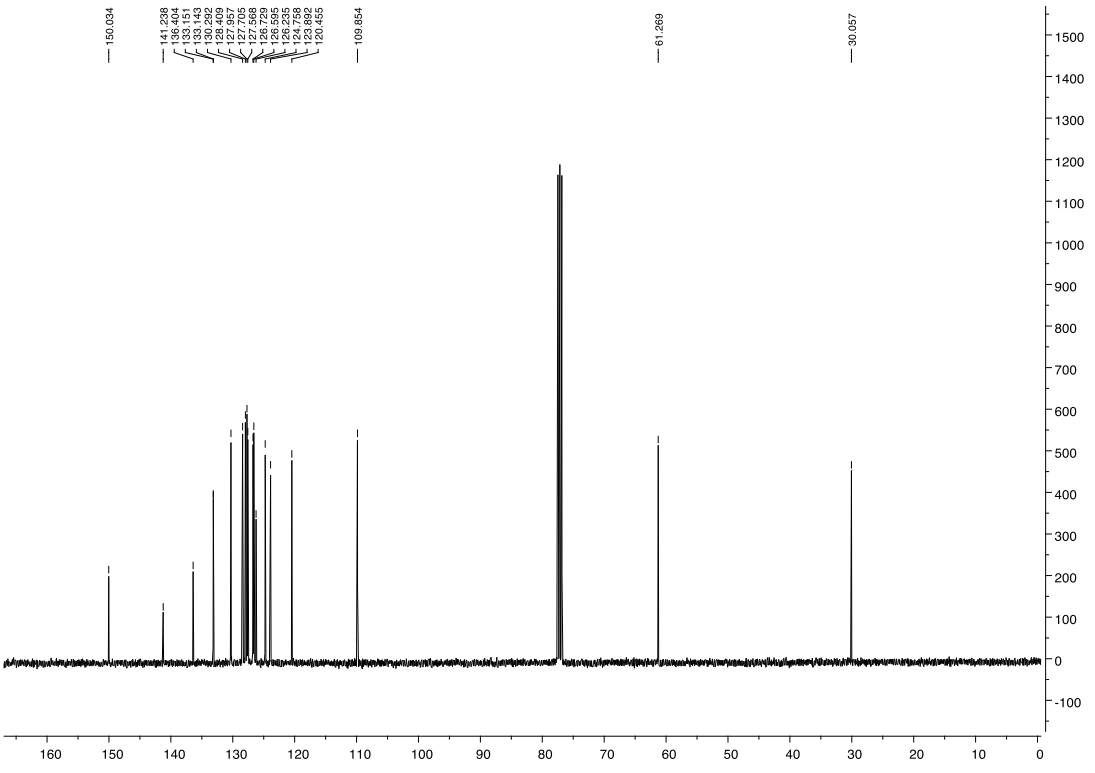
Detector A Channel 1 254nm

Peak#	Ret. Time	Area	Height	Height%	Area%
1	14.306	1018531	40008	9.311	5.933
2	24.972	16149837	389671	90.689	94.067
Total		17168368	429679	100.000	100.000


Me
N
O
S
N

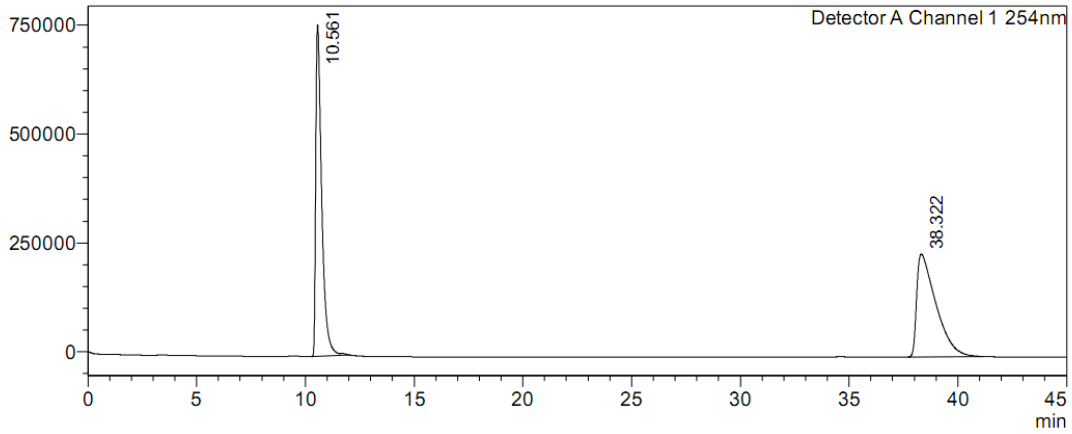
27f


7.892
7.887
7.878
7.873
7.871
7.782
7.763
7.687
7.645
7.632
7.613
7.575
7.213
7.211
7.205
7.196
7.191
7.077
7.073
7.056
7.052
4.636
4.683
4.703
4.671
3.351
7.487
7.484
7.470
7.467
7.451
7.446
7.431
7.428
7.414
7.410
7.407
7.403
7.389
7.385
7.381
7.374
7.366
7.362
7.358
7.344
7.340
1.01
1.03
0.93
0.89
4.00
0.97
0.97
1.00
1.00
2.97


150.034
141.238
136.404
133.151
133.143
129.292
128.499
127.957
127.705
127.568
126.729
126.595
126.235
124.758
123.892
120.455
109.854
61.269
30.057

YXY3192A-IB3-3010254230-100-R YXY3192A-IB3-3010254230-100-R.lcd

uV

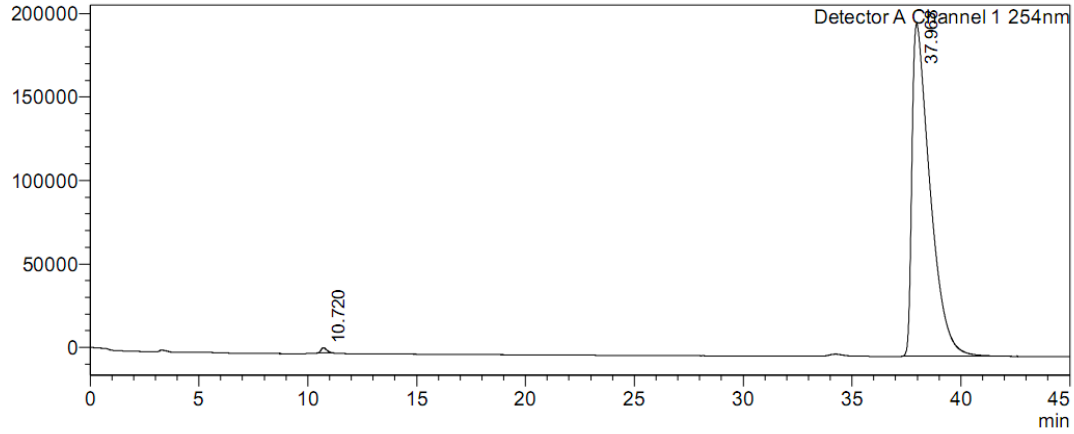


Detector A Channel 1 254nm

Peak#	Ret. Time	Area	Height	Height%	Area%
1	10.561	14573807	761242	76.291	49.966
2	38.322	14593517	236572	23.709	50.034
Total		29167324	997813	100.000	100.000

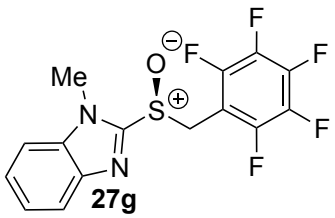
YXY3192B-IB3-3010254230-50 YXY3192B-IB3-3010254230-50.lcd

uV

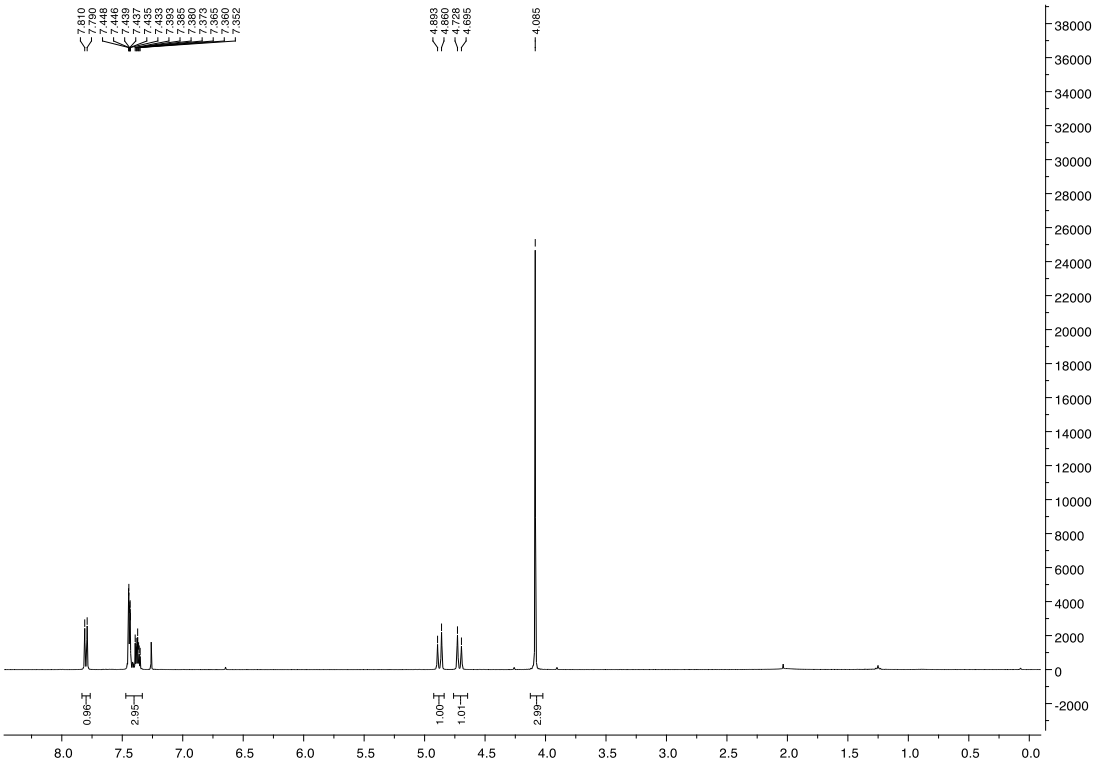


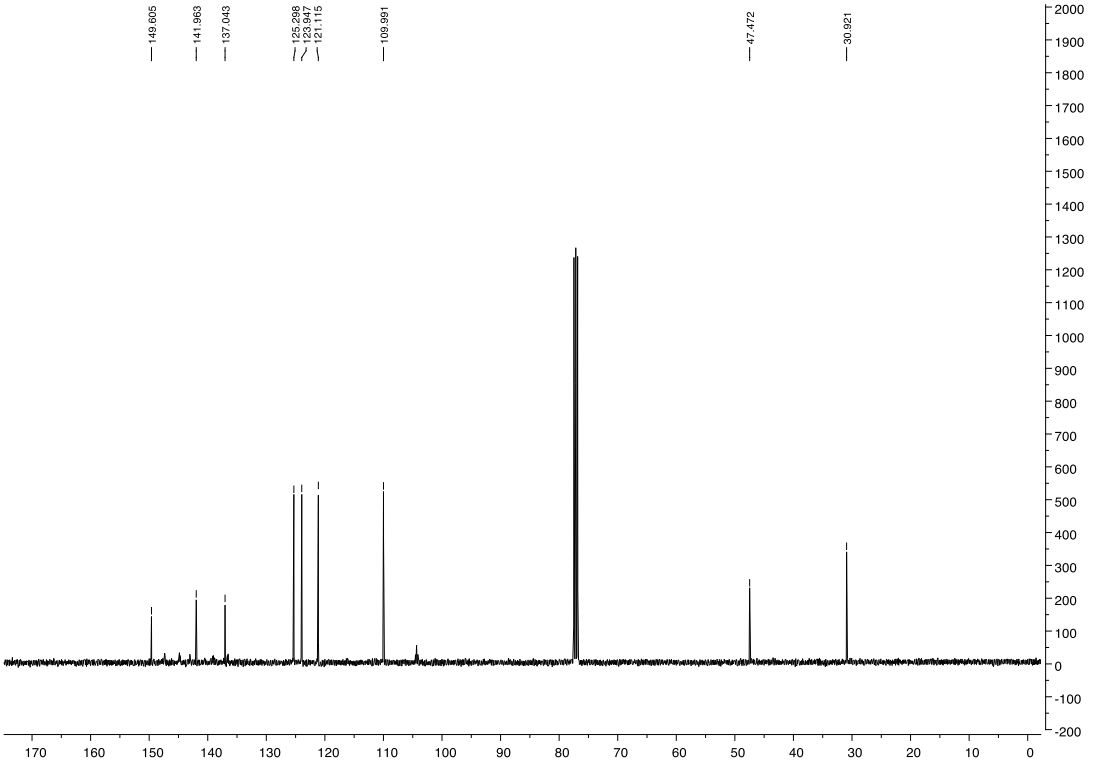
Detector A Channel 1 254nm

Peak#	Ret. Time	Area	Height	Height%	Area%
1	10.720	57575	3142	1.554	0.497
2	37.968	11525223	198996	98.446	99.503
Total		11582798	202138	100.000	100.000

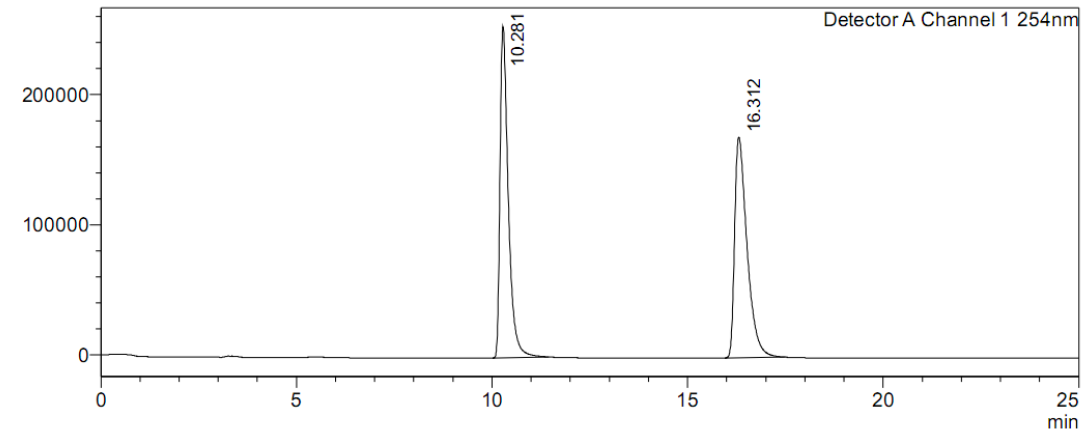

Me
N
O
S
F
F
F
F
F
N

27g


7.810
7.790
7.448
7.446
7.439
7.437
7.435
7.433
7.393
7.385
7.380
7.373
7.365
7.360
7.352
4.883
4.860
4.728
4.695
4.085
0.96
2.95
1.00
1.01
2.99


149.605
141.963
137.043
125.298
123.947
121.115
109.991
47.472
30.921

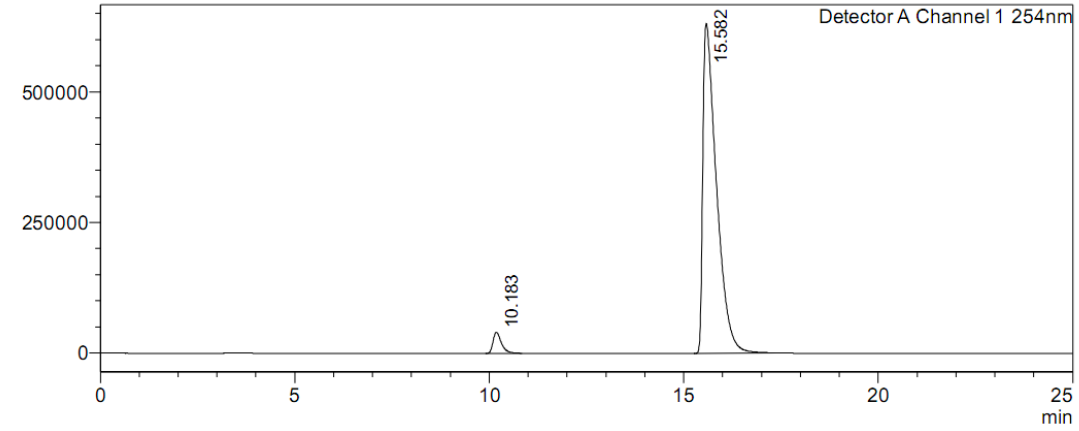
YXY3172B-IB3-3010254230-100-R YXY3172B-IB3-3010254230-100-R.lcd



Detector A Channel 1 254nm

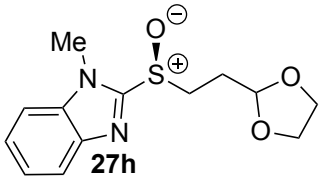
Peak#	Ret. Time	Area	Height	Height%	Area%
1	10.281	3775097	254634	60.014	50.158
2	16.312	3751267	169654	39.986	49.842
Total		7526363	424288	100.000	100.000

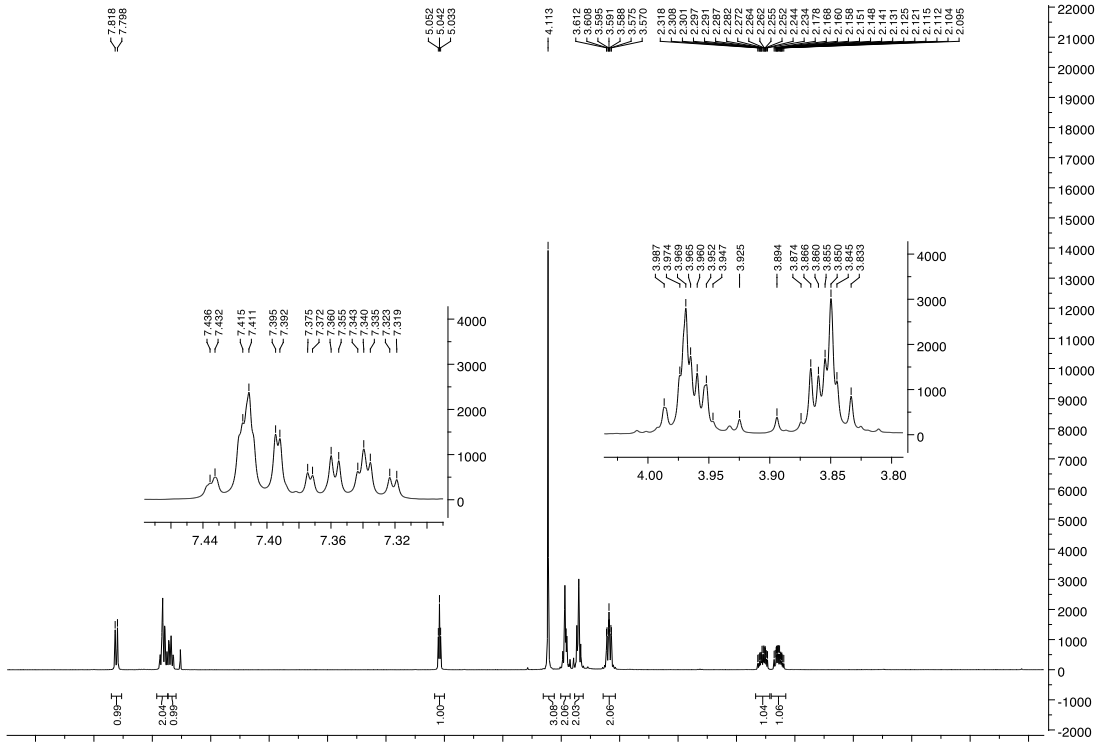
YXY3182-IB3-3010254230-25 YXY3182-IB3-3010254230-25.lcd

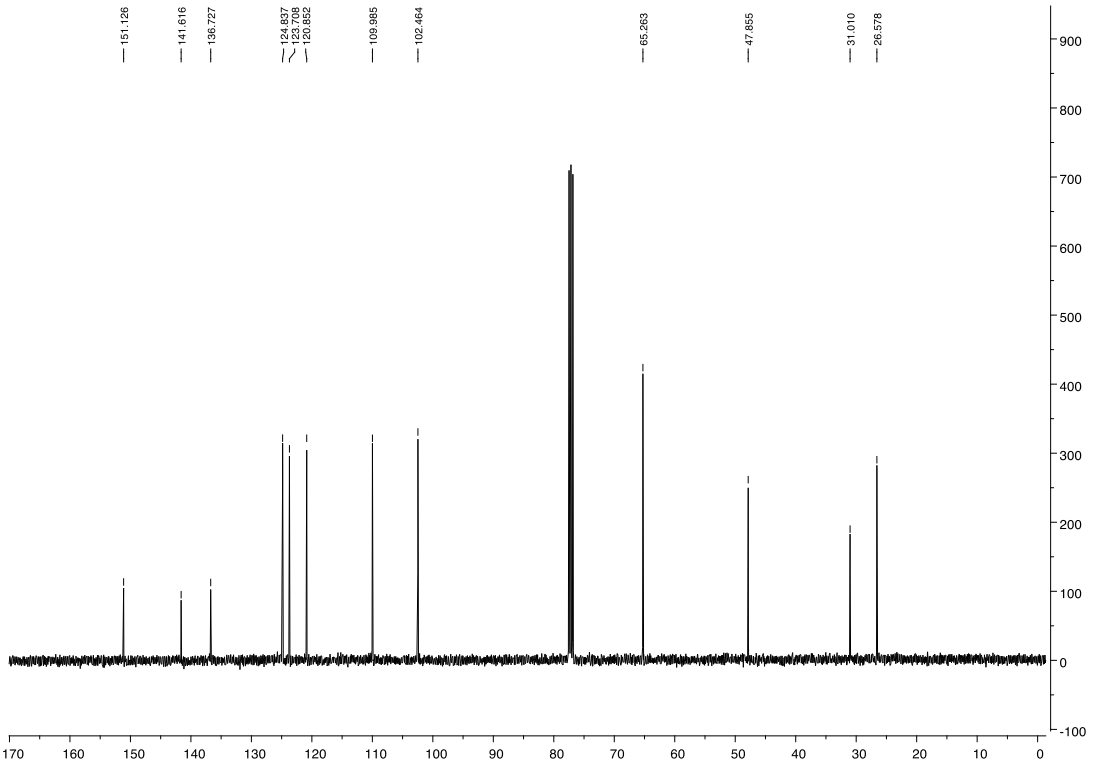


Detector A Channel 1 254nm

Peak#	Ret. Time	Area	Height	Height%	Area%
1	10.183	614364	40590	6.038	3.838
2	15.582	15393442	631604	93.962	96.162
Total		16007806	672195	100.000	100.000

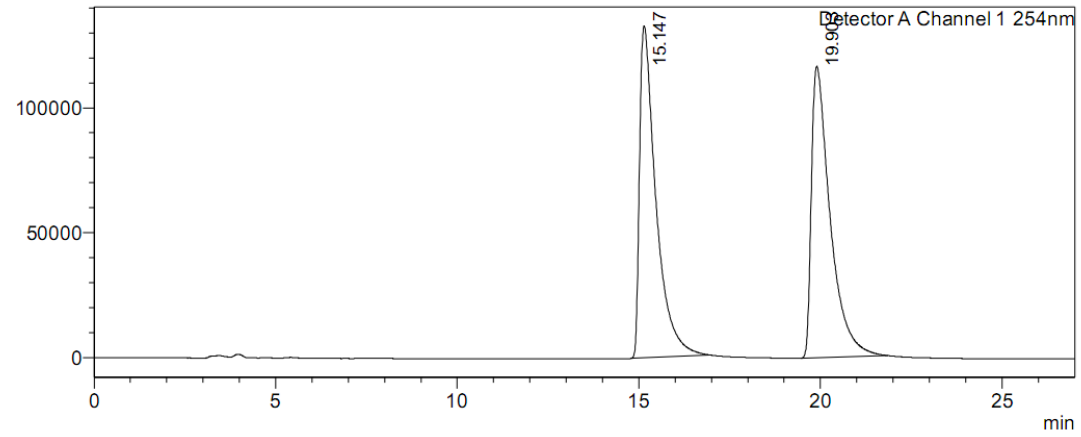

Me
N
S
O
O
N
O
27h


7.818
7.798
5.052
5.042
5.033
4.113
3.612
3.608
3.595
3.591
3.588
3.575
3.570
2.318
2.308
2.301
2.297
2.291
2.287
2.282
2.272
2.264
2.262
2.255
2.252
2.244
2.234
2.178
2.168
2.160
2.158
2.151
2.148
2.141
2.131
2.125
2.121
2.115
2.112
2.104
2.095
7.436
7.432
7.415
7.411
7.395
7.392
7.375
7.372
7.360
7.355
7.343
7.340
7.335
7.323
7.319
3.987
3.974
3.969
3.965
3.960
3.952
3.947
3.925
3.894
3.874
3.866
3.860
3.855
3.850
3.845
3.833
0.99
2.04
0.99
1.00
3.08
2.06
2.03
2.06
1.04
1.06


151.126
141.616
136.727
124.937
123.709
120.852
109.985
102.464
65.263
47.855
31.010
26.578

YXY3248A-IB3-3010254230-100-R YXY3248A-IB3-3010254230-100-R.lcd

uV

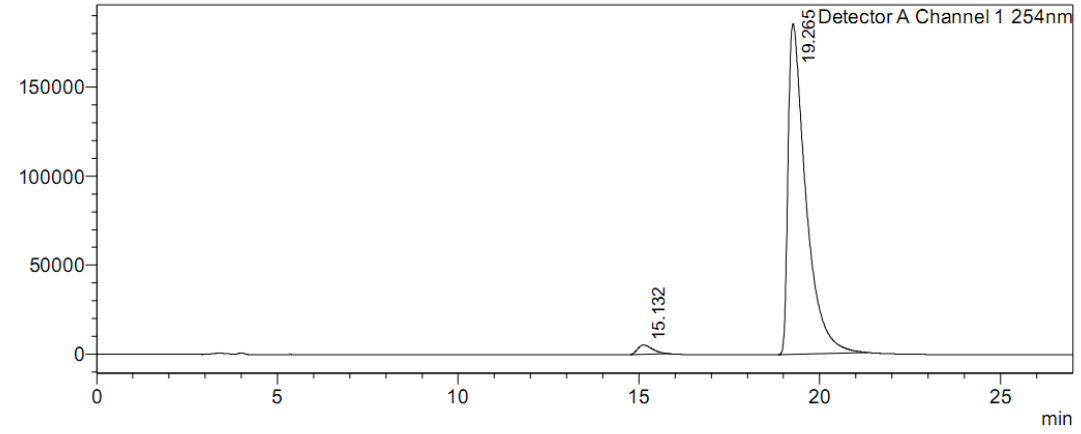


Detector A Channel 1 254nm

Peak#	Ret. Time	Area	Height	Height%	Area%
1	15.147	4189489	133053	53.288	49.991
2	19.903	4191050	116633	46.712	50.009
Total		8380539	249686	100.000	100.000

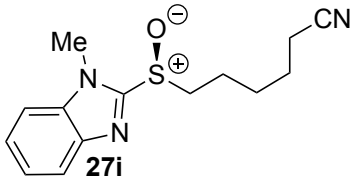
YXY3248B-IB3-3010254230-30 YXY3248B-IB3-3010254230-30.lcd

uV

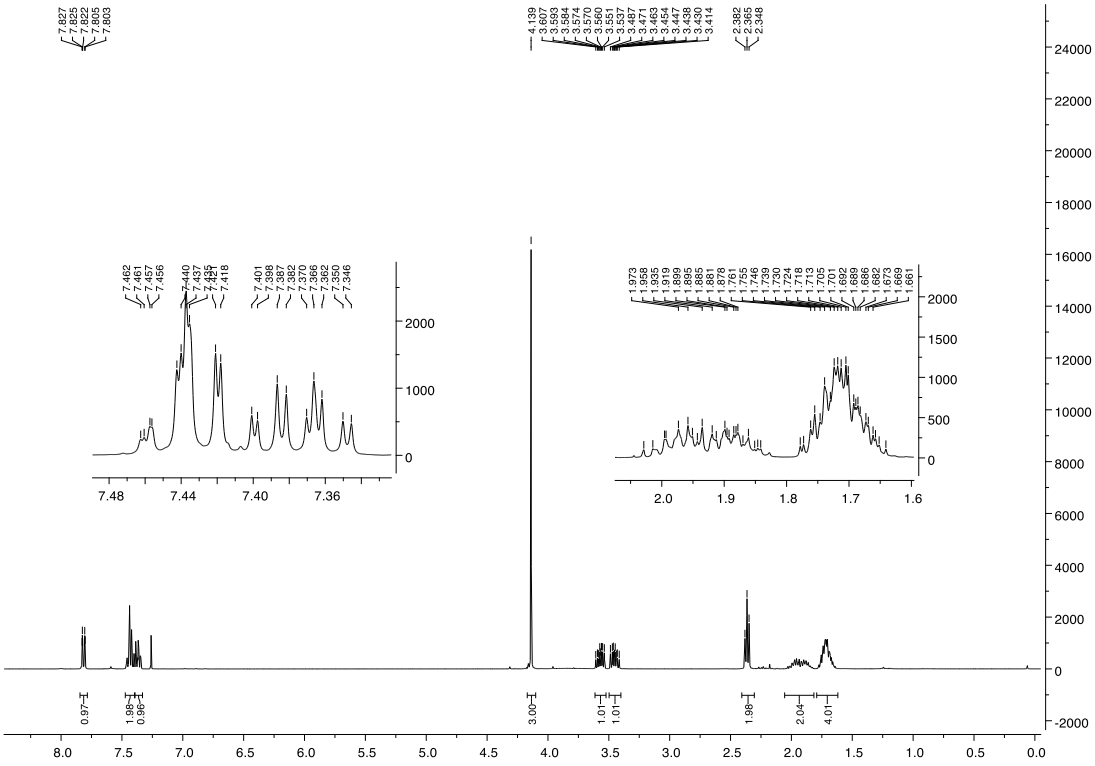


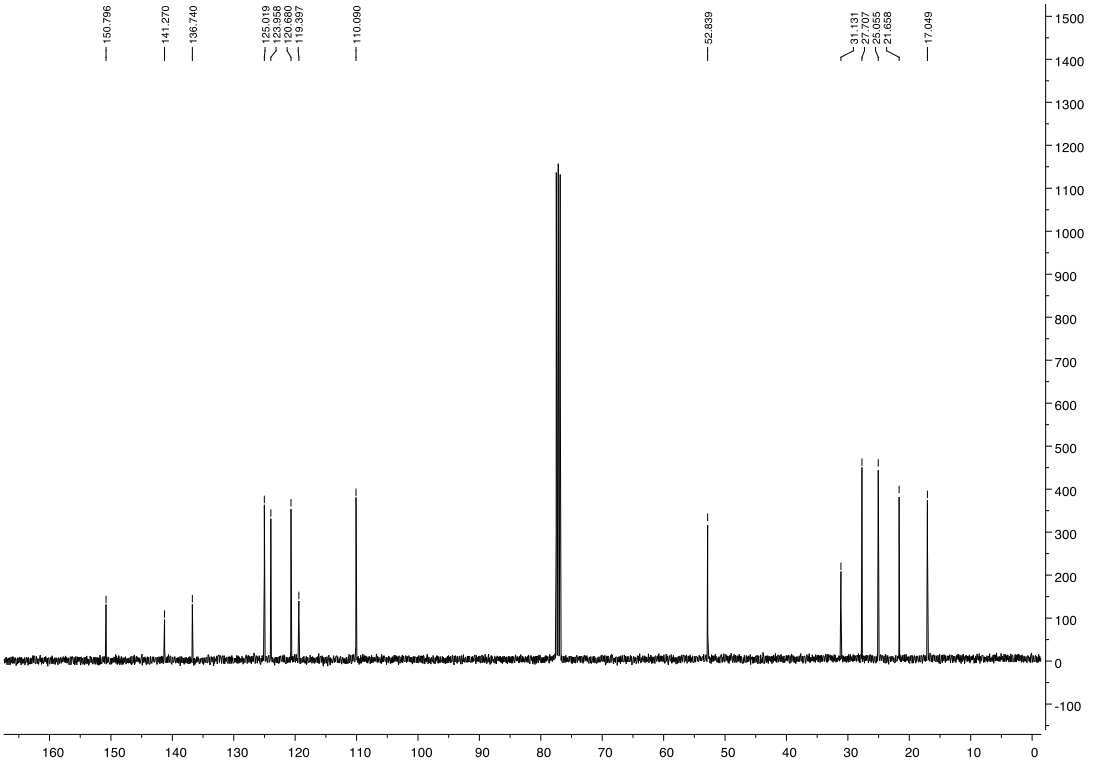
Detector A Channel 1 254nm

Peak#	Ret. Time	Area	Height	Height%	Area%
1	15.132	145996	5147	2.694	2.246
2	19.265	6353557	185876	97.306	97.754
Total		6499554	191023	100.000	100.000

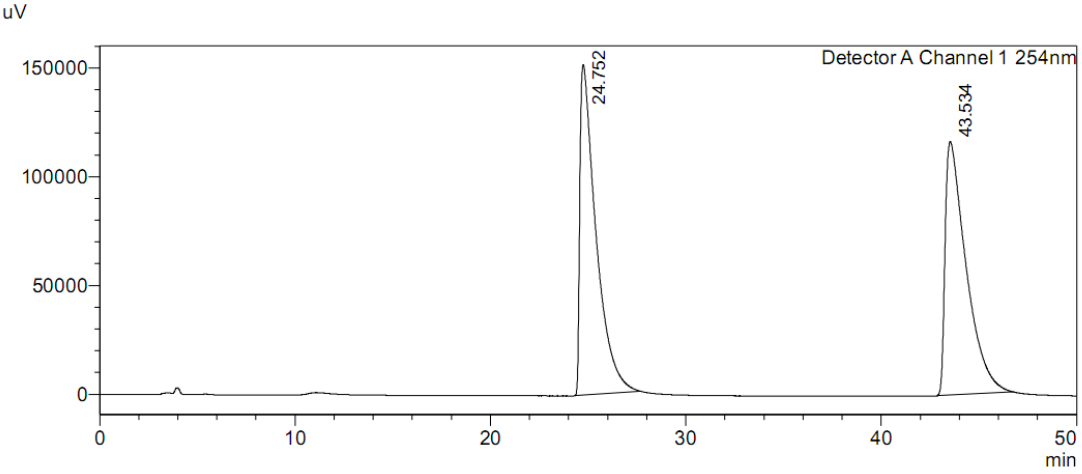


27i





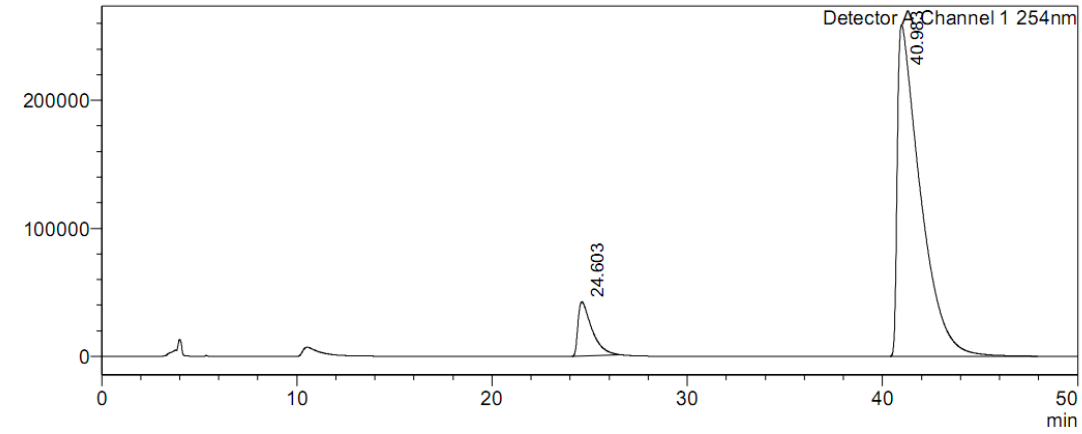
YXY3250A-IB3-3010254230-100-R YXY3250A-IB3-3010254230-100-R.lcd



Detector A Channel 1 254nm

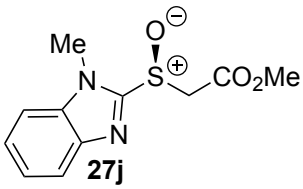
Peak#	Ret. Time	Area	Height	Height%	Area%
1	24.752	8728851	152023	56.608	50.045
2	43.534	8713116	116533	43.392	49.955
Total		17441967	268557	100.000	100.000

YXY3250B-IB3-3010254230-60 YXY3250B-IB3-3010254230-60.lcd

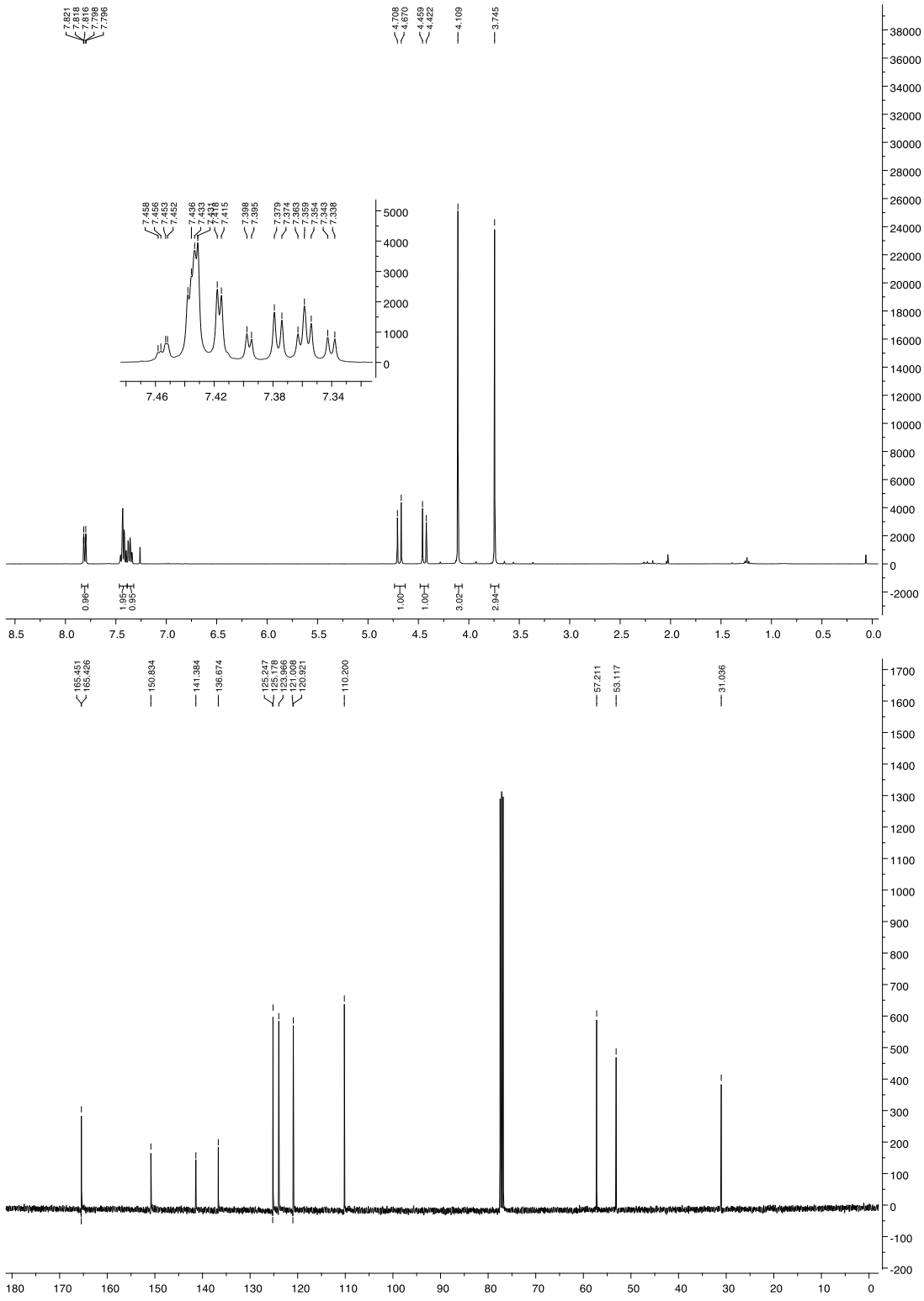


Detector A Channel 1 254nm

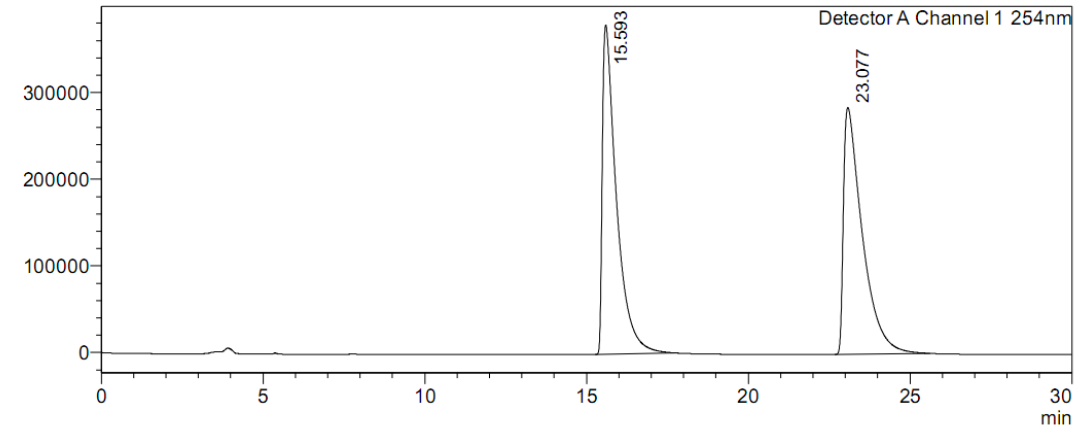
Peak#	Ret. Time	Area	Height	Height%	Area%
1	24.603	2099469	42298	14.042	9.041
2	40.983	21122932	258922	85.958	90.959
Total		23222401	301220	100.000	100.000


Me
N
O
S
CO2Me
N

27j


7.821
7.818
7.816
7.709
7.708
7.796
4.708
4.670
4.459
4.422
4.109
3.745
7.458
7.456
7.455
7.452
7.436
7.433
7.431
7.418
7.415
7.398
7.395
7.379
7.374
7.369
7.359
7.354
7.343
7.338
0.96
1.95
0.95
1.00
1.00
3.02
2.94
165.451
165.426
150.834
141.384
136.674
125.247
125.178
123.966
121.008
120.921
110.200
57.211
53.117
31.036

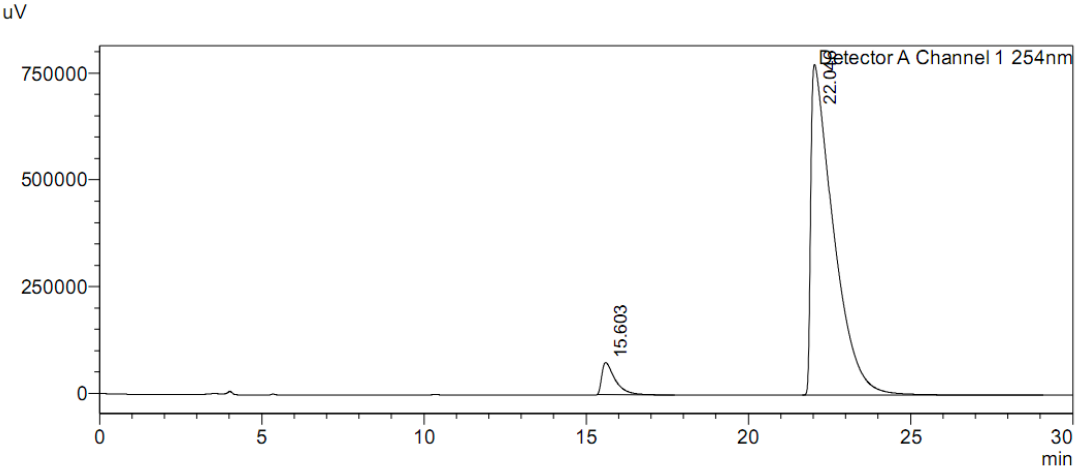
YXY3232A-IB3-3010254230-100-R YXY3232A-IB3-3010254230-100-R.lcd



Detector A Channel 1 254nm

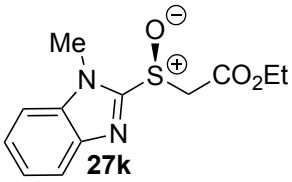
Peak#	Ret. Time	Area	Height	Height%	Area%
1	15.593	11563134	380259	57.169	49.952
2	23.077	11585415	284892	42.831	50.048
Total		23148549	665152	100.000	100.000

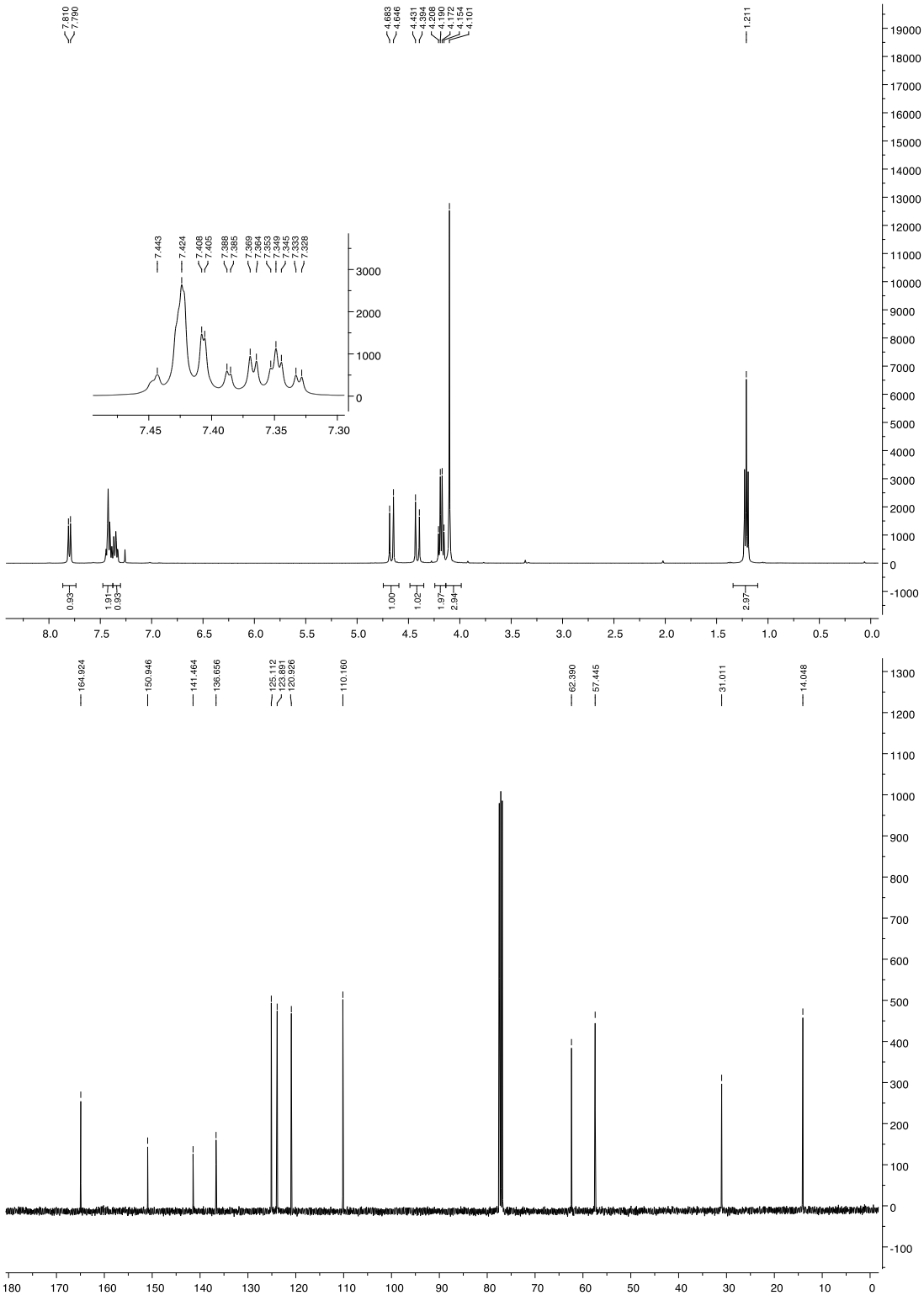
YXY3232B-IB3-3010254230-35 YXY3232B-IB3-3010254230-35.lcd



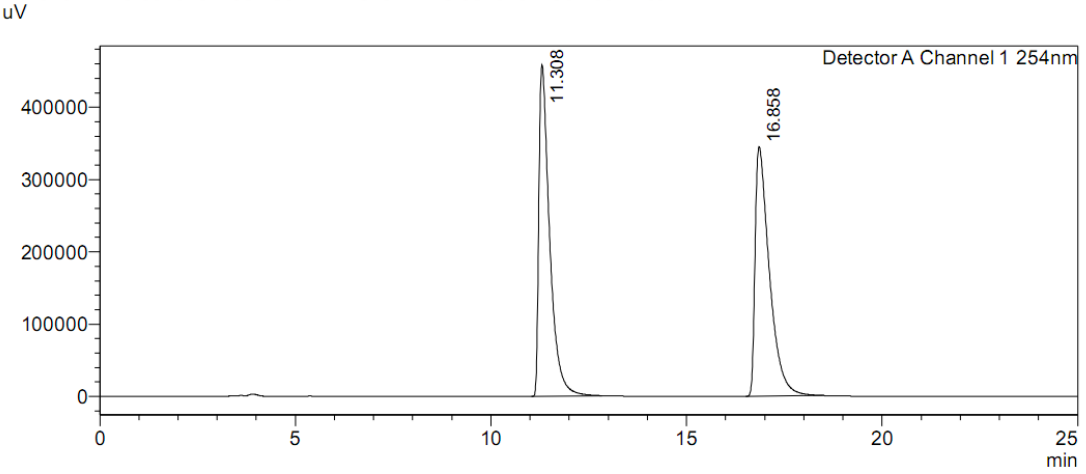
Detector A Channel 1 254nm

Peak#	Ret. Time	Area	Height	Height%	Area%
1	15.603	2152543	74999	8.822	5.411
2	22.046	37628485	775177	91.178	94.589
Total		39781028	850176	100.000	100.000


Me
N
O
S
CO2Et
N
27k


7.810
7.790
4.683
4.646
4.431
4.394
4.208
4.190
4.172
4.154
4.101
1.211
7.443
7.424
7.408
7.405
7.388
7.385
7.369
7.364
7.353
7.349
7.345
7.333
7.328
0.93
1.91
0.93
1.00
1.02
1.97
2.94
2.97
164.924
150.946
141.464
136.656
125.112
123.891
120.926
110.160
62.390
57.445
31.011
14.048

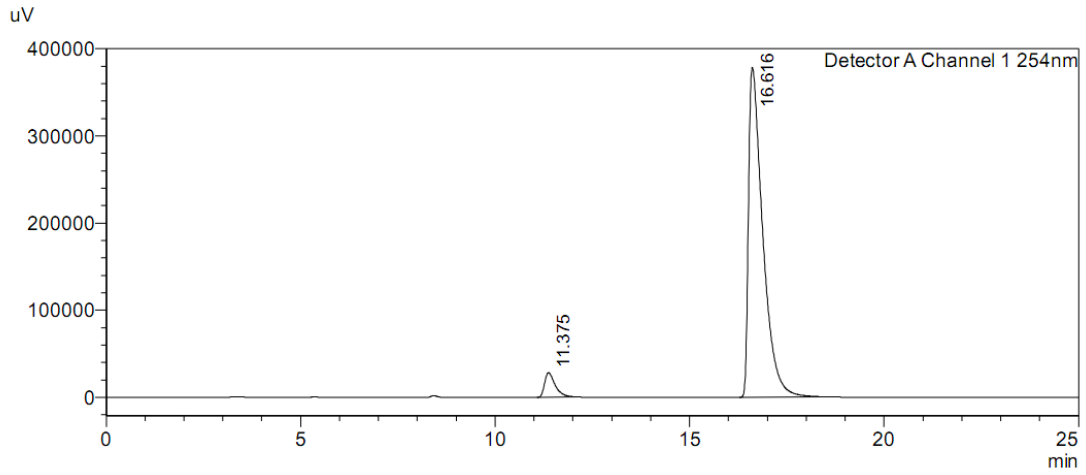
YXY3234A-IB3-3010254230-100-R YXY3234A-IB3-3010254230-100-R.lcd



Detector A Channel 1 254nm

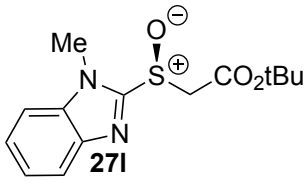
Peak#	Ret. Time	Area	Height	Height%	Area%
1	11.308	8811903	458927	57.063	49.972
2	16.858	8821841	345322	42.937	50.028
Total		17633744	804249	100.000	100.000

YXY3234B-IB3-3010254230-25 YXY3234B-IB3-3010254230-25.lcd

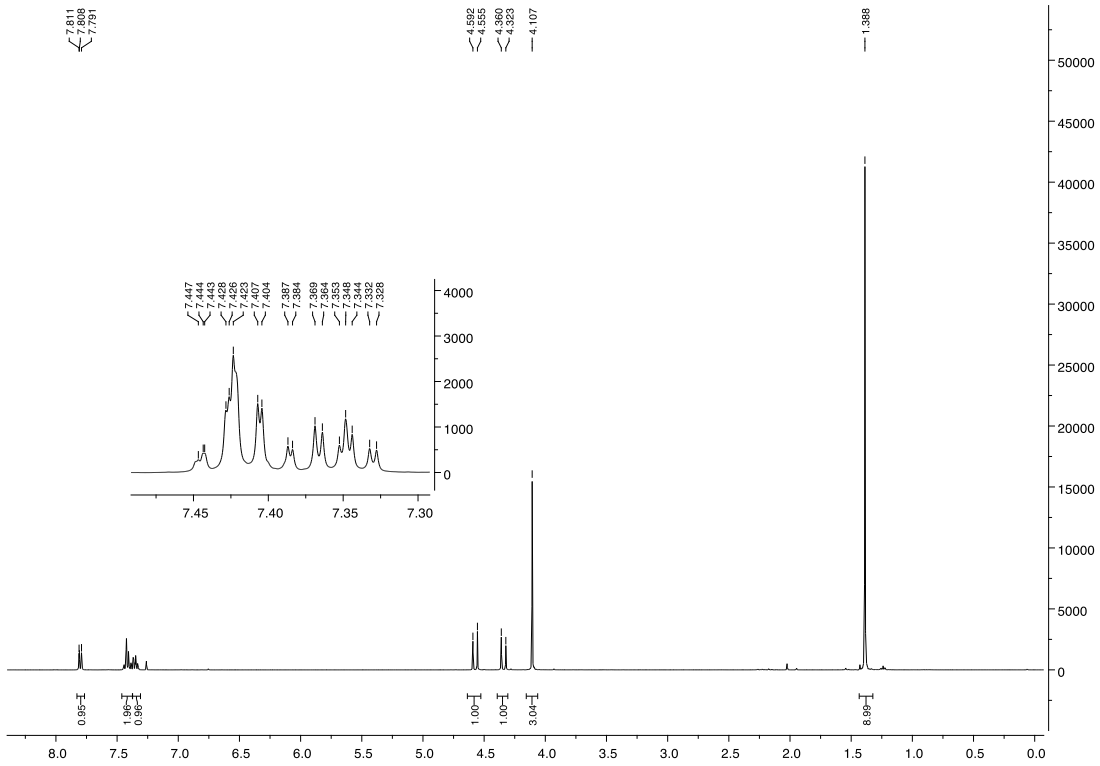


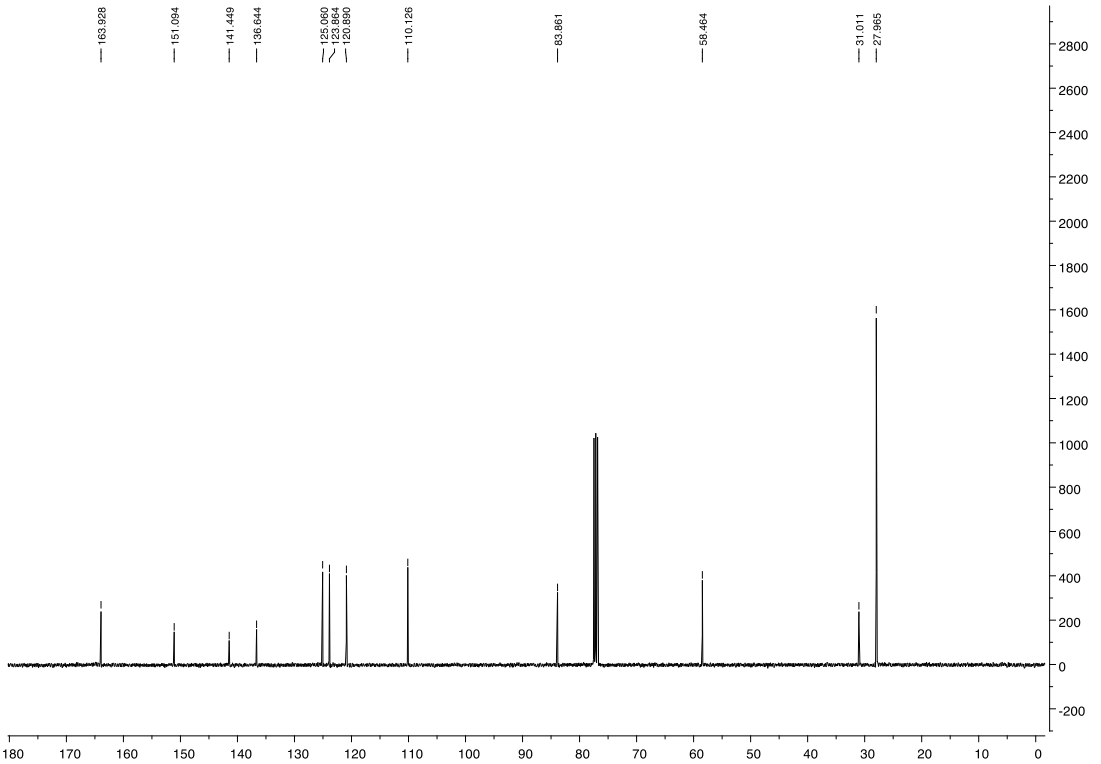
Detector A Channel 1 254nm

Peak#	Ret. Time	Area	Height	Height%	Area%
1	11.375	547635	28354	6.965	5.384
2	16.616	9623172	378755	93.035	94.616
Total		10170807	407110	100.000	100.000

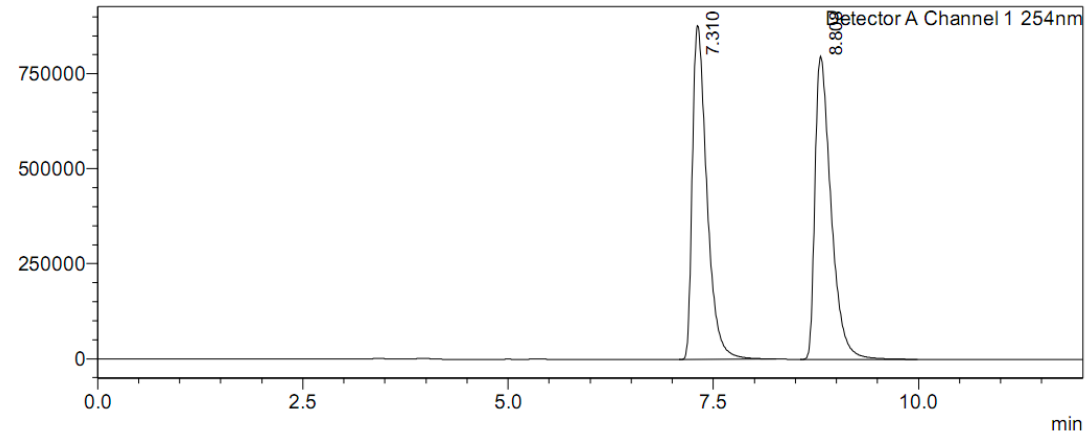

Me
N
O
S
CO2tBu
N

27l


7.811
7.808
7.791
4.592
4.555
4.360
4.323
4.107
1.388
7.447
7.444
7.443
7.428
7.426
7.423
7.407
7.404
7.387
7.384
7.369
7.364
7.353
7.348
7.344
7.332
7.328
0.95
1.95
0.96
1.00
1.00
3.04
8.99


163.928
151.094
141.449
136.644
125.060
123.864
120.890
110.126
83.861
58.464
31.011
27.965

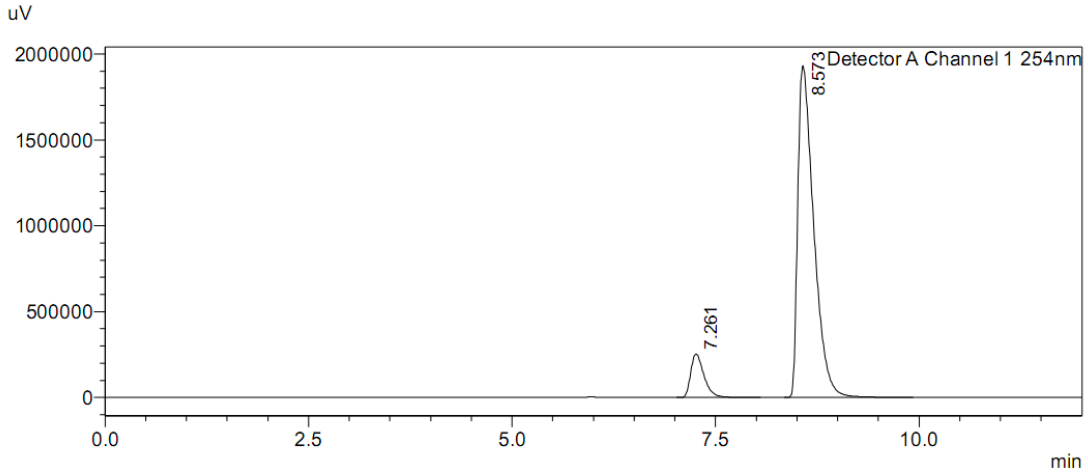
YXY3246A-IB3-3010254230-100-R YXY3246A-IB3-3010254230-100-R.lcd



Detector A Channel 1 254nm

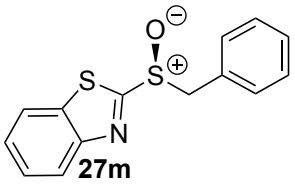
Peak#	Ret. Time	Area	Height	Height%	Area%
1	7.310	10861827	879418	52.428	49.926
2	8.808	10894095	797954	47.572	50.074
Total		21755923	1677371	100.000	100.000

YXY3246B-IB3-3010254230-12 YXY3246B-IB3-3010254230-12.lcd

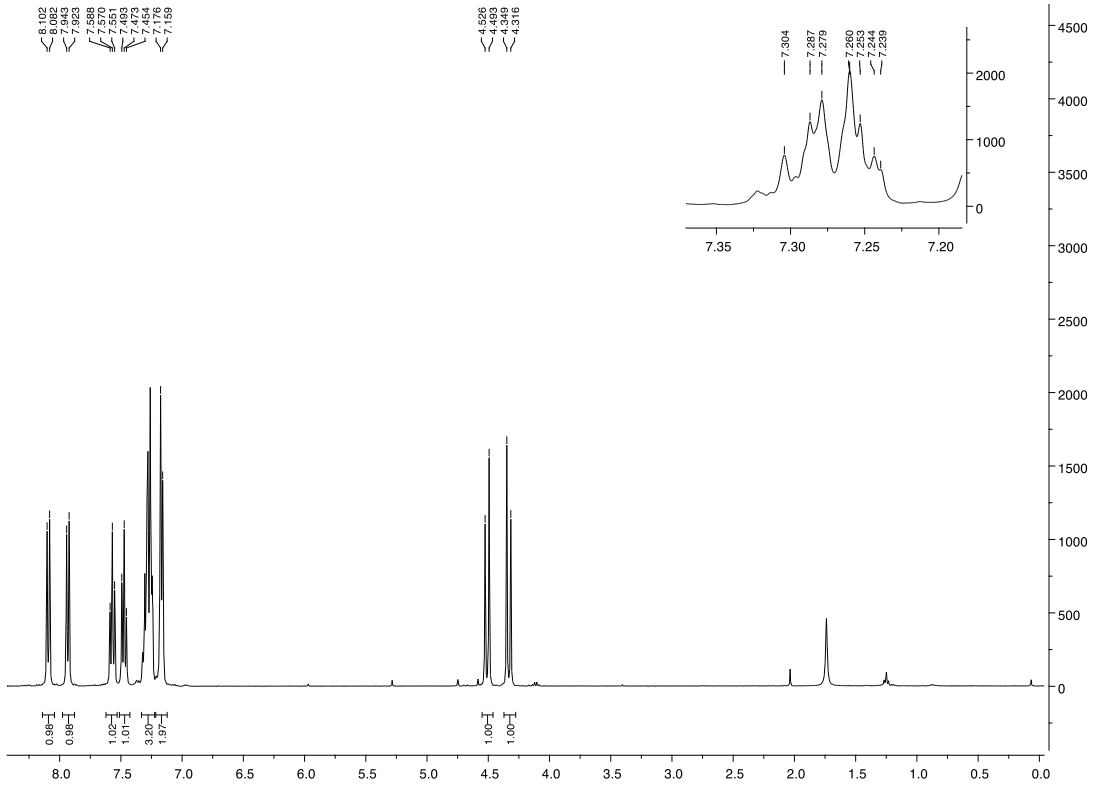


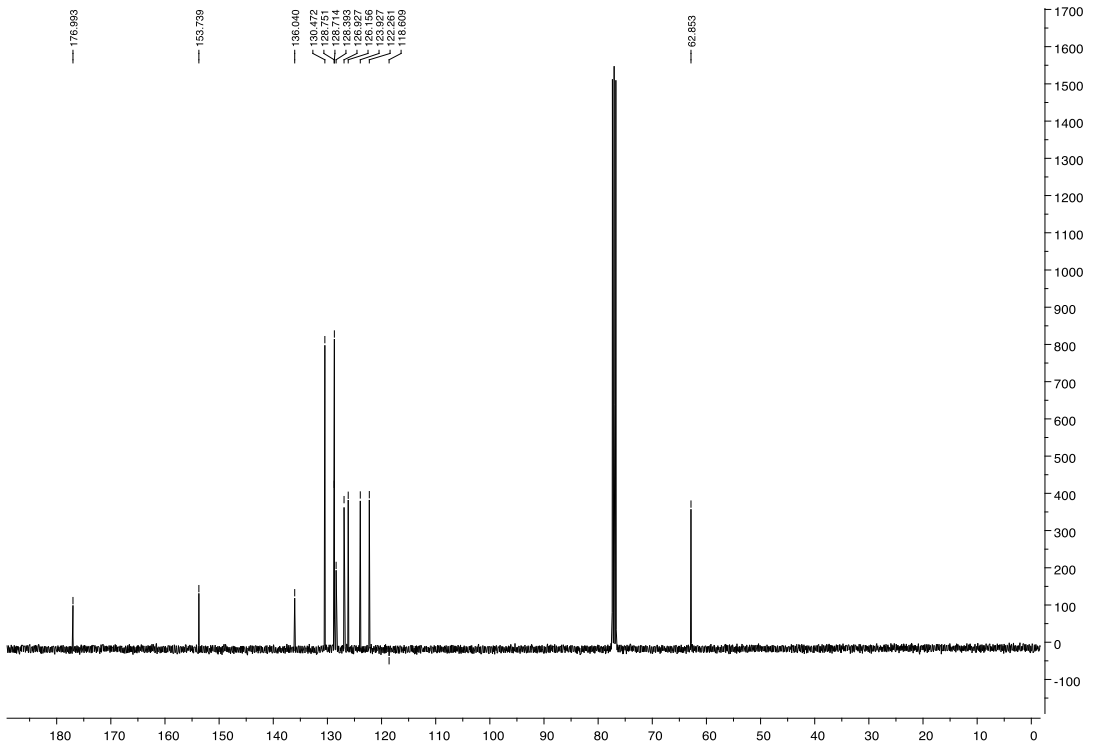
Detector A Channel 1 254nm

Peak#	Ret. Time	Area	Height	Height%	Area%
1	7.261	2898886	253488	11.597	9.896
2	8.573	26394966	1932382	88.403	90.104
Total		29293852	2185869	100.000	100.000

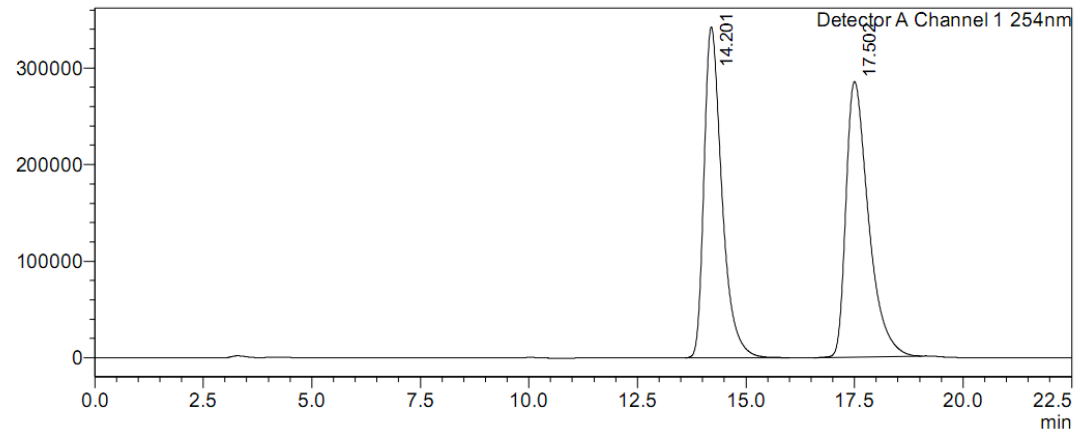

O
S
S
N

27m


8.102
8.082
7.943
7.923
7.588
7.570
7.551
7.493
7.473
7.454
7.176
7.159
4.526
4.493
4.349
4.316
7.304
7.287
7.279
7.260
7.253
7.244
7.239
0.98
0.98
1.02
1.01
3.20
1.97
1.00
1.00


176.993
153.739
136.040
130.472
128.751
128.734
128.393
126.927
126.156
125.967
122.261
118.609
62.853

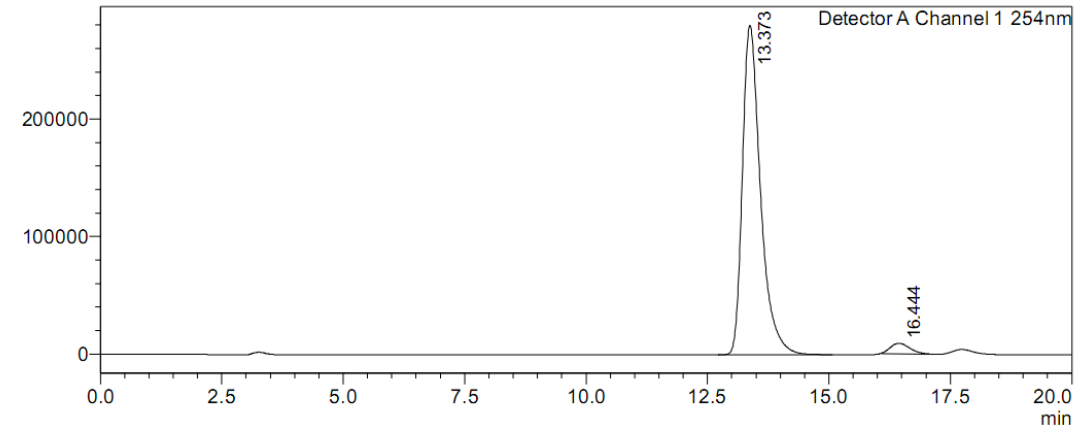
YXY2134B-ODH1010254230-25 YXY2134B-ODH1010254230-25.lcd



Detector A Channel 1 254nm

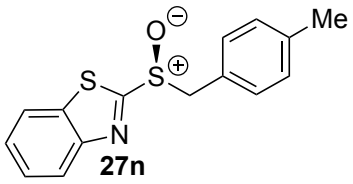
Peak#	Ret. Time	Area	Height	Height%	Area%
1	14.201	9833400	342482	54.577	48.942
2	17.502	10258342	285041	45.423	51.058
Total		20091743	627523	100.000	100.000

YXY3148A-ODH1010254230-25 YXY3148A-ODH1010254230-25.lcd

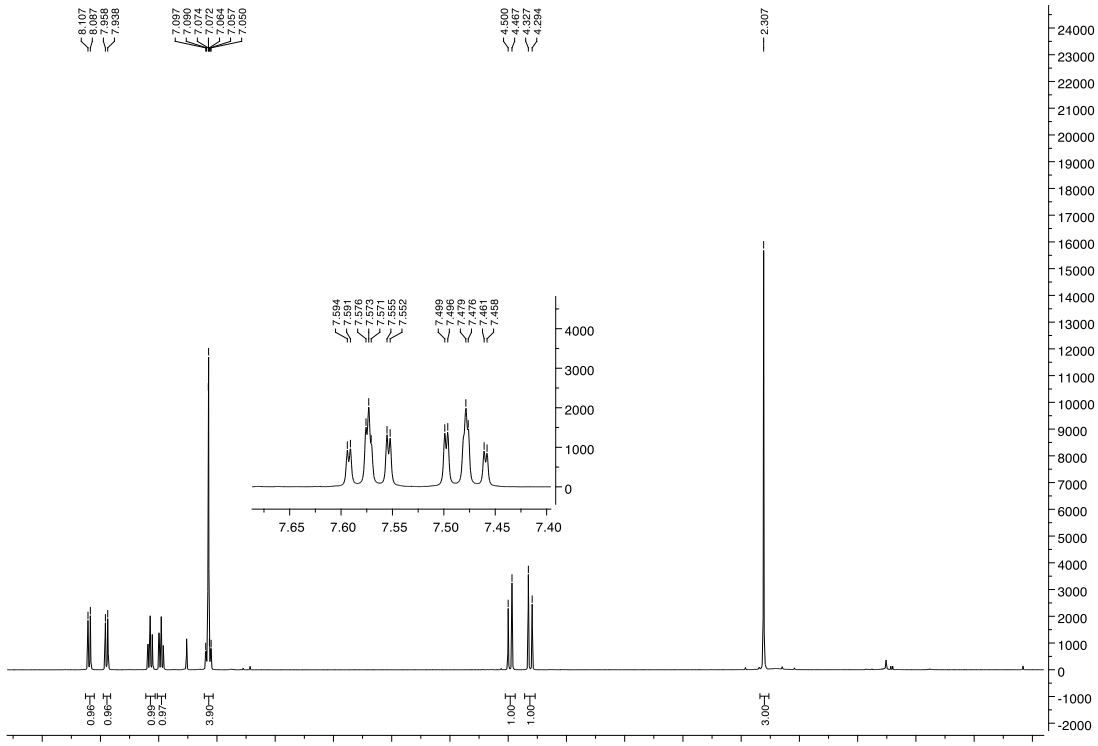


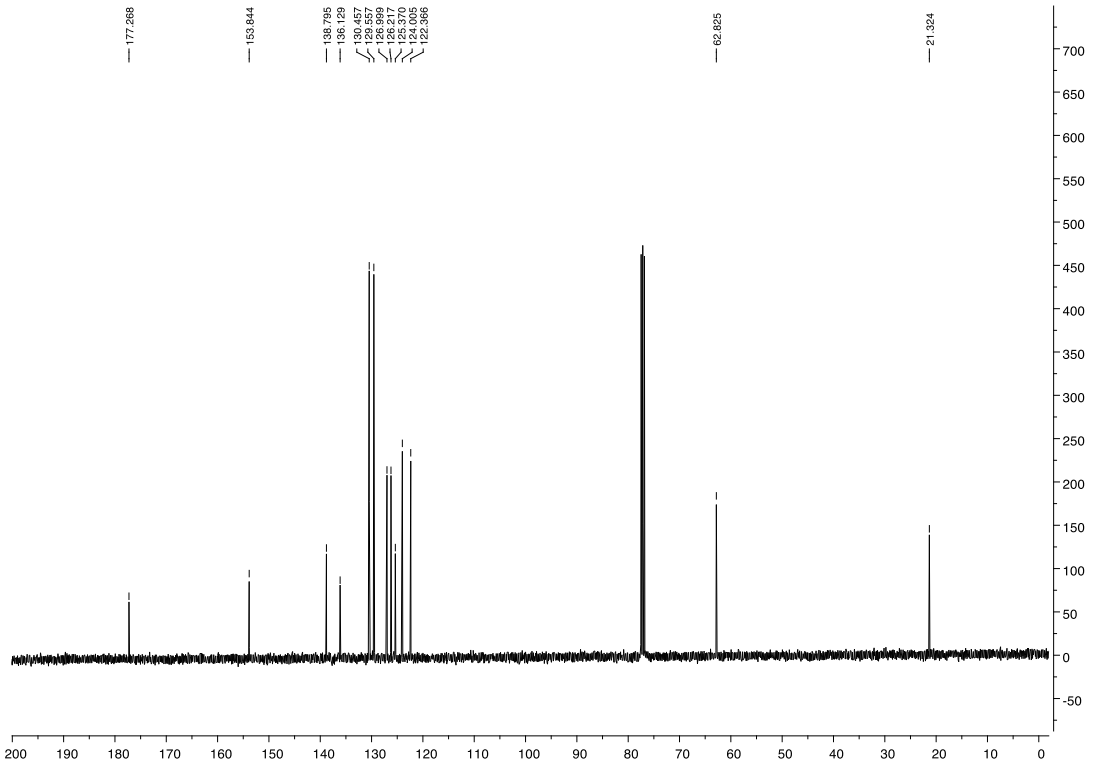
Detector A Channel 1 254nm

Peak#	Ret. Time	Area	Height	Height%	Area%
1	13.373	7249159	280279	96.840	96.580
2	16.444	256698	9145	3.160	3.420
Total		7505857	289424	100.000	100.000

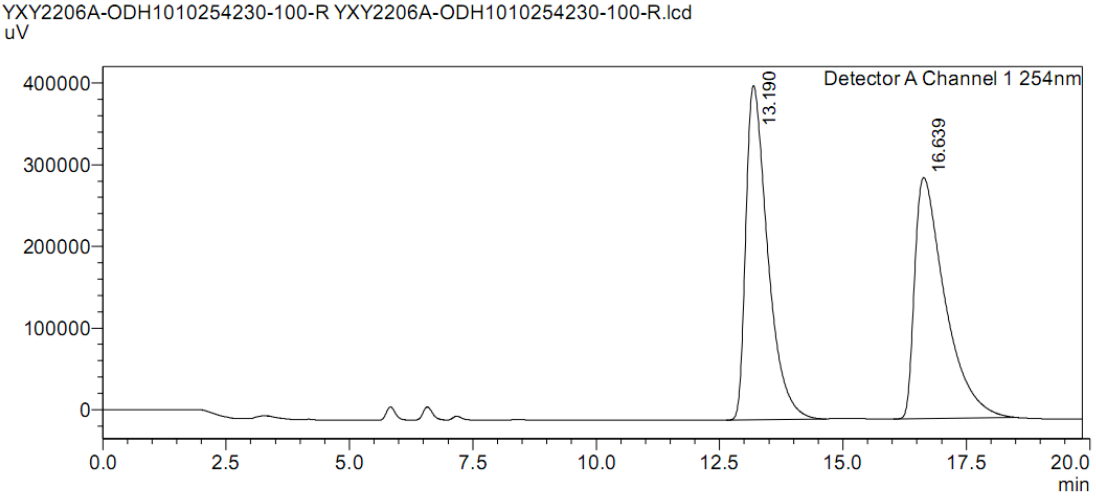

Me
O
S
S
N

27n


8.107
8.087
7.958
7.938
7.097
7.090
7.074
7.072
7.064
7.057
7.050
4.500
4.467
4.327
4.294
2.307
7.594
7.591
7.576
7.573
7.571
7.555
7.552
7.499
7.496
7.479
7.476
7.461
7.458
0.96
0.96
0.99
0.97
3.90
1.00
1.00
3.00


177.268
153.844
138.795
136.129
130.457
129.557
126.999
126.217
125.370
124.005
122.366
62.825
21.324

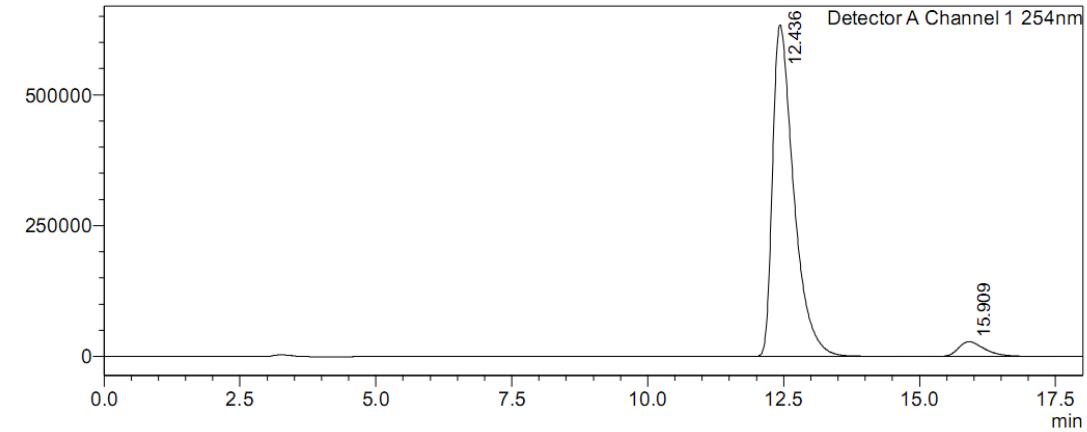
YXY2206A-ODH1010254230-100-R YXY2206A-ODH1010254230-100-R.lcd



Detector A Channel 1 254nm

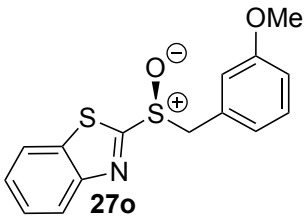
Peak#	Ret. Time	Area	Height	Height%	Area%
1	13.190	12618341	409443	58.119	50.020
2	16.639	12608245	295050	41.881	49.980
Total		25226586	704492	100.000	100.000

YXY3114A-ODH1010254230-25 YXY3114A-ODH1010254230-25.lcd

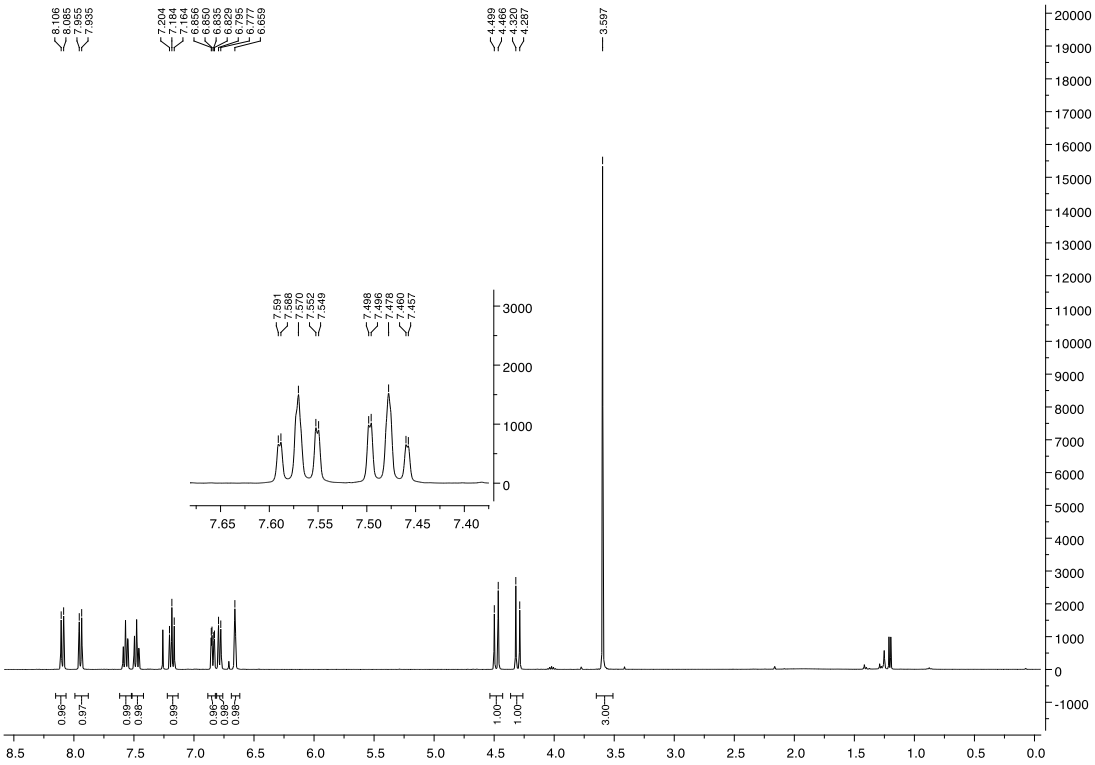


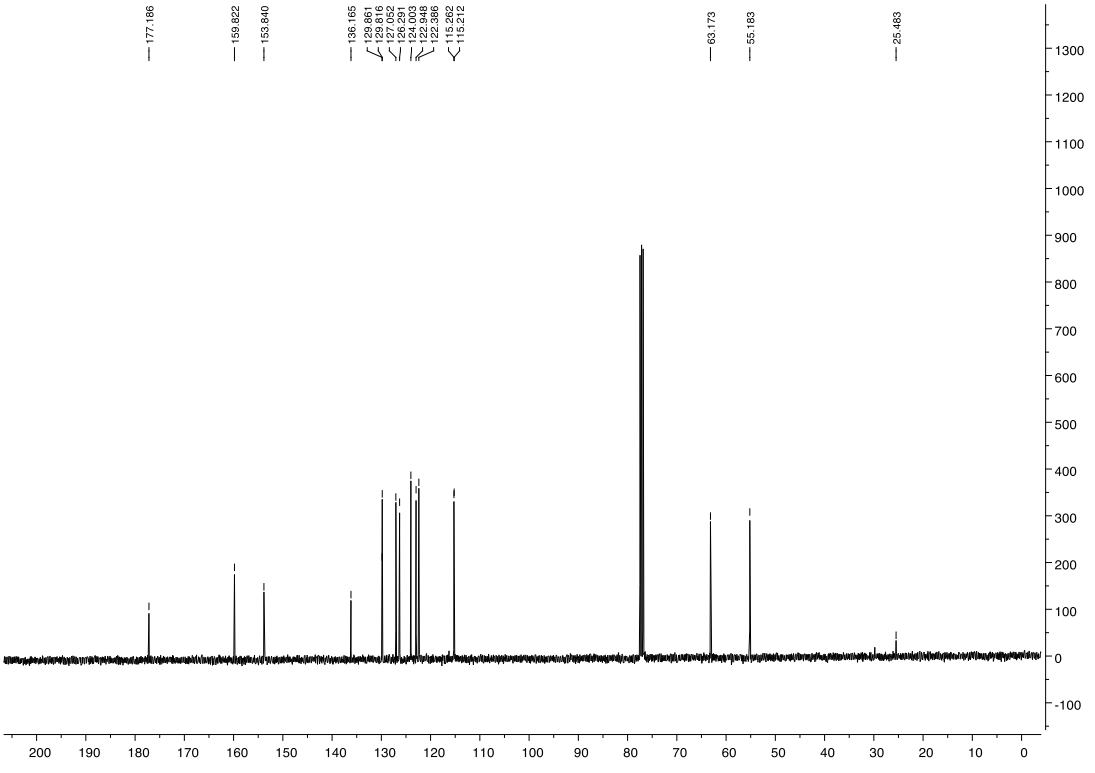
Detector A Channel 1 254nm

Peak#	Ret. Time	Area	Height	Height%	Area%
1	12.436	17192185	634067	95.734	94.653
2	15.909	971142	28258	4.266	5.347
Total		18163327	662325	100.000	100.000

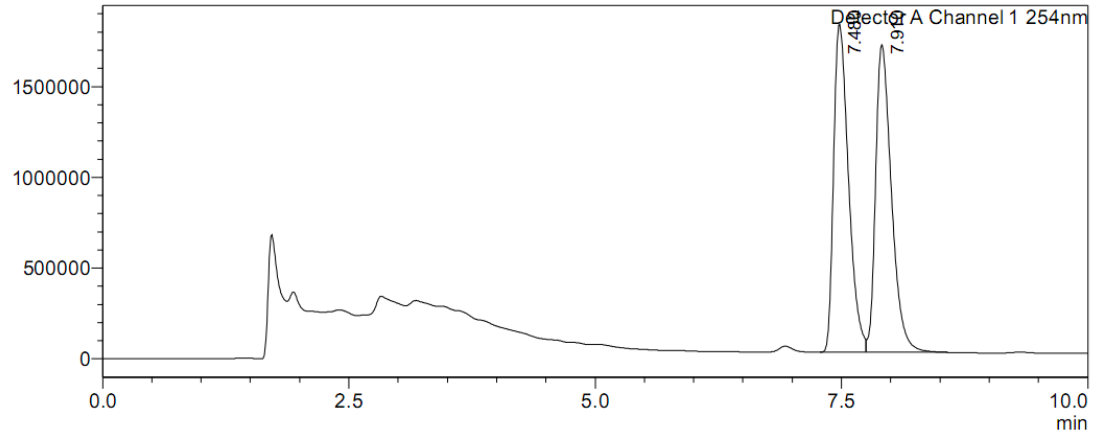

OMe
O
S
S
N

27o


8.106
8.085
7.955
7.935
7.204
7.184
7.164
6.856
6.850
6.835
6.829
6.795
6.777
6.659
4.499
4.466
4.320
4.287
3.597
7.591
7.588
7.570
7.552
7.549
7.498
7.496
7.478
7.460
7.457
0.96
0.97
0.99
0.98
0.99
0.96
0.98
0.98
1.00
1.00
3.00


177.186
159.822
153.840
136.165
129.861
129.816
129.052
126.291
124.003
122.948
122.386
115.262
115.212
63.173
55.183
25.483

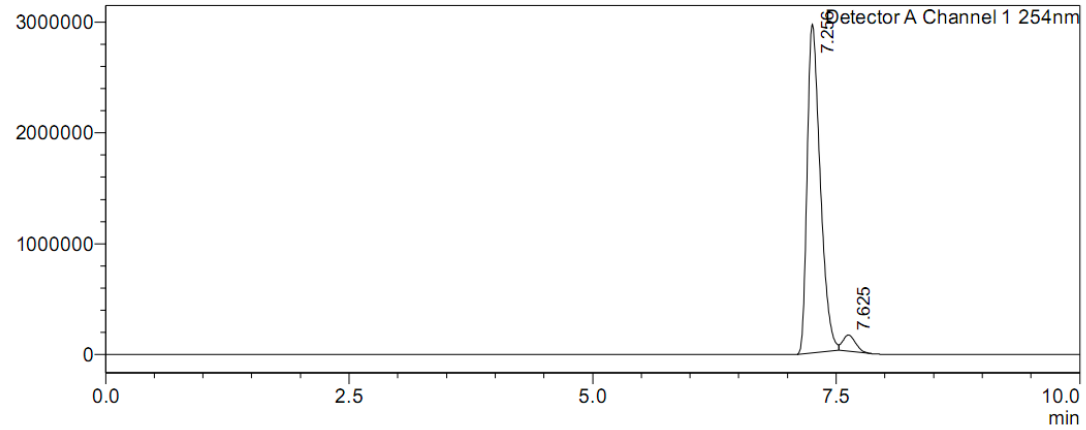
YXY2210A-IB3-3010254230-100-R YXY2210A-IB3-3010254230-100-R.lcd
uV



Detector A Channel 1 254nm

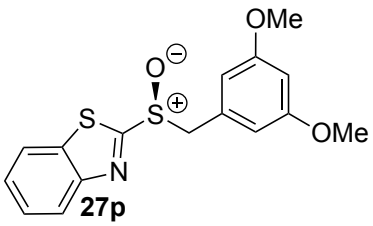
Peak#	Ret. Time	Area	Height	Height%	Area%
1	7.480	18799954	1806037	51.611	49.646
2	7.910	19068028	1693317	48.389	50.354
Total		37867981	3499354	100.000	100.000

YXY3102B-IB3-3010254230-12 YXY3102B-IB3-3010254230-12.lcd
uV

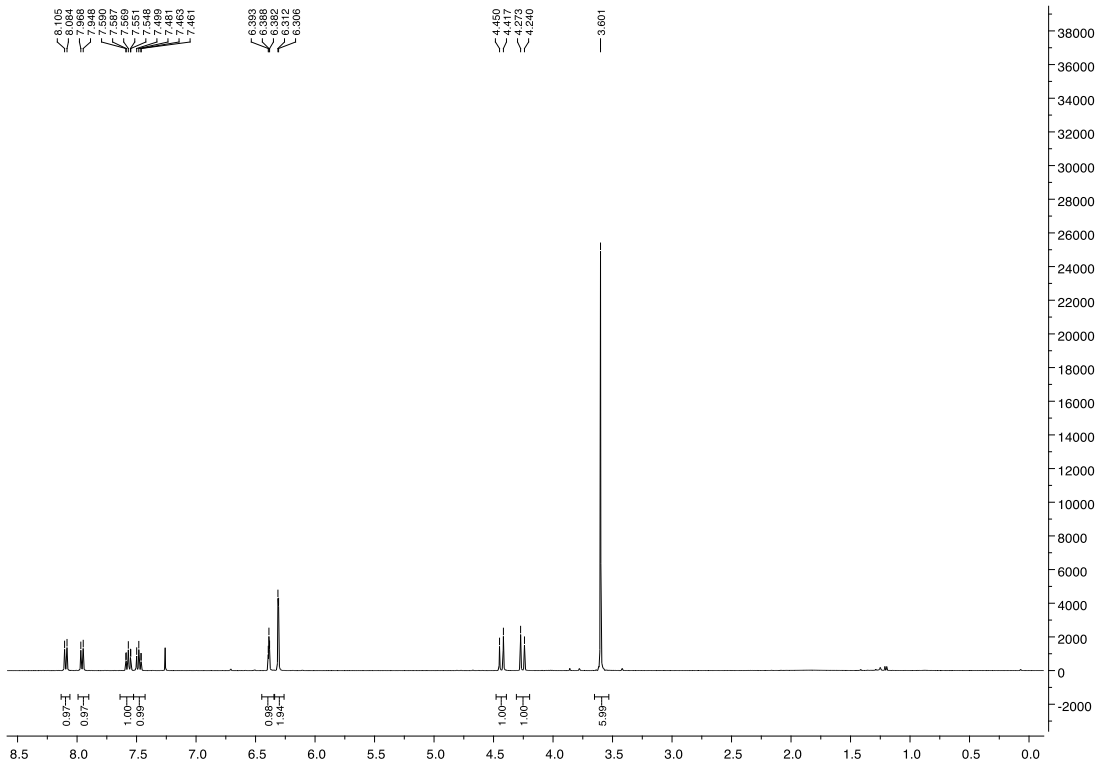


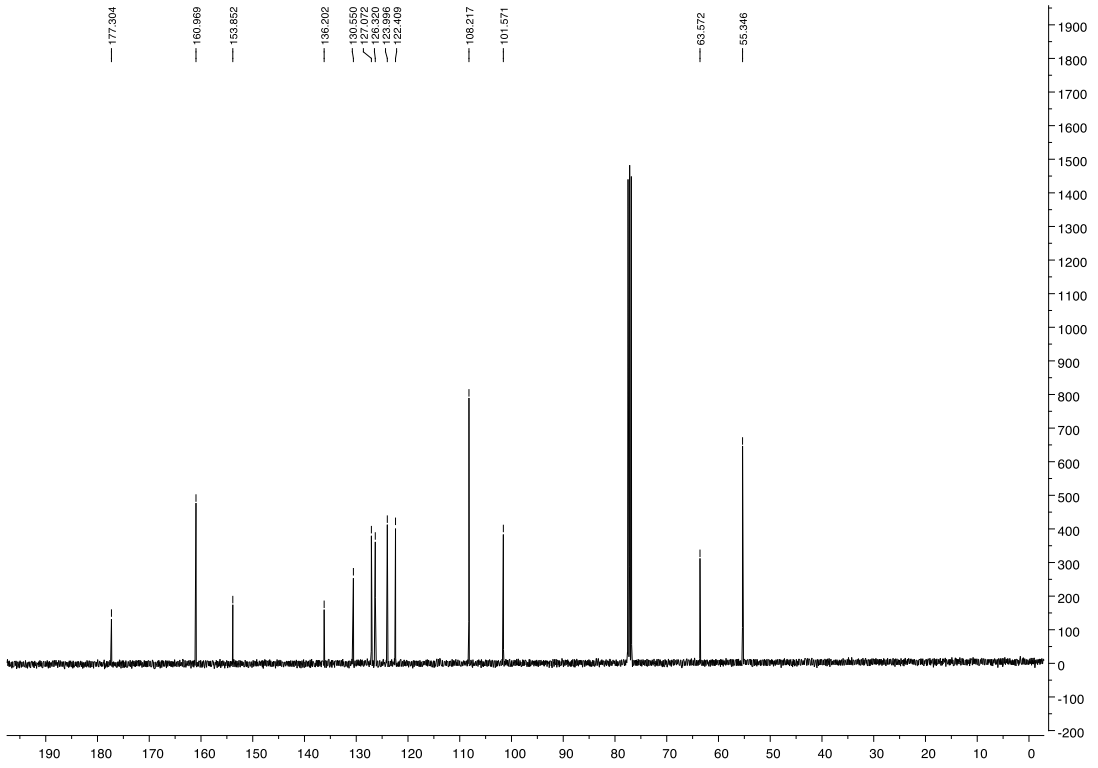
Detector A Channel 1 254nm

Peak#	Ret. Time	Area	Height	Height%	Area%
1	7.256	27730115	2963615	95.303	95.391
2	7.625	1339867	146074	4.697	4.609
Total		29069982	3109689	100.000	100.000


OMe
O
S
S
N
OMe

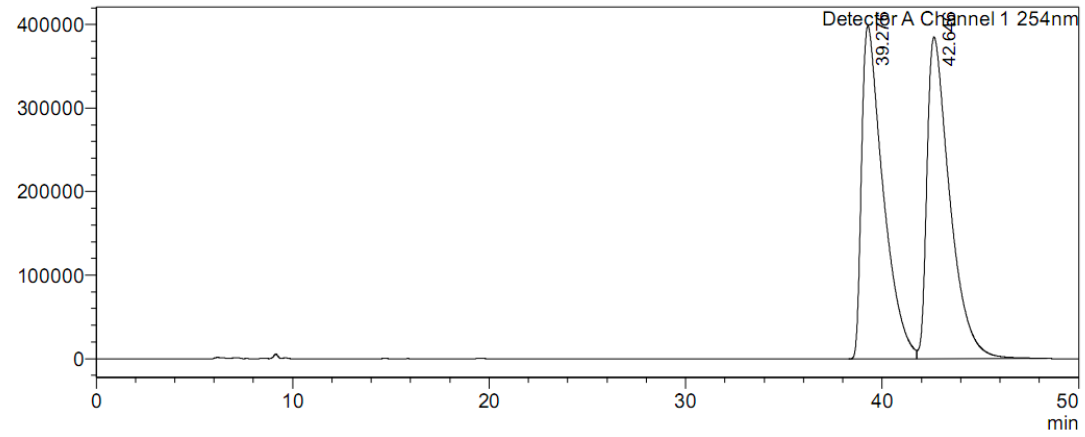
27p


8.105
8.084
7.968
7.948
7.590
7.587
7.569
7.551
7.548
7.489
7.481
7.463
7.461
6.393
6.388
6.382
6.312
6.306
4.450
4.417
4.273
4.240
3.601
0.97
0.97
1.00
0.99
0.98
1.94
1.00
1.00
5.99


177.304
160.969
153.852
136.202
130.550
127.070
126.320
123.996
122.409
108.217
101.571
63.572
55.346

YZY1153A-ODH10005254230-100-R YZY1153A-ODH10005254230-100-R.lcd

uV

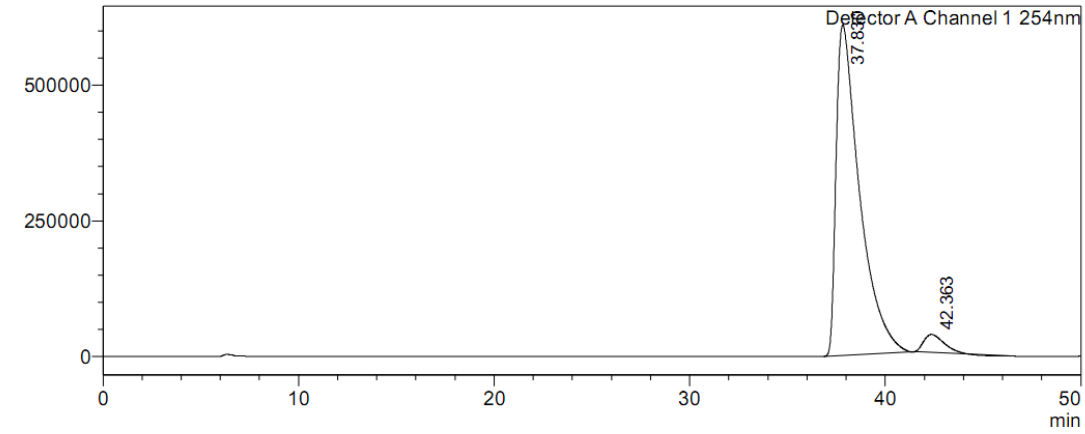


Detector A Channel 1 254nm

Peak#	Ret. Time	Area	Height	Height%	Area%
1	39.276	30473496	398999	50.865	49.414
2	42.646	31196694	385430	49.135	50.586
Total		61670189	784429	100.000	100.000

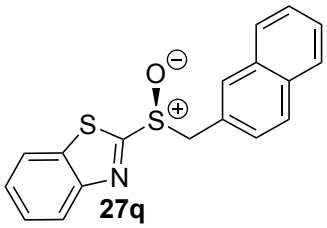
YXY3094B-ODH1005254230-55 YXY3094B-ODH1005254230-55.lcd

uV

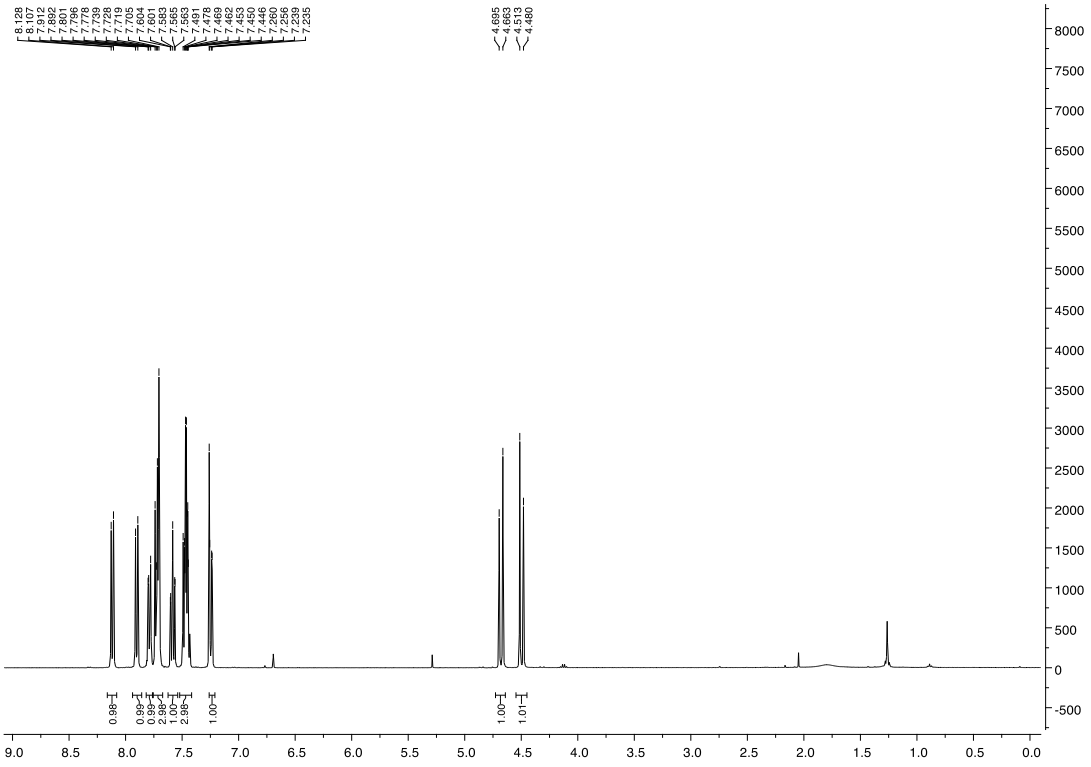


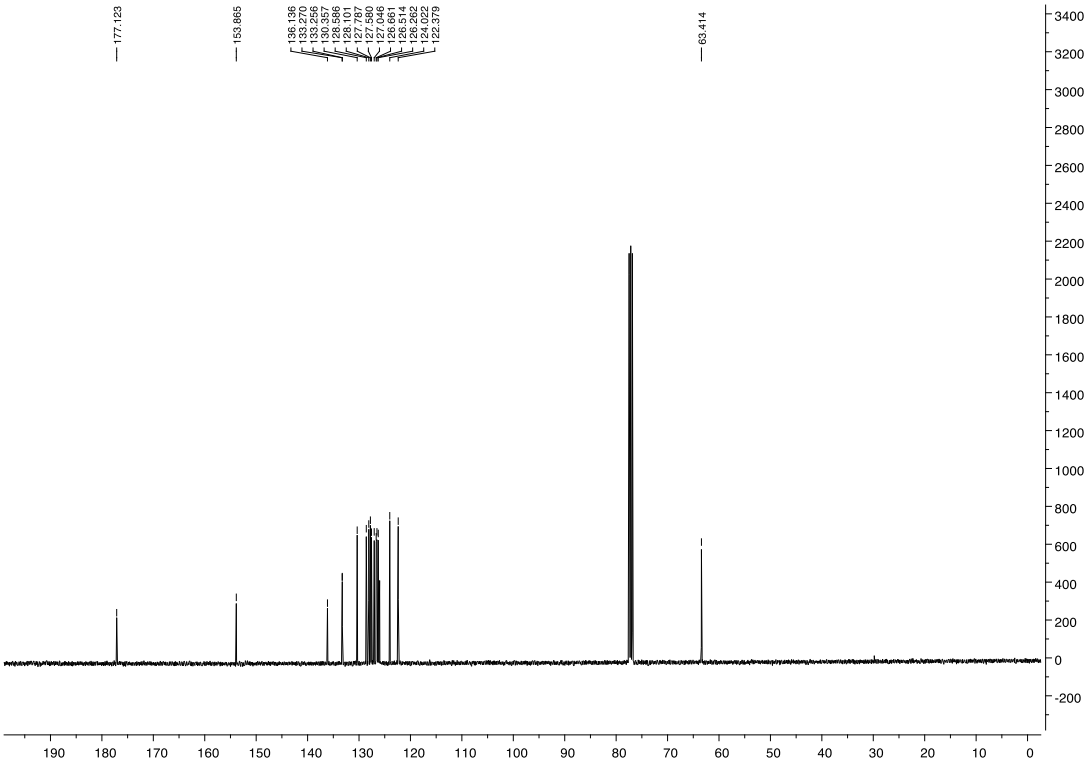
Detector A Channel 1 254nm

Peak#	Ret. Time	Area	Height	Height%	Area%
1	37.830	50760652	609872	94.897	95.751
2	42.363	2252274	32793	5.103	4.249
Total		53012927	642665	100.000	100.000

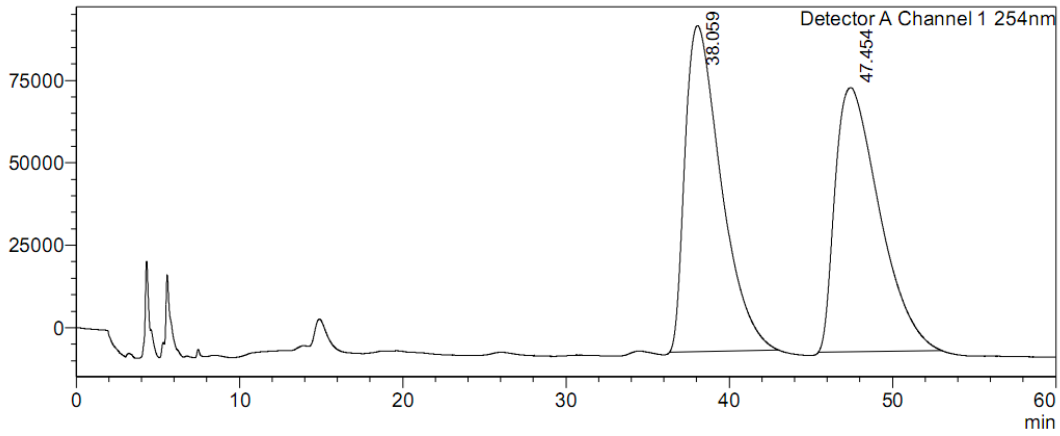

O
S
S
N

27q


8.128
8.107
7.812
7.802
7.801
7.796
7.778
7.758
7.728
7.719
7.705
7.604
7.601
7.583
7.565
7.563
7.491
7.478
7.469
7.462
7.453
7.450
7.446
7.260
7.256
7.239
7.235
4.695
4.663
4.513
4.480
0.98
0.99
0.99
2.88
1.00
2.98
1.00
1.00
1.01


177.123
153.865
136.136
133.270
133.256
130.357
128.586
128.510
127.787
127.580
127.046
126.661
126.514
126.262
124.022
122.379
63.414

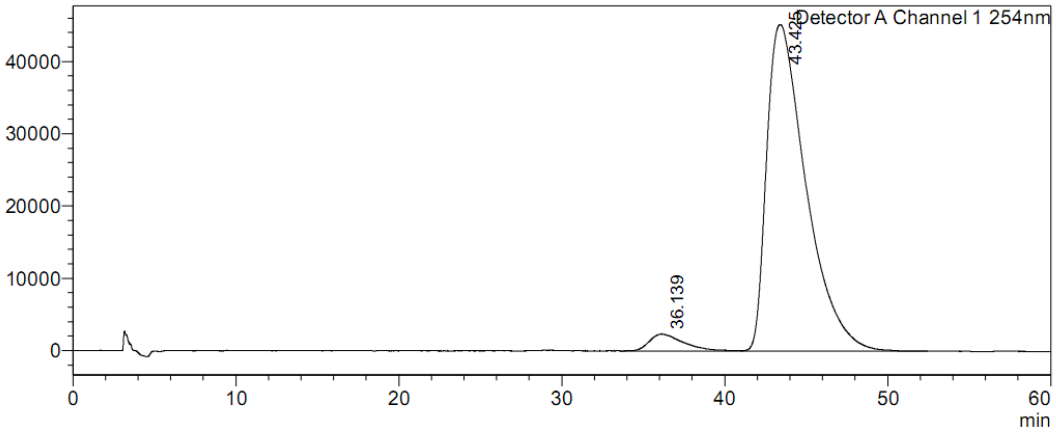
YXY2218A-ASH-1010254230-100-R YXY2218A-ASH-1010254230-100-R.lcd
uV



Detector A Channel 1 254nm

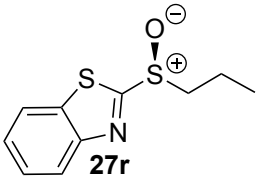
Peak#	Ret. Time	Area	Height	Height%	Area%
1	38.059	15179463	98870	55.246	50.077
2	47.454	15132551	80095	44.754	49.923
Total		30312013	178965	100.000	100.000

YXY3116A-ASH1010254230-60 YXY3116A-ASH1010254230-60.lcd
uV

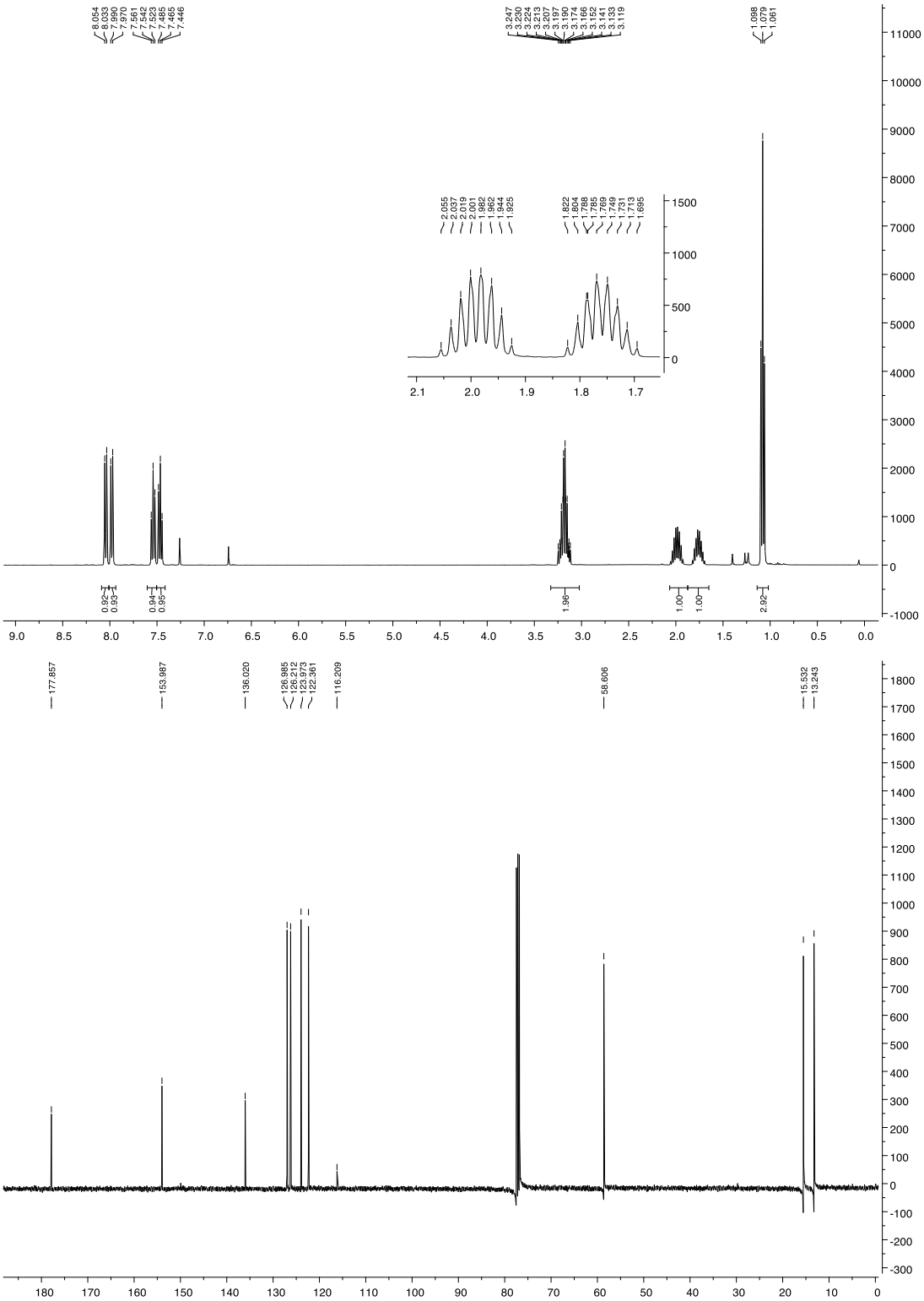


Detector A Channel 1 254nm

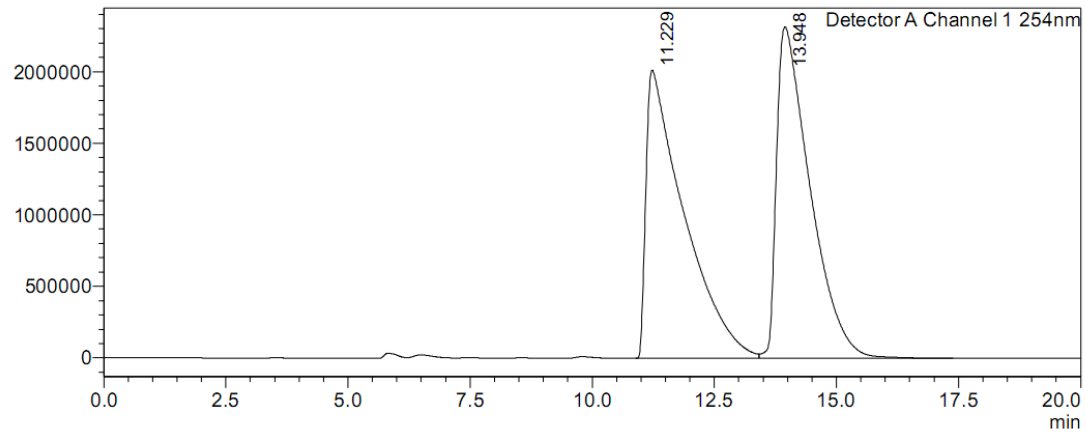
Peak#	Ret. Time	Area	Height	Height%	Area%
1	36.139	341816	2351	4.945	4.301
2	43.425	7604799	45202	95.055	95.699
Total		7946615	47553	100.000	100.000


O
S
S
N

27r


8.054
8.053
8.033
7.990
7.970
7.561
7.542
7.483
7.465
7.446
3.247
3.239
3.224
3.213
3.207
3.197
3.189
3.174
3.166
3.152
3.141
3.133
3.119
1.098
1.079
1.061
2.055
2.037
2.019
2.001
1.982
1.962
1.944
1.925
1.822
1.804
1.788
1.785
1.769
1.749
1.731
1.713
1.695
0.92
0.93
0.94
0.95
1.96
1.00
1.00
2.92
177.857
153.987
136.020
126.985
126.712
123.973
122.361
116.209
58.606
15.532
13.243

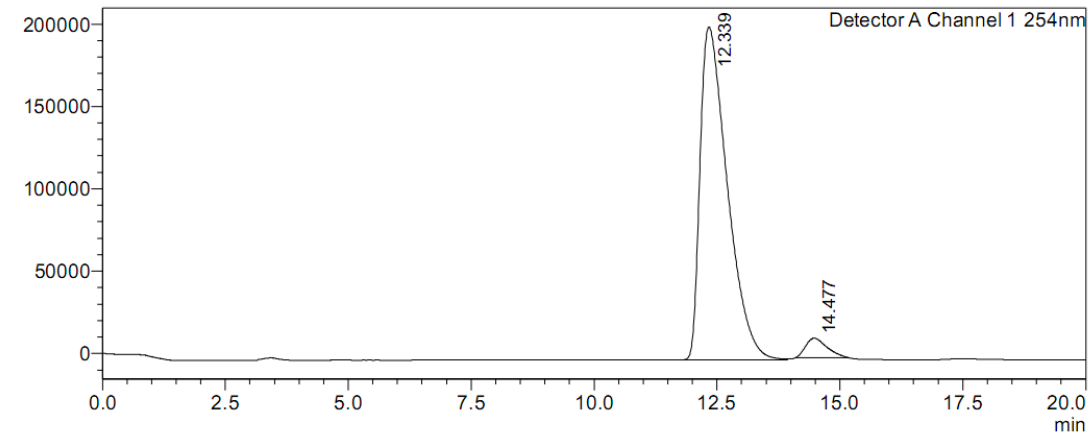
YZY1025B-OBH-1010254230-100-R YZY1025B-OBH-1010254230-100-R.lcd



Detector A Channel 1 254nm

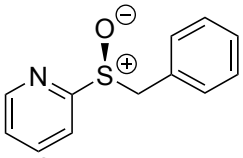
Peak#	Ret. Time	Area	Height	Height%	Area%
1	11.229	109380403	2015071	46.509	49.700
2	13.948	110703080	2317622	53.491	50.300
Total		220083484	4332693	100.000	100.000

YXY3148B-OBH1010254230-20 YXY3148B-OBH1010254230-20.lcd

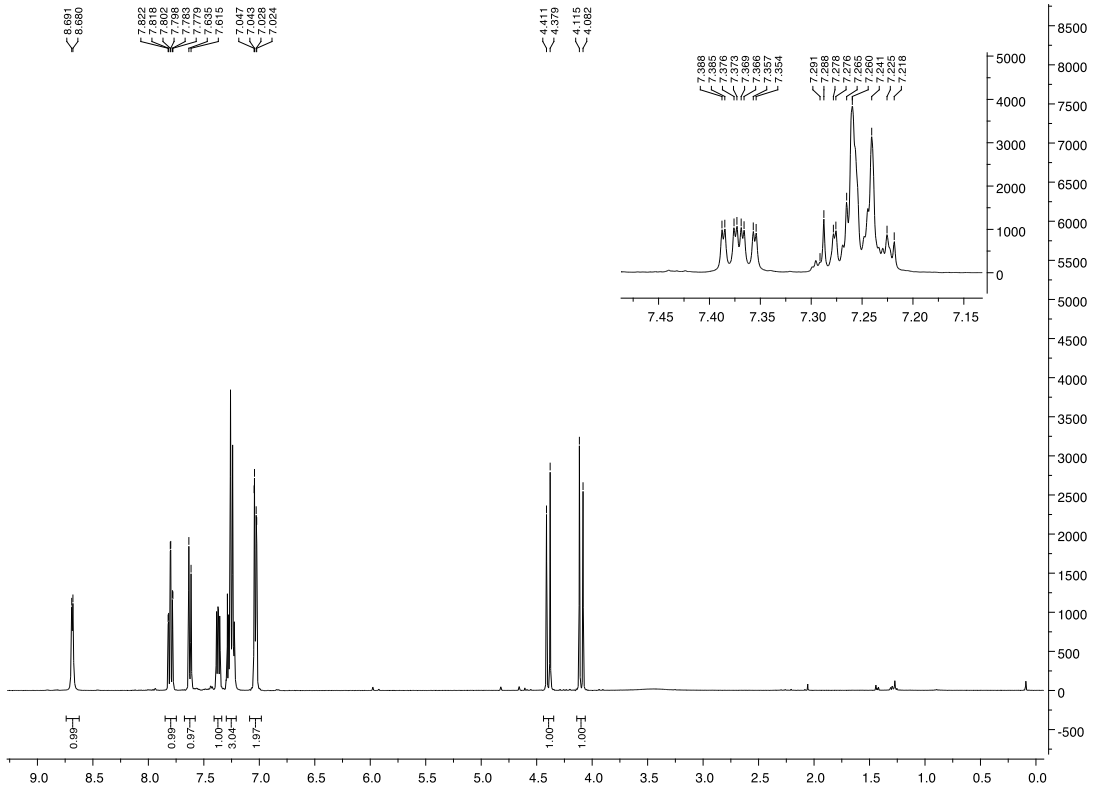


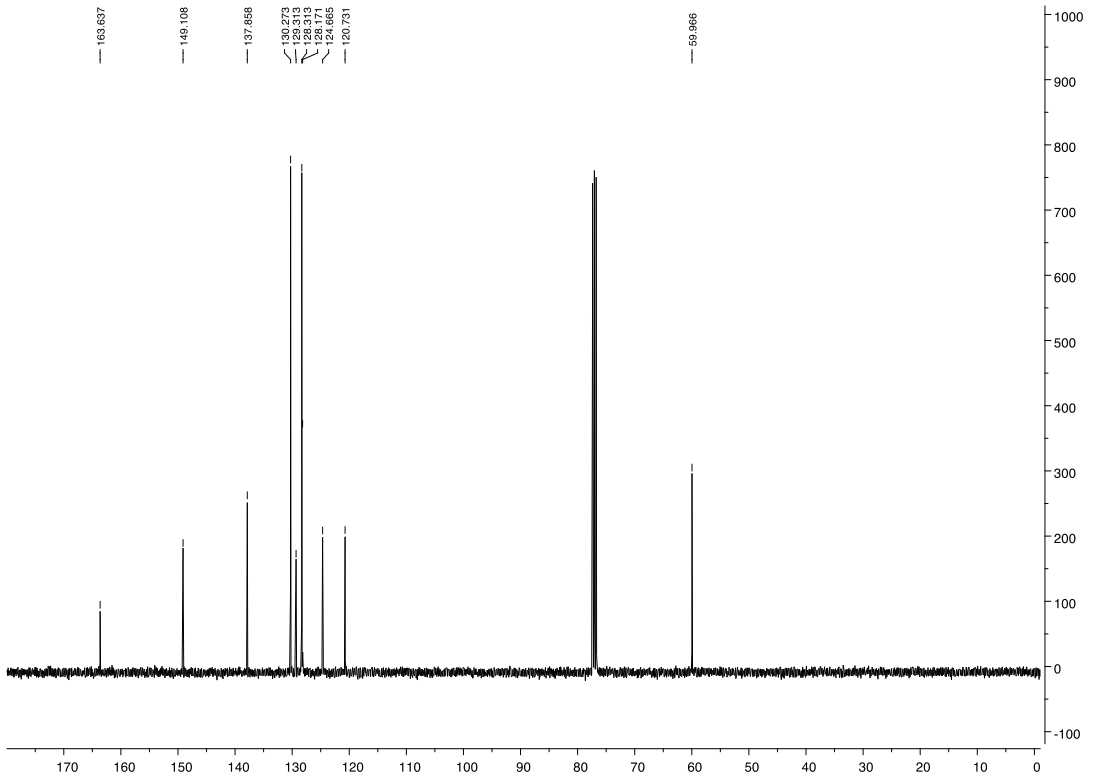
Detector A Channel 1 254nm

Peak#	Ret. Time	Area	Height	Height%	Area%
1	12.339	7775143	202177	94.505	95.653
2	14.477	353365	11756	5.495	4.347
Total		8128507	213933	100.000	100.000

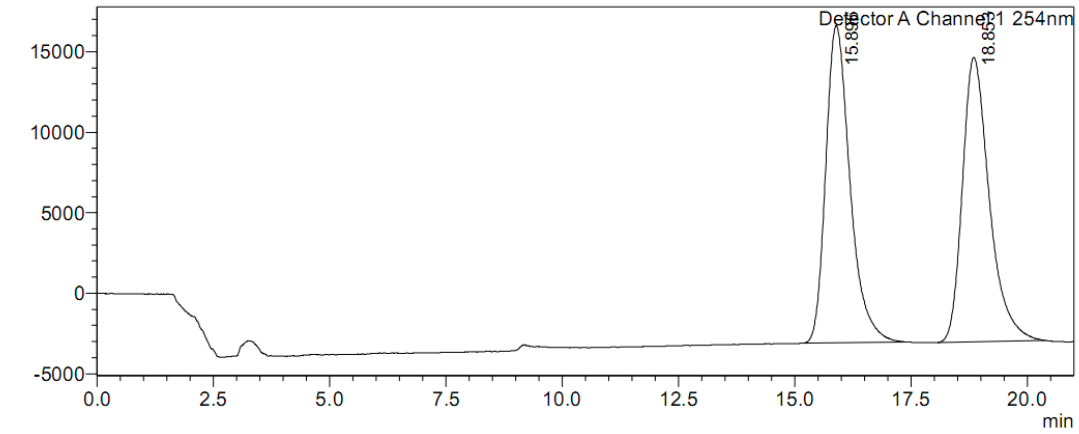


27s


8.691
8.680
7.822
7.818
7.802
7.798
7.783
7.779
7.635
7.615
7.047
7.043
7.028
7.024
4.411
4.379
4.115
4.082
7.388
7.385
7.376
7.373
7.369
7.366
7.357
7.354
7.291
7.288
7.278
7.276
7.265
7.260
7.241
7.225
7.218
0.99
0.99
0.97
1.00
3.04
1.97
1.00
1.00


163.637
149.108
137.858
130.273
129.313
129.313
128.171
124.665
120.731
59.966

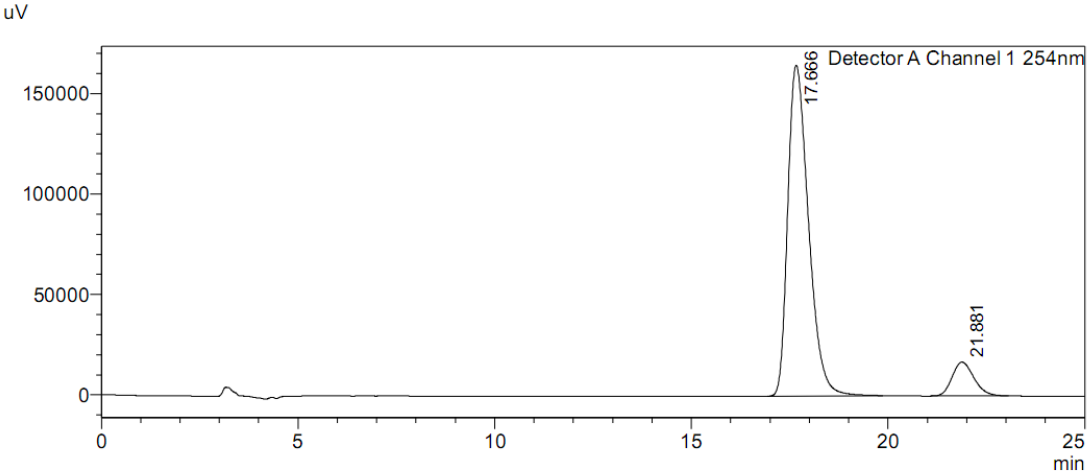
YZY1097A-ODH-1010254230-100-R YZY1097A-ODH-1010254230-100-R.lcd



Detector A Channel 1 254nm

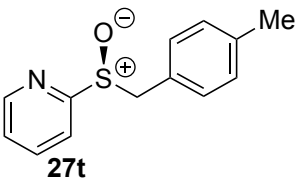
Peak#	Ret. Time	Area	Height	Height%	Area%
1	15.896	714147	19682	52.692	50.024
2	18.853	713458	17671	47.308	49.976
Total		1427605	37352	100.000	100.000

YXY3166B-ODH1010254230-25 YXY3166B-ODH1010254230-25.lcd

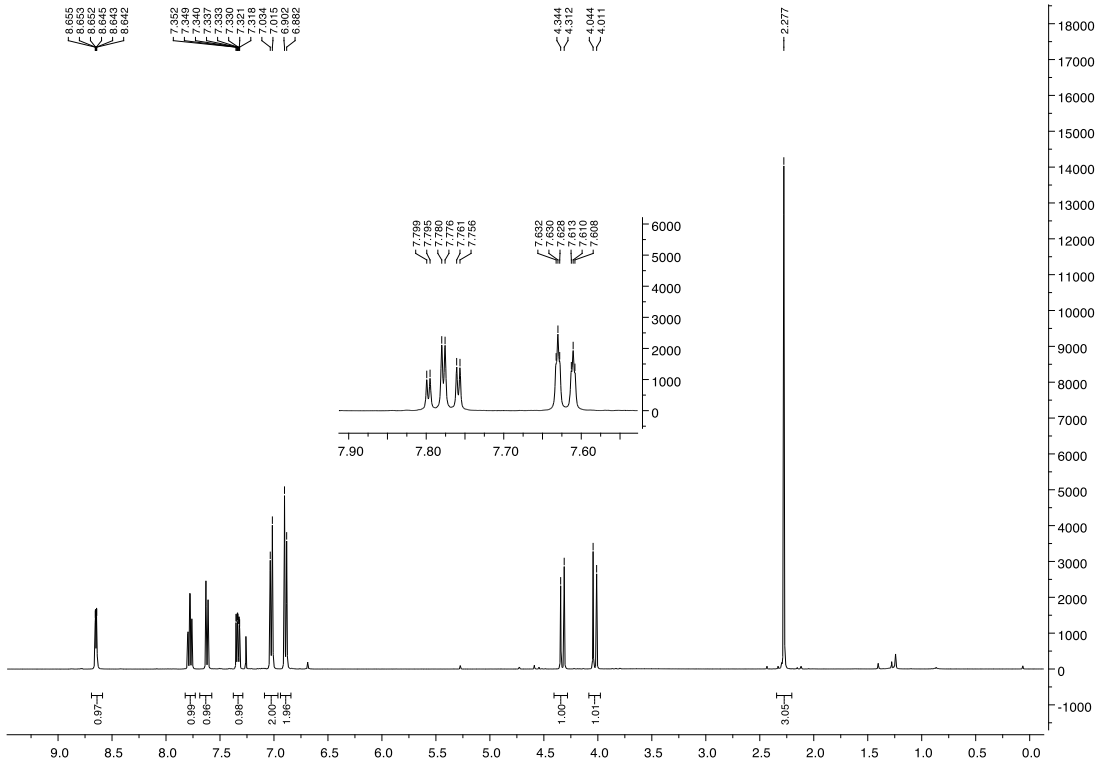


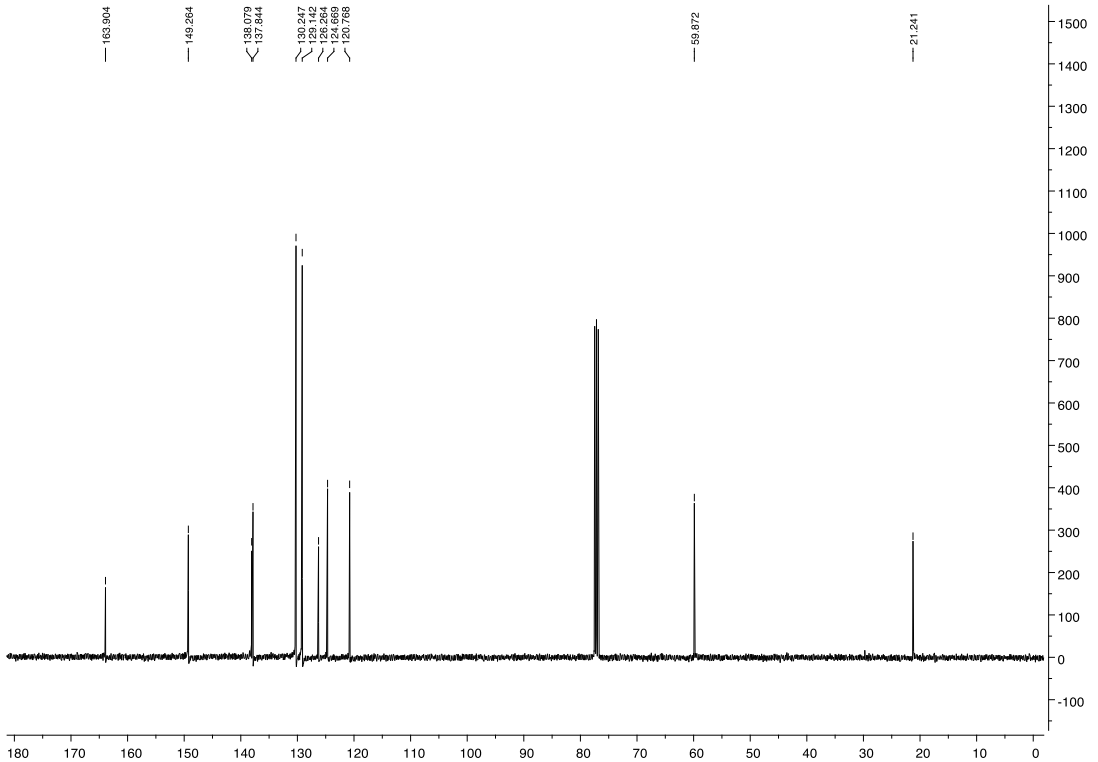
Detector A Channel 1 254nm

Peak#	Ret. Time	Area	Height	Height%	Area%
1	17.666	6039043	164809	90.714	90.289
2	21.881	649548	16870	9.286	9.711
Total		6688591	181679	100.000	100.000

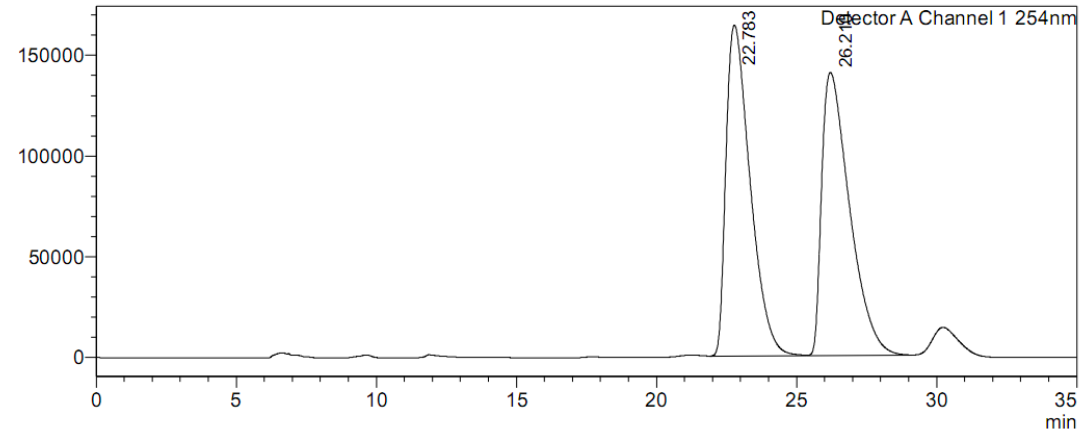

Me
O
N
S

27t


8.655
8.653
8.652
8.645
8.643
8.642
7.352
7.349
7.340
7.337
7.333
7.330
7.321
7.318
7.034
7.015
6.902
6.882
4.344
4.312
4.044
4.011
2.277
7.799
7.795
7.780
7.776
7.761
7.756
7.632
7.630
7.628
7.613
7.610
7.608
0.97
0.99
0.96
0.98
2.00
1.96
1.00
1.01
3.05


163.904
149.264
138.079
137.844
130.247
129.142
126.284
124.668
120.768
59.872
21.241

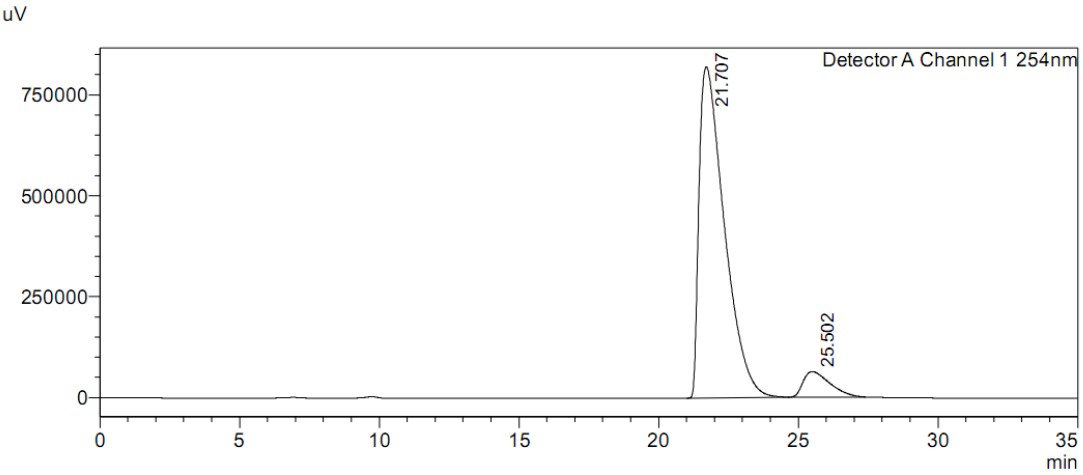
YZY1125A-OBH-1005254230-100-R YZY1125A-OBH-1005254230-100-R.lcd



Detector A Channel 1 254nm

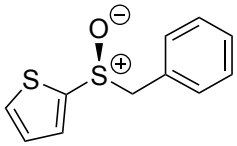
Peak#	Ret. Time	Area	Height	Height%	Area%
1	22.783	9843428	164241	53.895	50.326
2	26.210	9716080	140501	46.105	49.674
Total		19559508	304742	100.000	100.000

YXY3220A-OBH1005254230-35 YXY3220A-OBH1005254230-35.lcd

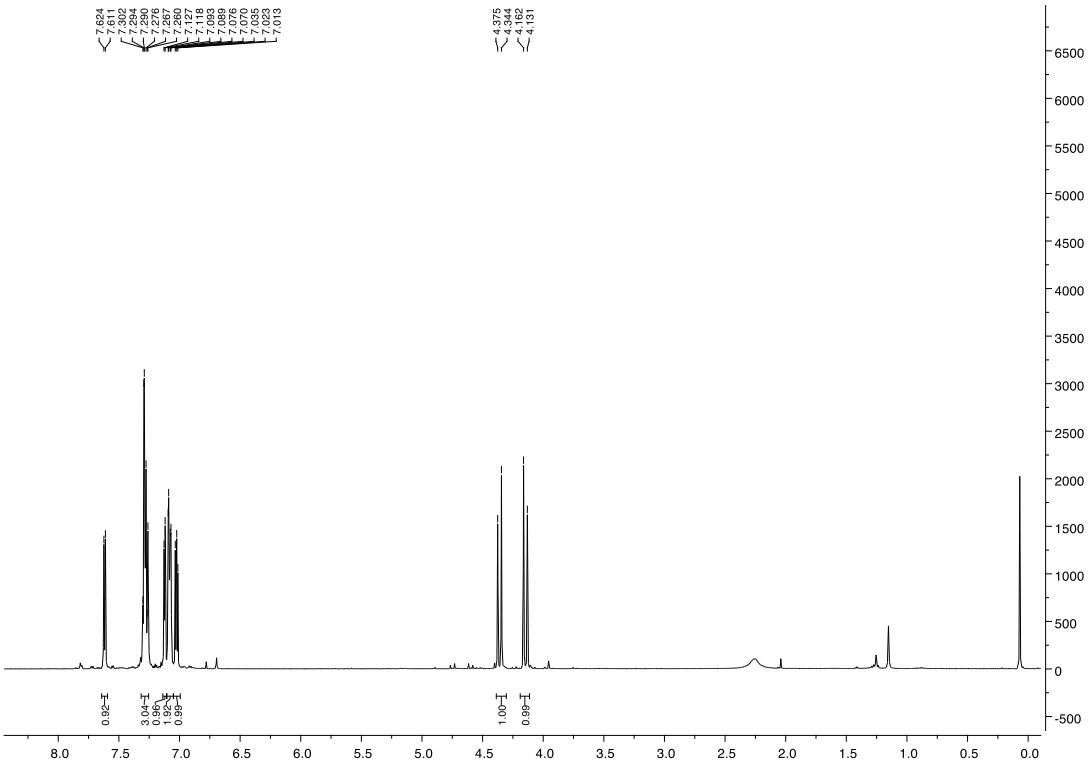


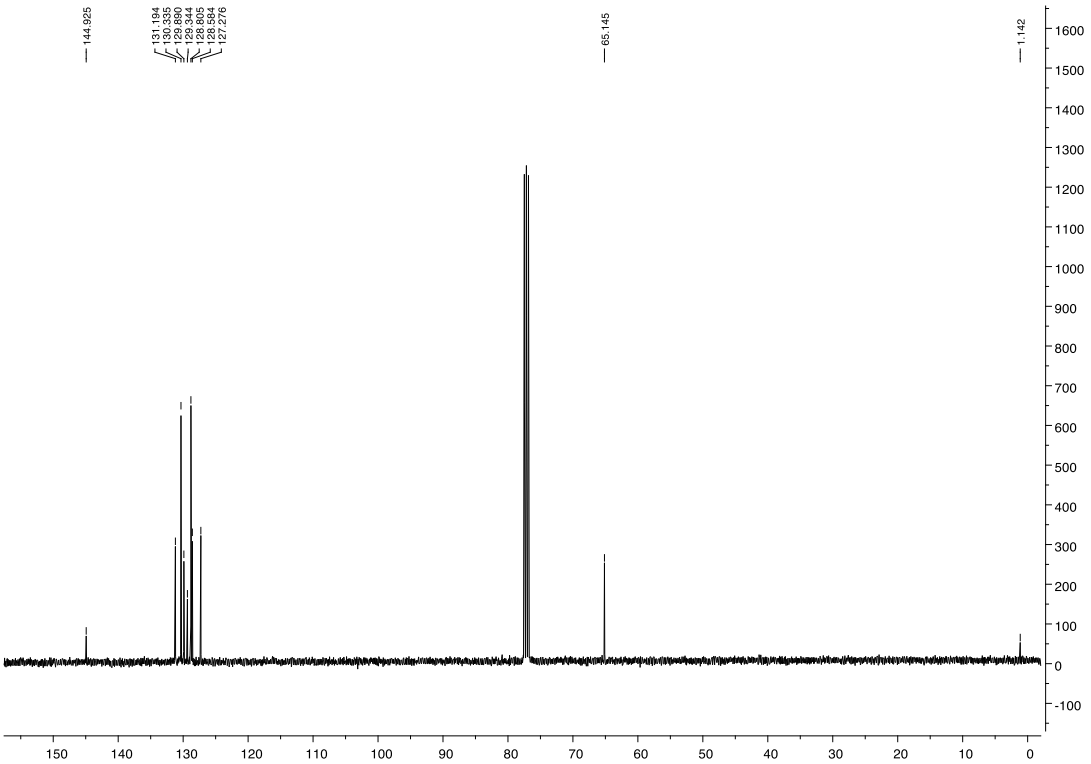
Detector A Channel 1 254nm

Peak#	Ret. Time	Area	Height	Height%	Area%
1	21.707	51586183	820459	92.856	92.475
2	25.502	4197800	63125	7.144	7.525
Total		55783983	883584	100.000	100.000

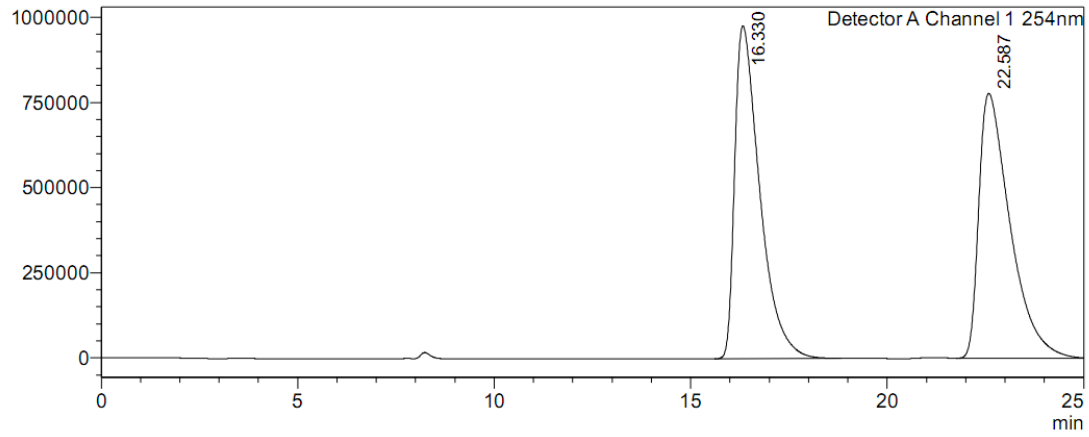


27u


7.624
7.611
7.302
7.284
7.290
7.276
7.267
7.260
7.127
7.118
7.093
7.089
7.076
7.070
7.035
7.023
7.013
4.375
4.344
4.162
4.131
0.92
3.04
0.96
1.92
0.88
1.00
0.99


144.925
131.194
130.935
130.880
129.344
128.805
128.584
127.276
65.145
1.142

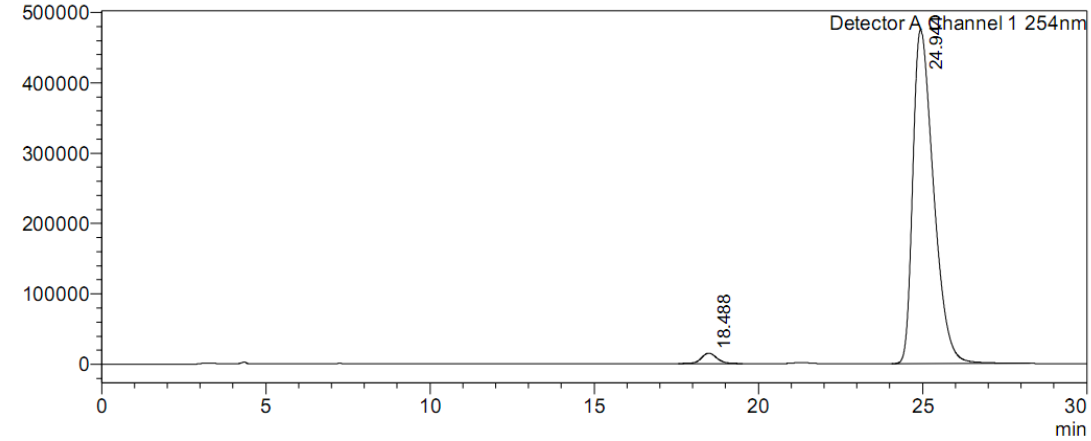
YZY1097C-ODH-1010254230-100-R YZY1097C-ODH-1010254230-100-R.lcd
uV



Detector A Channel 1 254nm

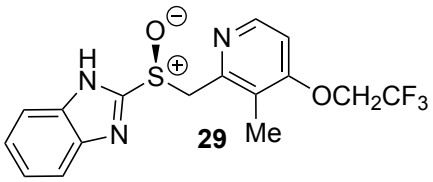
Peak#	Ret. Time	Area	Height	Height%	Area%
1	16.330	43376051	977905	55.697	50.163
2	22.587	43094210	777860	44.303	49.837
Total		86470261	1755765	100.000	100.000

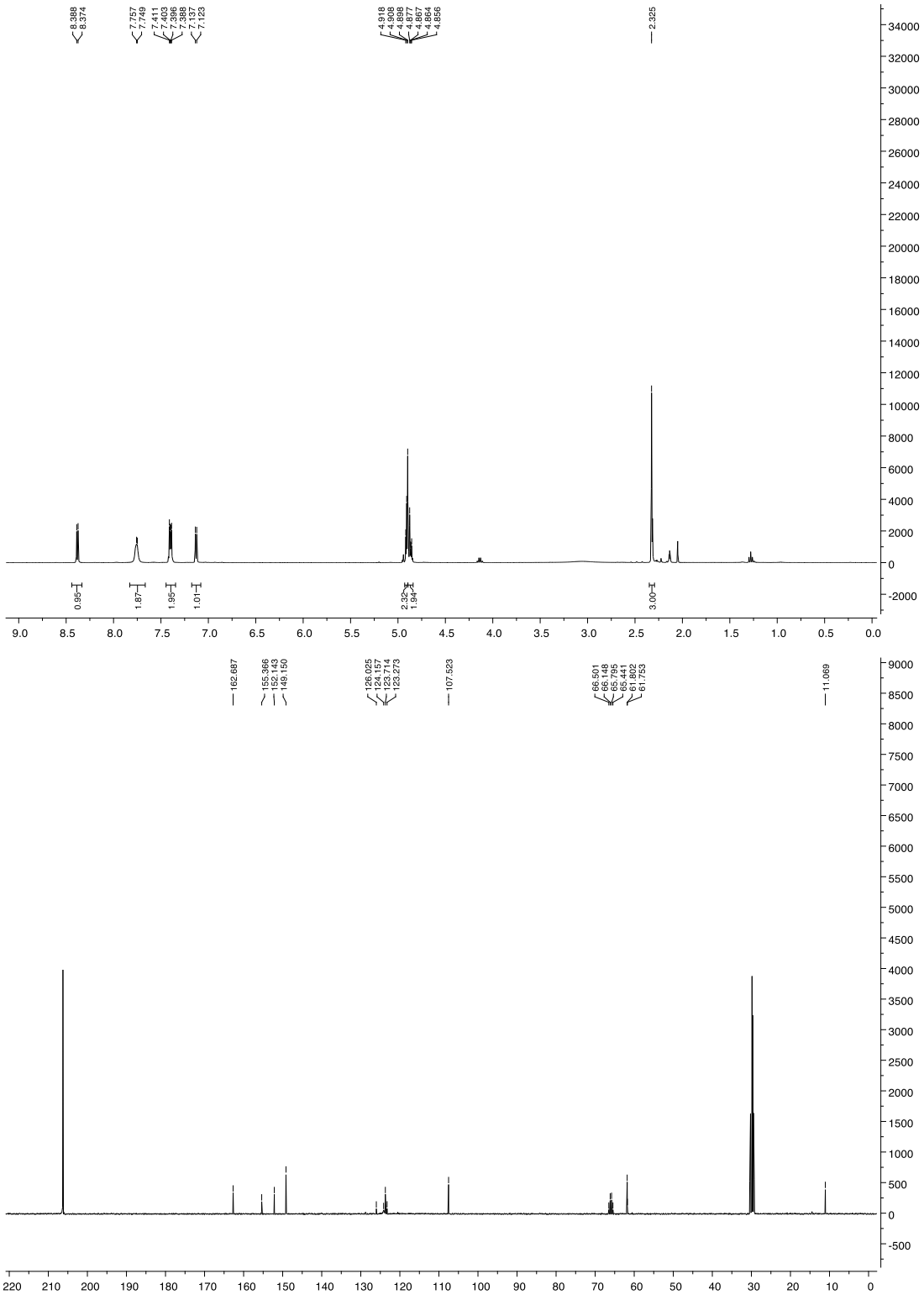
YXY3276B-ODH1010254230-35 YXY3276B-ODH1010254230-35.lcd
uV



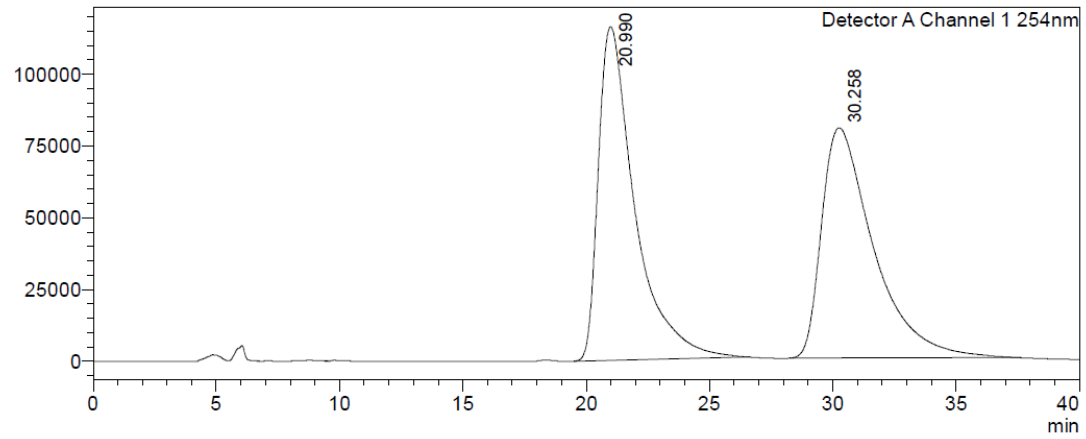
Detector A Channel 1 254nm

Peak#	Ret. Time	Area	Height	Height%	Area%
1	18.488	485581	14792	3.022	2.297
2	24.944	20658780	474650	96.978	97.703
Total		21144361	489442	100.000	100.000


O
N
H
S
N
N
OCH2CF3
29
Me


8.388
8.374
7.757
7.749
7.411
7.403
7.396
7.388
7.137
7.123
4.918
4.908
4.898
4.887
4.877
4.867
4.864
4.856
2.325
0.95
1.87
1.95
1.01
2.32
1.94
3.00
162.687
155.366
152.143
149.150
126.025
124.157
123.714
123.273
107.523
66.501
66.148
65.795
65.441
61.802
61.753
11.069

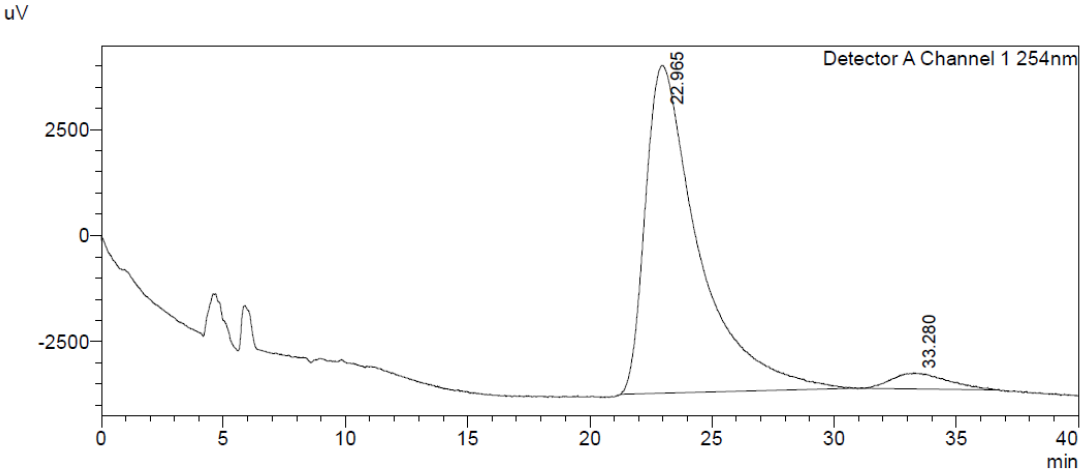
YXY4016A-ODH2007254230-100 YXY4016A-ODH2007254230-100.lcd



Detector A Channel 1 254nm

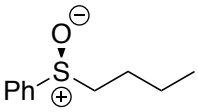
Peak#	Ret. Time	Area	Height	Height%	Area%
1	20.990	11936319	116253	59.153	50.365
2	30.258	11763522	80275	40.847	49.635
Total		23699840	196528	100.000	100.000

YXY4072B-ODH2007254230-50-2 YXY4072B-ODH2007254230-50-2.lcd

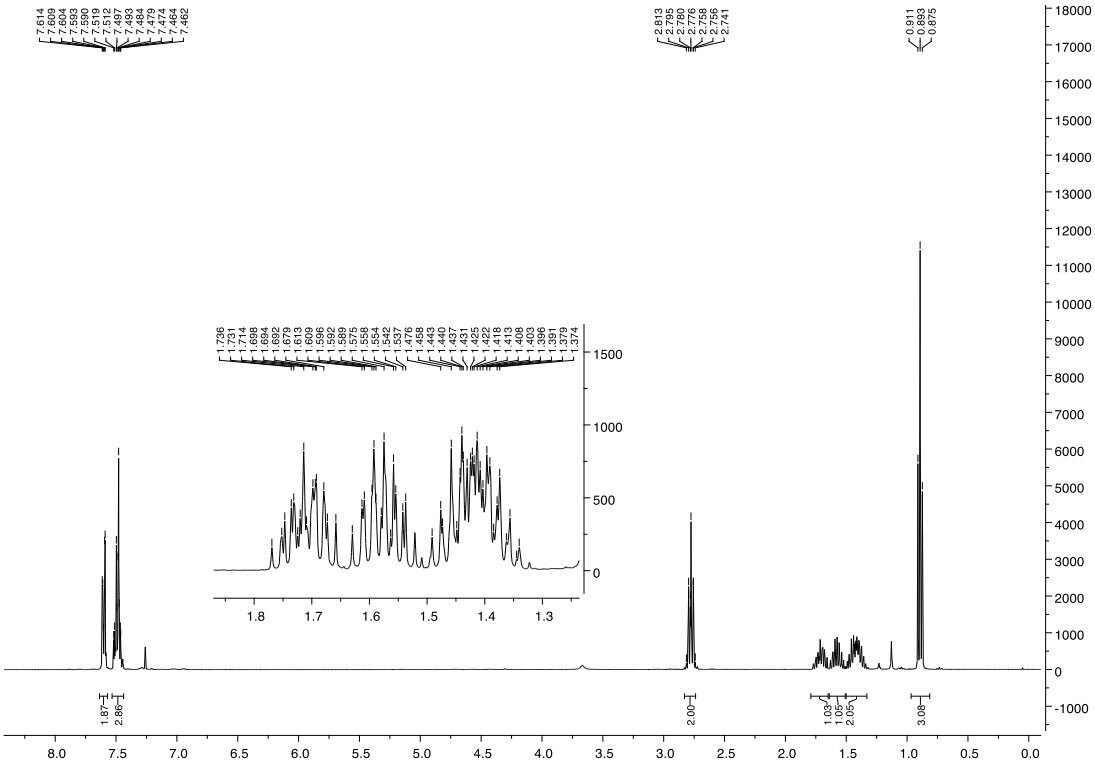


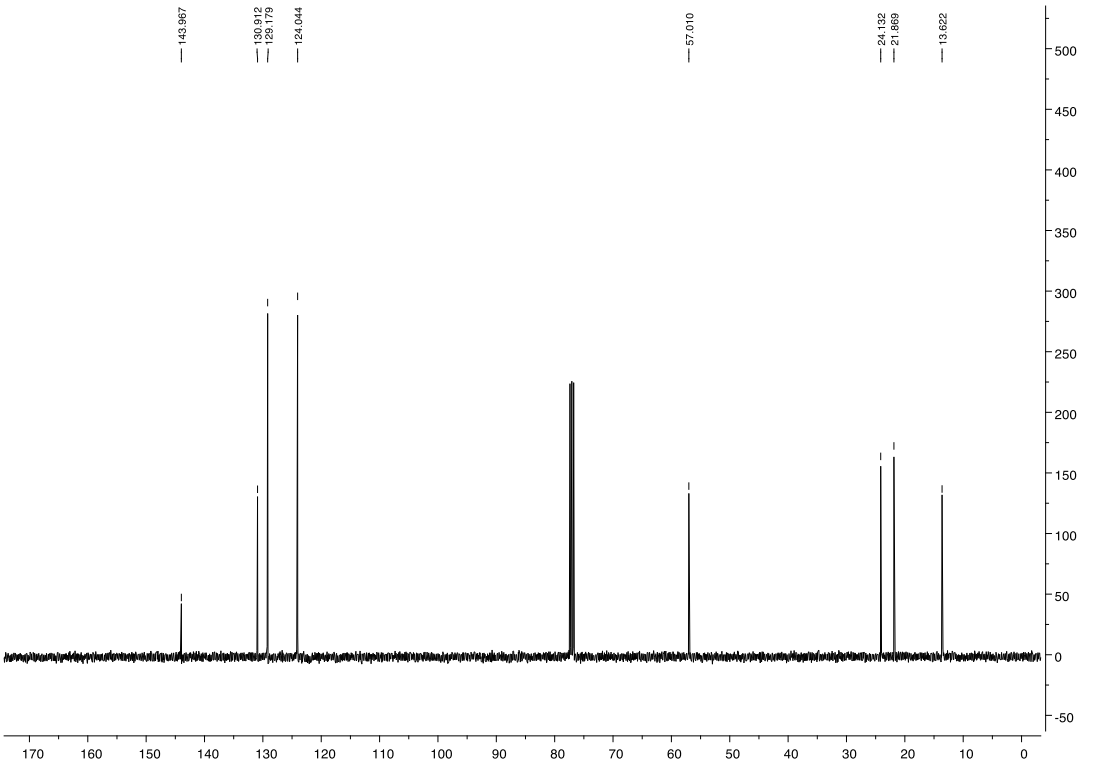
Detector A Channel 1 254nm

Peak#	Ret. Time	Area	Height	Height%	Area%
1	22.965	1169991	7727	95.430	95.200
2	33.280	58986	370	4.570	4.800
Total		1228977	8097	100.000	100.000



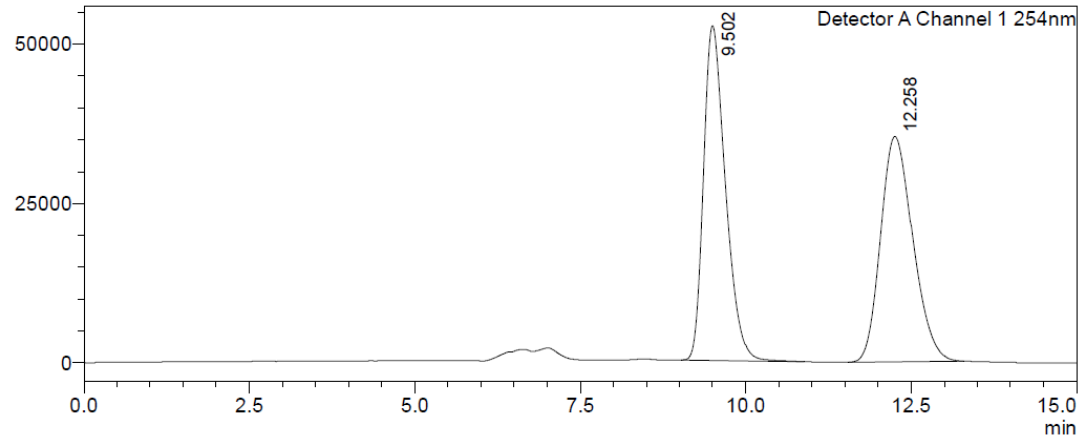
31a





YZY1095B-OBH-5005254230-100-R1 YZY1095B-OBH-5005254230-100-R1.lcd

uV

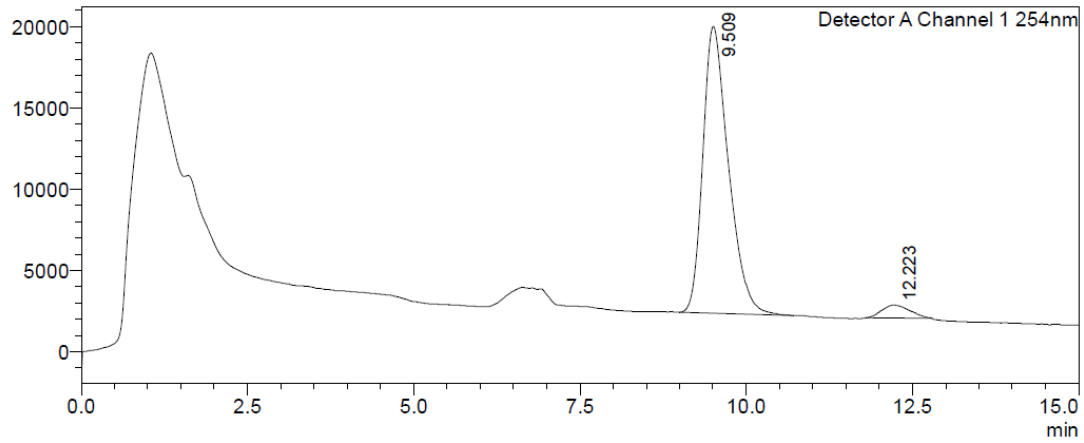


Detector A Channel 1 254nm

Peak#	Ret. Time	Area	Height	Height%	Area%
1	9.502	1214636	52574	59.776	50.405
2	12.258	1195128	35378	40.224	49.595
Total		2409763	87952	100.000	100.000

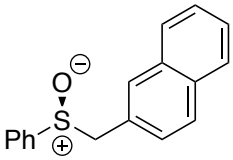
YXY4144-OBH5005254230-15 YXY4144-OBH5005254230-15.lcd

uV

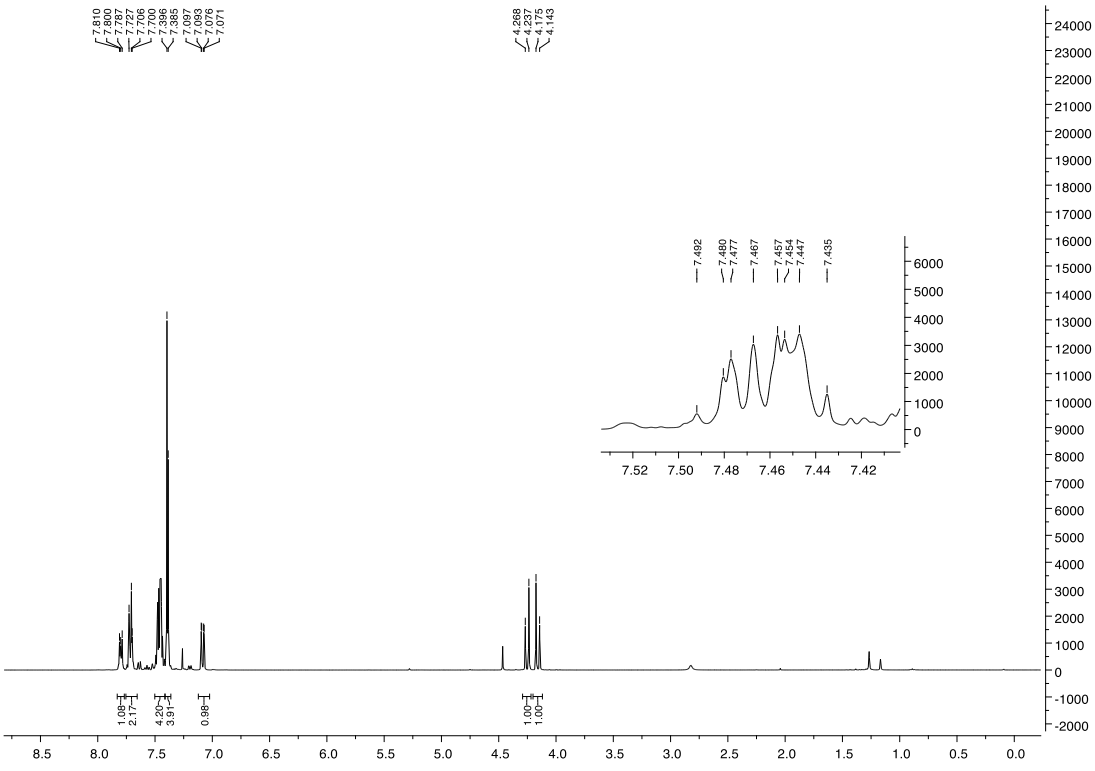


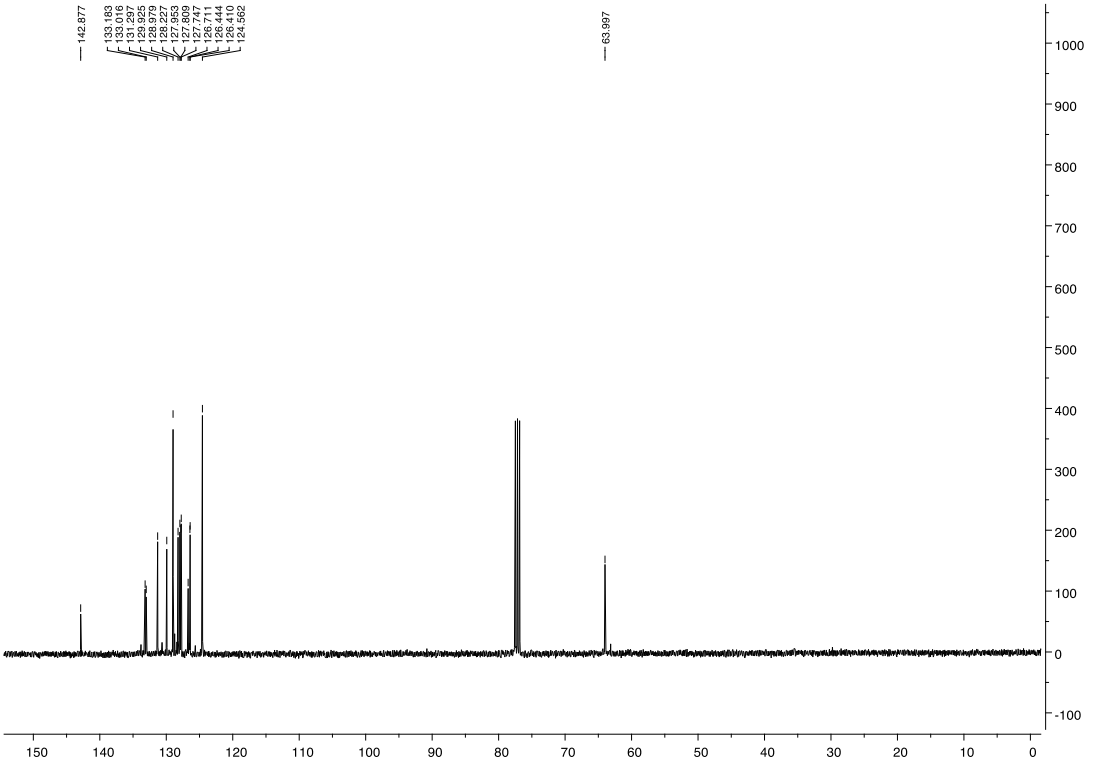
Detector A Channel 1 254nm

Peak#	Ret. Time	Area	Height	Height%	Area%
1	9.509	473982	17664	95.641	95.204
2	12.223	23878	805	4.359	4.796
Total		497860	18469	100.000	100.000

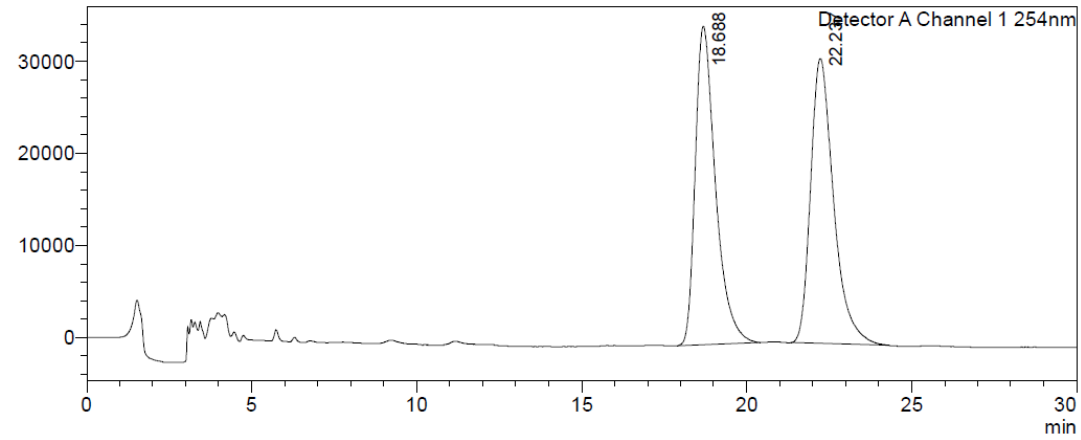


31b


7.810
7.800
7.787
7.727
7.706
7.700
7.396
7.385
7.097
7.093
7.076
7.071
4.268
4.237
4.175
4.143
7.492
7.480
7.477
7.467
7.457
7.454
7.447
7.435
1.08
2.17
4.20
3.91
0.98
1.00
1.00


142.877
133.183
133.016
131.297
129.925
129.079
128.227
127.953
127.809
127.747
126.771
126.444
126.410
124.562
63.997

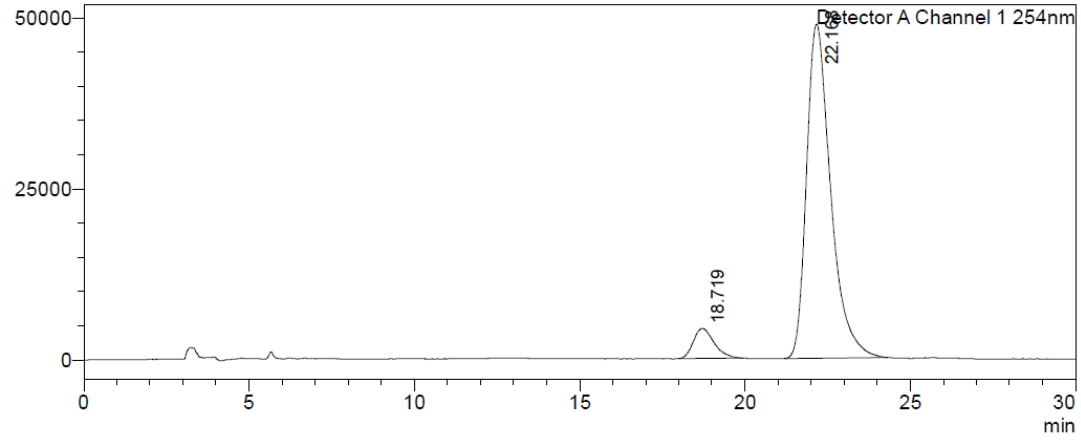
YXY4118A-ODH1010254230-100-R YXY4118A-ODH1010254230-100-R.lcd



Detector A Channel 1 254nm

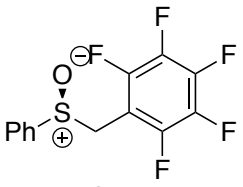
Peak#	Ret. Time	Area	Height	Height%	Area%
1	18.688	1479821	34615	52.795	49.730
2	22.237	1495906	30950	47.205	50.270
Total		2975727	65565	100.000	100.000

YXY4118B-ODH1010254230-30 YXY4118B-ODH1010254230-30.lcd

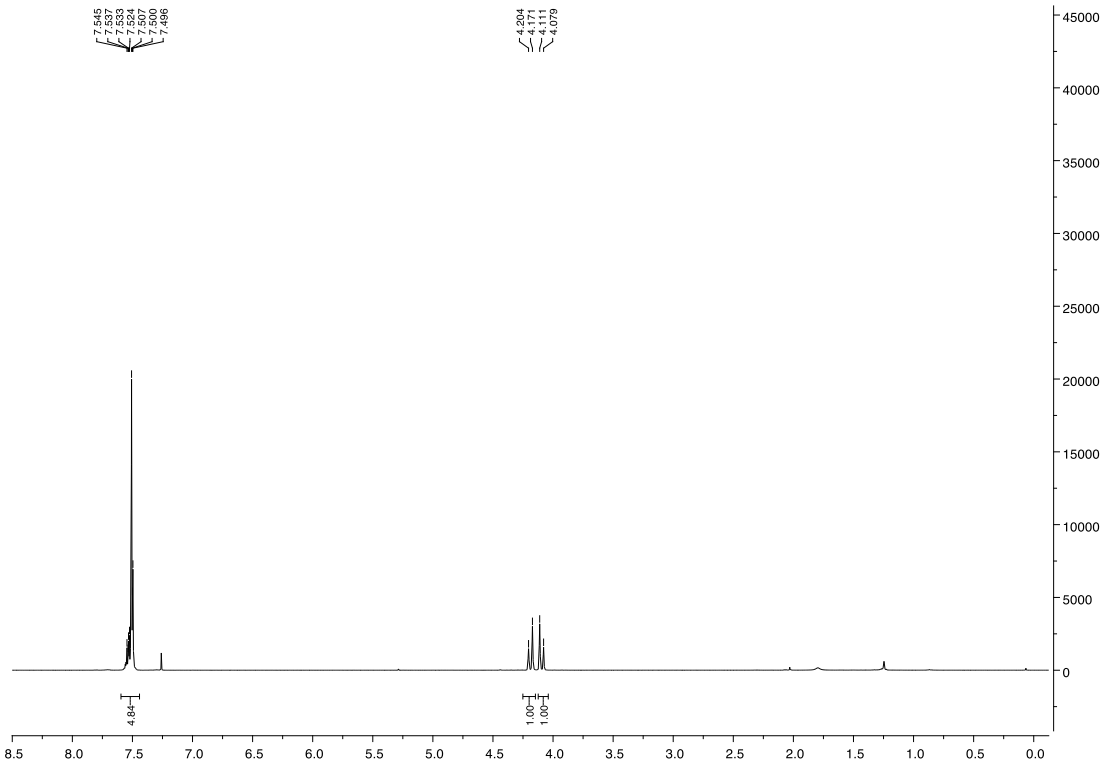


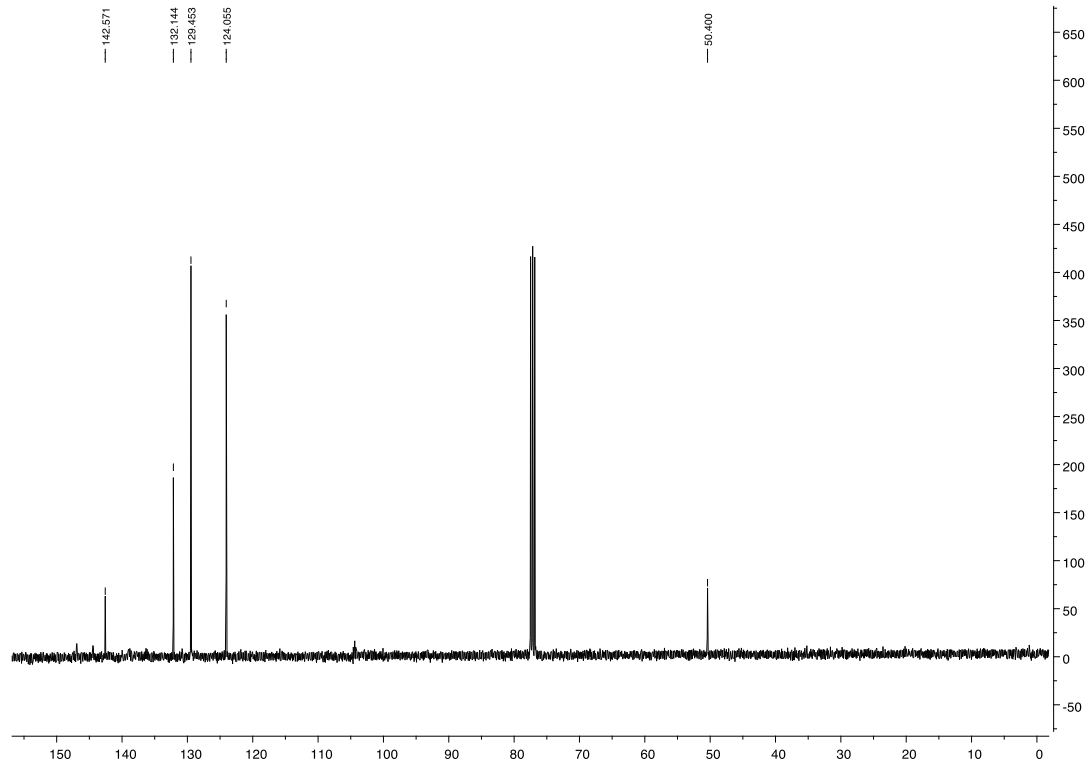
Detector A Channel 1 254nm

Peak#	Ret. Time	Area	Height	Height%	Area%
1	18.719	192003	4376	8.219	7.204
2	22.168	2473312	48864	91.781	92.796
Total		2665315	53240	100.000	100.000

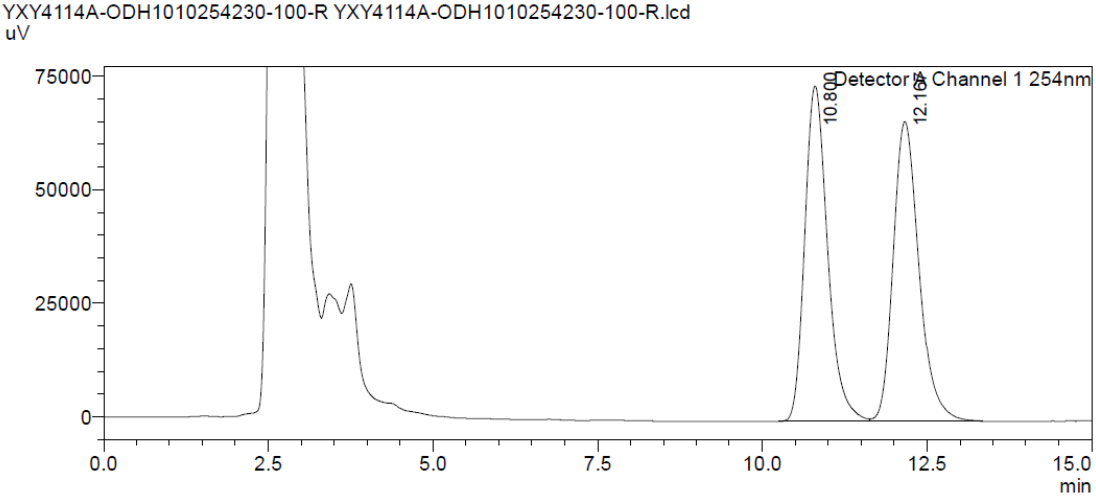


31c


7.545
7.537
7.533
7.504
7.507
7.500
7.496
4.204
4.171
4.111
4.079
4.84
1.00
1.00


142.571
132.144
129.453
124.055
50.400

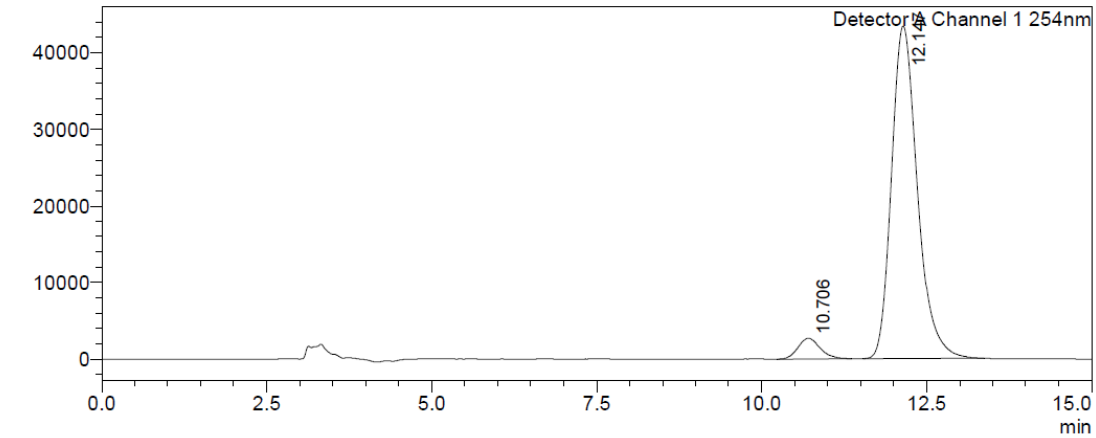
YXY4114A-ODH1010254230-100-R YXY4114A-ODH1010254230-100-R.lcd



Detector A Channel 1 254nm

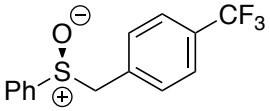
Peak#	Ret. Time	Area	Height	Height%	Area%
1	10.800	1795146	73946	52.826	49.963
2	12.167	1797818	66035	47.174	50.037
Total		3592964	139981	100.000	100.000

YXY4114D-ODH1010254230-15 YXY4114D-ODH1010254230-15.lcd

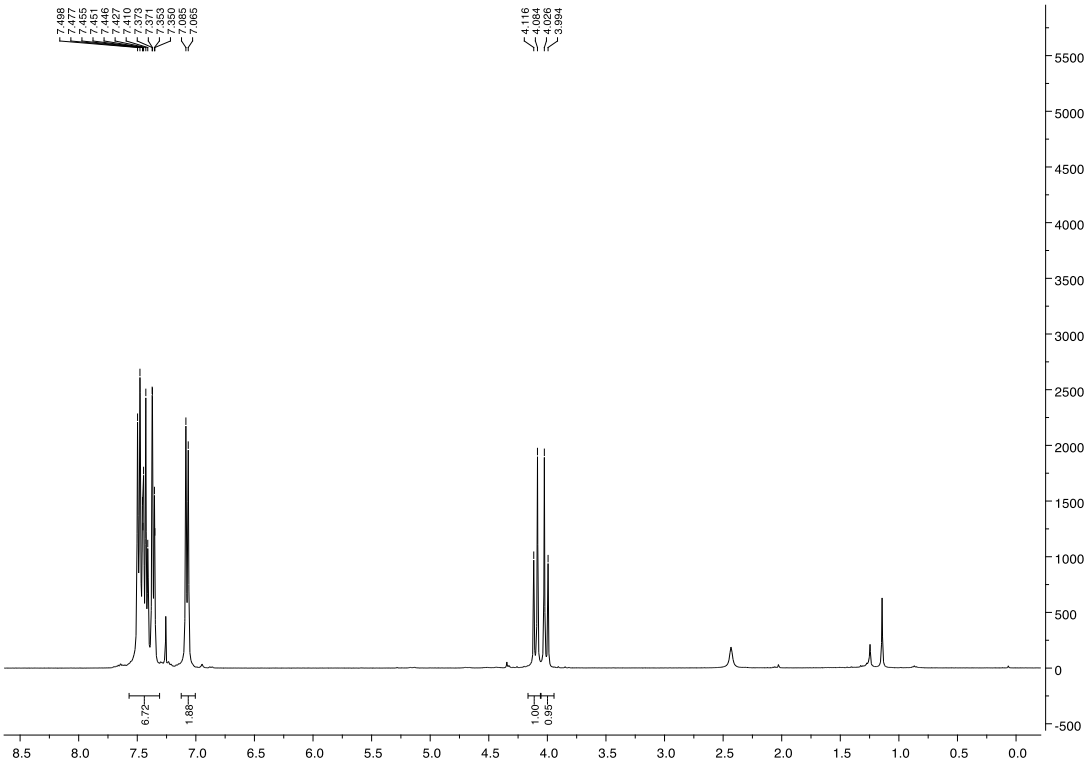


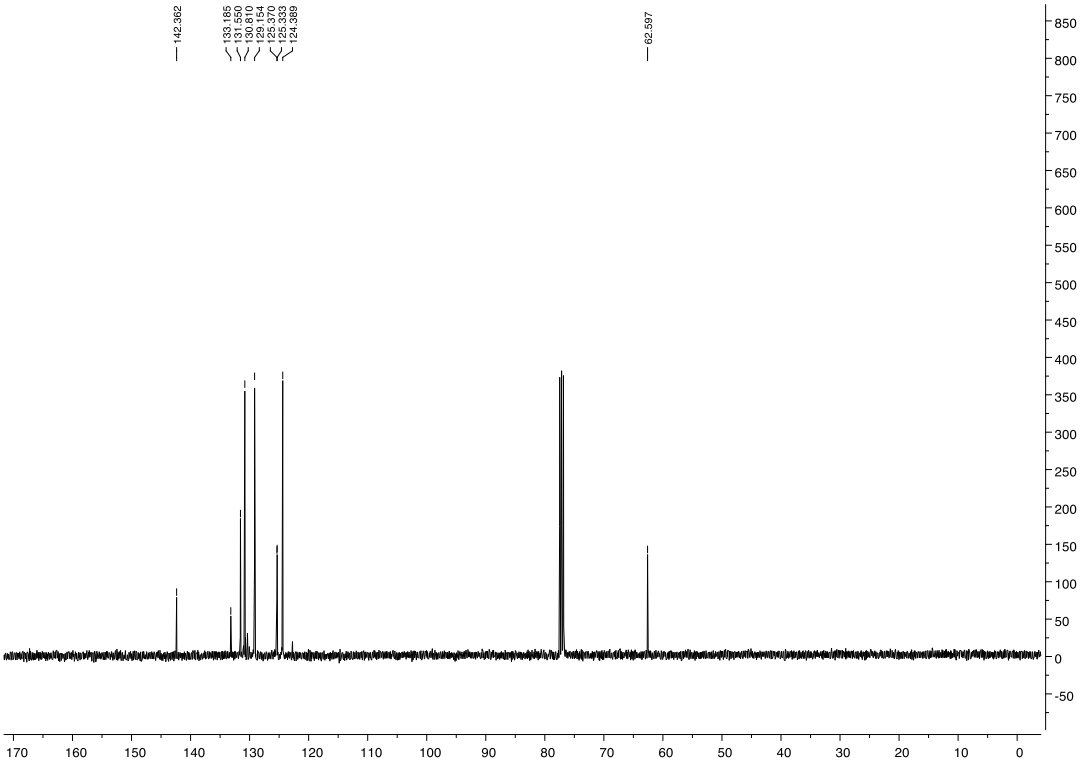
Detector A Channel 1 254nm

Peak#	Ret. Time	Area	Height	Height%	Area%
1	10.706	62851	2680	5.818	5.045
2	12.147	1183008	43379	94.182	94.955
Total		1245859	46059	100.000	100.000

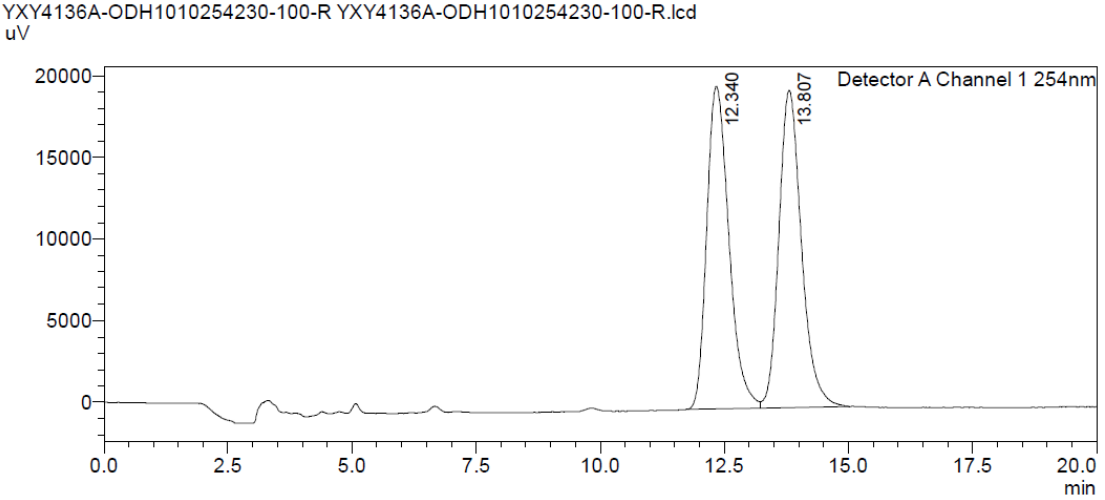

O
S
Ph
CF3

31d


7.498
7.477
7.455
7.451
7.446
7.427
7.410
7.373
7.371
7.353
7.350
7.085
7.065
4.116
4.084
4.026
3.994
6.72
1.88
1.00
0.95


142.362
133.185
131.850
131.510
129.154
125.370
125.333
124.389
62.597

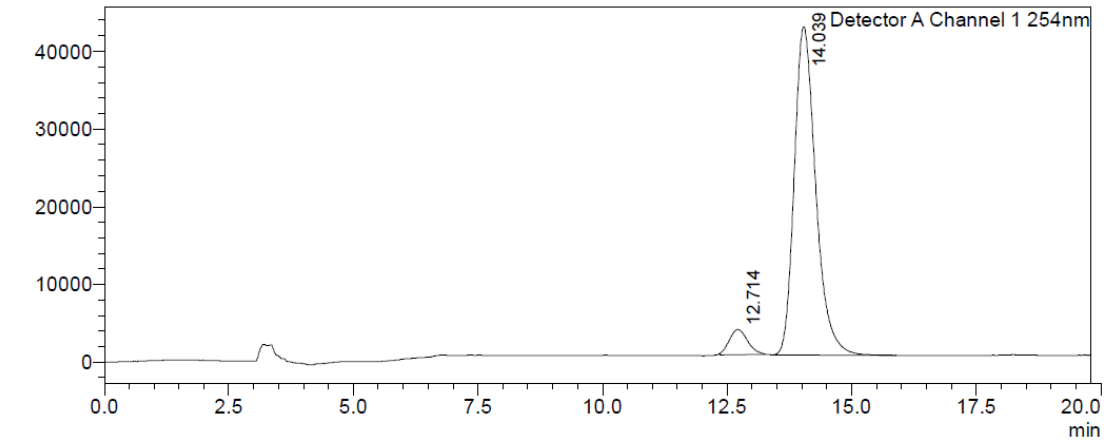
YXY4136A-ODH1010254230-100-R YXY4136A-ODH1010254230-100-R.lcd



Detector A Channel 1 254nm

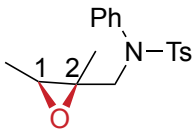
Peak#	Ret. Time	Area	Height	Height%	Area%
1	12.340	613612	19755	50.426	49.943
2	13.807	615006	19421	49.574	50.057
Total		1228618	39176	100.000	100.000

YXY4136B-ODH1010254230-20 YXY4136B-ODH1010254230-20.lcd

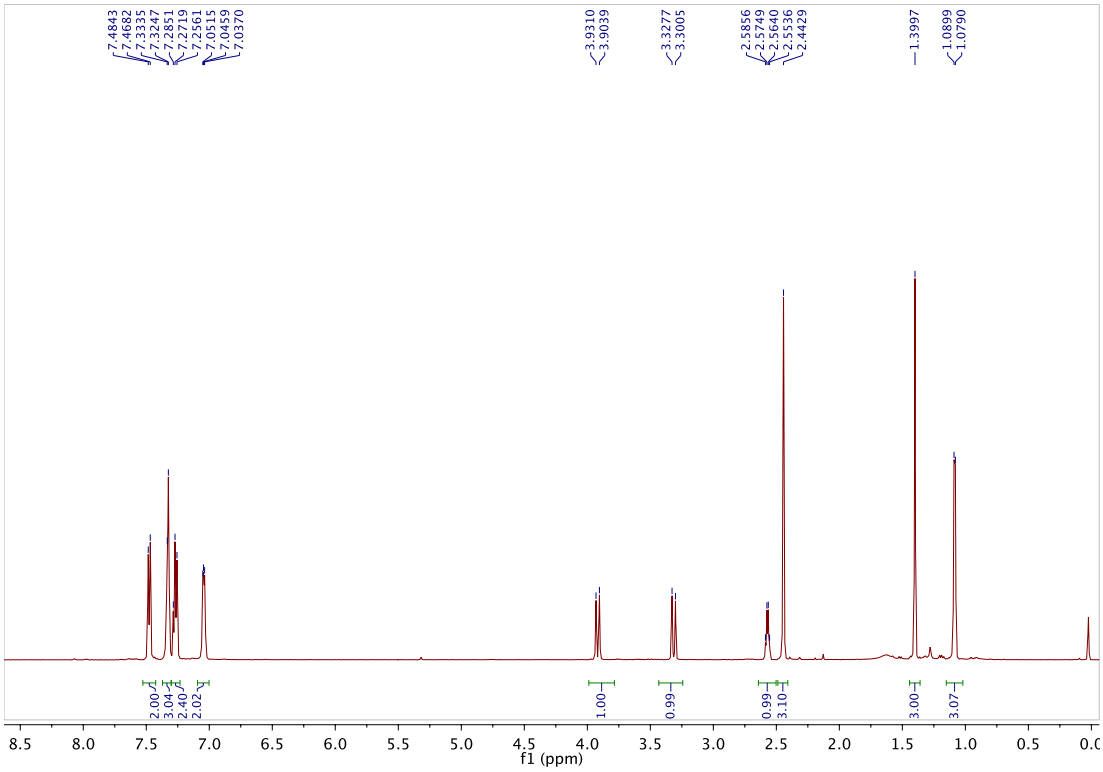


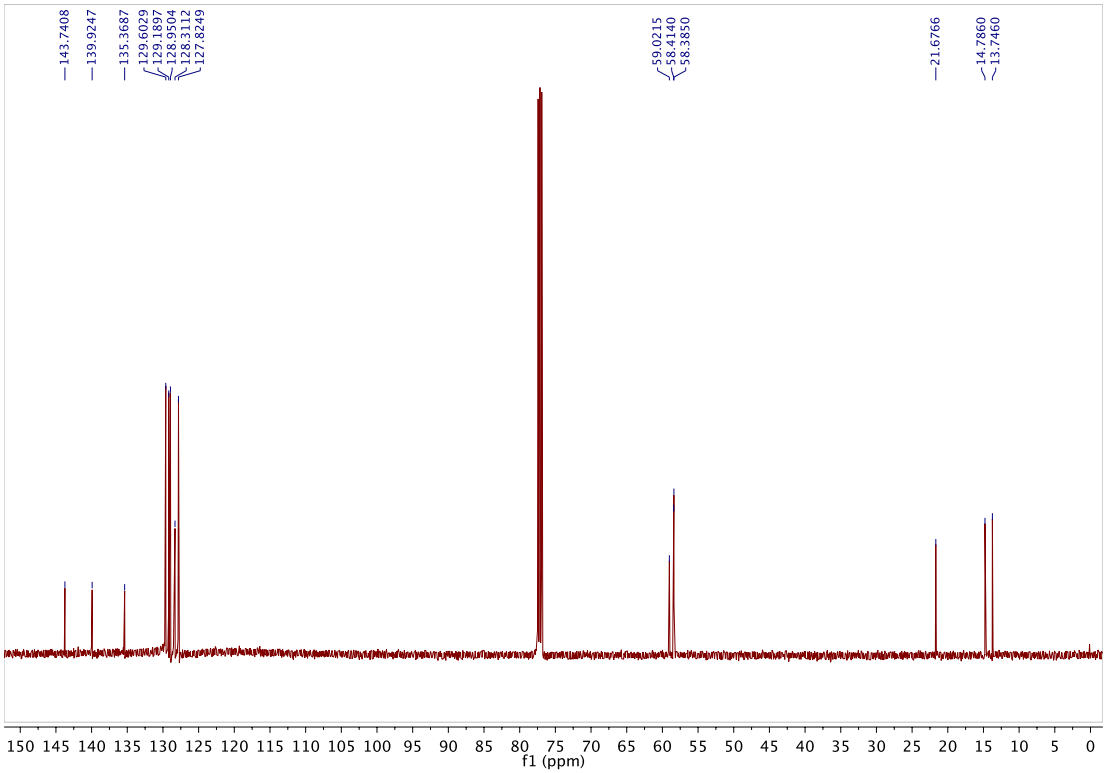
Detector A Channel 1 254nm

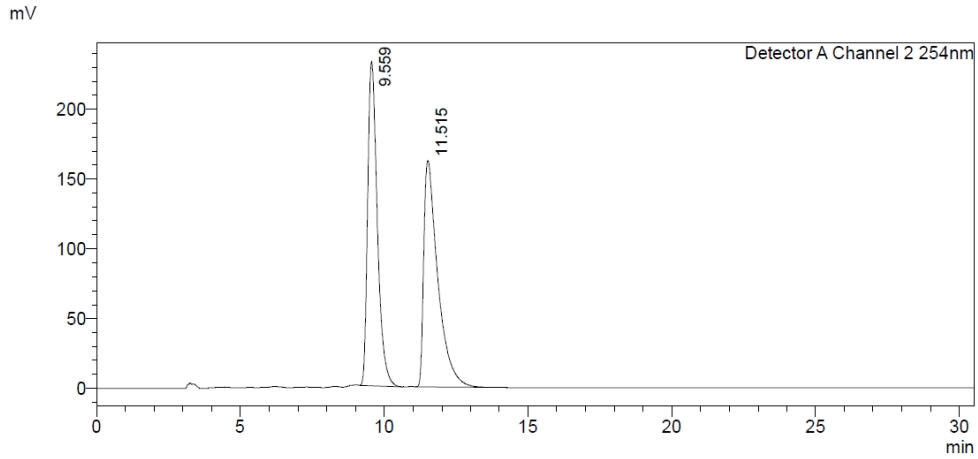
Peak#	Ret. Time	Area	Height	Height%	Area%
1	12.714	83661	3250	7.141	6.202
2	14.039	1265356	42266	92.859	93.798
Total		1349016	45516	100.000	100.000


Ph
N−Ts
1
2
O

35a

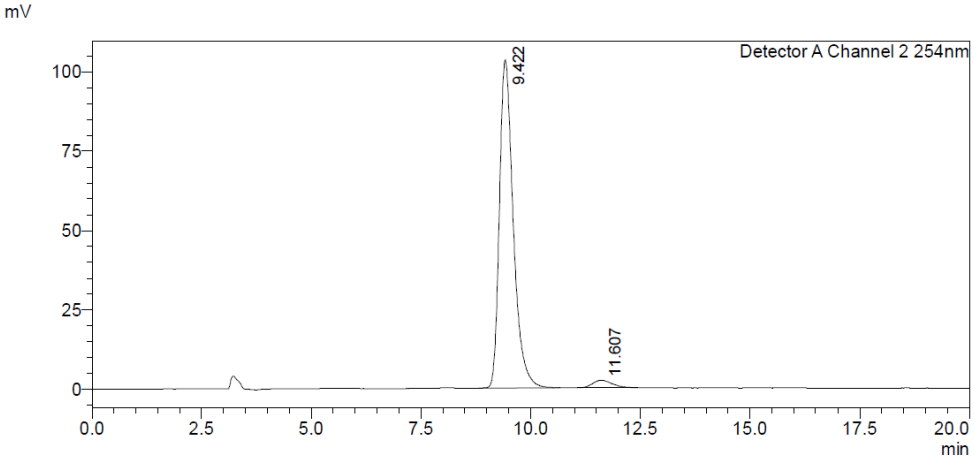

7.4843
7.4682
7.3335
7.3247
7.2851
7.2719
7.2561
7.0515
7.0459
7.0370
3.9310
3.9039
3.3277
3.3005
2.5856
2.5749
2.5640
2.5536
2.4429
1.3997
1.0899
1.0790
2.00
3.04
2.40
2.02
1.00
0.99
0.99
3.10
3.00
3.07
f1 (ppm)


143.7408
139.9247
135.3687
129.6029
129.1897
128.9504
128.3112
127.8249
59.0215
58.4140
58.3850
21.6766
14.7860
13.7460
f1 (ppm)



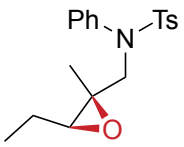
Detector A Channel 2 254nm

Peak#	Ret. Time	Area	Area%
1	9.559	5424617	49.544
2	11.515	5524374	50.456
Total		10948991	100.000

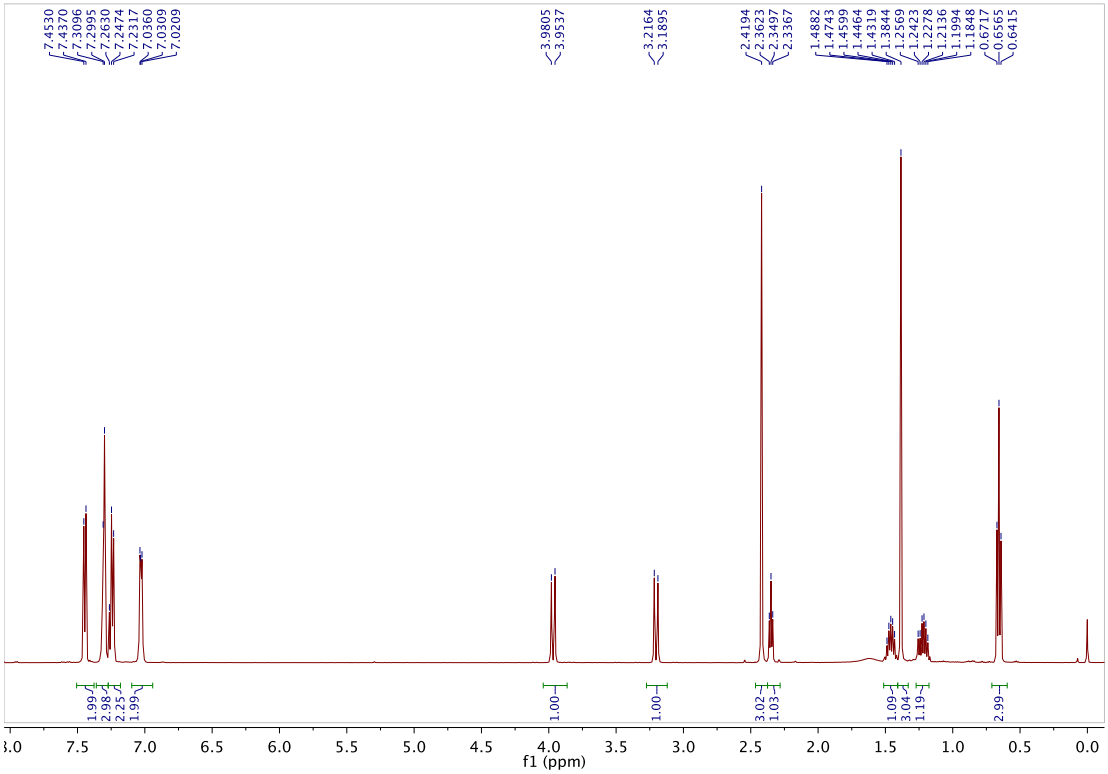


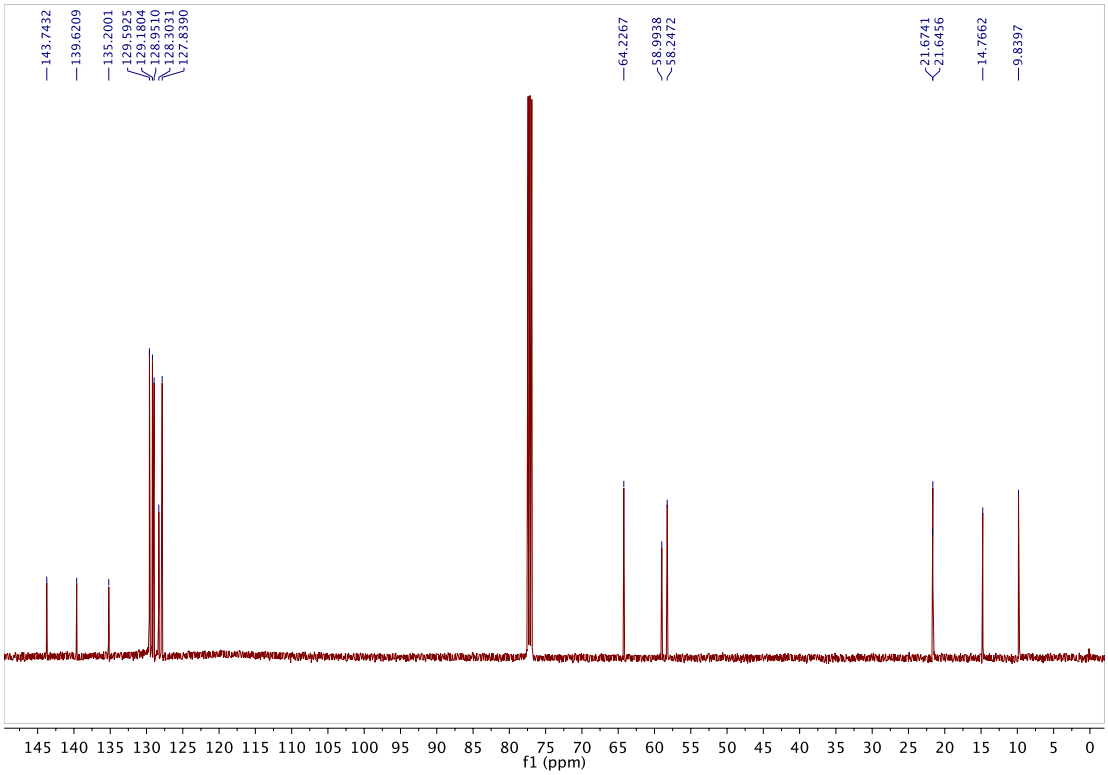
Detector A Channel 2 254nm

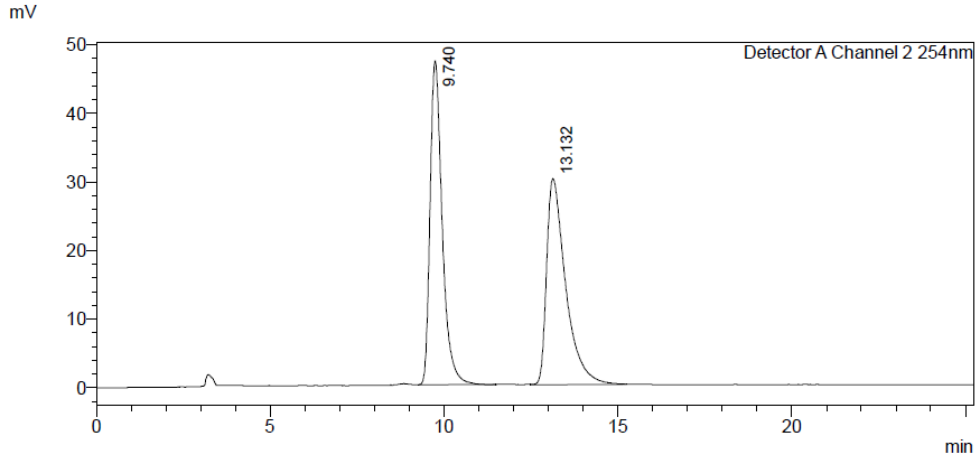
Peak#	Ret. Time	Area	Area%
1	9.422	2274822	96.820
2	11.607	74711	3.180
Total		2349533	100.000


Ph
N
Ts
O

35b

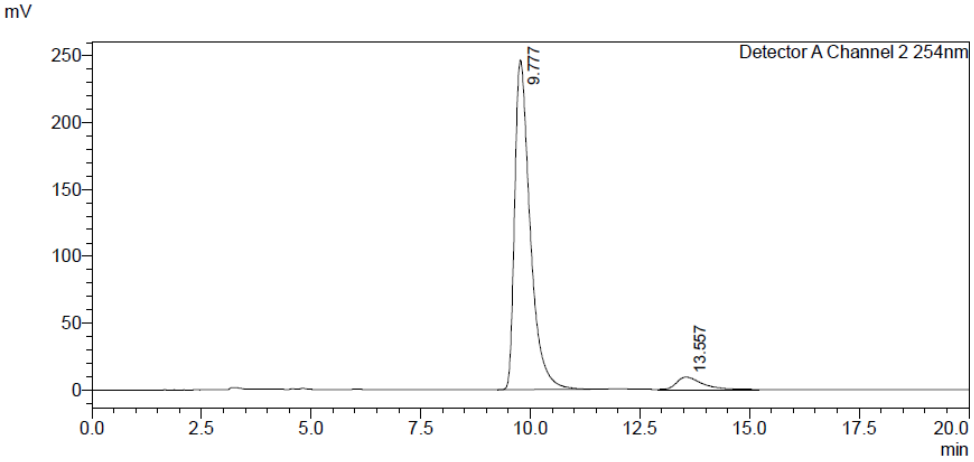

7.4530
7.4370
7.3096
7.2995
7.2630
7.2474
7.2317
7.0360
7.0309
7.0209
3.9805
3.9537
3.2164
3.1895
2.4194
2.3623
2.3497
2.3367
1.4482
1.4743
1.4599
1.4464
1.4319
1.3844
1.2569
1.2423
1.2278
1.2136
1.1994
1.1848
0.6717
0.6565
0.6415
1.99
2.98
2.25
1.99
1.00
1.00
3.02
1.03
1.09
3.04
1.19
2.99
f1 (ppm)


143.7432
139.6209
135.2001
129.5925
129.1804
128.9510
128.3031
127.8390
64.2267
58.9938
58.2472
21.6741
21.6456
14.7662
9.8397
f1 (ppm)



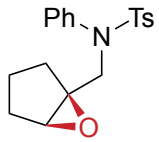
Detector A Channel 2 254nm

Peak#	Ret. Time	Area	Area%
1	9.740	1147201	50.036
2	13.132	1145558	49.964
Total		2292759	100.000

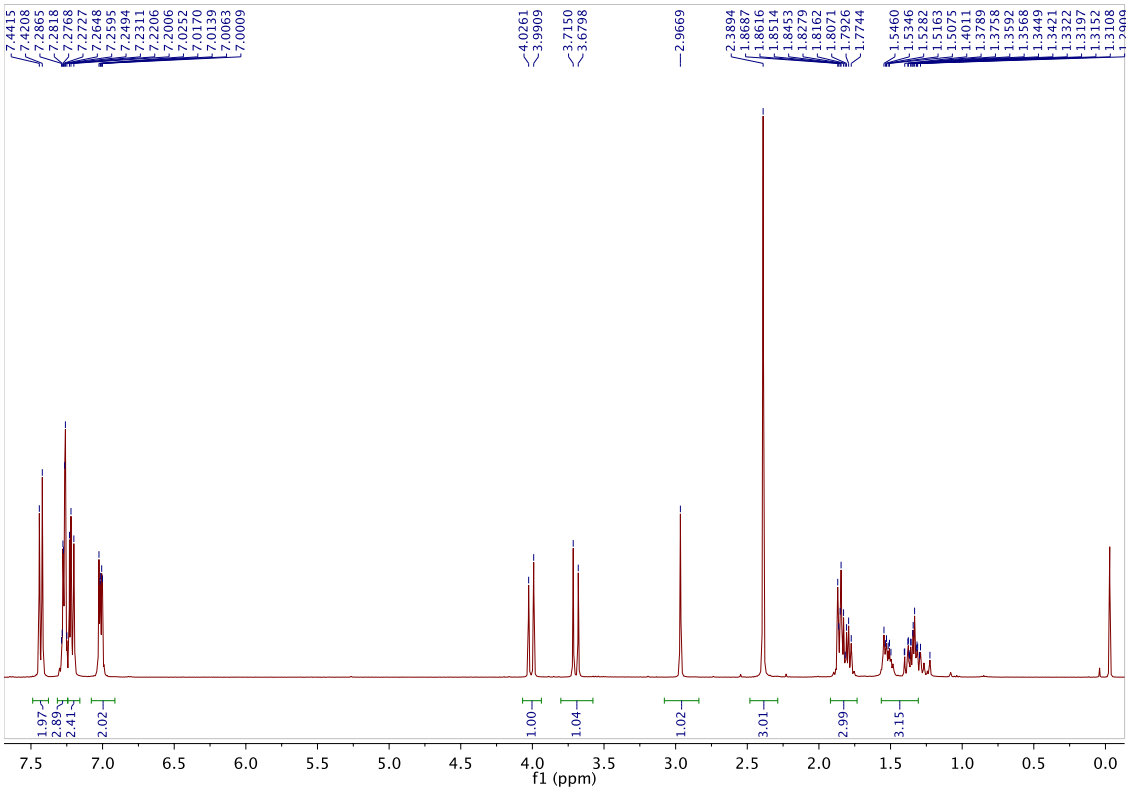


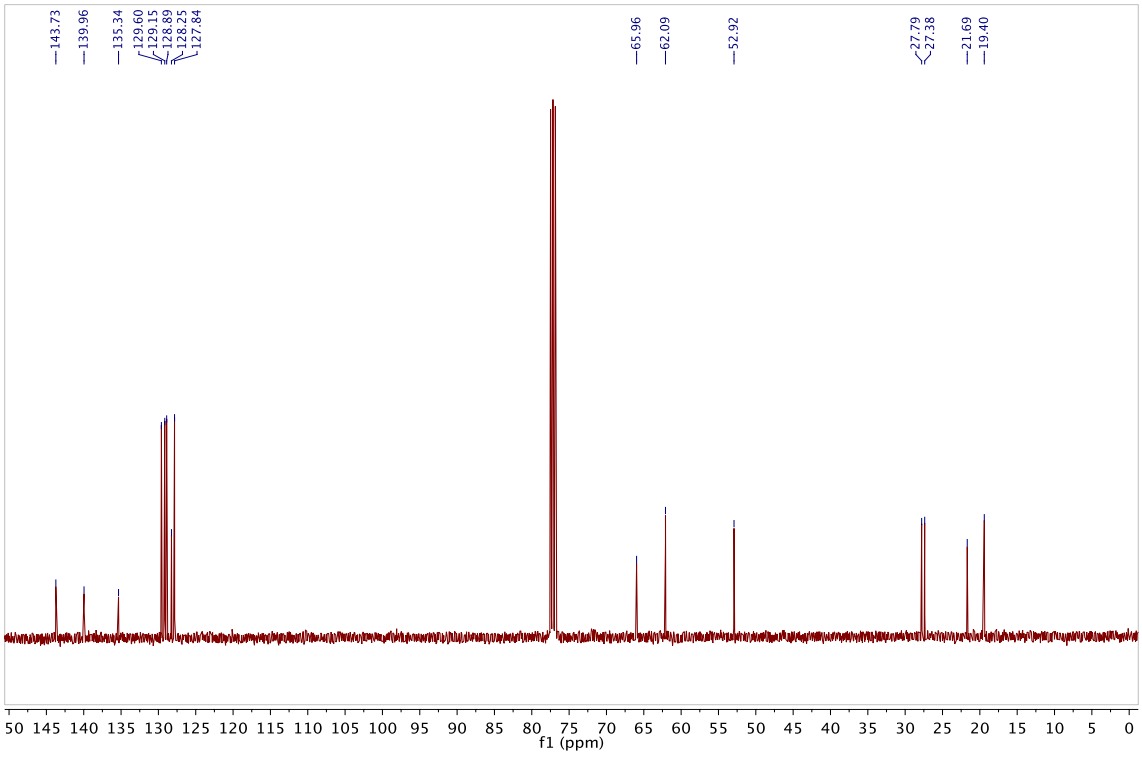
Detector A Channel 2 254nm

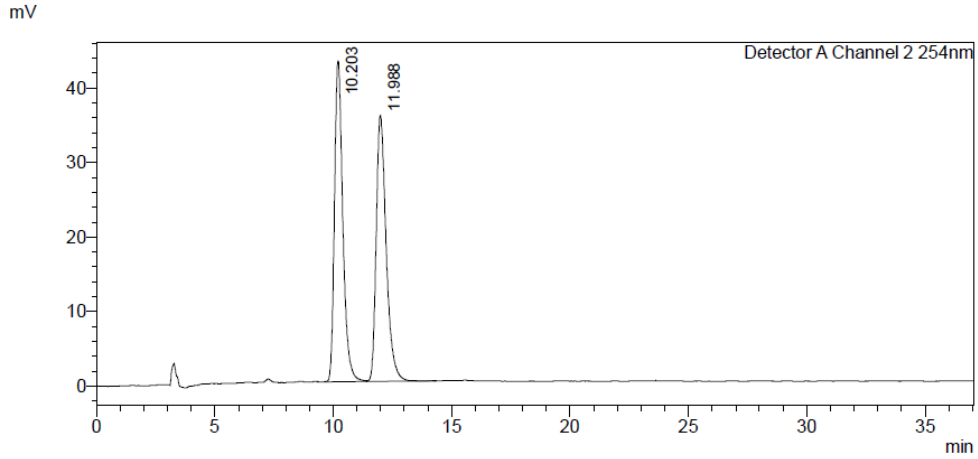
Peak#	Ret. Time	Area	Area%
1	9.777	6024082	94.110
2	13.557	376998	5.890
Total		6401080	100.000


Ph
N
Ts
O

35c

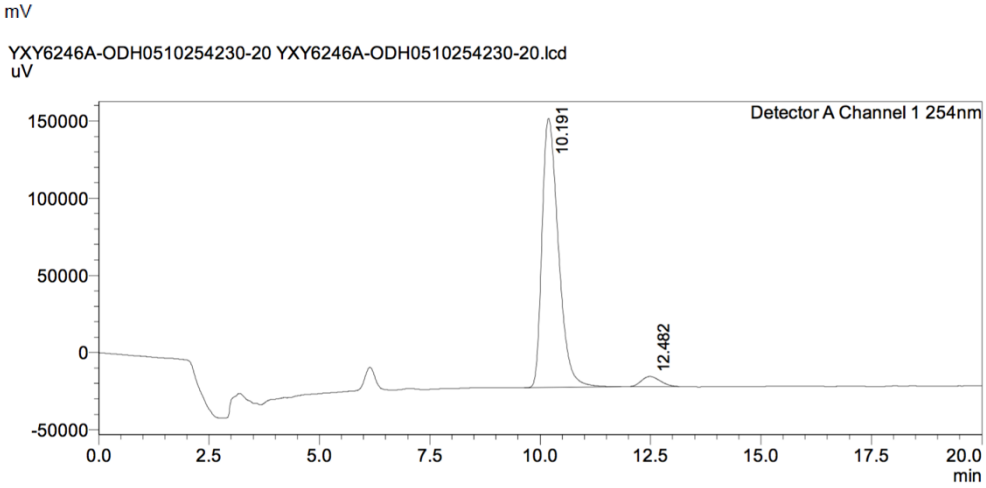

7.4415
7.4208
7.2865
7.2818
7.2768
7.2727
7.2648
7.2595
7.2494
7.2311
7.2206
7.2006
7.0252
7.0170
7.0139
7.0063
7.0009
4.0261
3.9909
3.7150
3.6798
2.9669
2.3894
1.8687
1.8616
1.8514
1.8453
1.8279
1.8162
1.8071
1.7926
1.7744
1.5460
1.5346
1.5282
1.5163
1.5075
1.4011
1.3789
1.3758
1.3592
1.3568
1.3449
1.3421
1.3322
1.3197
1.3152
1.3108
1.2900
1.97
2.89
2.41
2.02
1.00
1.04
1.02
3.01
2.99
3.15
7.5 7.0 6.5 6.0 5.5 5.0 4.5 4.0 3.5 3.0 2.5 2.0 1.5 1.0 0.5 0.0
f1 (ppm)


143.73
139.96
135.34
129.60
129.15
128.89
128.25
127.84
65.96
62.09
52.92
27.79
27.38
21.69
19.40
50 145 140 135 130 125 120 115 110 105 100 95 90 85 80 75 70 65 60 55 50 45 40 35 30 25 20 15 10 5 0
f1 (ppm)



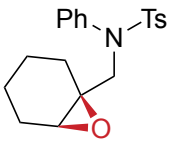
Detector A Channel 2 254nm

Peak#	Ret. Time	Area	Area%
1	10.203	1054717	50.284
2	11.988	1042790	49.716
Total		2097507	100.000

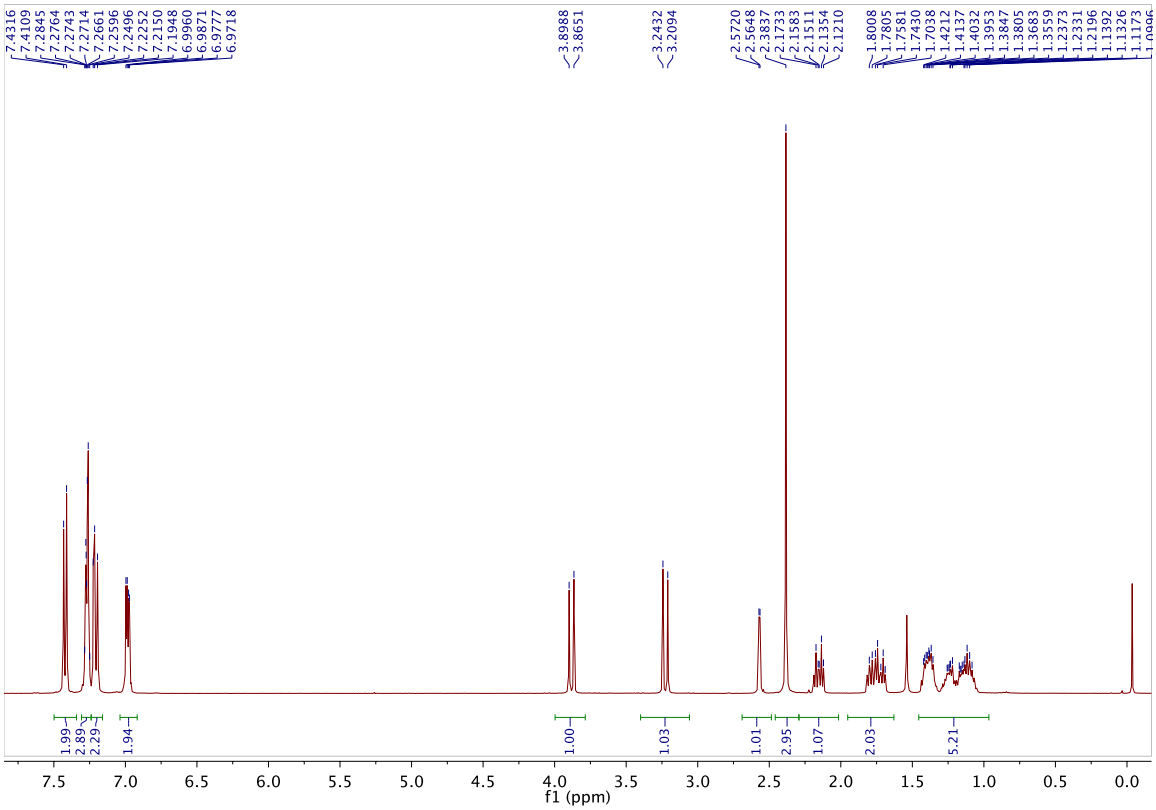


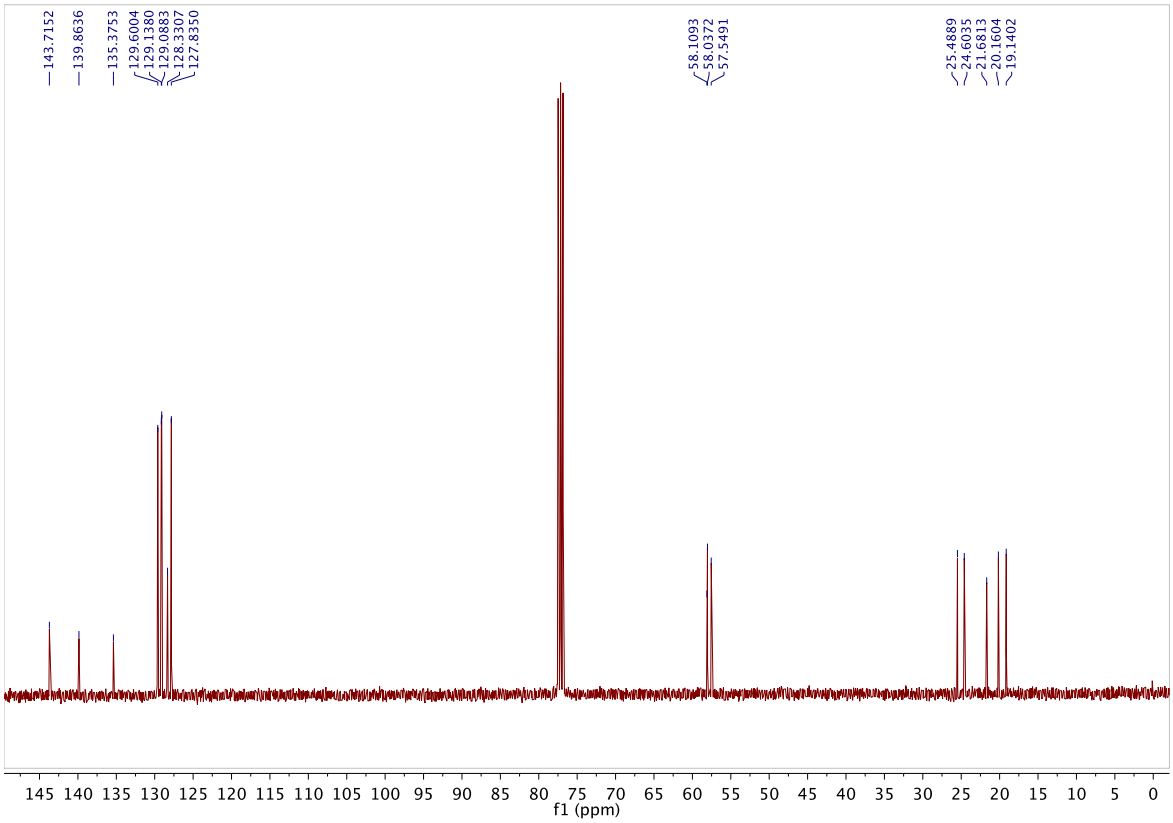
Detector A Channel 1 254nm

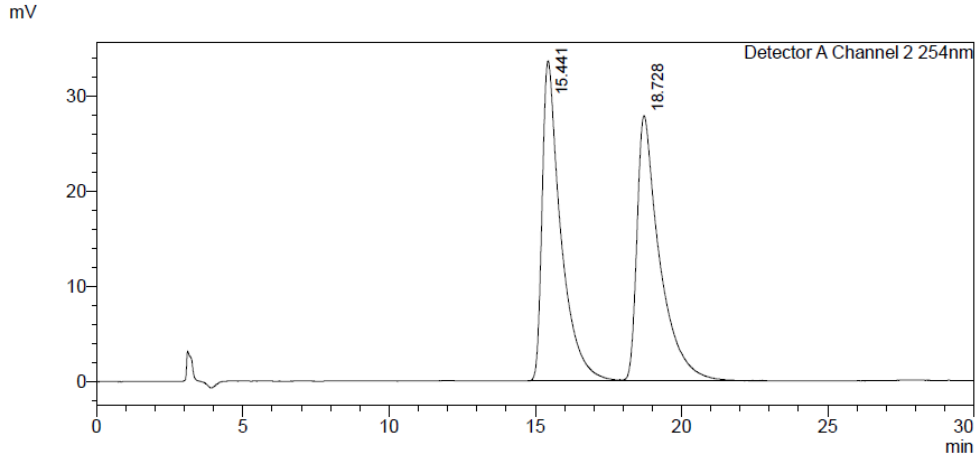
Peak#	Ret. Time	Area	Height	Height%	Area%
1	10.191	4520916	174374	96.419	95.938
2	12.482	191401	6476	3.581	4.062
Total		4712318	180850	100.000	100.000


Ph
N
Ts
O

35d

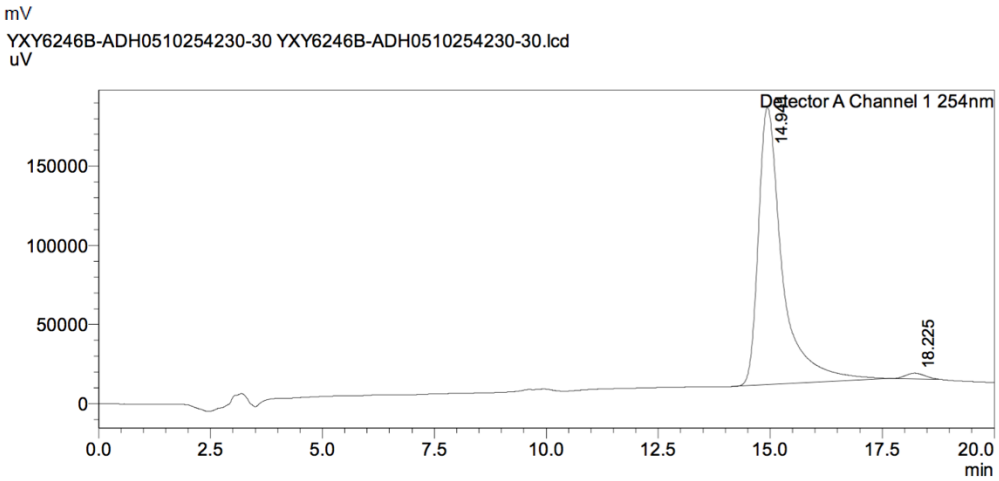

7.4316
7.4109
7.2845
7.2764
7.2743
7.2714
7.2661
7.2596
7.2496
7.2252
7.2150
7.1948
6.9960
6.9871
6.9777
6.9718
3.8988
3.8651
3.2432
3.2094
2.5720
2.5648
2.3837
2.1733
2.1583
2.1511
2.1354
2.1210
1.8008
1.7805
1.7581
1.7430
1.7038
1.4212
1.4137
1.4032
1.3953
1.3847
1.3805
1.3683
1.3559
1.2373
1.2331
1.2196
1.1392
1.1326
1.1173
1.0996
1.99
2.89
2.29
1.94
1.00
1.03
1.01
2.95
1.07
2.03
5.21
7.5
7.0
6.5
6.0
5.5
5.0
4.5
4.0
3.5
3.0
2.5
2.0
1.5
1.0
0.5
0.0
f1 (ppm)


143.7152
139.8636
135.3753
129.6004
129.1380
129.0883
128.3307
127.8350
58.1093
58.0372
57.5491
25.4889
24.6035
21.6813
20.1604
19.1402
145 140 135 130 125 120 115 110 105 100 95 90 85 80 75 70 65 60 55 50 45 40 35 30 25 20 15 10 5 0
f1 (ppm)



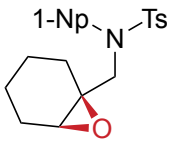
Detector A Channel 2 254nm

Peak#	Ret. Time	Area	Area%
1	15.441	1492532	49.874
2	18.728	1500053	50.126
Total		2992585	100.000

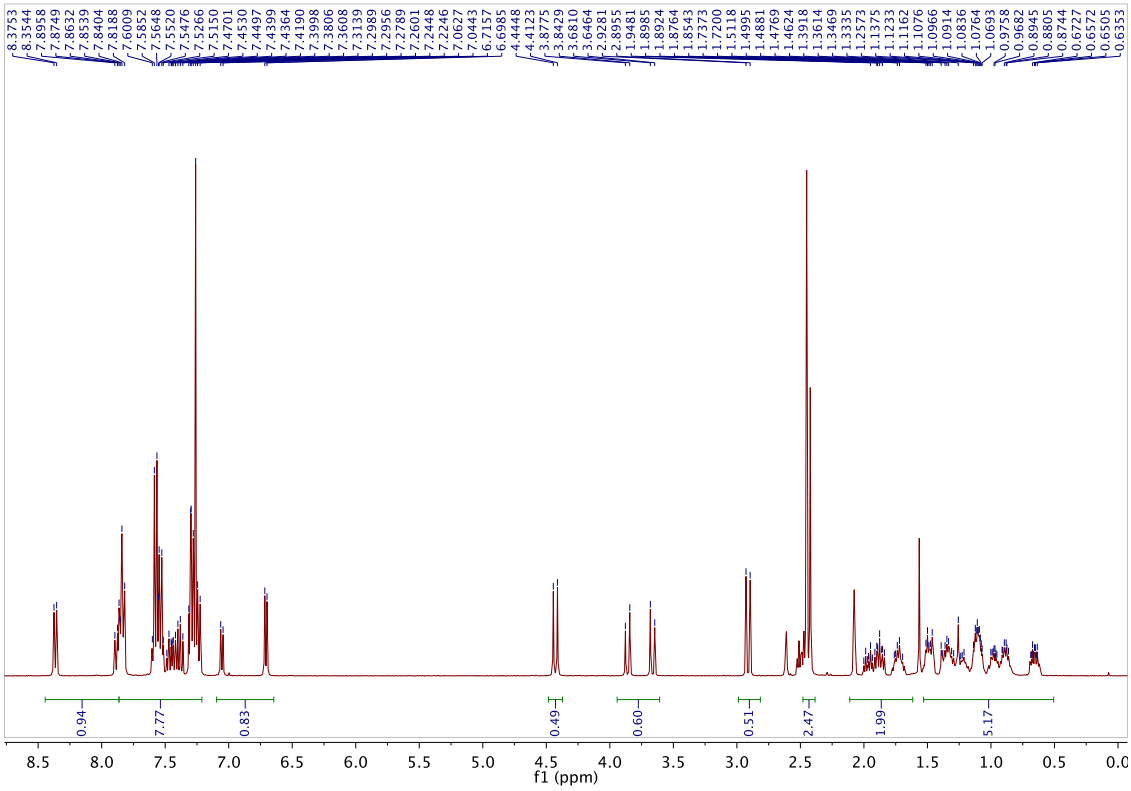


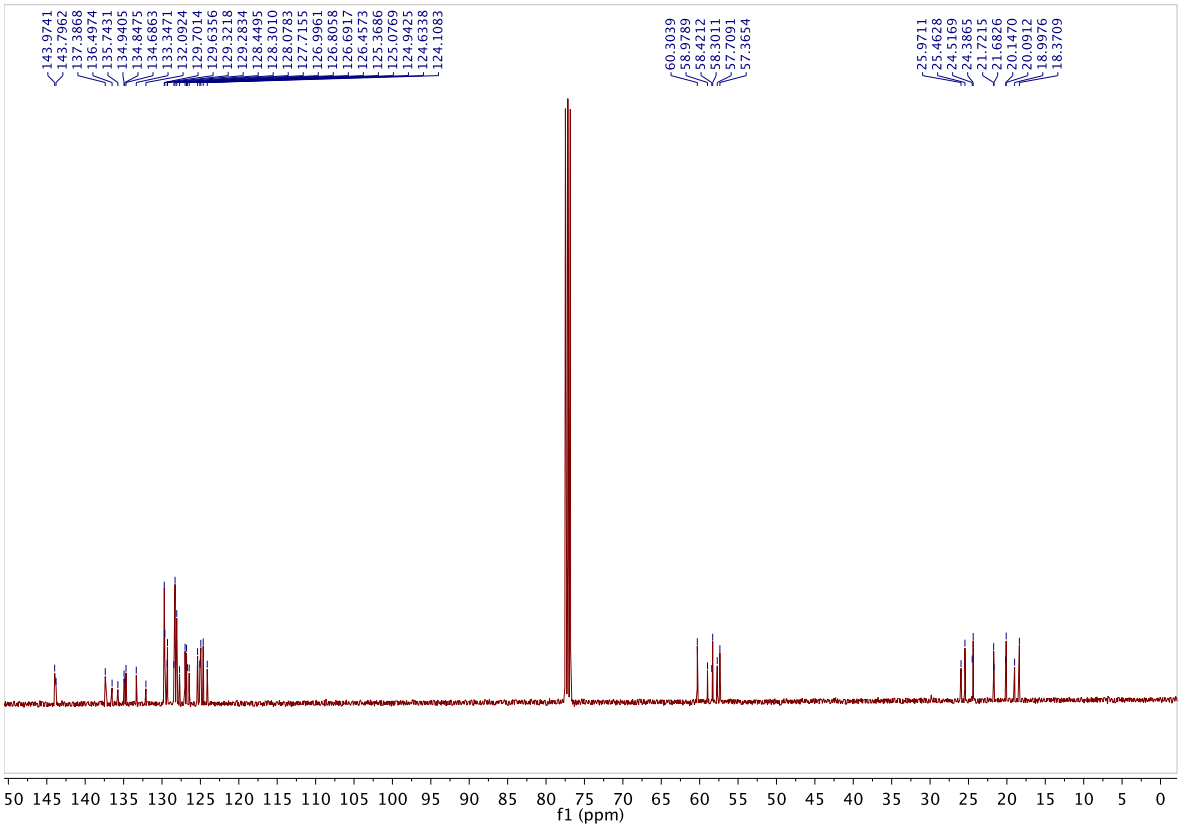
Detector A Channel 1 254nm

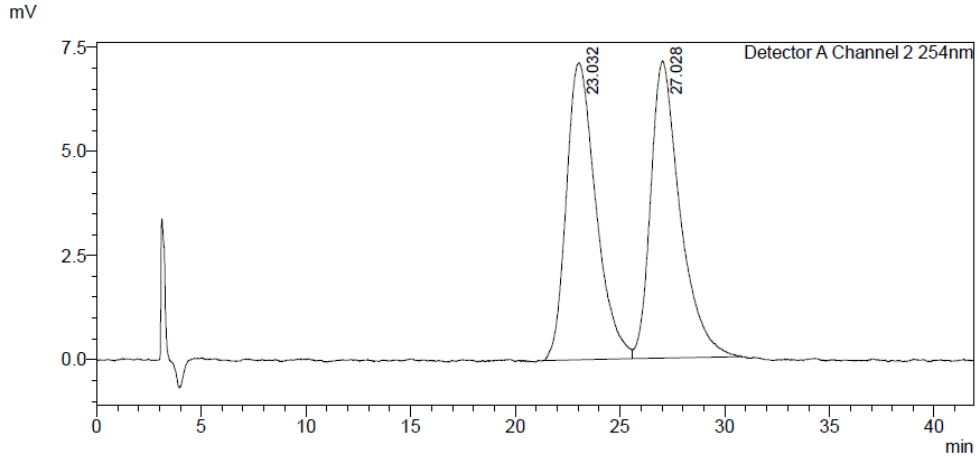
Peak#	Ret. Time	Area	Height	Height%	Area%
1	14.941	6553186	175176	98.009	98.421
2	18.225	105149	3558	1.991	1.579
Total		6658336	178734	100.000	100.000


1-Np
N
Ts
O

35e

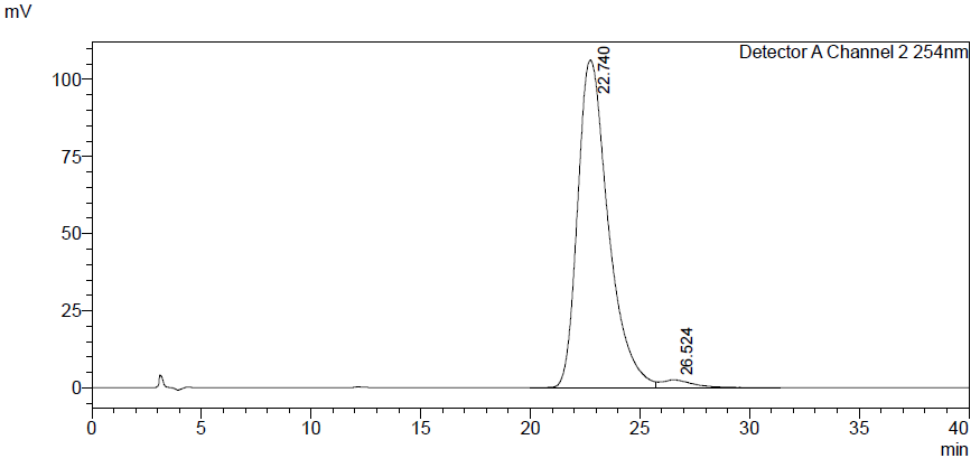

8.3753
8.3544
7.8958
7.8749
7.8632
7.8539
7.8404
7.8188
7.6009
7.5852
7.5648
7.5520
7.5476
7.5266
7.5150
7.4701
7.4530
7.4497
7.4399
7.4364
7.4190
7.3998
7.3806
7.3608
7.3139
7.2989
7.2956
7.2789
7.2601
7.2448
7.2246
7.0627
7.0443
6.7157
6.6985
4.4448
4.4123
3.8775
3.8429
3.6810
3.6464
2.9281
2.8955
1.9481
1.8985
1.8924
1.8764
1.8543
1.7373
1.7200
1.5118
1.4995
1.4881
1.4769
1.4624
1.3918
1.3614
1.3469
1.3335
1.2573
1.1375
1.1233
1.1162
1.1076
1.0966
1.0914
1.0836
1.0764
1.0693
0.9758
0.9682
0.8945
0.8805
0.8744
0.6727
0.6572
0.6505
0.6353
0.94
7.77
0.83
0.49
0.60
0.51
2.47
1.99
5.17
8.5
8.0
7.5
7.0
6.5
6.0
5.5
5.0
4.5
4.0
3.5
3.0
2.5
2.0
1.5
1.0
0.5
0.0
f1 (ppm)


143.9741
143.7962
137.3868
136.4974
135.7431
134.9405
134.8475
134.6863
133.3471
132.0924
129.7014
129.6356
129.3218
129.2834
128.4495
128.3010
128.0783
127.7155
126.9961
126.8058
126.6917
126.4573
125.3686
125.0769
124.9425
124.6338
124.1083
60.3039
58.9789
58.4212
58.3011
57.7091
57.3654
25.9711
25.4628
24.5169
24.3865
21.7215
21.6826
20.1470
20.0912
18.9976
18.3709
50 145 140 135 130 125 120 115 110 105 100 95 90 85 80 75 70 65 60 55 50 45 40 35 30 25 20 15 10 5 0
f1 (ppm)



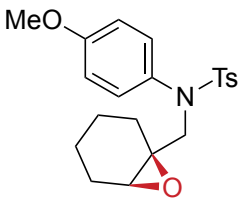
Detector A Channel 2 254nm

Peak#	Ret. Time	Area	Area%
1	23.032	702549	50.125
2	27.028	699043	49.875
Total		1401591	100.000

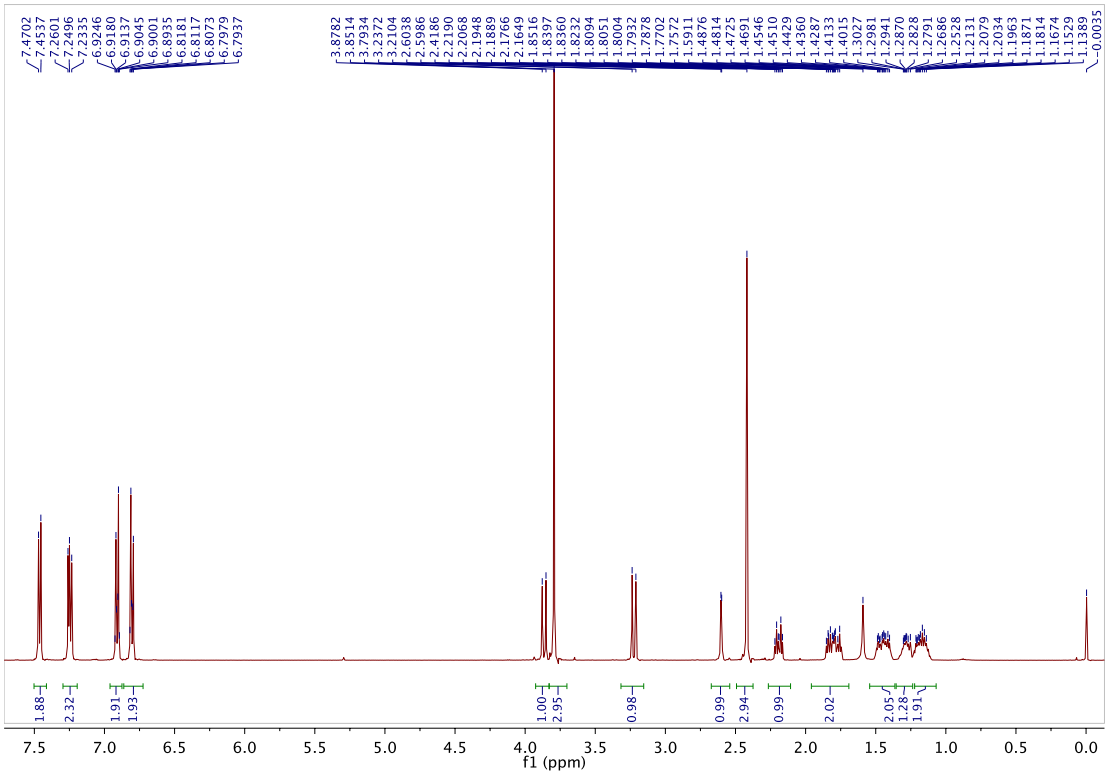


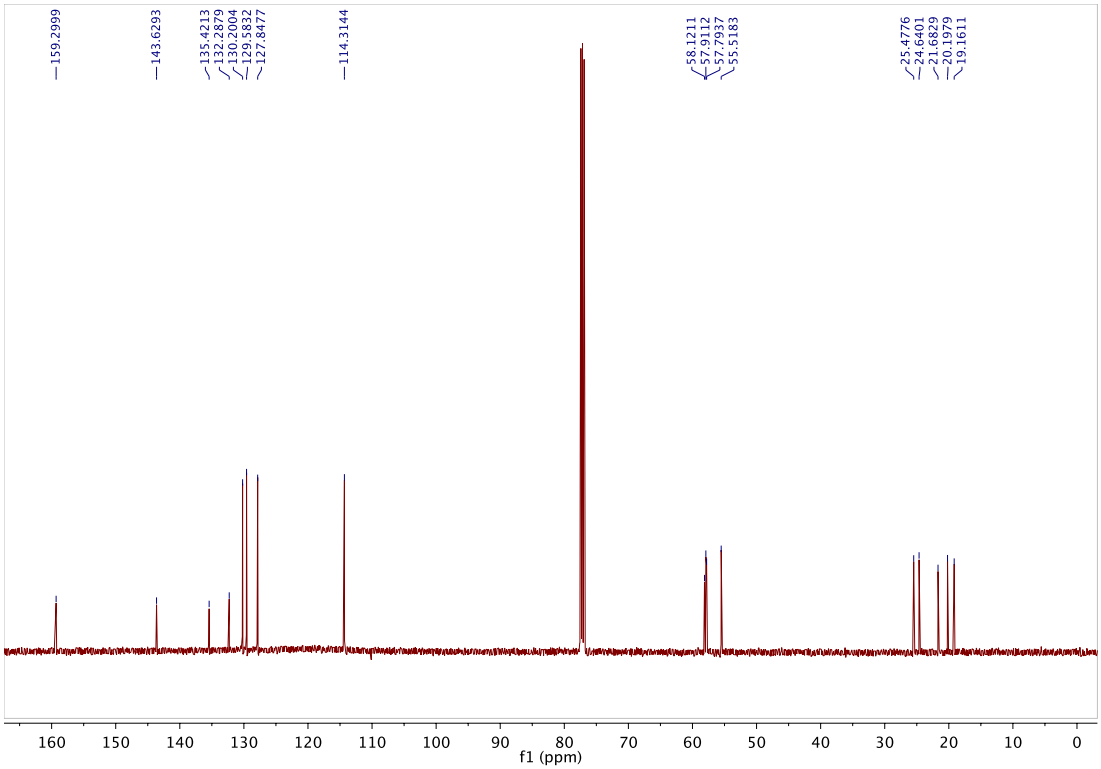
Detector A Channel 2 254nm

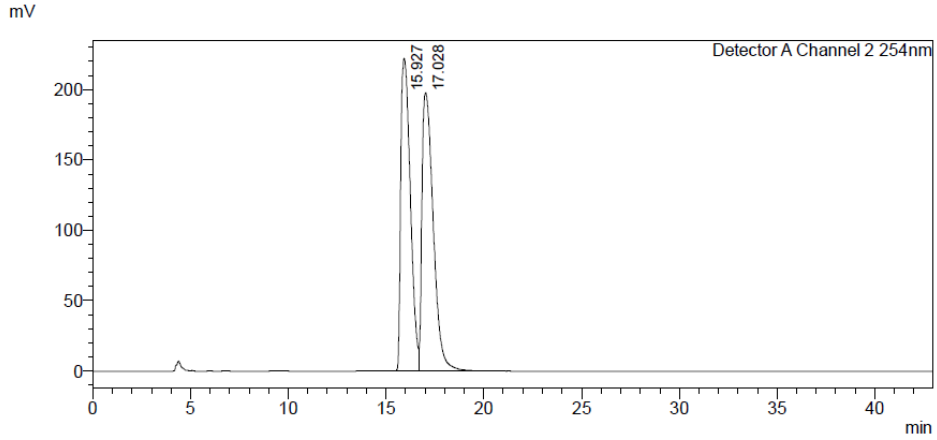
Peak#	Ret. Time	Area	Area%
1	22.740	10360614	97.431
2	26.524	273177	2.569
Total		10633791	100.000


MeO
N
Ts
O

35f

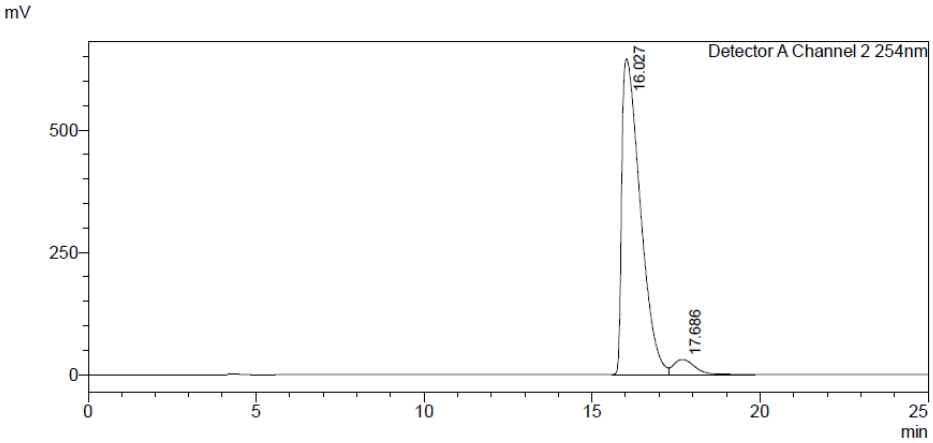

7.4702
7.4537
7.2601
7.2496
7.2335
6.9246
6.9180
6.9137
6.9045
6.9001
6.8935
6.8181
6.8117
6.8073
6.7979
6.7937
3.8782
3.8514
3.7934
3.2372
3.2104
2.6038
2.5986
2.4186
2.2190
2.2068
2.1948
2.1889
2.1766
2.1649
1.8516
1.8397
1.8360
1.8232
1.8094
1.8051
1.8004
1.7932
1.7878
1.7702
1.7572
1.5911
1.4876
1.4814
1.4725
1.4691
1.4546
1.4510
1.4429
1.4360
1.4287
1.4133
1.4015
1.3027
1.2981
1.2941
1.2870
1.2828
1.2791
1.2686
1.2528
1.2131
1.2079
1.2034
1.1963
1.1871
1.1814
1.1674
1.1529
1.1389
-0.0035
1.88
2.32
1.91
1.93
1.00
2.95
0.98
0.99
2.94
0.99
2.02
2.05
1.28
1.91
7.5
7.0
6.5
6.0
5.5
5.0
4.5
4.0
3.5
3.0
2.5
2.0
1.5
1.0
0.5
0.0
f1 (ppm)


159.2999
143.6293
135.4213
132.2879
130.2004
129.5832
127.8477
114.3144
58.1211
57.9112
57.7937
55.5183
25.4776
24.6401
21.6829
20.1979
19.1611
160
150
140
130
120
110
100
90
80
70
60
50
40
30
20
10
0
f1 (ppm)



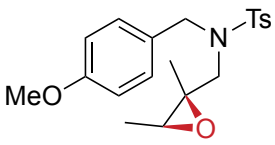
Detector A Channel 2 254nm

Peak#	Ret. Time	Area	Area%
1	15.927	7539694	48.737
2	17.028	7930587	51.263
Total		15470281	100.000

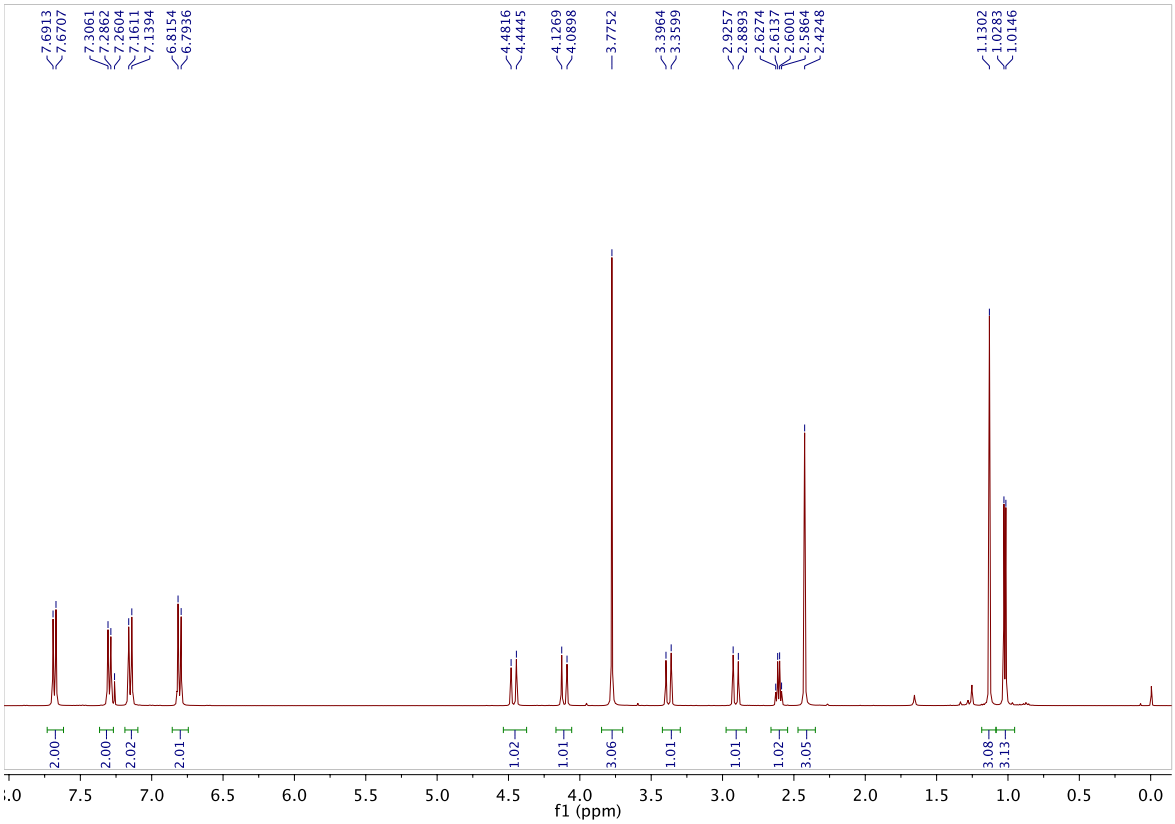


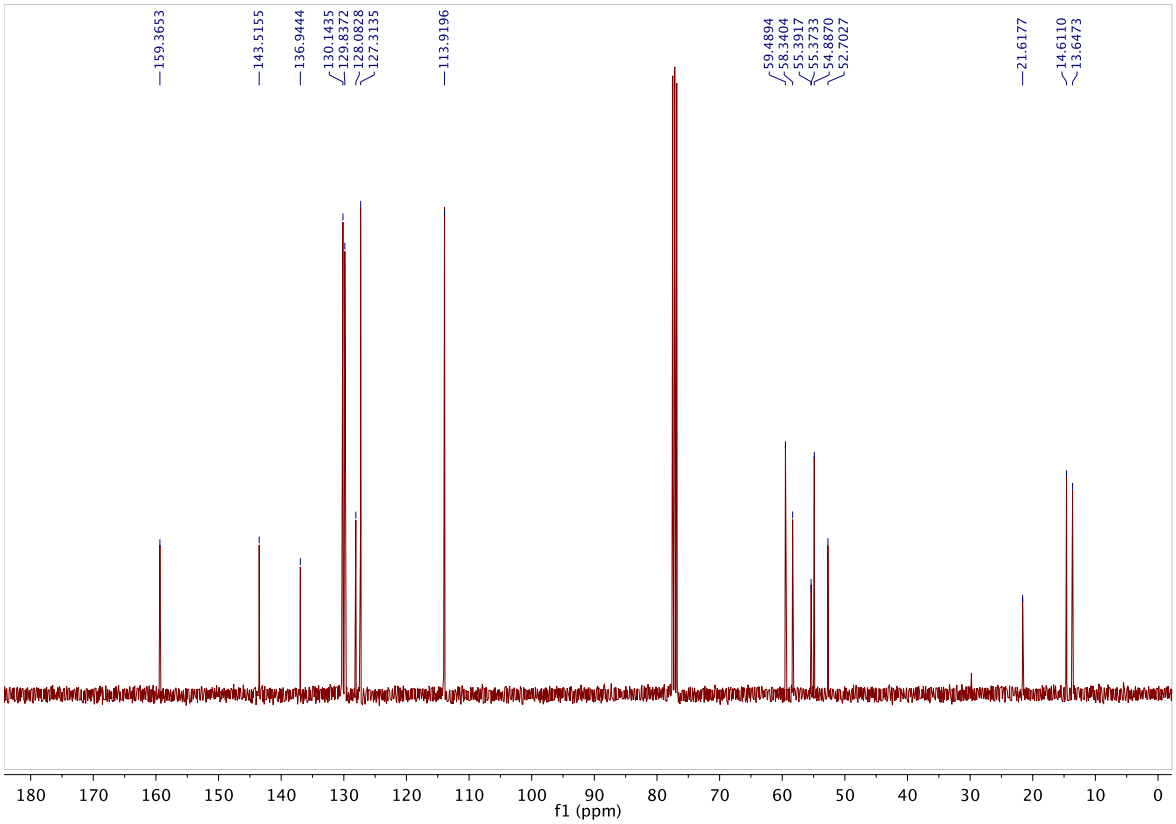
Detector A Channel 2 254nm

Peak#	Ret. Time	Area	Area%
1	16.027	24610266	94.764
2	17.686	1359757	5.236
Total		25970024	100.000

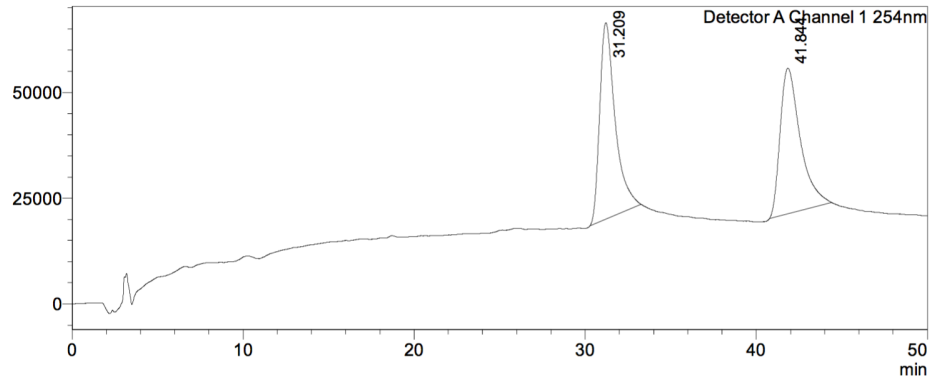

Ts
N
MeO
O

35g


7.6913
7.6707
7.3061
7.2862
7.2604
7.1611
7.1394
6.8154
6.7936
4.4816
4.4445
4.1269
4.0898
3.7752
3.3964
3.3599
2.9257
2.8893
2.6274
2.6137
2.6001
2.5864
2.4248
1.1302
1.0283
1.0146
2.00
2.00
2.02
2.01
1.02
1.01
3.06
1.01
1.01
1.02
3.05
3.08
3.13
f1 (ppm)


159.3653
143.5155
136.9444
130.1435
129.8372
128.0828
127.3135
113.9196
59.4894
58.3404
55.3917
55.3733
54.8870
52.7027
21.6177
14.6110
13.6473
f1 (ppm)

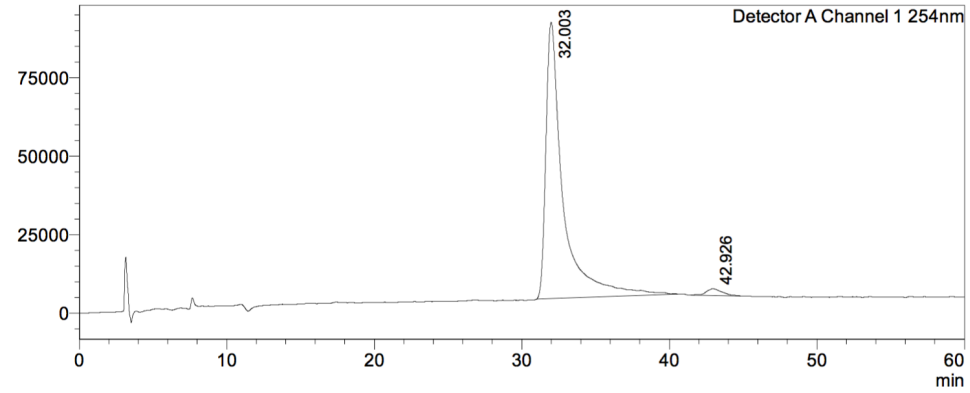
YXY7008A-ADH0510254230-60 YXY7008A-ADH0510254230-60.lcd
uV



Detector A Channel 1 254nm

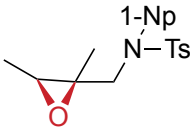
Peak#	Ret. Time	Area	Height	Height%	Area%
1	32.003	7085578	87921	97.630	97.823
2	42.926	157689	2135	2.370	2.177
Total		7243267	90056	100.000	100.000

YXY7008B-ADH0510254230-60 YXY7008B-ADH0510254230-60.lcd
uV

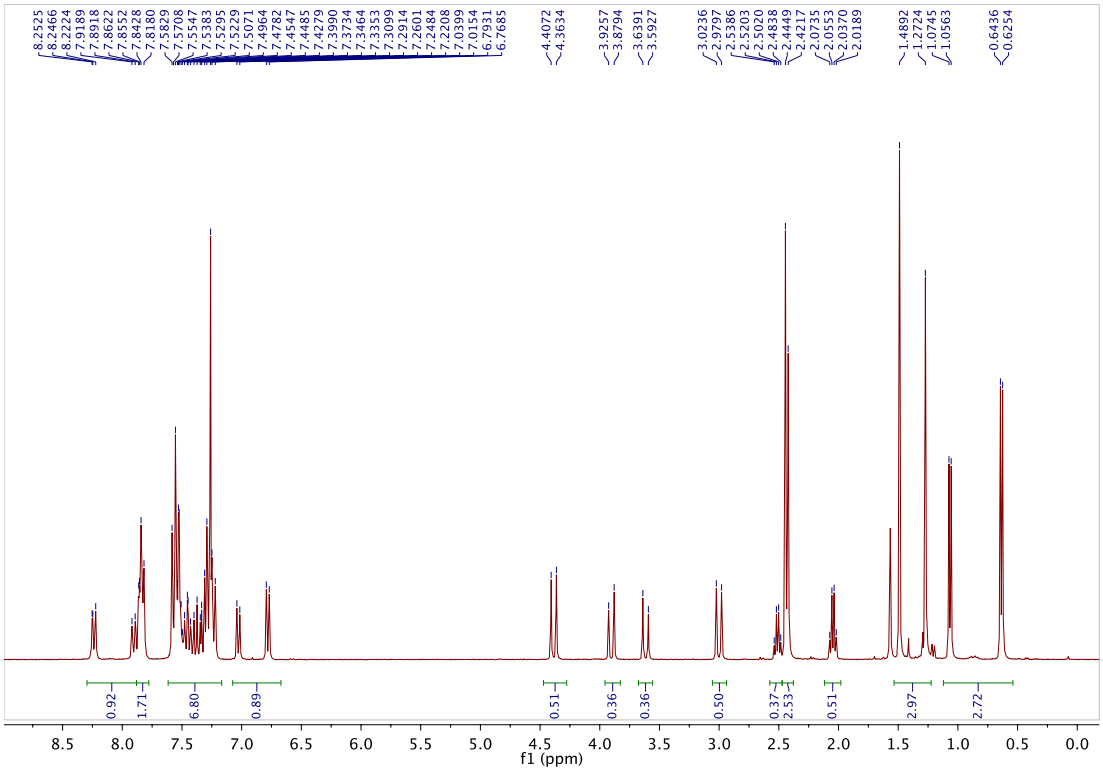


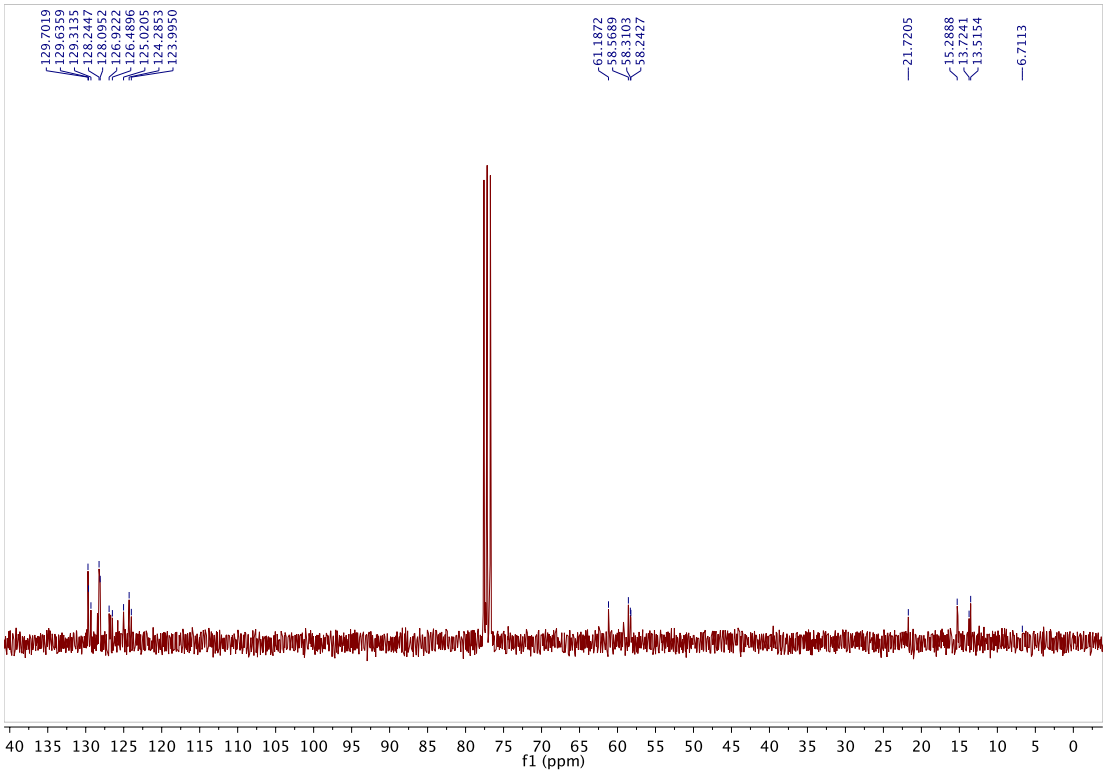
Detector A Channel 1 254nm

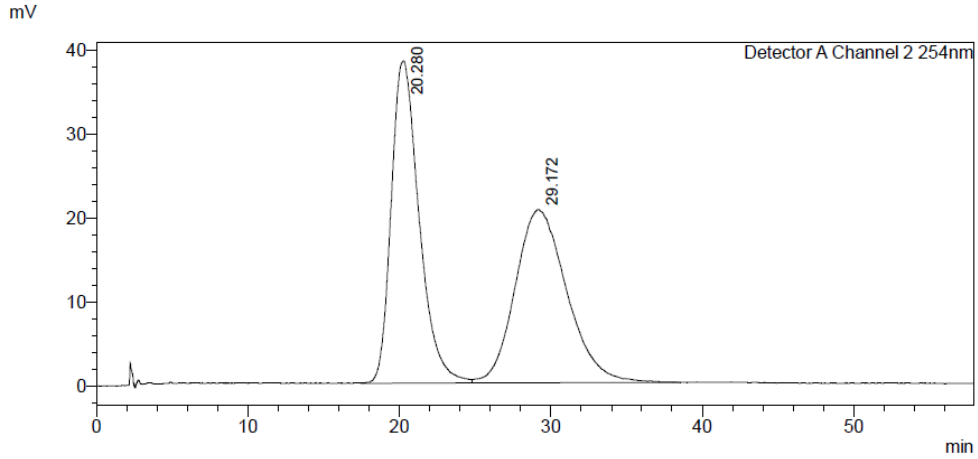
Peak#	Ret. Time	Area	Height	Height%	Area%
1	32.003	7085578	87921	97.630	97.823
2	42.926	157689	2135	2.370	2.177
Total		7243267	90056	100.000	100.000


1-Np
N—Ts
O

35h

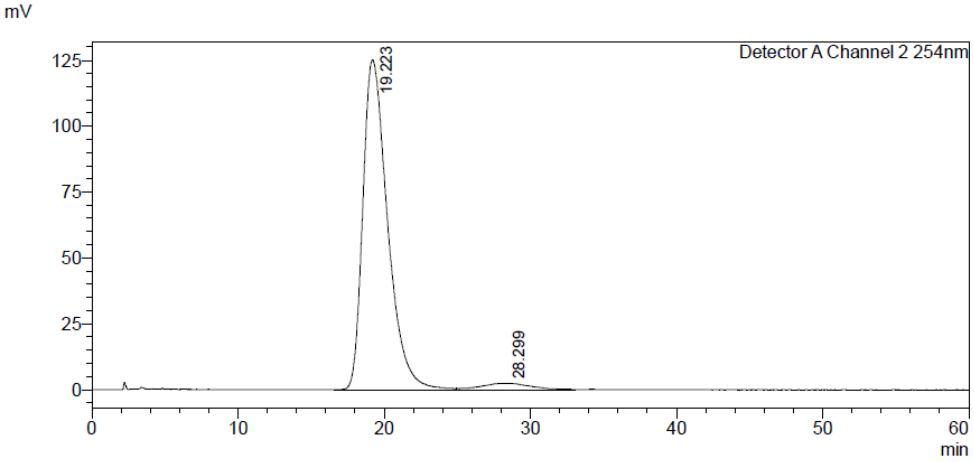

8.2525
8.2466
8.2224
7.9189
7.8918
7.8622
7.8552
7.8428
7.8180
7.5829
7.5708
7.5547
7.5383
7.5295
7.5229
7.5071
7.4964
7.4782
7.4547
7.4485
7.4279
7.3990
7.3734
7.3464
7.3353
7.3099
7.2914
7.2601
7.2484
7.2208
7.0399
7.0154
6.7931
6.7685
4.4072
4.3634
3.9257
3.8794
3.6391
3.5927
3.0236
2.9797
2.5386
2.5203
2.5020
2.4838
2.4649
2.4417
2.0737
2.0553
2.0370
2.0189
1.4892
1.2724
1.0745
1.0563
0.6436
0.6254
0.92
1.71
6.80
0.89
0.51
0.36
0.36
0.50
0.37
2.33
0.51
2.97
2.72
8.5
8.0
7.5
7.0
6.5
6.0
5.5
5.0
4.5
4.0
3.5
3.0
2.5
2.0
1.5
1.0
0.5
0.0
f1 (ppm)


129.7019
129.6359
129.3135
128.2447
128.0952
126.9222
126.4896
125.0205
124.2853
123.9950
61.1872
58.5689
58.3103
58.2427
21.7205
15.2888
13.7241
13.5154
6.7113
40
135
130
125
120
115
110
105
100
95
90
85
80
75
70
65
60
55
50
45
40
35
30
25
20
15
10
5
0
f1 (ppm)



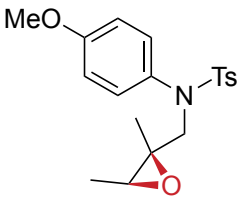
Detector A Channel 2 254nm

Peak#	Ret. Time	Area	Area%
1	20.280	4916144	50.136
2	29.172	4889389	49.864
Total		9805533	100.000

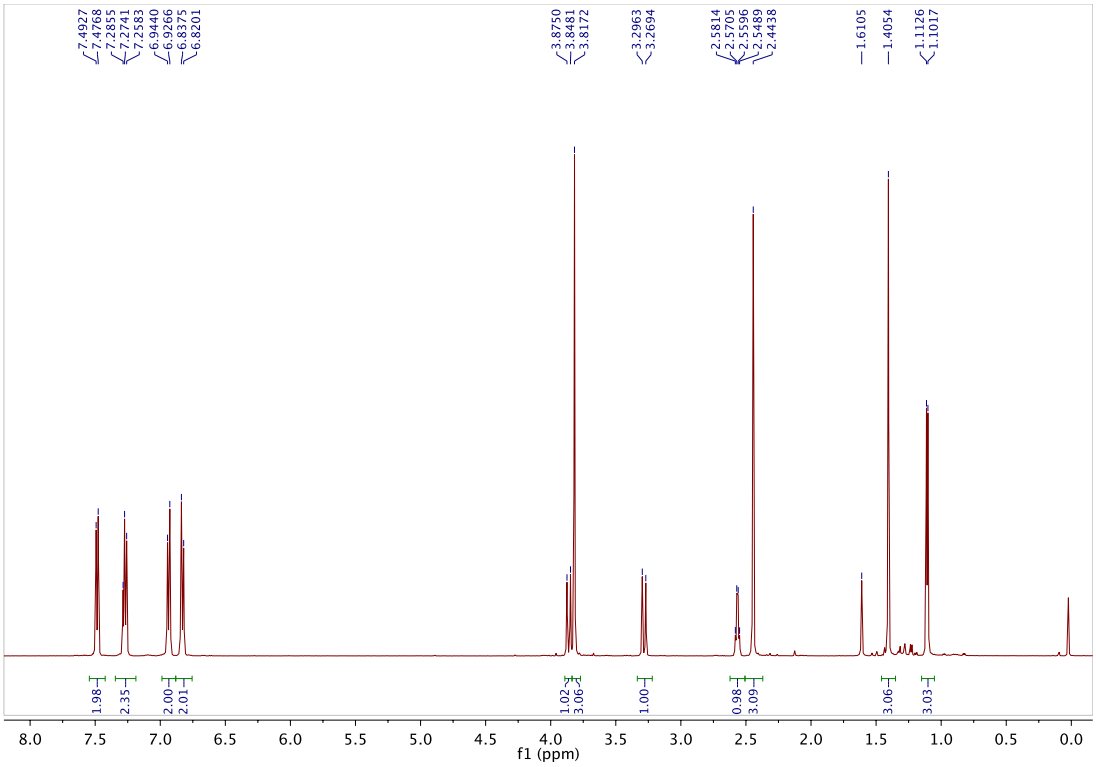


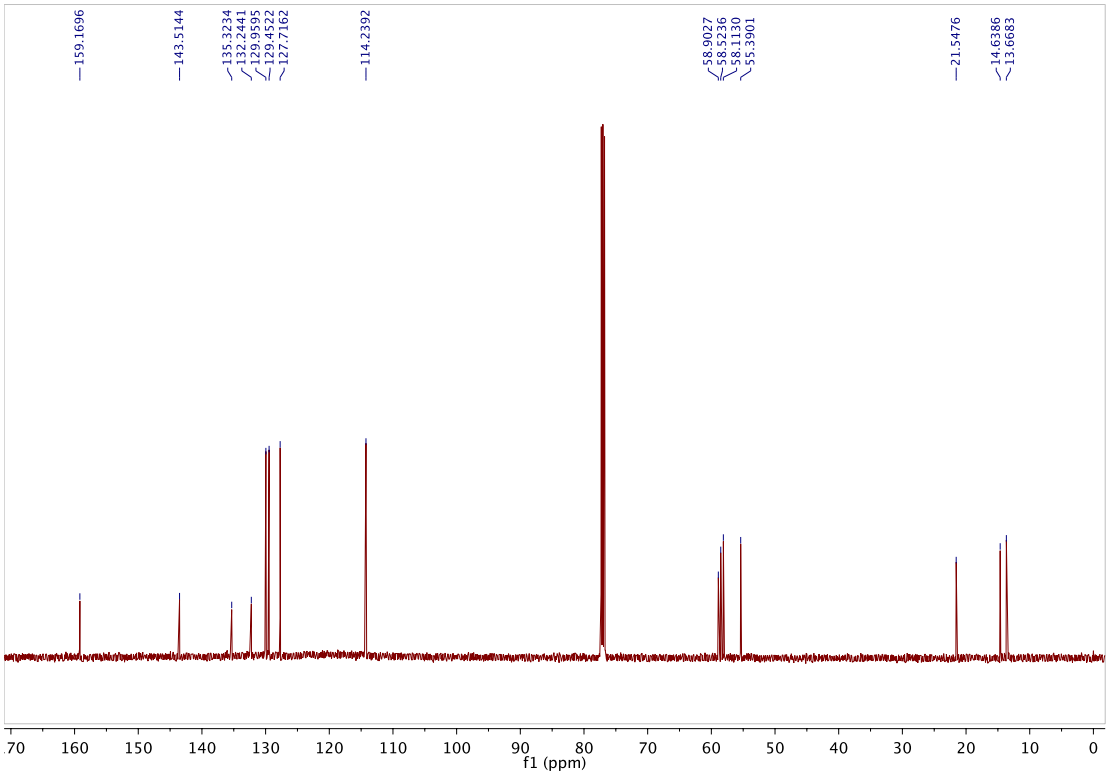
Detector A Channel 2 254nm

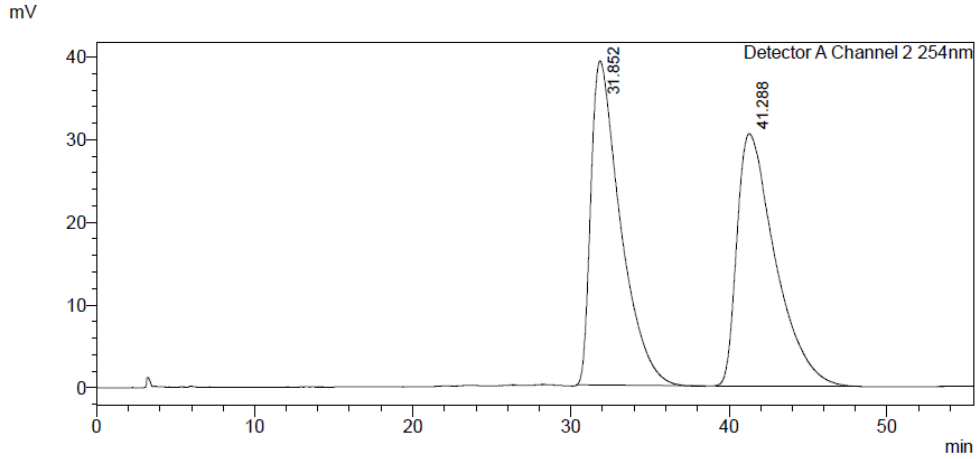
Peak#	Ret. Time	Area	Area%
1	19.223	14713412	96.475
2	28.299	537664	3.525
Total		15251076	100.000


MeO
N
Ts
O

35i


7.4927
7.4768
7.2855
7.2741
7.2583
6.9440
6.9266
6.8375
6.8201
3.8750
3.8481
3.8172
3.2963
3.2694
2.5814
2.5705
2.5596
2.5489
2.4438
1.6105
1.4054
1.1126
1.1017
1.98
2.35
2.00
2.01
1.02
3.06
1.00
0.98
3.09
3.06
3.03
f1 (ppm)


159.1696
143.5144
135.3234
132.2441
129.9595
129.4522
127.7162
114.2392
58.9027
58.5236
58.1130
55.3901
21.5476
14.6386
13.6683
f1 (ppm)



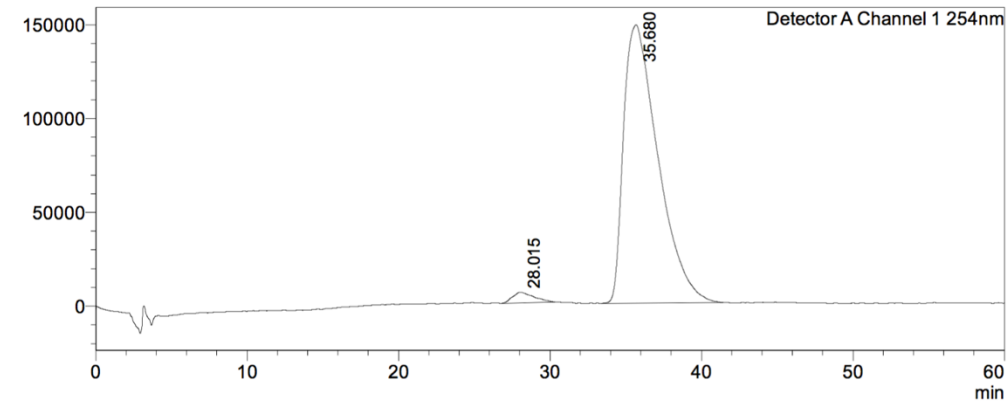
Detector A Channel 2 254nm

Peak#	Ret. Time	Area	Area%
1	31.852	5097901	49.824
2	41.288	5133853	50.176
Total		10231755	100.000

mV

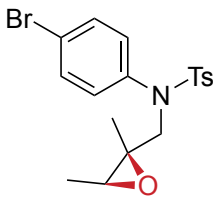
YXY6252B-ASH0510254230-60 YXY6262B-ASH0510254230-60.lcd

uV

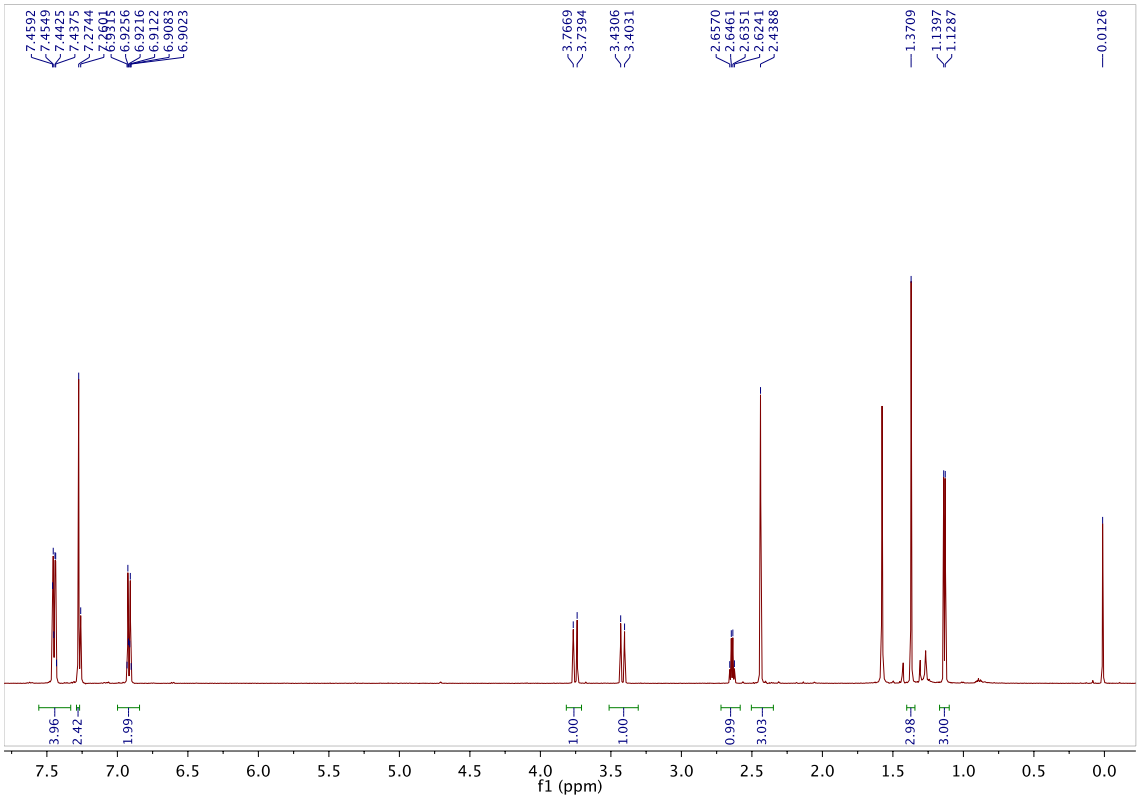


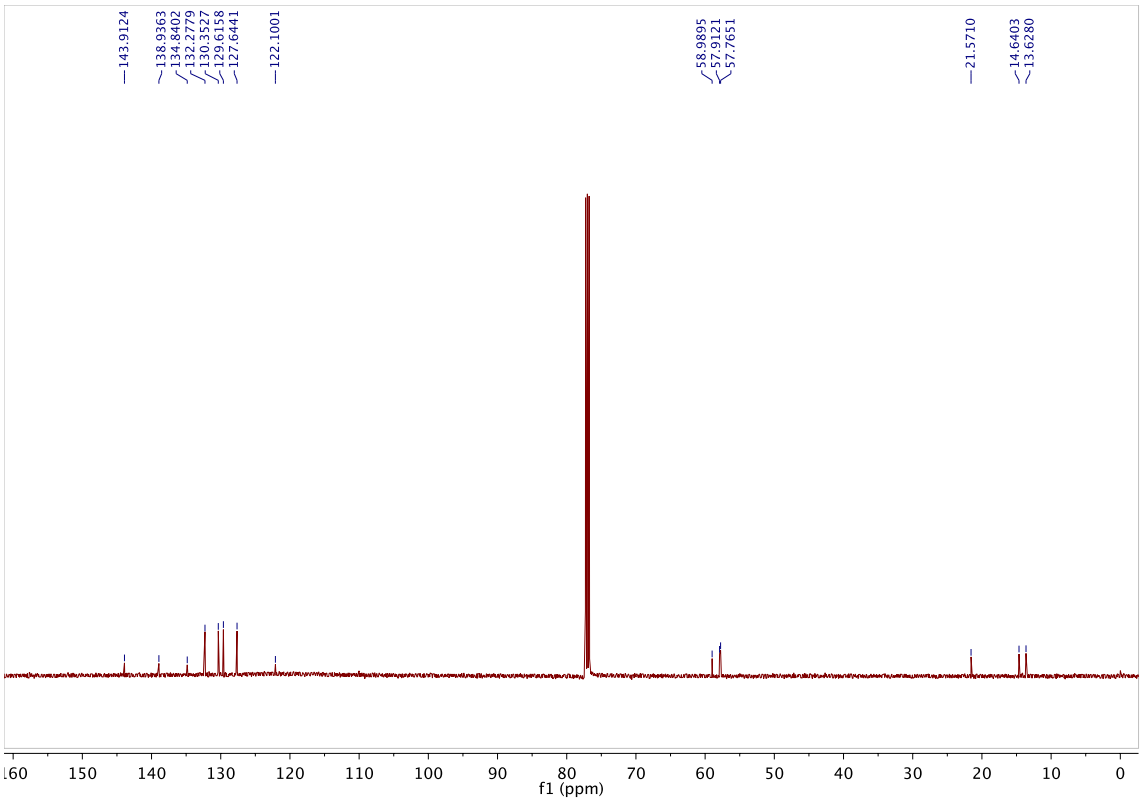
Detector A Channel 1 254nm

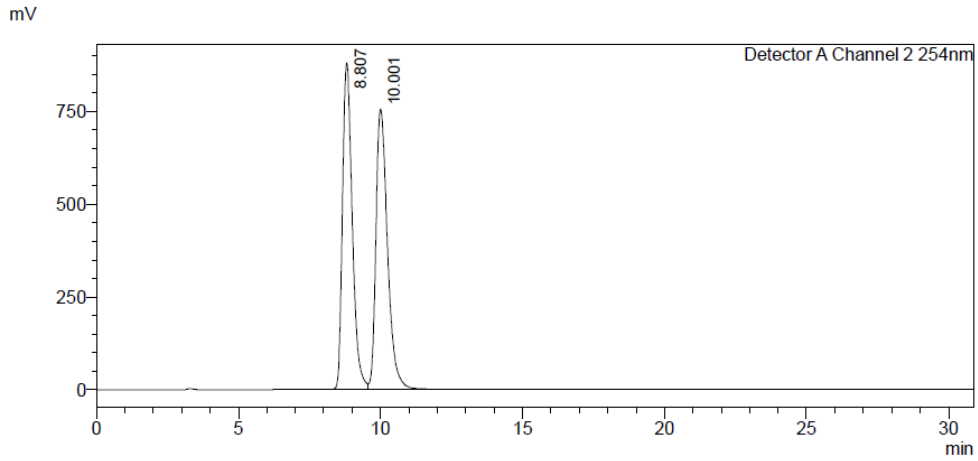
Peak#	Ret. Time	Area	Height	Height%	Area%
1	28.015	548236	5690	3.691	2.278
2	35.680	23523156	148491	96.309	97.722
Total		24071392	154181	100.000	100.000


Br
N
Ts
O

35j

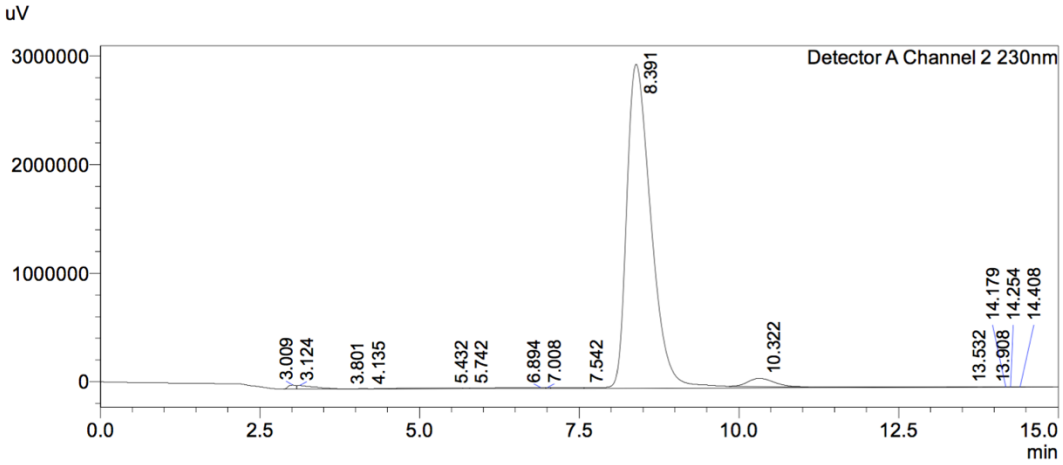

7.4592
7.4549
7.4425
7.4375
7.2744
7.2601
6.9315
6.9256
6.9216
6.9122
6.9083
6.9023
3.7669
3.7394
3.4306
3.4031
2.6570
2.6461
2.6351
2.6241
2.4388
1.3709
1.1397
1.1287
0.0126
3.96
2.42
1.99
1.00
1.00
0.99
3.03
2.98
3.00
f1 (ppm)


143.9124
138.9363
134.8402
132.2779
130.3527
129.6158
127.6441
122.1001
58.9895
57.9121
57.7651
21.5710
14.6403
13.6280
f1 (ppm)



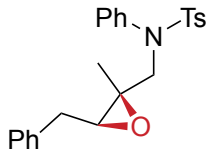
Detector A Channel 2 254nm

Peak#	Ret. Time	Area	Area%
1	8.807	21017769	49.548
2	10.001	21401614	50.452
Total		42419383	100.000

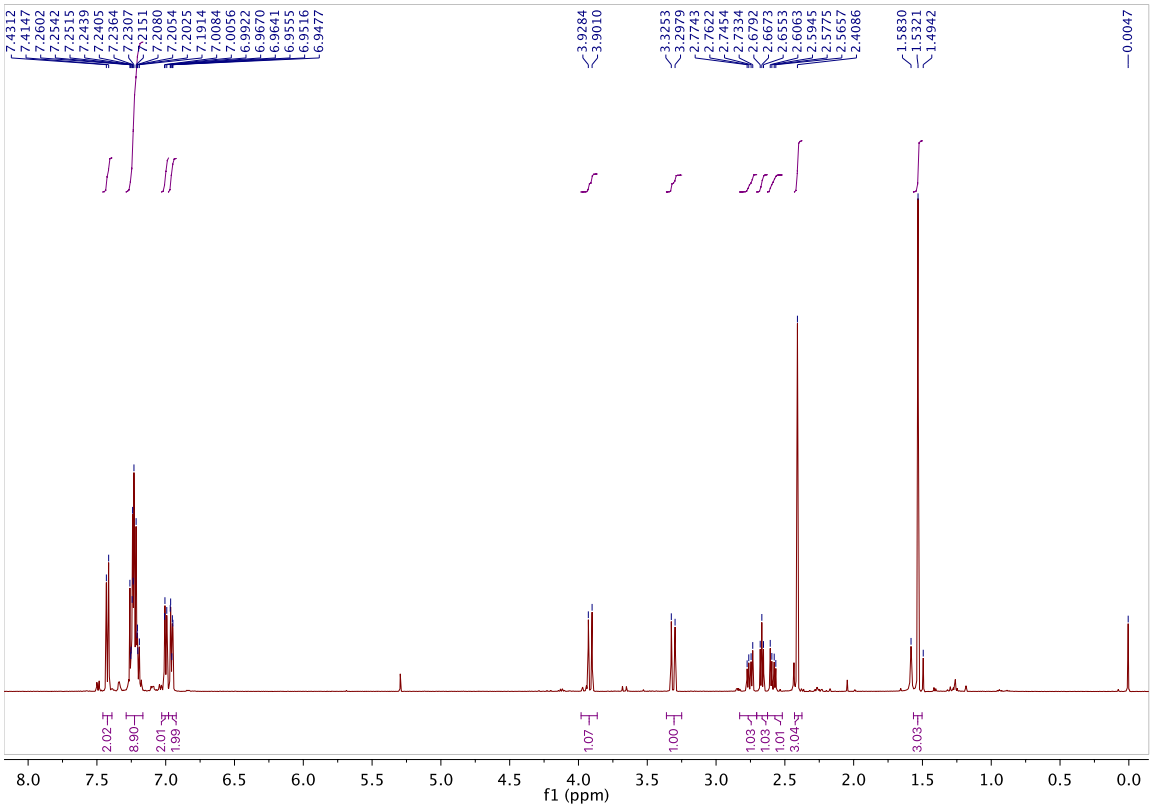


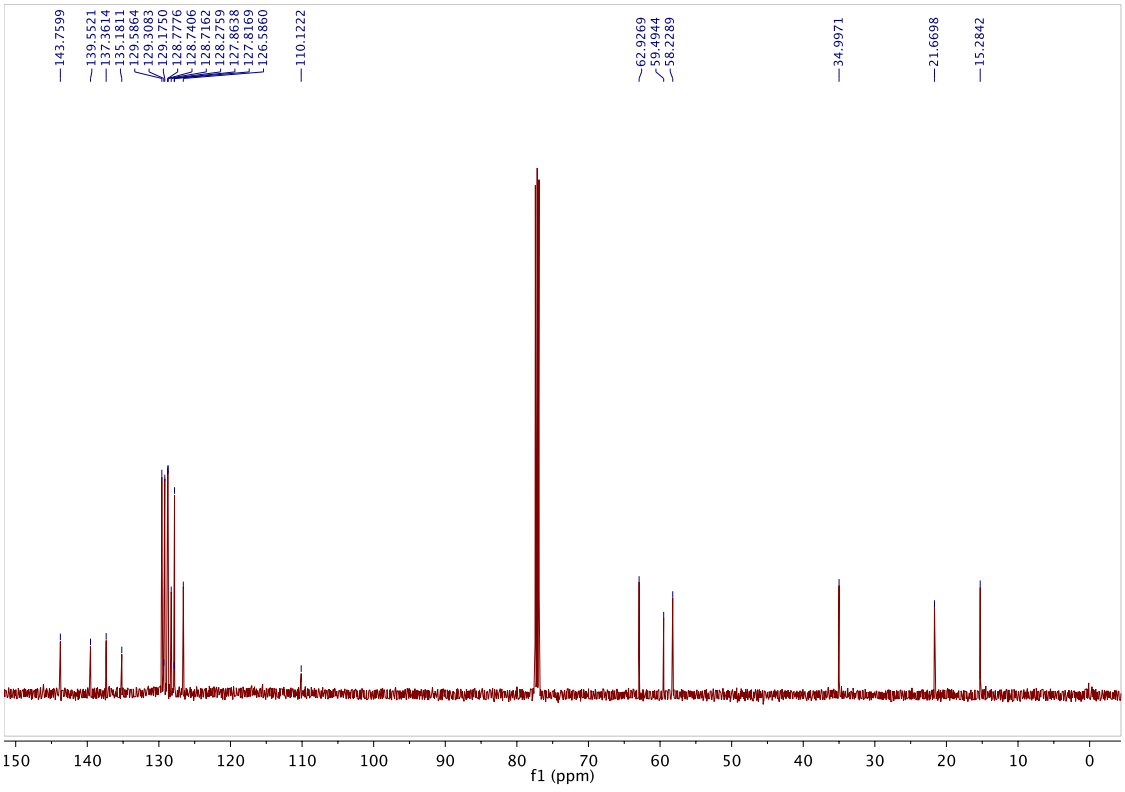
Detector A Channel 1 254nm

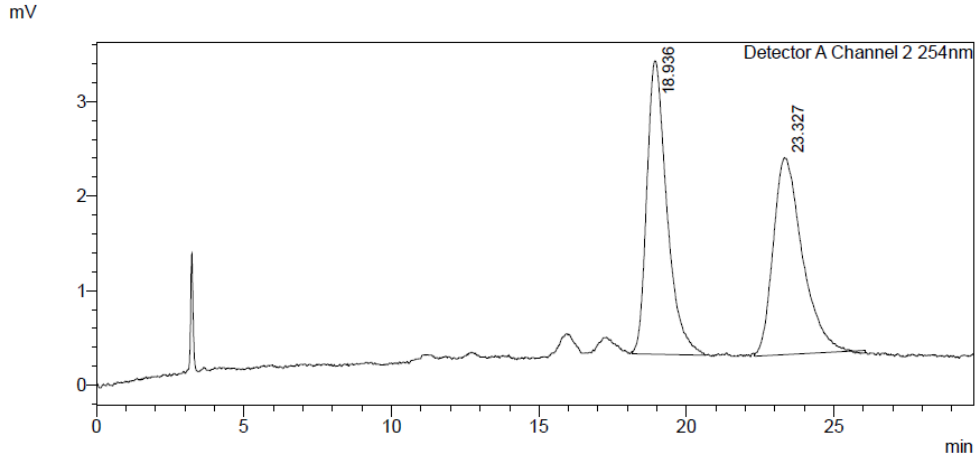
Peak#	Ret. Time	Area	Height	Height%	Area%
1	8.391	40408448	1517216	97.558	97.644
2	10.321	975037	37975	2.442	2.356
Total		41383485	1555191	100.000	100.000


Ph
N
Ts
Ph
O

35k

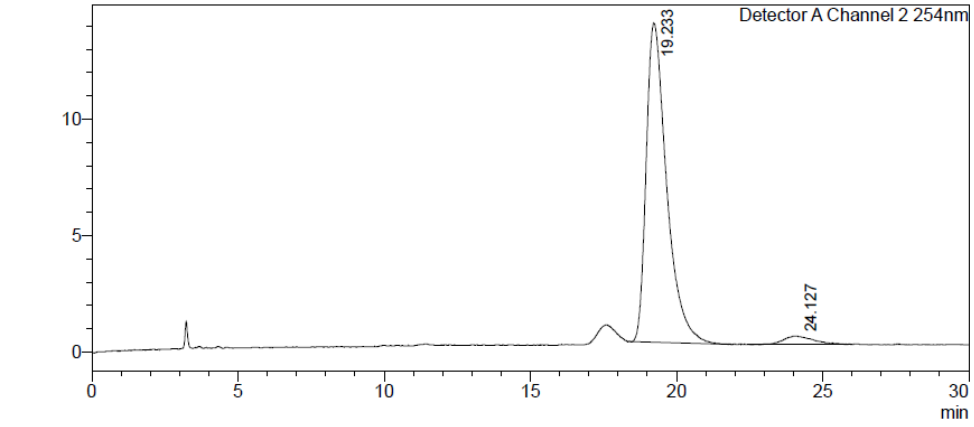

7.4312
7.4147
7.2602
7.2542
7.2515
7.2439
7.2405
7.2364
7.2307
7.2151
7.2080
7.2054
7.2025
7.1914
7.0084
7.0056
6.9922
6.9670
6.9641
6.9555
6.9516
6.9477
3.9284
3.9010
3.3253
3.2979
2.7743
2.7622
2.7454
2.7334
2.6792
2.6673
2.6553
2.6063
2.5945
2.5775
2.5657
2.4086
1.5830
1.5321
1.4942
0.0047
2.02
8.90
2.01
1.99
1.07
1.00
1.03
1.03
1.01
3.04
3.03
f1 (ppm)


143.7599
139.5521
137.3614
135.1811
129.5864
129.3083
129.1750
128.7776
128.7406
128.7162
128.2759
127.8638
127.8169
126.5860
110.1222
62.9269
59.4944
58.2289
34.9971
21.6698
15.2842
f1 (ppm)



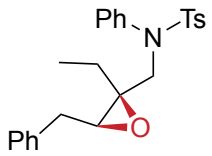
Detector A Channel 2 254nm

Peak#	Ret. Time	Area	Area%
1	18.936	147254	50.716
2	23.327	143094	49.284
Total		290348	100.000

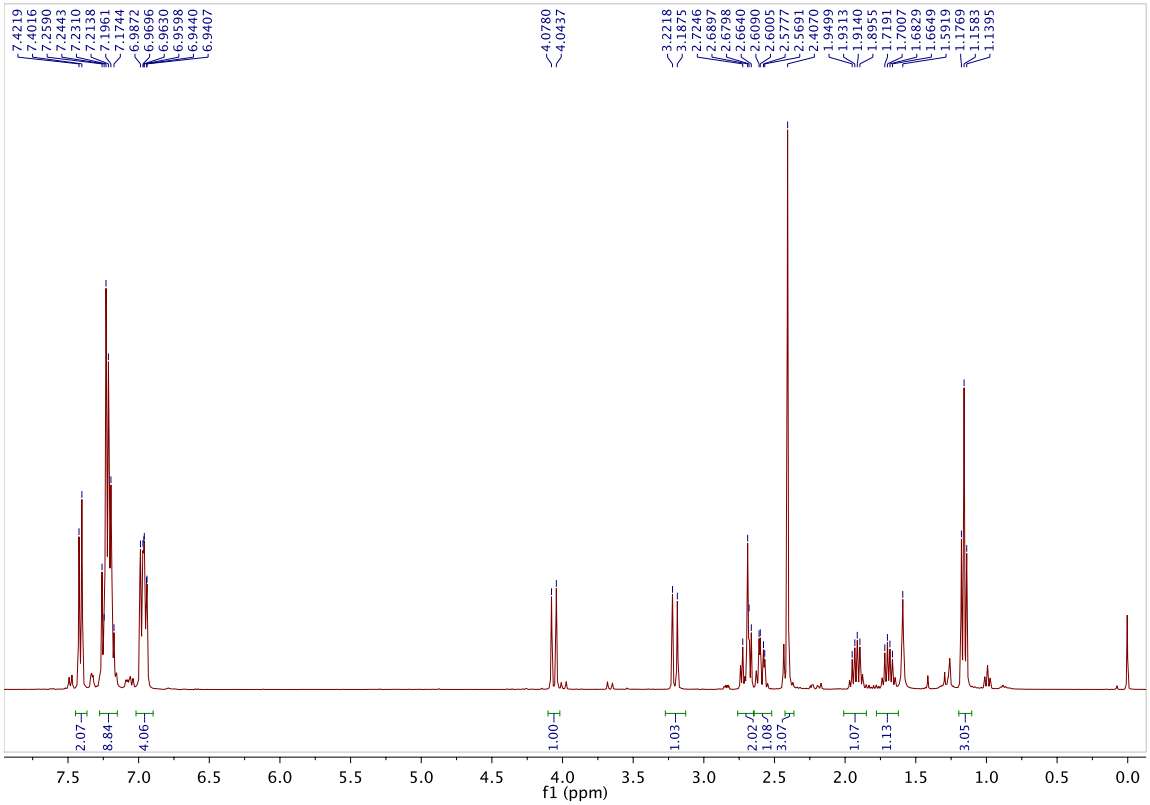


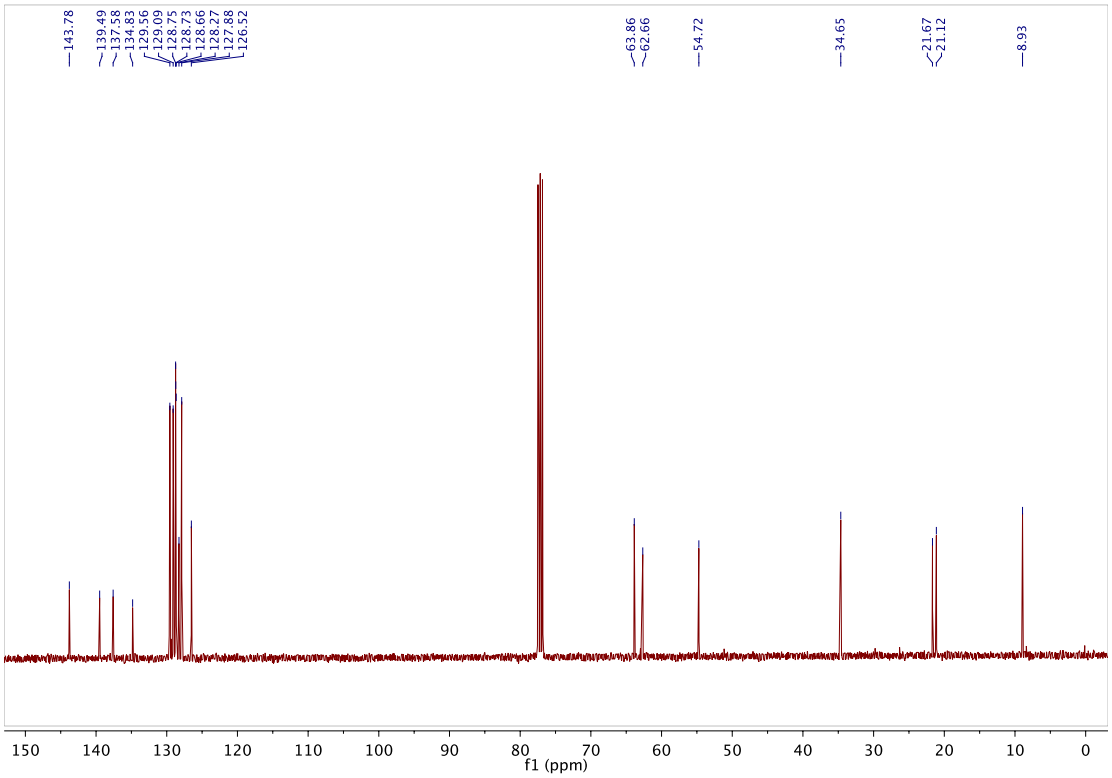
Detector A Channel 2 254nm

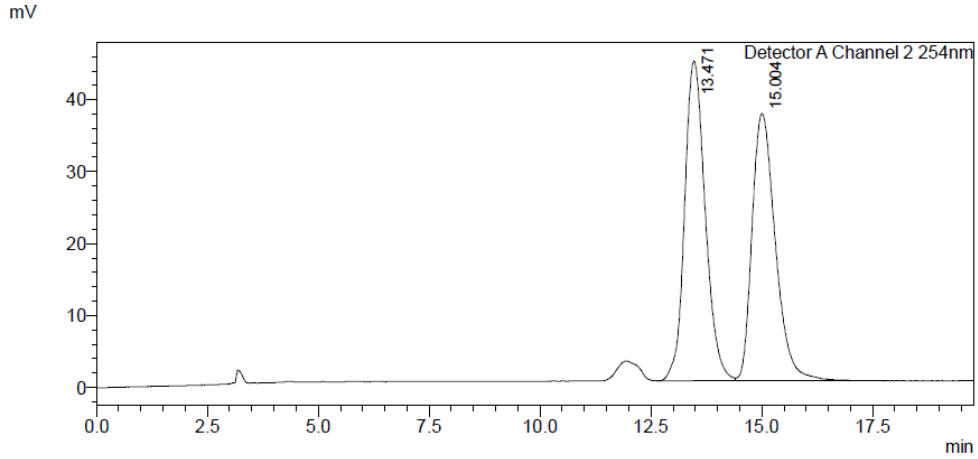
Peak#	Ret. Time	Area	Area%
1	19.233	667911	96.360
2	24.127	25233	3.640
Total		693144	100.000


Ph
N
Ts
Ph
O

35l


7.4219
7.4016
7.2590
7.2443
7.2310
7.2138
7.1961
7.1744
7.1744
6.9872
6.9696
6.9630
6.9598
6.9440
6.9407
4.0780
4.0437
3.2218
3.1875
2.7246
2.6897
2.6798
2.6640
2.6090
2.6005
2.5777
2.5691
2.4070
1.9499
1.9313
1.9140
1.8955
1.7191
1.7007
1.6829
1.6649
1.5919
1.1769
1.1583
1.1395
2.07
8.84
4.06
1.00
1.03
2.02
1.08
3.07
1.07
1.13
3.05
7.5
7.0
6.5
6.0
5.5
5.0
4.5
4.0
3.5
3.0
2.5
2.0
1.5
1.0
0.5
0.0
f1 (ppm)


143.78
139.49
137.38
134.83
129.56
129.09
128.75
128.73
128.66
128.27
127.88
126.52
63.86
62.66
54.72
34.65
21.67
21.12
8.93
150
140
130
120
110
100
90
80
70
60
50
40
30
20
10
0
f1 (ppm)



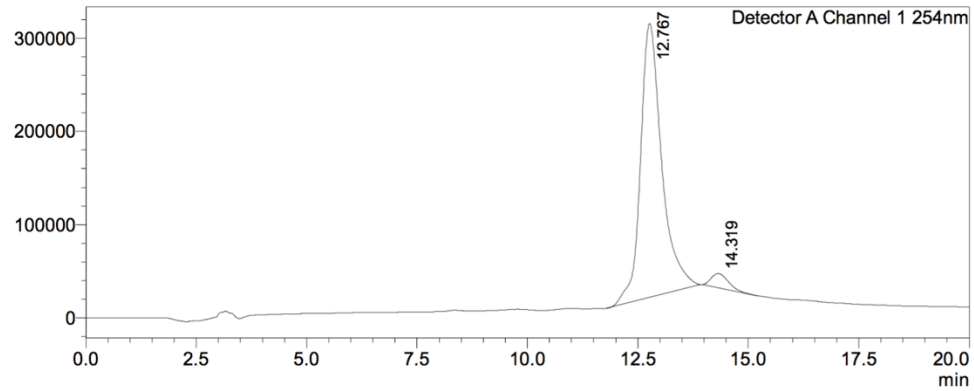
Detector A Channel 2 254nm

Peak#	Ret. Time	Area	Area%
1	13.471	1440308	51.524
2	15.004	1355111	48.476
Total		2795419	100.000

mV

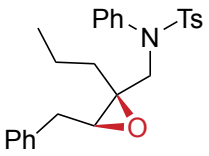
YXY6268B-ADH0510254230-20 YXY6268B-ADH0510254230-20.lcd

uV

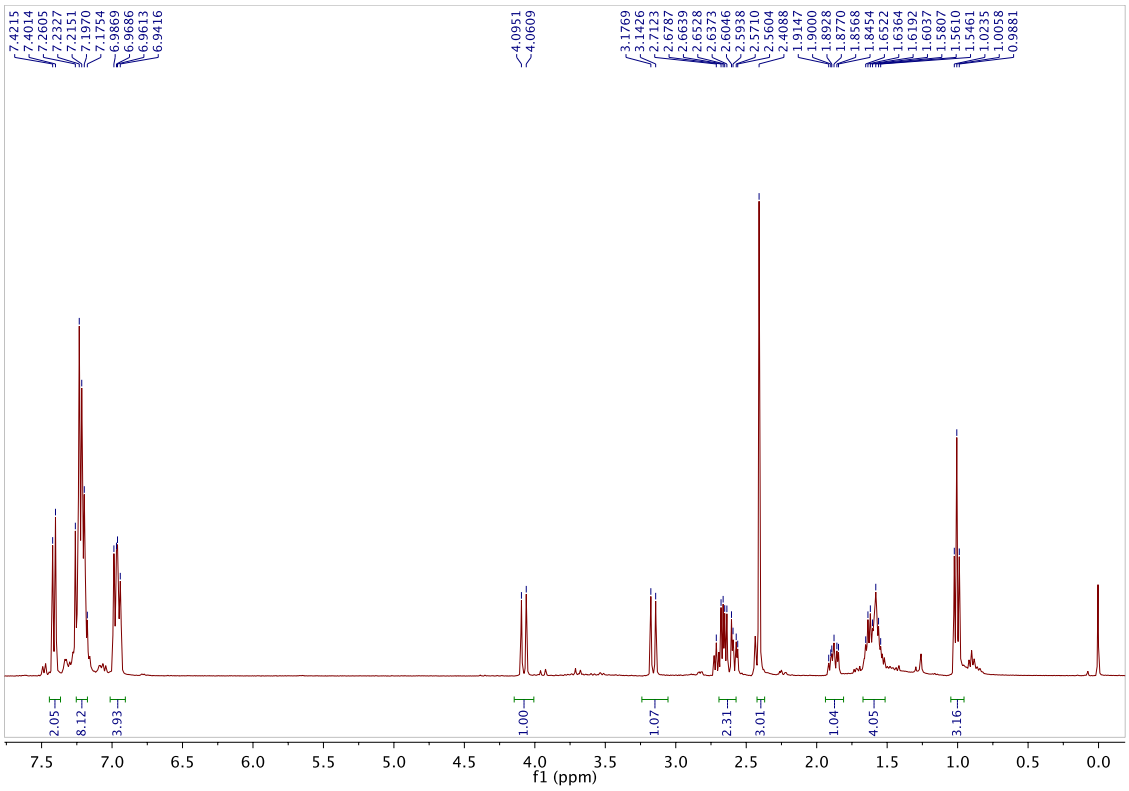


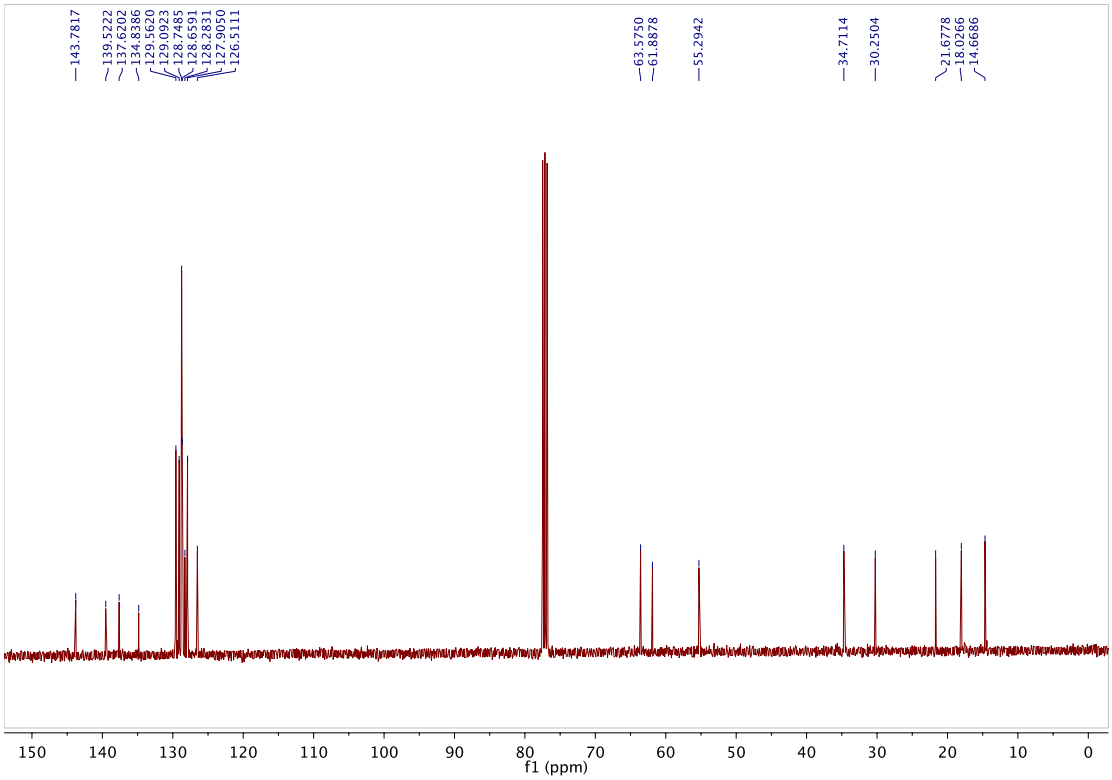
Detector A Channel 1 254nm

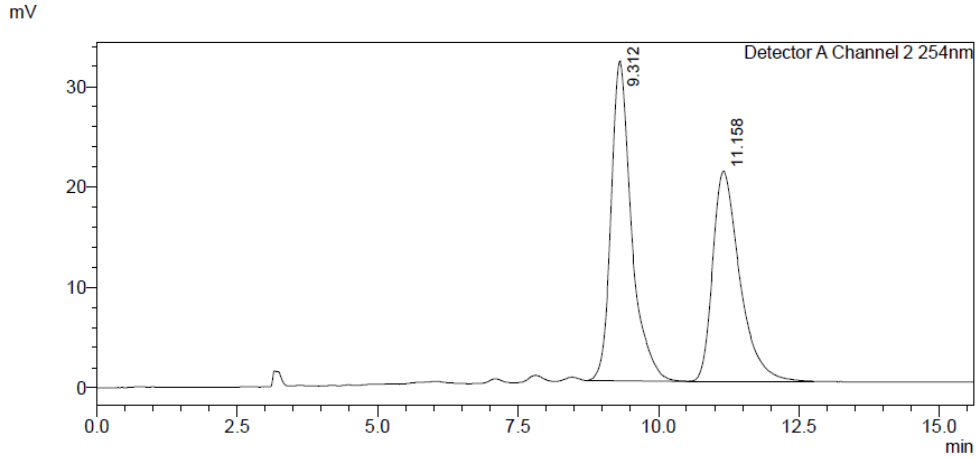
Peak#	Ret. Time	Area	Height	Height%	Area%
1	12.767	9871535	293559	95.020	95.903
2	14.319	421679	15385	4.980	4.097
Total		10293213	308943	100.000	100.000


Ph
N
Ts
O
Ph

35m

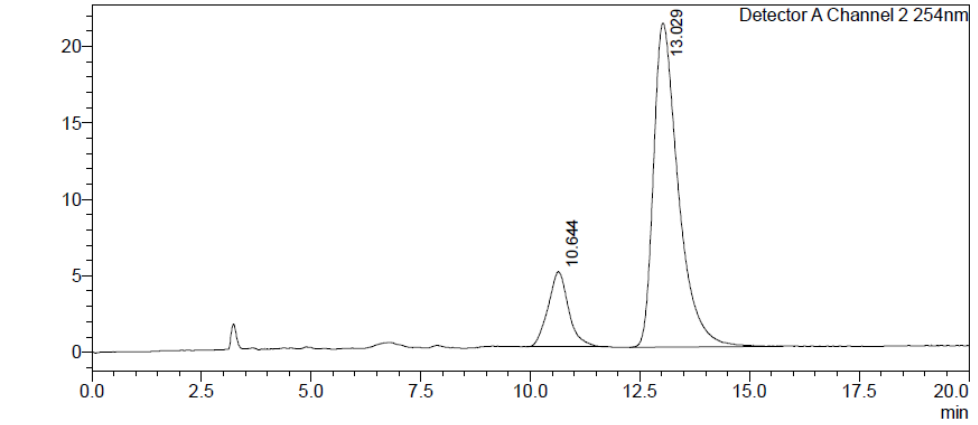

7.4215
7.4014
7.2605
7.2327
7.2151
7.1970
7.1754
6.9869
6.9686
6.9613
6.9416
4.0951
4.0609
3.1769
3.1426
2.7123
2.6787
2.6639
2.6528
2.6373
2.6046
2.5938
2.5710
2.5604
2.4088
1.9147
1.9000
1.8928
1.8770
1.8568
1.8454
1.6552
1.6364
1.6192
1.6037
1.5807
1.5610
1.5461
1.0235
1.0058
0.9881
2.05
8.12
3.93
1.00
1.07
2.31
3.01
1.04
4.05
3.16
7.5
7.0
6.5
6.0
5.5
5.0
4.5
4.0
3.5
3.0
2.5
2.0
1.5
1.0
0.5
0.0
f1 (ppm)


143.7817
139.5222
137.6202
134.8386
129.3620
129.0923
128.7485
128.6591
128.2831
127.9050
126.5111
63.5750
61.8878
55.2942
34.7114
30.2504
21.6778
18.0266
14.6686
150
140
130
120
110
100
90
80
70
60
50
40
30
20
10
0
f1 (ppm)



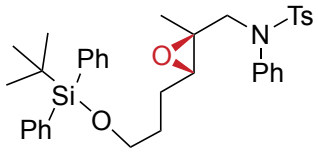
Detector A Channel 2 254nm

Peak#	Ret. Time	Area	Area%
1	9.312	807678	53.510
2	11.158	701718	46.490
Total		1509396	100.000

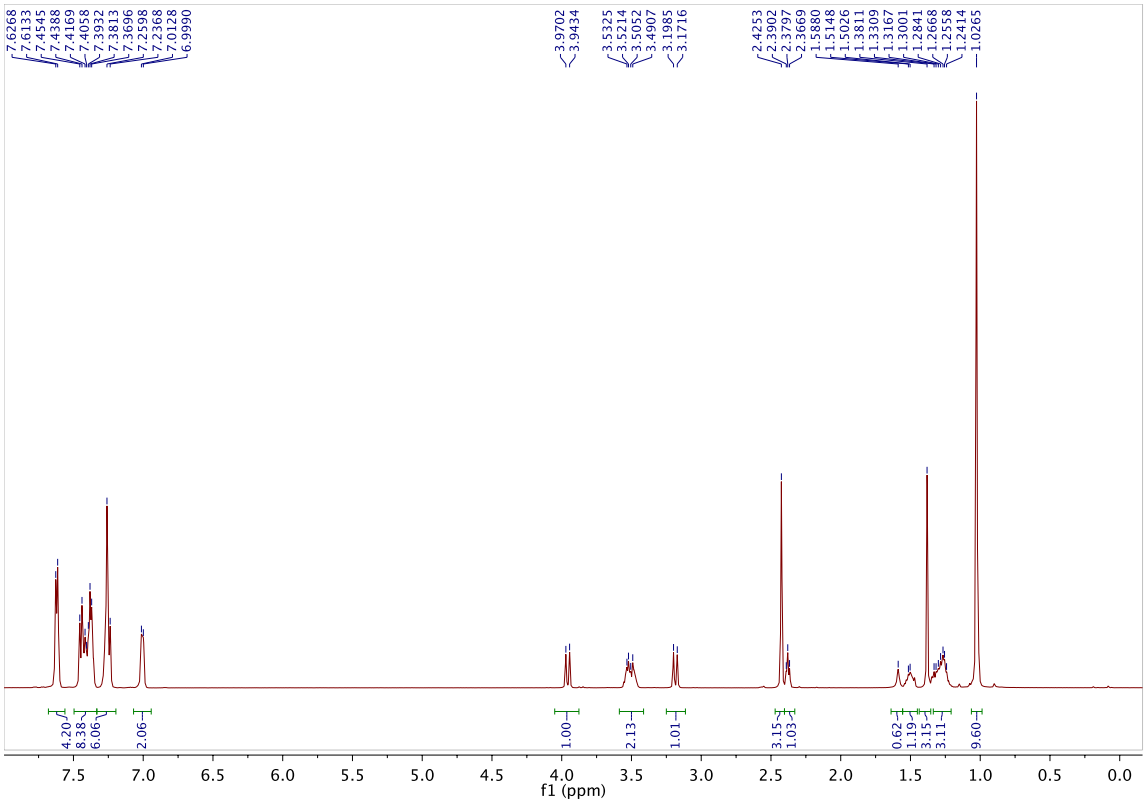


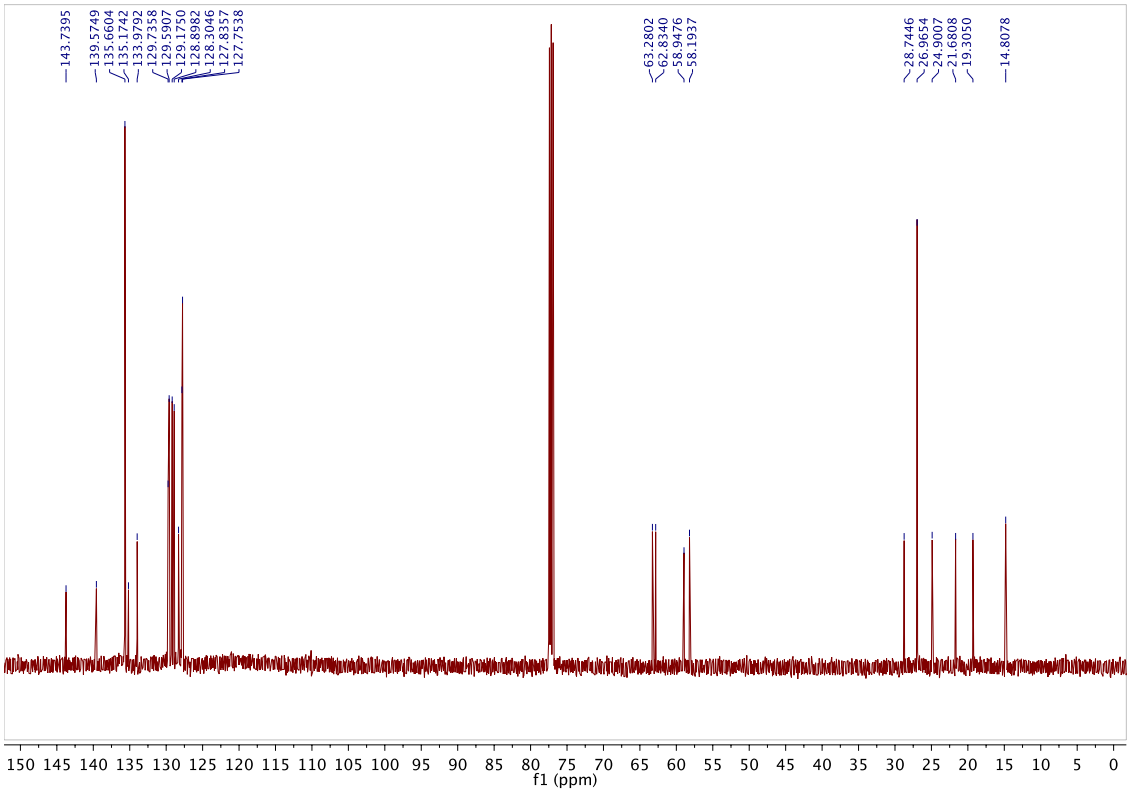
Detector A Channel 2 254nm

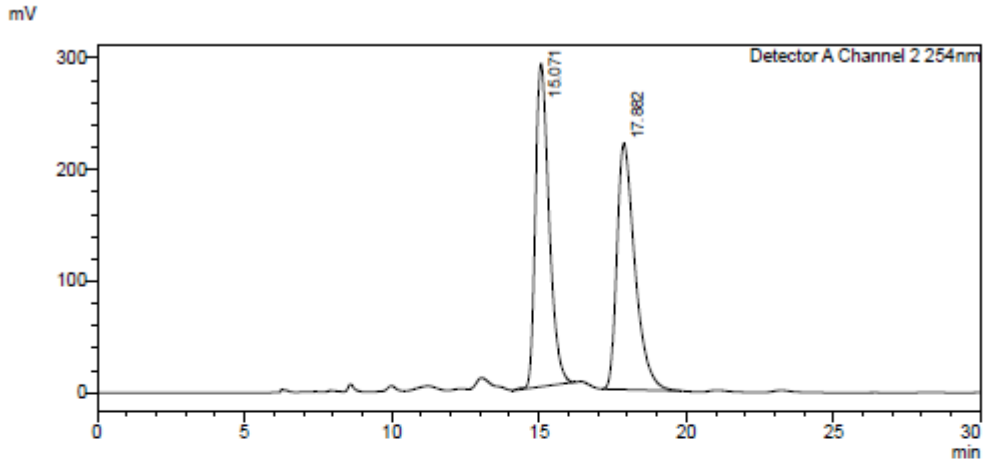
Peak#	Ret. Time	Area	Area%
1	10.644	160983	16.178
2	13.029	834083	83.822
Total		995066	100.000


Ts
N
Ph
O
Ph
Si
Ph
O

35n

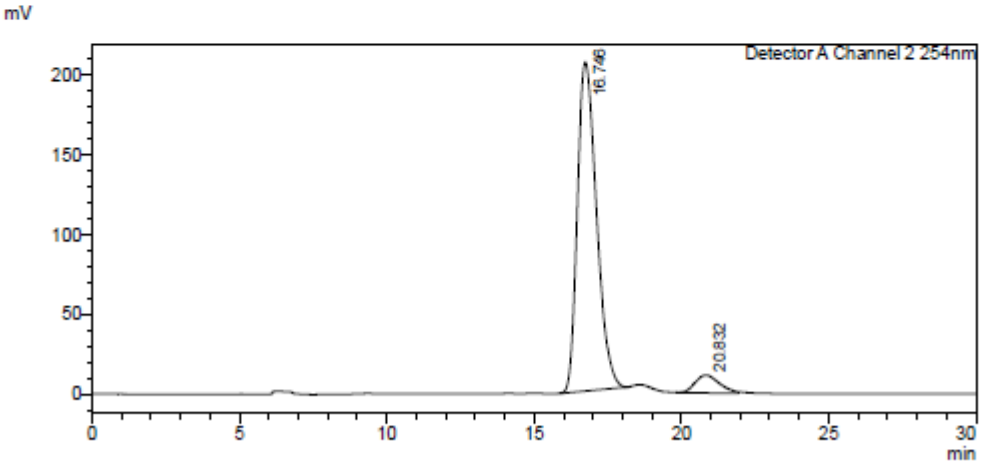

7.6268
7.6133
7.4545
7.4388
7.4169
7.4058
7.3932
7.3813
7.3696
7.2598
7.2368
7.0128
6.9990
3.9702
3.9434
3.5325
3.5214
3.5052
3.4907
3.1985
3.1716
2.4253
2.3902
2.3797
2.3669
1.5880
1.5148
1.5026
1.3811
1.3309
1.3167
1.3001
1.2841
1.2668
1.2358
1.2414
1.0265
4.20
8.38
6.06
2.06
1.00
2.13
1.01
3.15
1.03
0.62
1.19
3.15
3.11
9.60
f1 (ppm)


143.7395
139.5749
135.6604
135.1742
133.9792
129.7358
129.5907
129.1750
128.8982
128.3046
127.8357
127.7538
63.2802
62.8340
58.9476
58.1937
28.7446
26.9654
24.9007
21.6808
19.3050
14.8078
f1 (ppm)



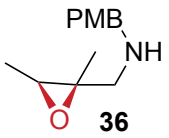
Detector A Channel 2 254nm

Peak#	Ret. Time	Area	Area%
1	15.071	9224248	49.501
2	17.882	9410313	50.499
Total		18634562	100.000

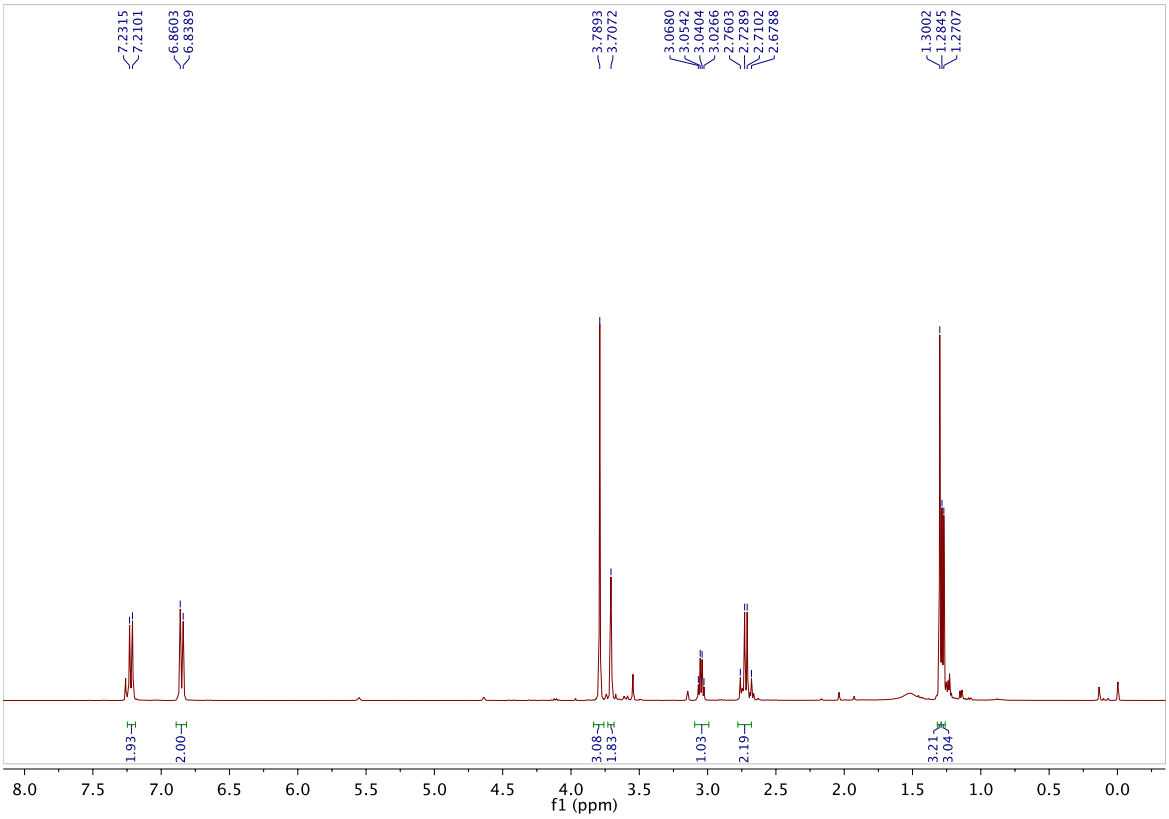


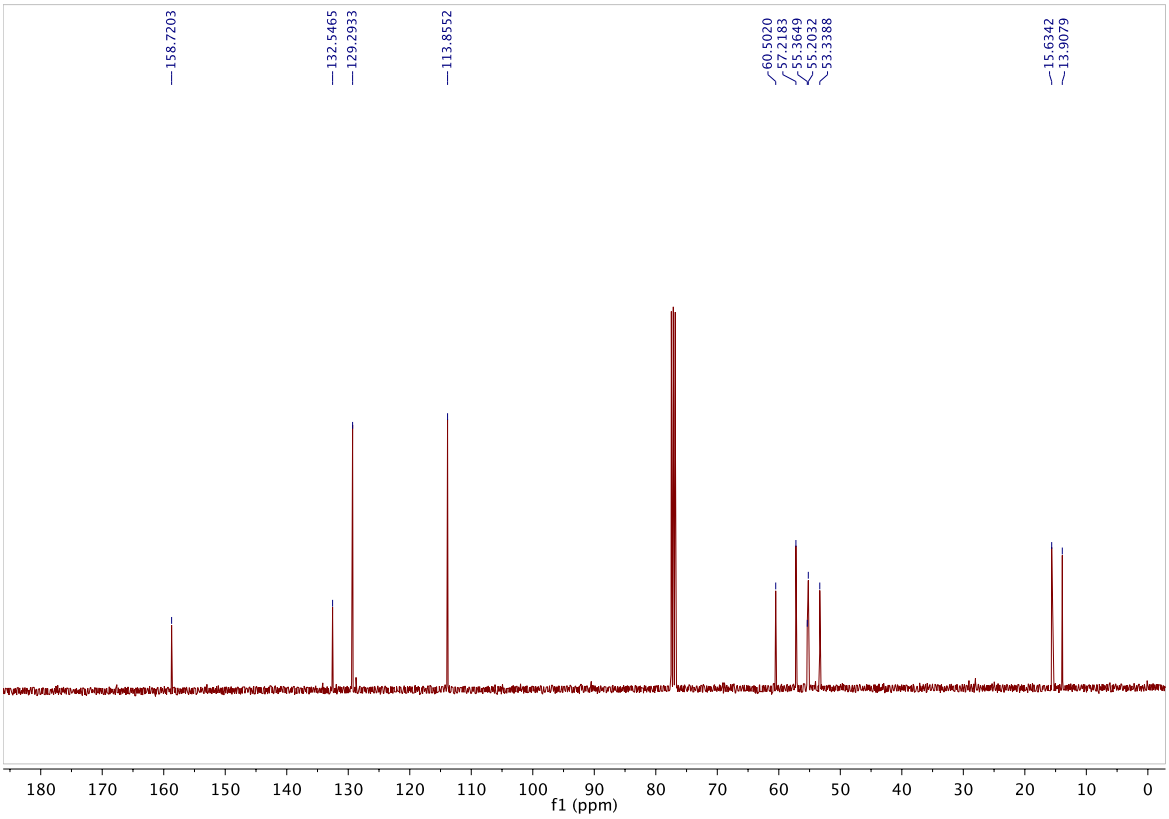
Detector A Channel 2 254nm

Peak#	Ret. Time	Area	Area%
1	16.746	9331885	93.424
2	20.832	656883	6.576
Total		9988768	100.000

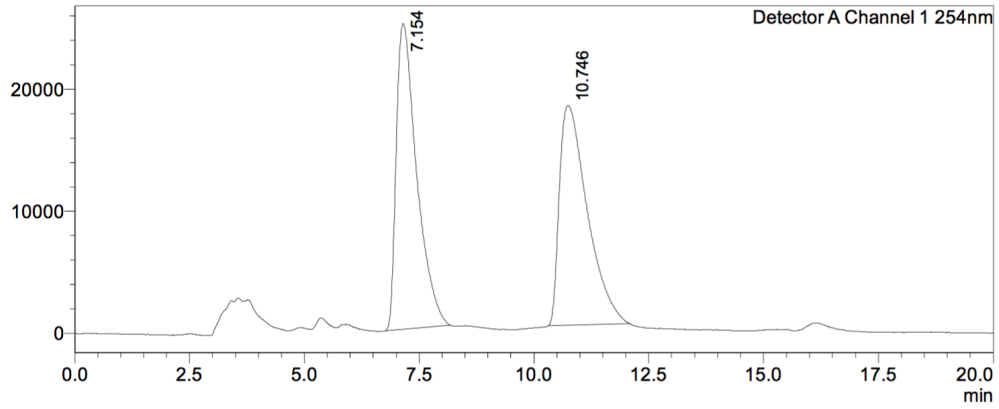

PMB
NH
O

36


7.2315
7.2101
6.8603
6.8389
3.7893
3.7072
3.0680
3.0542
3.0404
3.0266
2.7603
2.7289
2.7102
2.6788
1.3002
1.2845
1.2707
1.93
2.00
3.08
1.83
1.03
2.19
3.21
3.04
f1 (ppm)


158.7203
132.5465
129.2933
113.8552
60.5020
57.2183
55.3649
55.2032
53.3388
15.6342
13.9079
f1 (ppm)

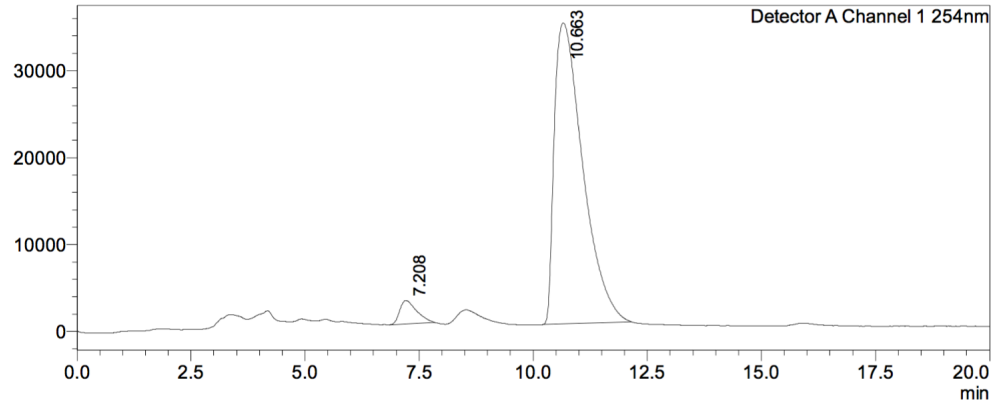
YXY7104-2-ASH2010254230-30R YXY7104-2-ASH2010254230-30R.lcd
uV



Detector A Channel 1 254nm

Peak#	Ret. Time	Area	Height	Height%	Area%
1	7.154	777228	25027	58.188	50.615
2	10.746	758327	17984	41.812	49.385
Total		1535555	43010	100.000	100.000

YXY7102-2-ASH1510254230-20redo YXY7102-2-ASH2010254230-20redo.lcd
uV



Detector A Channel 1 254nm

Peak#	Ret. Time	Area	Height	Height%	Area%
1	7.208	69656	2701	7.237	4.431
2	10.663	1502231	34617	92.763	95.569
Total		1571886	37318	100.000	100.000